SYNTHESIS AND CHARACTERIZATION OF LARGE LINEAR HETEROACENES AND THEIR DERIVATIVES

A Thesis
Presented to
The Academic Faculty

by

Anthony Lucas Appleton

In Partial Fulfillment
of the Requirements for the Degree
Doctor of Philosophy in the
School of Chemistry and Biochemistry

Georgia Institute of Technology
December 2010

SYNTHESIS AND CHARACTERIZATION OF LARGE LINEAR HETEROACENES AND THEIR DERIVATIVES

Approved by:

Dr. Uwe H.F. Bunz, Advisor
School of Chemistry and Biochemistry
Georgia Institute of Technology

Dr. Jean-Luc Brédas
School of Chemistry and Biochemistry
Georgia Institute of Technology

Dr. Laren Tolbert
School of Chemistry and Biochemistry
Georgia Institute of Technology

Dr. Seth R. Marder
School of Chemistry and Biochemistry
Georgia Institute of Technology

Dr. Bernard Kippelen
School of Electrical and Computer Engineering
Georgia Institute of Technology

Date Approved: November 8, 2010

To Cortney Leigh Donovan, the person who saved my soul.

ACKNOWLEDGEMENTS

There are many people whom have assisted me in the work throughout this Thesis, not only scientifically but also personally. If I have forgotten anyone, my sincerest apologies to you.

Beginning with the Bunz Group itself, I would like to offer thanks to Dr. Shaobin Miao, Dr. Scott M. Brombosz, Drew Zappas II, and Yexiang Zhang for their direct help on the work that went into our publications and my Thesis; also, I would like to offer special thanks to Evan Davey, Jonny Bryant, Chris Kub, Imani Jones, Stephen Hayden, Dr. Psarus McGrier, and Dr. AJ Zucchero for their support and wonderful discussions on science, life, economics, government, and general bullshit. Let us never forget the day when Bohemian Rhapsody came over the radio, and without acknowledgement to each other while in our hoods, took different parts of the chorus and blasted the worst karaoke rendition ever heard! A special note to Dr. Juan Tolosa and David Schweinfurth for helping to establish the best annual party ever, as well as being dear friends and fellow soccer fans. Dr. Ronnie Phillips will always hold a special place in my heart, as he was the one individual who taught me more than just science; it is no wonder I asked him to be a groomsman at my wedding.

Outside of the Bunz Group, I formed many professional and personal relationships. First, allow me to thank my fellow scientists: Dr. Brian Lawrence, you are the man for sticking with us during our first publication and never getting agitated at the long, odd hours we worked; Dr. Stephen Barlow, a wonderful person who has provided more help with more projects than any other person I could ever thank; Jose Baltazar and

Prof. Cliff Henderson for their continuing effort to fabricate a working device (a task I now have great respect and admiration for); Anthony Baldridge for being the most reliable member of GSF and never hesitating to help a fellow graduate student; Dr. Richard Mason for having the ability to hear me bitch and moan, all the while preparing a statement that would put my mind at ease and place the current situation in perspective; Dr. Kenneth Hardcastle for understanding the pressures of the Bunz group and always coming through in a pinch with crystallographic determinations, many times on very short notice, and always with a smile; and Dr. John S. Sears for running huge computational studies of our molecules and making the latest publications really special.

There are many people that assist in the operation of a group beyond the actual science. These folks are critical to Georgia Tech flourishing as a top-ranked research facility: Carmen Rivera, the most reliable administrative assistant we have ever had and also the most beautiful soul in the department; Marsha Lamb, who assisted in paperwork many times, even though she is not part of our group; the entire Accounting Office for their understanding and patience in dealing with matters related to finances in the Bunz Group; Jeff Curtiss for always making sure the lab was operating and getting us through some disasters of moving into in a new building; Kevin and Jason of VWR for never taking the term "back ordered" seriously and always finding a way to get what I needed for the next experiment.

I would like to especially thank my committee for not accepting me as a decent graduate student, but pushing me to become the best possible scientist even when it meant a trial by fire. Without these five people, I would not be the person I am today, nor would I have such a wonderful opportunity as a postdoctoral fellow at Stanford

University in the Bao Research Group. Prof. Laren Tolbert served as the best possible "step" Advisor anyone could ask for. Prof. Seth Marder for treating me like his own graduate student when it really mattered. I gained more from you in the shortest of time, thank you. Prof. Brédas and Prof. Bernard Kippelen for allowing me to sit at their table at the f-π-9 banquet. It was truly unforgettable and one of my fondest memories of graduate school. And to Prof. Uwe H.F. Bunz for always giving me enough rope to hang myself. I learned to make baskets quickly.

Before I arrived at GT, my career was launched by a single person: Dr. Tegan Eve. Dr. Eve offered me my first teaching position in chemistry, which proved more beneficial to my education than any classes could have ever taught me. This led to a summer job offer by Prof. Francisço Raymo in his lab under the guidance of Dr. Massimiliano Tamasulo. The skills I had aquired in a relatively short time coupled with my experiences there, led me to ultimately pursue a graduate career in chemistry. I am forever indebted to these wonderful people, and hope to be able to repay them someday. Its great to be a Miami Hurricane!

My father, Jeffrey Appleton, has always made sure I had everything I needed to succeed through the entirety of my academic career. Even in the face of hell, he never waivored and only became more vigilant. To my MIG, the first person to teach me how to cook, and so should be actually recognized as the person who got me involved in chemistry. At least her chemistry resulted in tasty meals and expanded the scope of my pallet beyond our borders; licking the spoon in her lab was permitted! To the rest of the Appleton clan for always being supportive, even at a distance. There truly is no family like ours!

Lastly, my fiancé, Cortney Leigh Donovan, has been my rock in more ways than anyone could describe in a lifetime. So, it must be recognized that her parents, Denny and Kitty, instilled in her qualities that every man dreams of in their soulmate. I do not view them as in-laws, but true family. And really, it is not about the science, but what you come home to at the end of the day.

TABLE OF CONTENTS

LIST OF TABLES

LIST OF FIGURES

LIST OF SCHEMES

LIST OF SYMBOLS AND ABBREVIATIONS

PV	photovoltaic
LED	light-emitting diode
TFT	thin-film transistor
OLED	organic light-emitting diode
OPV	organic photovoltaic
TIPS-pent	6,13-bis((triisopropylsilyl)ethynyl)pentacene
P3HT	poly-3-hexylthiophene
PVT	physical vapor transport
SAM	self-assembled monolayer
OTS	octadecyltrichlorosilane
Me	methyl
Et	ethyl
iso-Pr	*iso*-propyl
cm	centimeter
V	volt
s	second
μ_-	electron mobility
μ_+	hole mobility
p	para
o	ortho
TIPS	triisopropylsilyl
TES	triethylsilyl
TMS	trimethylsilyl

nm	nanometer
λ_{max}	wavelength maximum
DFT	Density Functional Theory
FMO	frontier molecular orbital
BTD	acenothiadiazoles
ADTP	bis(trialkylsilylethynyl)acenodithiophenes
THF	tetrahydrofuran
M	molar
eV	electron volt
mL	milliliter
g	gram
mmol	millimol
h	hour
mg	milligram
°C	degree Celsius
m.p.	melting point
v	volume
DMF	dimethylformamide
d	days
mol	mole
ϕ	quantum yield
ε	molar absorptivity
aq	aqueous
eq	equivalent
ns	nanosecond

τ	lifetime
Cpd	compound
DCM	dichloromethane
abs	absorption
TFA	trifluoroacetic acid
μ	micromolar
HOMO (H)	highest occupied molecular orbital
LUMO (L)	lowest unoccupied molecular orbital
Å	angstrom
min	minutes
TD-DFT	Time-Dependent Density Functional Theory
tol	toluene
MeCN	acetonitrile
μ	ground-state dipole moment
S	state
IP	ionization potential
EA	electron affinity
LAH	lithium aluminum hydride
CV	cyclic voltammetry
ND	not determined
NA	not available
EBE	exciton binding energy

SUMMARY

The work presented in this Thesis is primarily concerned with the synthesis and characterization of large, linear heteroacenes and their derivatives. We have been able to significantly expand on the types of materials available for application in organic electronic devices. In particular, the work focused on solution processible and novel derivatives of thiadiazoles, diazatetracenes, diazapentacenes, tetrazapentacences, and *N,N*-dihydrotetraazaheptacene. Extensive computational studies have been performed in order to better understand the optoelectronic properties of these materials. Although no devices have been fabricated that show appreciable hole or electron mobility values, the properties of these materials are very promising. Besides our work on organic electronic materials for application in optoelectronic devices, we have also been able to develop, via the Click reaction, a series of aqueous metal sensors for copper (II), nickel (II), and silver (I) based upon fluorescence quenching. The use of a modified Stern-Volmer equation was necessary to fit the data in order to obtain binding constants. The exploration of new materials and their properties in the area of organic electronics is an exciting field for the synthetic organic chemist, as the goals associated with this work strive to impact humanity in a positive manner by reducing energy costs.

CHAPTER 1

INTRODUCTION

1.1 Background

Organic electronics encompasses many facets of science: organic synthesis, analytical techniques, computational methods, chemical engineering, etc. So to be able to flourish in this blossoming area of science, one must become a type of Renaissance scientist or form multiple collaborations for a single, complete project. A goal of organic electronics is to produce cost effective, solution processible materials to be utilized in flexible device architectures for applications in photovoltaic (PV) cells, light-emitting diodes (LED), and thin-film transistors (TFT). This area of research is not purely academic, but seeks to impact humanity in almost every aspect of daily life. Interestingly, this can be seen today by going to a local electronics department store to find organic LEDs (OLED) for holiday lighting, high definition monitors, and even electric shaver screens. Even TFTs have made their way into mobile technology such as e-book readers. Although organic PVs (OPV) appear to lag behind in the market place, once the cost is reduced and the efficiency increased, it may then be possible for these types of devices to become ubiquitous. The picture is big, so do not get lost on your way through the organic electronic jungle.

Organic semiconductors utilized within these devices can be classified into three categories: hole-transporter, electron-transporter, or ambipolar (hole and electron) transporter. Much progress has been made in the area of small molecule hole-transporting materials, but small molecule electron-transporting materials are not as

prevalent, as shown in the following sections. Almost more important than the development of electron-transporting materials themselves is the development of electron-transporting materials which are environmentally stable and able to function under ambient conditions so as to avoid the electrons being trapped by oxygen. Although computational studies assist in the development of these materials, it is not until they are synthesized, purified, characterized, and applied as the semiconducting layer within a device that their efficiency and efficacy can be evaluated. It would be beneficial to have the ability to easily modify the transfer integral or degree of wavefunction overlap between adjacent molecules and/or surfaces within the device in order to enhance hole/electron mobility and thus overall efficiency.

Within this thesis is a focus on the synthetic strategy to produce novel, potential electron-transporting small molecules and understand their properties. Due to the functional handles in the materials presented herein, we have been able to utilize the same core materials for other applications as well. Although the efficiency of these materials utilized in organic electronic devices needs to be addressed and improved, the versatility of the reactions presented here is paramount to further expand the library of available small molecules for device applications. An historical overview of the development of these materials is quite instructive.

1.2 Acene Materials

Pentacene (**1.1**) is ubiquitous throughout the literature (3,548 papers as of August 2010 on Web of Science) and has been known since 1929 (Scheme 1.1).[1] Its high charge carrier mobility of 35 $cm^2V^{-1}s^{-1}$ (single crystal, room temperature)[2] and 6 $cm^2V^{-1}s^{-1}$ (thermally deposited)[3] has fueled its use as a hole-transporting material. However, it has

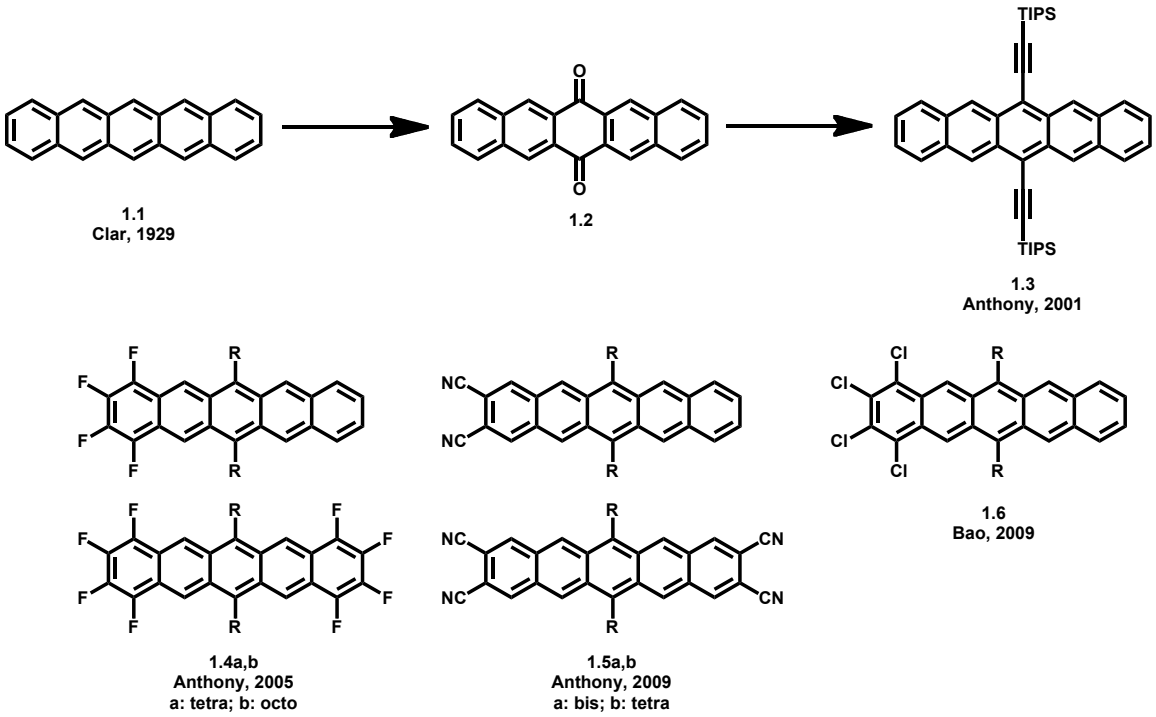

Scheme 1.1. Selected acenes. R is a substituted ethynyl group.

two points of concern: 1. Pentacene oxidizes to 6,13-pentacenequinone (**1.2**) in the presence of light under ambient conditions[4] and 2. It has very low solubility and therefore must be thermally deposited onto substrates. John Anthony and his group have addressed both of these concerns in a single reaction: the transformation of **1.2** into 6,13-bis((triisopropylsilyl)ethynyl)pentacene (TIPS-pent, **1.3**).[5] This now solution processible derivative has been utilized as a hole-transporting material (0.4 $cm^2V^{-1}s^{-1}$, solution processed).[5] Electron mobility values have not been reported using this material. However, the Anthony group,[6] as well as the Bao group,[7] have made progress towards electron-transporting analogues of TIPS-pent by appending electron withdrawing groups (F: **1.4**, CN: **1.5**, Cl: **1.6**) around the periphery of the acene core to varying degrees of substitution. These materials (**1.4**/**1.6**) have been observed to behave as ambipolar transporters in TFTs (μ_+ = 0.07-0.11 $cm^2V^{-1}s^{-1}$; μ_- = 0.06-0.41 $cm^2V^{-1}s^{-1}$),[8] and **1.5** and

derivatives thereof have been utilized as the electron-transporting layer in OPVs with power conversion efficiencies of 0.10 in a 1:1 blend with poly-3-hexylthiophene (P3HT).[9]

1.3 Heteroacene Materials

We, on the other hand, wanted to focus on substitution within the core of acenes utilizing nitrogen to replace two to four carbon atoms. Our goal was to generate air-stable, solution processible, electron-transporting analogues that could operate under ambient conditions. Interestingly, the chemistry of these types of materials predates that of pentacene by almost forty years, but their application in organic electronic devices has been modest at best and as hole-transporting semi-conductor materials.

In 1890, Fischer and Hepp began the work that still influences the chemistry of heteroacenes today.[10] They began with the synthesis of **1.7**, shortly followed by the synthesis of homofluoroindine **1.13**. Ten years later, Hinsberg[11] synthesized **1.9** and investigated the oxidation of **1.7** and **1.9**. Hinsberg was able to oxidize **1.9** into **1.10** using Jones conditions, but was unable to obtain the oxidation product of **1.7**. Then in 1967, Kummer and Zimmermann[12] obtained the oxidation product **1.8** by using *p*-chloranil as the oxidizing agent. Preceeding the work of Kummer and Zimmermann by less than a year was Leete et al.'s[13] work on the diazapentacene derivative **1.12**, which was obtained by using copper acetate to oxidize the dihydro precursor **1.11**. Fischer's homofluoroindine **1.13** has been the subject of debate as to whether the correct structure is that shown (Scheme 1.2) or takes on a quinoidal form. This was resolved by Armand et al.[14] and Dunsch et al.[15] utilizing NMR spectroscopy; from the date first synthesized

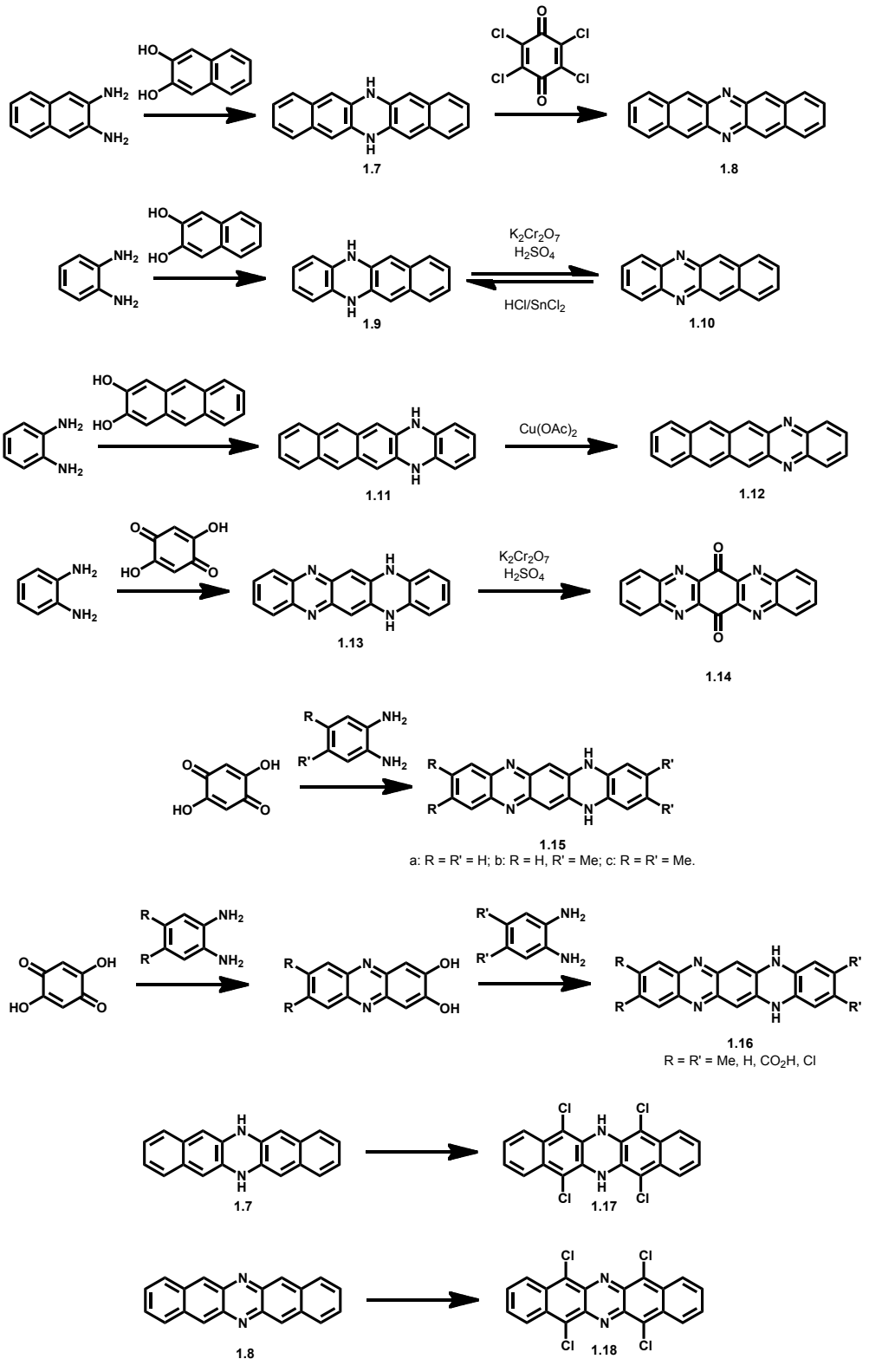

Scheme 1.2. Selected historical heteroacenes.

in Fischer's lab to the date of structural confirmation was 101 years! The oxidation of **1.13** into **1.14** was shown to proceed using Jones conditions by Petit and Badger in 1951;[16] this oxidation product was later utilized by our group[17] for the development of the first solution processible tetraazapentacene derivative, which was highlighted in Synfacts by T. Swager.[18] Building upon the work of the early 20th century, Zhu et al.[19] in 2005 synthesized **1.15**, peripherally methylated derivatives of **1.13**. A year later, Siri et al.[20] expanded on this work by synthesizing differently substituted homofluoroindine derivatives **1.16**, which now incorporate not only methyl groups, but also carboxylic acid groups and chlorine atoms at select positions around the periphery. In 2009, Weng et al.[21] were able to synthesize differently halogenated diazapentacene derivatives from **1.7** and **1.8** to produce **1.17** and **1.18**, respectively.

Ma et al.'s[19] work on derivatives of **1.16** thermally deposited directly on top of SiO_2 functioned as a hole-transporting material with a mobility value of 2×10^{-2} $cm^2V^{-1}s^{-1}$ with an on/off ratio on the order of 10^5. However, Nuckolls et al.[22] using **1.7** and **1.11** thermally deposited on TFTs achieved hole mobility values of 5×10^{-5} and 3-6 $\times 10^{-3}$ $cm^2V^{-1}s^{-1}$, respectively; their device architecture and method of fabrication is essentially the same as that of Ma et al.[19] Although the mobility values of these two materials are low, their on/off ratios were on the order of 10^3. Six years later in 2009, Miao et al.[23] found that three polymorphs of **1.7** exist in the solid state, one of which was found to display a good hole mobility value of 0.45 $cm^2V^{-1}s^{-1}$ by a thermally vacuum deposited TFT. This highlights that the same material can behave differently depending on device fabrication procedures. Nuckolls et al.[22] recrystallized their materials directly from the reaction mixture, whereas Miao et al.[23] performed physical vapor transport (PVT) to

purify the same material. Even by PVT, **1.7** was only 99% pure with 1% of **1.8** (its oxidized form) present. Also, Nuckolls et al.[22] did not use any self-assembled monolayer (SAM) on top of their SiO_2 dielectric, whereas Miao et al.[23] found the highest mobility values of the same material to be achieved on top of a SAM of octadecyltrichlorosilane (OTS) treated SiO_2, otherwise their device architectures were nearly identical. The work of Weng et al.[21] using **1.17** and **1.18** also led to the fabrication of TFTs with hole mobility values of 1.4 and 0.13 $cm^2V^{-1}s^{-1}$, respectively. Interestingly, these materials only showed a field-effect mobility when deposited by thermal evaporation on top of a pentacene buffer layer prepared on a rubbed monolayer of *n*-nonyltrichlorosilane on an Si/SiO_2 surface. However, no electron mobility has been reported for the heteroacene materials presented thus far and none of these devices were fabricated with solution processing of the semiconductor material.

In order to achieve solution processible derivatives of phenazine, **1.9**/**1.10**, **1.11**/**1.12**, and **1.13**/**1.14** we took a page from the J.E. Anthony playbook: bis((triisopropylsilyl)ethynyl) substitution.[6] In order to prepare derivatives of phenazine and **1.9**-**1.12**, this required the development of three key starting materials: **1.19**, **1.20**, and **1.21** (Scheme 1.3).[24] These materials can then be transformed into their *o*-diamine forms (**1.22**-**1.24**, respectively) via reduction, which then allows for the condensation of an appropriately substituted *o*-dione to achieve the diazaacene derivative of interest (**1.25**-**1.27**, respectively).[25,26] Interestingly, the versatility of **1.19** and **1.20** is shown by their utilization as water-soluble metal sensors via a deprotection reaction followed by Click chemistry to furnish bistriazoles (**1.30**-**1.31**) that display binding toward select

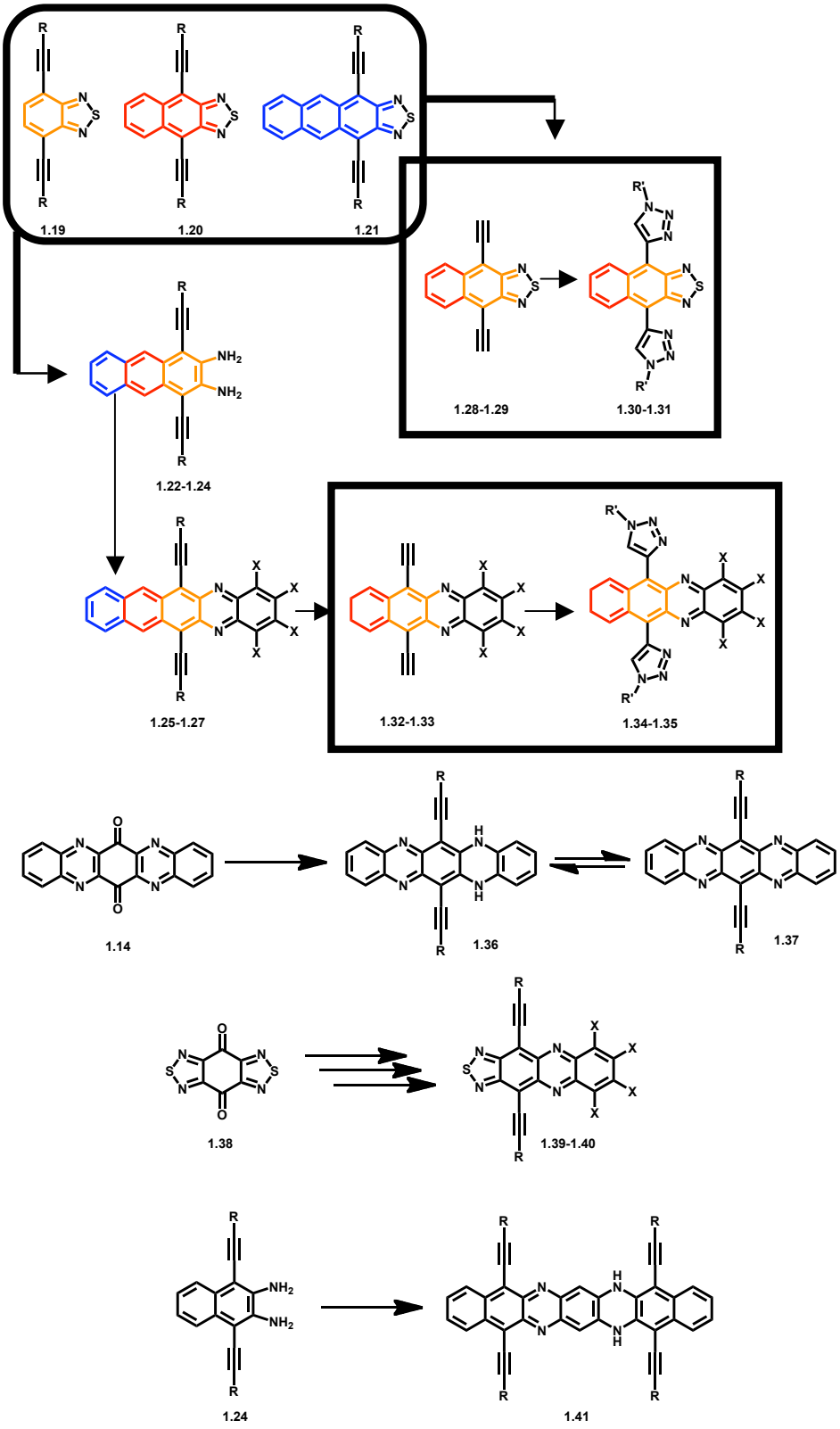

Scheme 1.3. Synthetic roadmap to solution processible *N*-heteroacene derivatives, as well as the metal sensing bistriazoles. R = TIPS, TES, or TMS; R' = oligoethylene glycol; X = H, Cl, or Br.

metal cations.[27] Recently, we have expanded our metal sensing library to now include phenazine and diazatretracene derivatives (**1.34**-**1.35**).[28] To transform **1.13**/**1.14** into solution processible derivatives, we utilized Petit and Badger's oxidized product **1.14**[16] to generate **1.36**/**1.37**.[17] In an effort to lower the electron affinity and ionization potential to a level stabilized enough to create an air-stable electron-transporting small molecule, we functionalized our thiadiazole derivatives with a pyrazine moiety and/or peripheral halogen substitution to produce **1.39**-**1.40**. An exercise in the limits of stability and synthetic methodology, we have produced the first *N,N*-dihydrotetrazaheptacene derivative **1.41**. Although our group has made significant progress in the development of novel, solution processible materials for application in organic electronic devices, we have been unable to make any meaningful progress in the area of device fabrication.

Section 1.4 Estimating the Exciton Binding Energy

The exciton binding energy (EBE), the energy required to separate an exciton into a hole and electron, i.e., for the excited state of a molecule, typically in a solid film, to dissociate to give a free radical cation and radical anion, can be estimated from experimental data. The process of separating the hole and electron is represented by the following equation:

$$A^* + A \rightarrow A^+ + A^- \qquad (1)$$

where A* represents the lowest excited singlet state of A, and A^+ and A– represent radical anions and cations sufficiently distant from one another in the solid that the Coulombic attraction between them is negligible. The free-energy change for this reaction (ΔG_{rxn}) is defined as the EBE. Considering only orbital energies of the neutral

molecule, as shown in Figure 1.1, one would anticipate zero EBE. However, this overlooks the fact that the hole and electron in the excited state (exciton, left side of figure 1.1) experience considerable mutual electrostatic attraction absent in the radical cation and anion, substantially stabilizing the exciton with respect to a pair of radical ions. How does one estimate the EBE using the above equation and experimental data? Figure 1.1 shows schematically the processes for which we can measure the free-energy changes and thereby estimate the EBE.

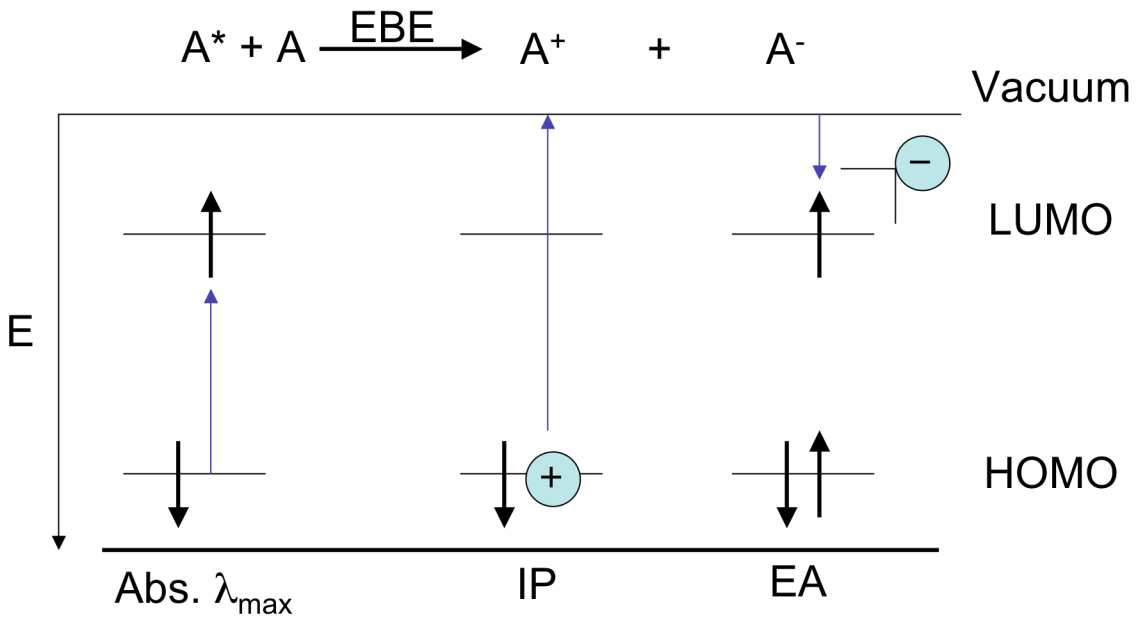

Figure 1.1. Pictorial representation of the formation of A* (exciton) and the separation of the exciton into a hole (A^+) and an electron (A^-) in terms of experimentally observable phenomena. The blue lines indicate the process being observed.

On the reactant side of the equation 1, there are two molecules of A before anything happens. Then one molecule of A absorbs a photon of light that is capable of exciting A from its ground-state (S_0) to its lowest excited-state (S_1), which in many cases can be well-approximated as a promotion of an electron from the HOMO to the LUMO. This

process is energetically represented by the long wavelength λ_{max} from the absorbance profile. The energy of the excited state estimated by this method is sometimes known as the Optical Gap. To convert this value, usually obtained in nm, to a more easily comparable value for the other two processes shown in Figure 1.1, we must convert nm to eV. This is accomplished using the following conversion:

$$E = h\nu = \frac{hc}{\lambda} \tag{2}$$

where E is energy (we want this to be in eV), *h* is Planck's constant (6.6 x 10^{-34} Js, 4.14 x 10^{-15} eVs), ν is the frequency (ν = 1/T in Hz), and c is the speed of light (3.0 x 10^{8} m/s). Solving for λ (where E = 1.6 x 10^{-19} J = 1 eV), we arrive at a value of 1239.85 nm (in most cases, this is utilized as 1240 nm). This means that wavelength in nm and energy in eV can be interconverted according to:

$$E(eV) = \frac{1240(nm \bullet eV)}{\lambda(nm)} \tag{3}$$

Now, any value obtained from the absorbance profile for the long wavelength absorption can easily be converted to the unit of eV. This is important, as the next set of measurements obtained by cyclic voltammetry experiments is typically measured in V.

Figure 1.1 shows that the energy required to remove an electron from A to infinity (meanig beyond the Coulombic influence of the hole, i.e., the vacuum level), leaving a hole on an A molecule is the ionization potential (IP), while the energy released on bringing an electron from infinity to A is the electron affinity (EA). The IP and EA in solid films can be directly measured using UV-photoelectron spectroscopy and inverse photoelectron spectroscopy. However, they are commonly estimated from solution

electrochemical measurements according to IP = $eE_{1/2}^{+/0}$ + c and EA = $eE_{1/2}^{0/-}$ + c where $E_{1/2}^{+/0}$ and $E_{1/2}^{0/-}$ are half-wave potentials corresponding to molecular oxidation and reduction, respectively, e is the electronic charge, and c is a constant offset (often assumed to be 4.8 eV when the potentials are quoted vs. ferrocenium/ferrocene). However, as discussed below, this approach assumes comparable stabilization energies for the hole and electron in solution and in the solid state. The difference between $E_{1/2}^{+/0}$ and $E_{1/2}^{0/-}$ is known as the electrochemical gap, whereas the difference between EA and IP (either directly measured or estimated from electrochemical data) is known as the Transport Gap.

Now we have all of the pieces in order to estimate the EBE from the difference between the Optical Gap (OG) and the Transport Gap (TG) using the following equation:

$$EBE = TG - OG \qquad (4)$$

where numerical values are usually in eV, or both TG and OG are in the same units. Now we have an estimate for the exciton binding energy of molecule A.

An interesting question is why in equation 4 is TG – OG? The TG is expected be larger that the OG due to Coulombic effects stabilizing the exciton relative to the pair of ions. When measuring the OG, the exciton is stabilized because the electron and the hole are still coulombically bound together (A*) on the same molecule. In contrast, IP and EA related to the energy required to remove an electron or released upon addition of an electron, respectively. The hole or electron injected into A to generate either A^+ or A^- is not stabilized relative to A* (hole in the HOMO and electron in the LUMO) because there is only a hole (HOMO) or electron (LUMO) being added to the system at a time. This should result in a larger Transport Gap than Optical Gap.

A caveat to estimation of the EBE using electrochemical estimates of the transport gap is that all measurements have been taken in solution, but the actual process we are describing takes place in the solid-state. This presents error in the actual EBE observed in the solid-state process versus an estimation from solution data. The EBE calculated using equation 4 generally results in a lower estimated value when electrochemical data are used in place of UPS/IPES data. This is because there are more stabilizing forces in solution than there are in the solid-state. Polar solvent molecules can reorient in solution to stabilize A*, A^+, and A^-. Also, cyclic voltammetry experiments are carried out in a polar solvent with a conducting electrolyte solution. This is in stark contrast to the solid-state process where molecules cannot move like the solvent or electrolyte molecules, and will only be able to provide stabilization to A*, A^+, and A^- by polarization effects. So, the exciton binding energy estimated from solution phase data should be assumed to be a lower limit of the EBE expected in the solid-state.

1.5 Conclusion

This is an exciting time to be a scientist in the area of organic electronics. As demonstrated with the historical perspective, there are materials that predate the development of the field of organic electronics by almost a century. However, as elucidated in the last paragraph, synthesizing these types of materials is half the battle. In order to fully comprehend the utility of these materials they must be fabricated into a functioning device. The Renaissance or collaborative scientist will benefit from being able to pull together the three key areas (organic synthesis, computational studies, and chemical engineering) in a synergistic manner in order to make the next great impact on

the scientific community and humanity at large: the production of cost effective and efficient organic electronic components for application in TFT, LED, and PV devices that can be scaled-up to include manufacturing.

1.6 References

[1] E. Clar. *Chem. Ber.* **1929**, *62*, 30.

[2] O.D. Jurchescu, J. Baas, T.T.M. Palstra. *Appl. Phys. Lett.* **2004**, *84*, 3061.

[3] H. Klauk, M. Halik, U. Zschieschang, G. Scmid, W. Radlick, W. Weber. *J. Appl. Phys*. **2002**, *92*, 5259.

[4] [a] I. Lewis, L. Singer. *J. Phys. Chem.* **1981**, *85*, 354; [b] J. Birks, J. Appleyard, R. Pope. *Photochem. Photobiol.* **1963**, *2*, 493; [c] M. Yamada, I. Ikemoto, H. Kuroda. *Bull. Chem. Soc. Jpn.* **1988**, *61*, 1057; [d] E. Clar. Polycyclic Aromatic Hydrocarbons; Academic Press: London, **1964**, Vol. 1.

[5] C.D. Sheraw, T.N. Jackson, D.L. Eaton, J.E. Anthony. *Advanced Materials.* **2003**, *15*, 2009.

[6] C.R. Swartz, S.R. Parkin, J.E. Bullock, J.E. Anthony, A.C. Mayer, G.G. Malliaras. *Org. Lett.* **2005**, *7*, 2005.

[7] M.L. Tang, J.H. Oh, A.D. Reichardt, Z. Bao. *J. Am. Chem. Soc.* **2009**, *131*, 3733.

[8] M.L. Tang, A.D. Reichardt, P. Wei, Z. Bao. *J. Am. Chem. Soc.* **2009**, *131*, 5264.

[9] Y-F. Lim, Y. Shu, S.R. Parkin, J.E. Anthony, G.G. Malliaras. *J. Mater. Chem.* **2009**, *19*, 3049.

[10] [a] O. Fischer, E. Hepp. *Chem. Ber.* **1890**, *23*, 2789; [b] O. Fischer, E. Hepp. *Chem Ber.* **1895**, *28*, 293.

[11] O. Hinsberg. *Liebigs Ann. Chem.* **1901**, *319*, 257.

[12] F. Kummer, H. Zimmermann. *Ber. Bunsenges.* **1967**, *71*, 1119.

[13] E. Leete, O. Ekechukwu, P. Delvigs. *J. Org. Chem.* **1966**, *31*, 3734.

[14] J. Armand, L. Boulares, C. Bellec, J. Pinson. *Can. J. Chem.* **1987**, *65*, 1619.

[15] L. Sawtschenko, K. Jobst, A. Neudeck, L. Dunsch. *Electrochim. Acta.* **1996**, *41*, 123.

[16] G.M. Badger, R. Petit. *J. Chem. Soc.* **1951**, 3211.

[17] S. Miao, A.L. Appleton, N.J. Berger, S. Barlow, S.R. Marder, K.I. Hardcastle, U.H.F. Bunz. *Chem. Eur. J.* **2009**, *15*, 4990.

[18] T.M. Swager, T.L. Andrew. *Synfacts.* **2009**, *8*, 0857.

[19] Y. Ma, Y. Sun, Y. Liu, J. Gao, S. Chen, X. Sun, W. Qiu, G. Yu, G. Cui, W. Hu, D. Zhu. *J. Mater. Chem.* **2005**, *15*, 4894.

[20] C. Seillan, H. Brisset, O. Siri. *Org. Lett.* **2008**, *10*, 4013.

[21] S.Z. Weng, P. Shukla, M.Y. Kuo, Y.C. Chang, H.S. Sheu, I. Chao, Y.T. Tao. *ACS Appl. Mat. & Interfaces.* **2009**, *1*, 2071.

[22] Q. Miao, T.Q. Nguyen, T. Someva, G.B. Blanchet, C. Nuckolls. *J. Am. Chem. Soc.* **2003**, *125*, 10284.

[23] Q. Tang, D. Zhang, S. Wang, N. Ke, J. Xu, J.C. Yu, Q. Miao. *Chem. Mater.* **2009**, *21*, 1400.

[24] A.L. Appleton, S. Miao, S.M. Brombosz, N.J. Berger, S. Barlow, S.R. Marder, K.I. Hardcastle, U.H.F. Bunz. *Org. Lett.* **2009**, *11*, 5222.

[25] S. Miao, S.M. Brombosz, P.v.R. Schleyer, J.I Wu, S. Barlow, S.R. Marder, K.I. Hardcastle, U.H.F. Bunz. *J. Am. Chem. Soc.* **2008**, *130*, 7339.

[26] A.L. Appleton, S.M. Brombosz, S. Barlow, J.S. Sears, J-L. Brédas, S.R. Marder, U.H.F. Bunz. *Nature Communications.* **2010**, 1:90.

[27] S.M. Brombosz, A.L. Appleton, A.J. Zappas, U.H.F. Bunz. *Chem. Comm.* **2010**, *46*, 1419.

[28] Y. Zhang, A.L. Appleton, S.M. Brombosz, A.J. Zappas, X. Qian, U.H.F. Bunz. *Chem. Comm*. **Submitted**.

CHAPTER 2

ALKYNYLATED ACENO[2,1,3]THIADIAZOLES

2.1 Introduction

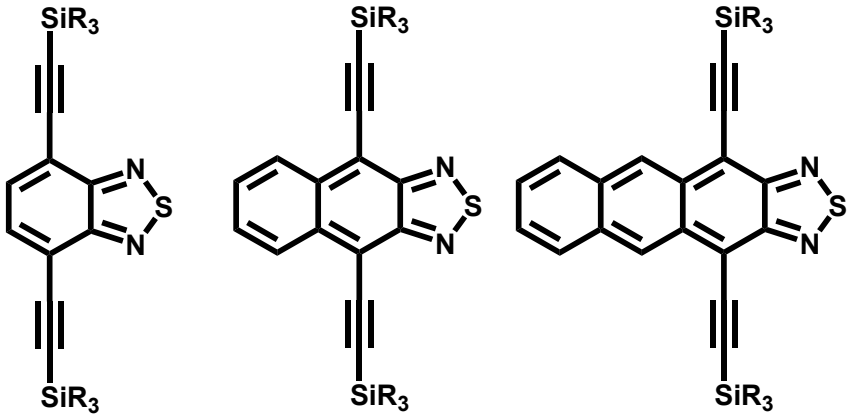

Scheme 2.1. Structures of compounds **2.1**-**2.3**, **a**: R = Me, **b**: R = Et, **c**: R = *iso*-Pr.

In order to gain access to organosoluble *N*-heteroacene derivatives, a series of acenothiadiazoles needed to be synthesized first. The utility of these compounds can clearly be seen throughout this work, underscoring their synthetic versatility. Also, they are a good example of the chemical and physical tunability of organic materials at an early stage of development via their R-groups and size-dependent optical properties.

Organic electronics[1] utilizes organic synthesis, combined with processing technology, thin-film and surface science, and electrical engineering to ideally deliver low cost, effective, and easily processible, flexible devices. While advances have been

made in the development of materials for organic electronics there is still a need for stable, solution processible organic materials with high charge-carrier mobilities, especially for electron transport. A possible reason for the lack of electron-transporting small molecules may be the unavailability of suitable starting materials, which we hope to expand on with the synthesis of alkynylated acenothiadiazoles.

For organic electronic devices, such as organic light-emitting diodes, thin-film transistors or photovoltaic cells, the materials must have and be able to be processed to have the correct molecular and solid-state properties to be effective.[2,3,4] The larger acenes have had and continue to have a significant impact in organic electronics with the hole-transporting pentacenes and rubrene (tetraphenyltetracene) being most popular. Anthony et al. have exploited alkynylated pentacene and thiophene-fused pentacene derivatives as easily solution processible organic electronic building blocks and demonstrated their utility.[5]

2.2 Results and Discussion

Here, we introduce thiadiazole-based heterocyclic[6] materials[7-10] with size-dependent optical properties and with promising electrochemical and solid-state packing properties as potential materials in which electrons can hopefully be easily injected. The synthesis of **2.1a-c** (Scheme 2.2) is achieved by Sonogashira alkynylation of **2.4** in 33-47% yield,[11] while **2.2a-c** are obtained from **2.5** in yields ranging from 11-87% in a procedure adapted from reference 12. As derivatives of **2.3** are unknown, we started from **2.6**, which was synthesized according to a modification of the procedures of reference 13. Reaction of **2.6** with potassium phthalimide **2.7**, followed by treatment with hydrazine, afforded the diaminoquinone **2.8** in 31% yield. Dissolution of **2.8** in

refluxing thionyl chloride forms the thiadiazole ring to give **2.9** in 78% yield, which is then combined with suitable alkynyllithiums. After hydrolysis, the corresponding diols are directly reduced by sodium hypophosphite and potassium iodide in hot acetic acid to afford **2.3a-c** in 9-92% yield after column chromatography over silica gel as blue-black crystalline materials, displaying a metallic luster.

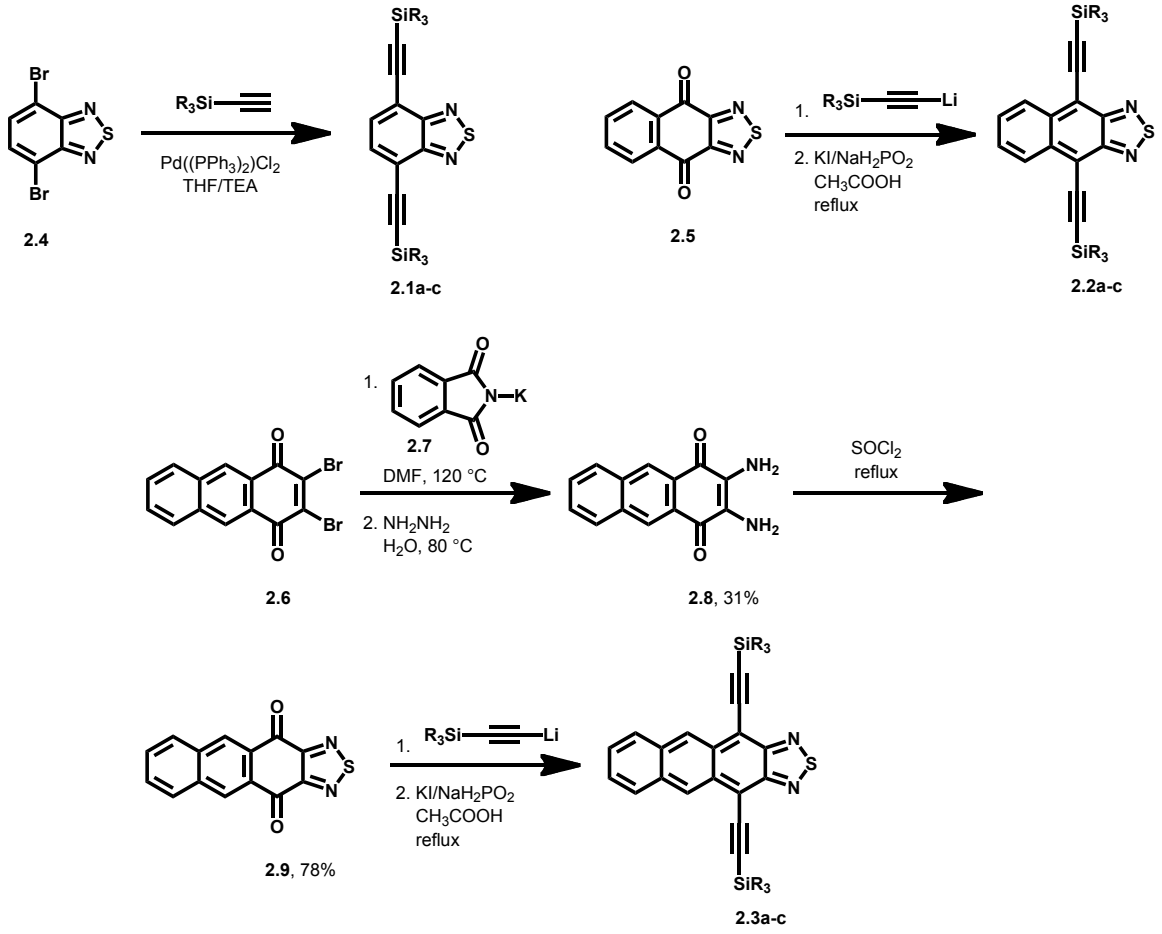

Scheme 2.2. Synthesis of compounds **2.1-2.3a-c**.

The UV-vis absorption and emission spectra (Figure 2.1) of **1b-3b** in hexanes solution provide insight into the electronic structure of the molecules. **2.1b** has a broad,

featureless absorption with a maximum at 382 nm and a comparably broad emission peaking at 439 nm. In the case of **2.2b** an absorption spectrum with significant vibronic structure (λ_{max} = 530 nm) and an emission peaking at 536 nm is observed.[14] In the case of **2.3b**, the absorption is also structured with the λ_{max} = 654 nm, while the emission is centered at 659 nm and is strongly 0-0 peaked. As expected, the Stokes shifts for **2.2** and **2.3** are small due to the rigidity of the molecules; however, the small spectral bandwidths and the occurrence of vibronic structure in the emission spectra are unusual when compared to the spectra of diethynylacenes of analogous structure. The Density Functional Theory (DFT) method was applied to **2.1a**-**2.3a** using the B3LYP functional with the 6-31G**//6-31G** basis set (Prof. Bunz). We have shown via the development of the frontier molecular orbital (FMO) positions that the highest occupied molecular orbital (HOMO) becomes destabilized and the lowest unoccupied molecular orbital (LUMO) becomes stabilized upon increasing the size of the acenothiadiazole core.

Table 2.1. Comparison of calculated and measured HOMO, LUMO, and H-L gap. [a] Obtained by SPARTAN 08/Windows using the B3LYP functional with the 6-31G**//6-31G** basis set (Prof. Bunz). [b] Gap obtained from the λ_{max} of absorption (10^7/nm = cm^{-1}).

Compound	HOMO[a] (eV)	LUMO[a] (eV)	H-L Gap[a] (cm^{-1})	Optical Gap[b] (cm^{-1})
2.1a	-5.90	-2.67	2.60×10^4	2.62×10^4
2.2a	-5.38	-2.98	1.93×10^4	1.88×10^4
2.3a	-5.03	-3.16	1.51×10^4	1.53×10^4

Figure 2.2 shows the dependence of the absorption maxima, λ_{max}, of **2.1-2.3** on the number of rings in comparison to the dependencies seen for Anthony's

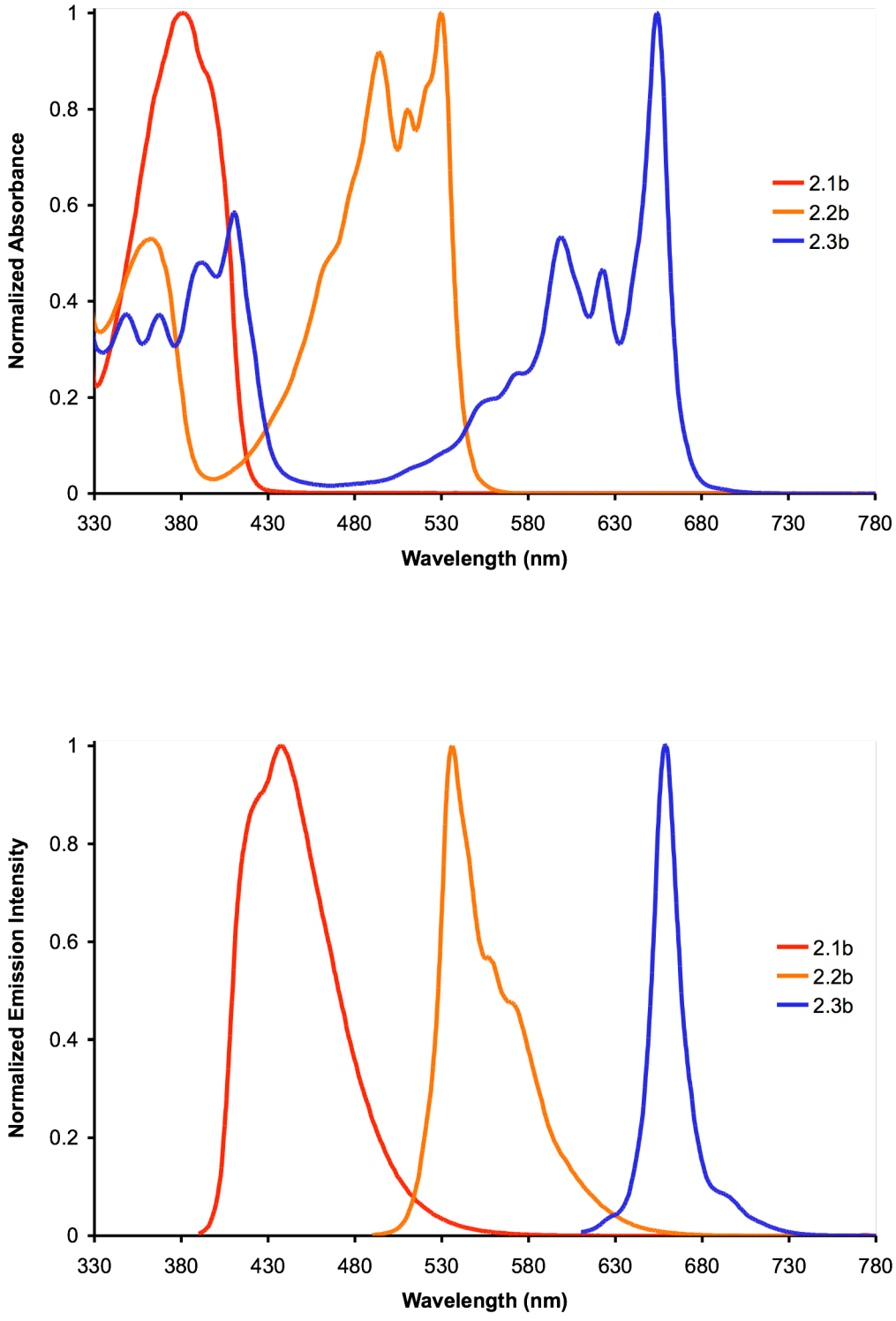

Figure 2.1. Normalized absorption (top) and emission (bottom) spectra of **2.1**-**2.3b**.

dialkynylacenes[5,7] and dialkynylanthradithiophenes.[14] Naphthothiadiazole **2.2**, which contains a total of three rings, displays similar optical properties to the four-ring tetracene and the five-ring anthradithiophenes, while **2.3** has a similar absorption maximum as TIPS-pent and the six-ring acenodithiophenes. A similar observation has been made by Wudl et al in the case of the isoquinolones.[15]

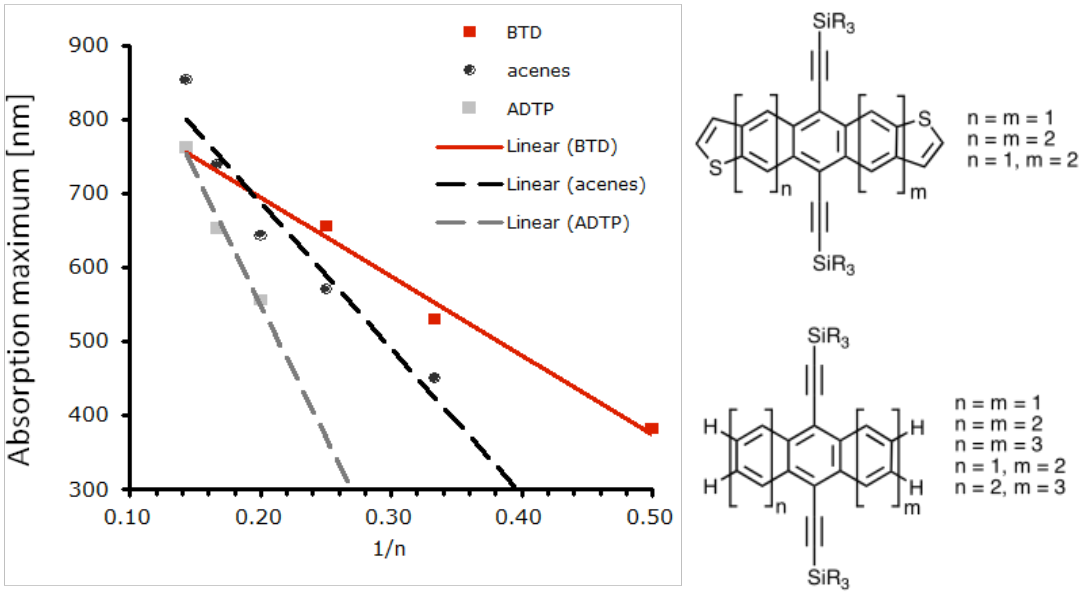

Figure 2.2. Plot of the absorption maxima versus 1/n, with n being the number of rings in a specific class of compounds. BTD: acenothiadiazoles **2.1**-**2.3**. Acenes: 9,10-bis(trimethylsilylethynyl)anthracene, bis(trialkylsilylethynyl)tetracene, bis(trialkyl-silylethynyl)pentacene, bis(trialkylsilylethynyl)hexacene, and bis(trialkyl-silylethynyl)heptacene.[5,7] ADTP: bis(trialkylsilylethynyl) acenodithiophenes.[13] (Prof. Bunz).

The ease of oxidation and reduction of compound **2.3** was investigated using cyclic voltammtery of **2.3c** in deoxygenated THF / 0.1 M $^{n}Bu_4NPF_6$ solution and ferrocene was used as an internal reference. One reversible oxidation at +0.74 V and two reversible reductions at -1.18 and -1.78 V were observed. The transport gap (the

difference between the first reduction (EA) and first oxidation (IP) potential) of 1.92 V correlates well with the H-L gap obtained by the DFT method (1.87 eV) and the optical gap of 1.90 eV. The exciton binding energy for **2.3** is ~0.02 eV (the difference between the optical and transport gaps). The reduction potential of **2.3c** is similar to that for a four-ring dialkynyldiazatetracene (-1.2 V)[12] and close to those for perylene diimides (circa -1.0 V), which are a well-established class of materials for electron transport within field-effect transistors,[16] indicating the possibility of facile electron injection.

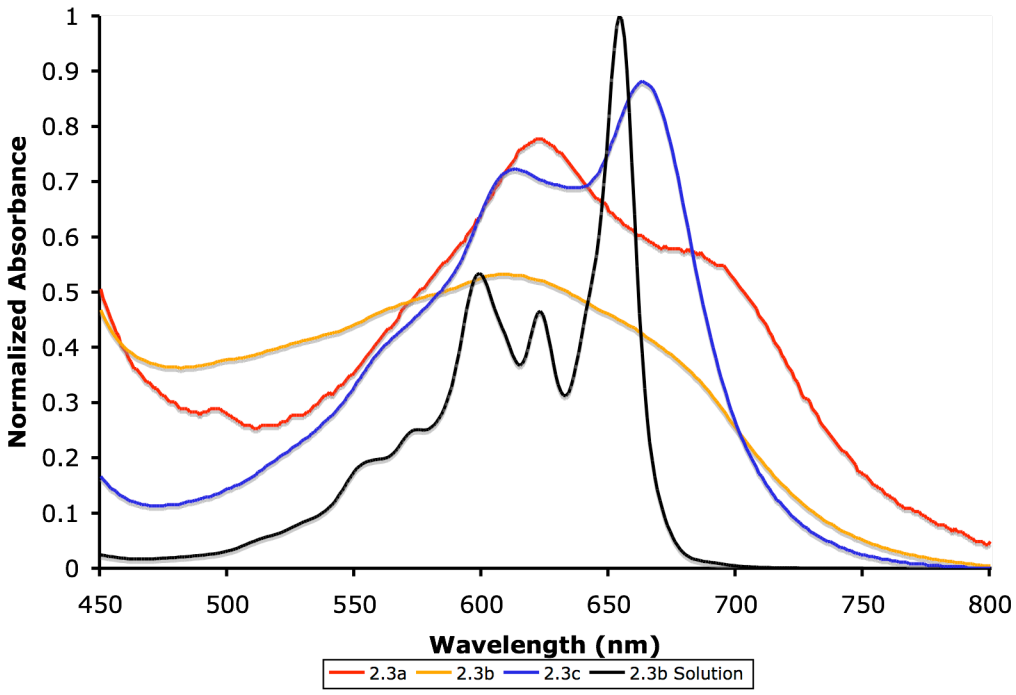

Figure 2.3. Thin-film UV-vis absorption spectra of **2.3a-c**; and **2.3b** in hexane solution for comparison.

The thin-film UV-vis absorption spectra of **2.3a-c** (Figure 2.3) are bathochromically shifted from that of **2.3b** (shown for reference) in hexane solution. In the case of **2.3c**, well-resolved features result, while the spectra of **2.3a** and **2.3b** are more

red-shifted and significantly broadened. **2.3a** and **2.3b** form microcrystalline films and **2.3c** forms amorphous transparent films; scattering effects lead to a somewhat featureless UV-vis spectrum for **2.3b**. However, the λ_{max} of **2.3a** is shifted to 685 nm in the solid state, while that of amorphous **2.3c** is recorded at 664 nm, only 10 nm shifted from its solution value. However, the spectrum is also broadened and the onset of absorption in the solid state for **2.3a-b** is greater than 750 nm. This suggests interaction of the π-systems of **2.3a-b** in the solid state.[17]

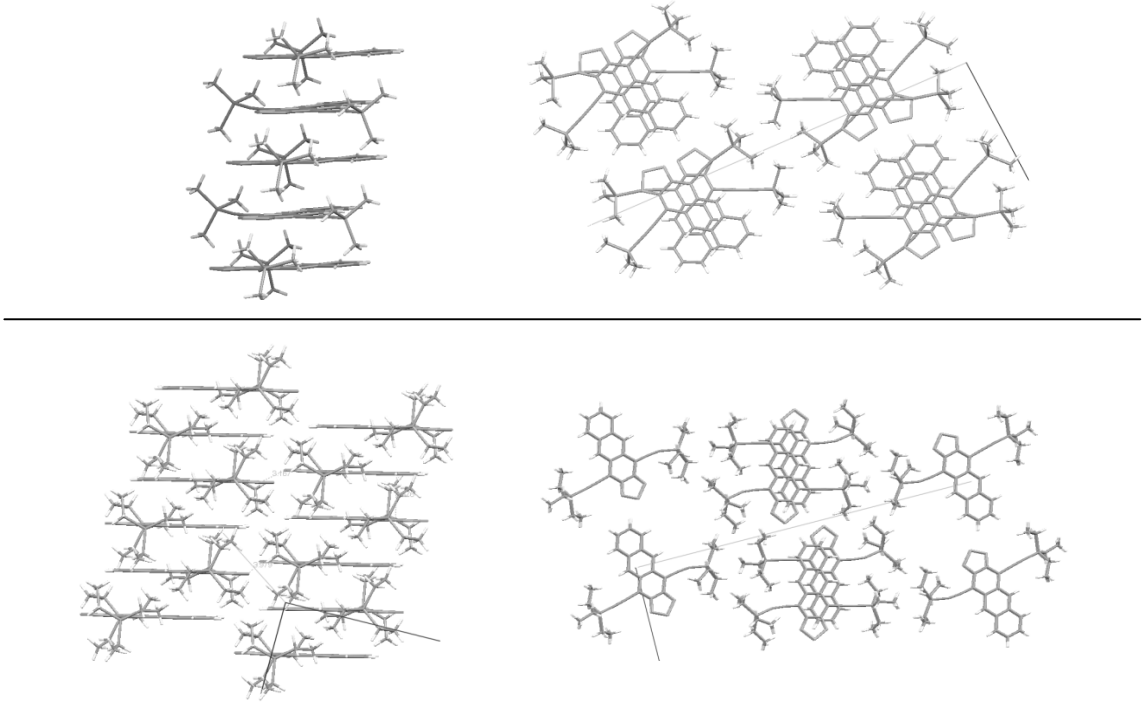

Figure 2.4. X-ray crystal structures of compounds **2.3a** (top) and **2.3b** (bottom). The left column corresponds to the vertical axis, not associated with any crystallographic axis; the right column for **2.3a** is the *c*-axis and for **2.3b** is the *a*-axis.

Single crystal X-ray analyses of **2.3a-c** reveal that the intrastack intermolecular distance is the same for each single crystal structure at approximately 3.4 Å (Figure 2.4). In the case of **2.3a** the π-systems of adjacent columns are isolated, while in **2.3b** adjacent

columns interact via sulfur-nitrogen interactions. Noticeable is the absence of π-π interactions between different columns, a hallmark of the diethynylacenes[14] and diethynylheteroacenes,[12] only allowing for two-dimensional particle (hole/electron) mobility. The π-stacking interactions seen in the crystal structures of **2.3a** and **2.3b** are presumably responsible for the observation of the larger spectral shifts to lower energy and broadening as compared to amorphous **2.3c**. The crystal packing shows good physical overlap of adjacent molecules, however attempts to fabricate devices from these materials failed.

2.3 Conclusion

In conclusion, we have prepared a series of acenothiadiazoles with differently functionalized R-groups (TMS, TES, TIPS), of which the three largest members **2.3a-c** were completely unknown. In relation to their size, **2.1-2.3** display lower energy optical transitions. They are also observed to have facile and reversible reduction potentials, a result likely to originate from their lower LUMO energies than the corresponding acene analogues. Derivatives of **2.3** also displayed solid-state optical properties that appear dependent upon the R-group. This is a good example of optoelectronic tenability via development of the core structure, as well as using of different solubilizing groups that impact the solid-state properties.

This work has been published in *Organic Letters*:

Anthony Lucas Appleton, Shaobin Miao, Scott M. Brombosz, Nancy J. Berger, Stephen Barlow, Seth R. Marder, Kenneth I. Hardcastle, Uwe H.F. Bunz. *Organic Letters*, **2009**, *11*, 5222.

2.4 Experimental Information

General Data. Reagent grade solvents were dried by standard procedures and were freshly distilled prior to use. Infrared spectra were recorded on a SHIMADZU FTIR-8400S spectrophotometer. ^{1}H-NMR spectra were recorded on a Varian Inova 300 spectrometer operating at 300 MHz. ^{13}C-NMR spectra were recorded on a Bruker 500 spectrometer operating at 125 MHz and were proton decoupled. Mass spectra were recorded on a VG70DE mass spectrometer using electron impact ionization. Electrochemical measurements were carried out under nitrogen on dry, deoxygenated solvent solutions ca. 10^{-4} M in analyte and 0.1 M in tetra-*n*-butylammonium hexafluorophosphate using a BAS Potentiostat, a glassy carbon working electrode, a platinum auxillary electrode, and, as a pseudo-reference electrode, a silver wire anodized in 1 M aqueous potassium chloride. Potentials were referenced to ferrocenium / ferrocene by addition of ferrocene to the sample cell. Cyclic voltammograms were recorded at a scan rate of 50 mVs^{-1}. Unless otherwise noted, this applies to all subsequent chapters.

2.4.1 4,7-bis((trimethylsilyl)ethynyl)benzo[c][1,2,5]thiadiazole, 2.1a

To an oven-dried Schlenk flask was added dry THF (20 mL) and triethylamine (20 mL), which was then vacuum degassed three times. 4,7-dibromobenzo[*c*][1,2,5]thiadiazole **2.4** (1.43 g, 4.86 mmol), trimethylsilylacetylene (2.13 mL, 15.0 mmol), copper(I) iodide (9.26 mg, 0.05 mmol), and bis(triphenylphosphine)palladium(II) chloride (35.10 mg, 0.05 mmol) were all added at room temperature. The Schlenk flask was sealed and heated to 80°C, whereupon the solution was stirred for 12 h. After the reaction was cooled to room temperature, water (200 mL) was added to the mixture and the aqueous solution was extracted with dichloromethane (2 x 100 mL). The combined organic layers were washed with water (3 x 200 mL), dried with magnesium sulfate, filtered, and dried *in vacuo*. The residue was purified by column chromatography on silica gel using pure hexane. Compound **2.1a** (0.70 g, 45% yield) was isolated as yellow crystals. m.p. = 104 °C. **2.1a**: IR (ATR, cm^{-1}) 3050, 2955, 2898, 2370, 2331, 2151, 1876, 1487, 1356, 1337, 1252, 1165. ^{1}H NMR (δ in $CDCl_3$): 7.692 (s, 2H), 0.323 (s, 18H). ^{13}C NMR (δ in $CDCl_3$): 154.201, 133.124, 117.245, 103.618, 99.974, -0.136. Accurate mass for $C_{16}H_{20}N_2SSi_2$: *m/z* = 328.09065 [M^+], calc. *m/z* = 328.09008.

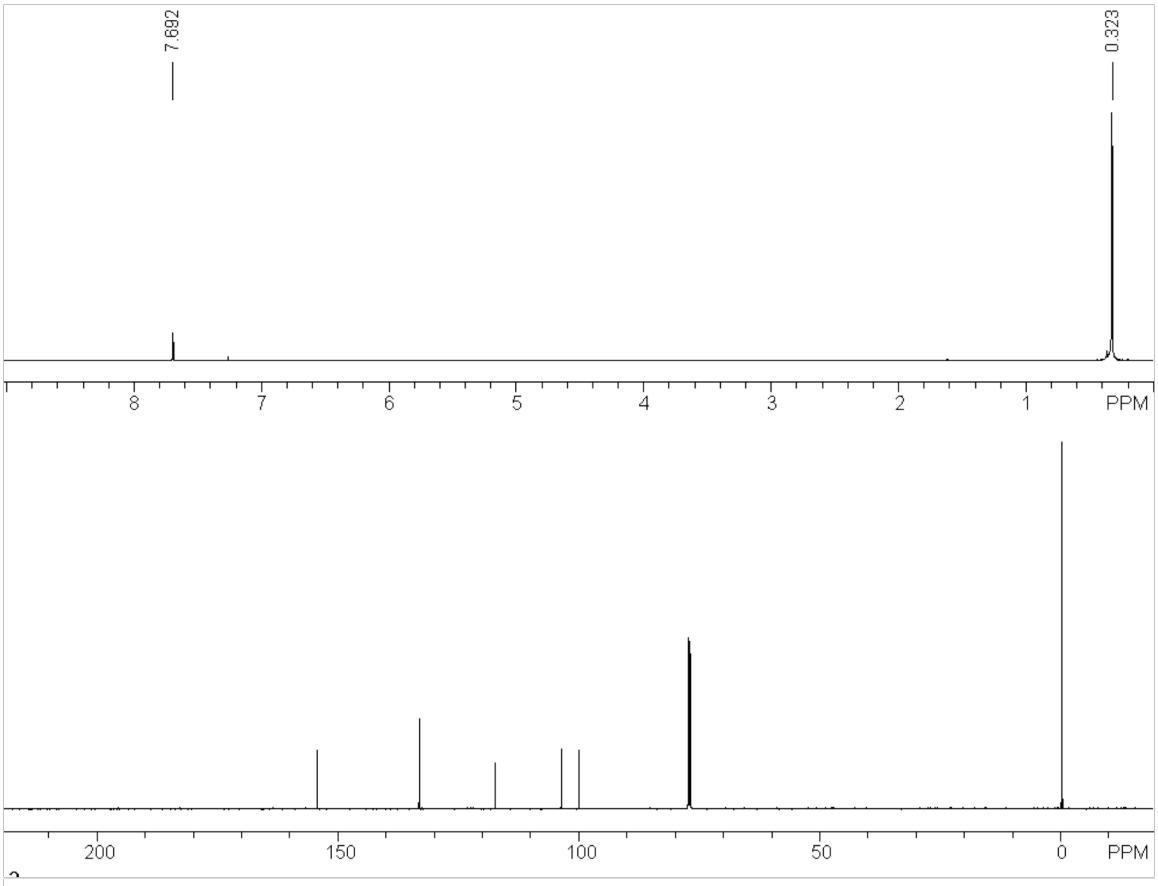

Figure 2.5. ^{1}H NMR (top) and ^{13}C NMR (bottom) of **2.1a**.

2.4.2 4,7-bis((triethylsilyl)ethynyl)benzo[c][1,2,5]thiadiazole, 2.1b

In a procedure identical to that of **2.1a**, **2.1b** was synthesized in 33% yield and isolated as yellow crystals. m.p. = 35-37 ^{o}C. **2.1b**: IR (ATR, cm^{-1}) 3054, 2972, 2954, 2922, 2899, 2796, 2730, 2681, 2635, 2586, 2197, 2147, 1866, 1231, 1169. ^{1}H NMR (δ in $CDCl_3$): 7.693 (s, 2H), 1.100 (t, J = 4.5 Hz, 18H), 0.754 (q, J = 4.8 Hz, 12H). ^{13}C NMR (δ in $CDCl_3$): 154.403, 132.942, 117.339, 101.354, 101.269, 7.471, 4.331. Accurate mass for $C_{22}H_{32}N_2SSi_2$: *m/z* = 412.18351 [M^+], calc. *m/z* = 412.18398.

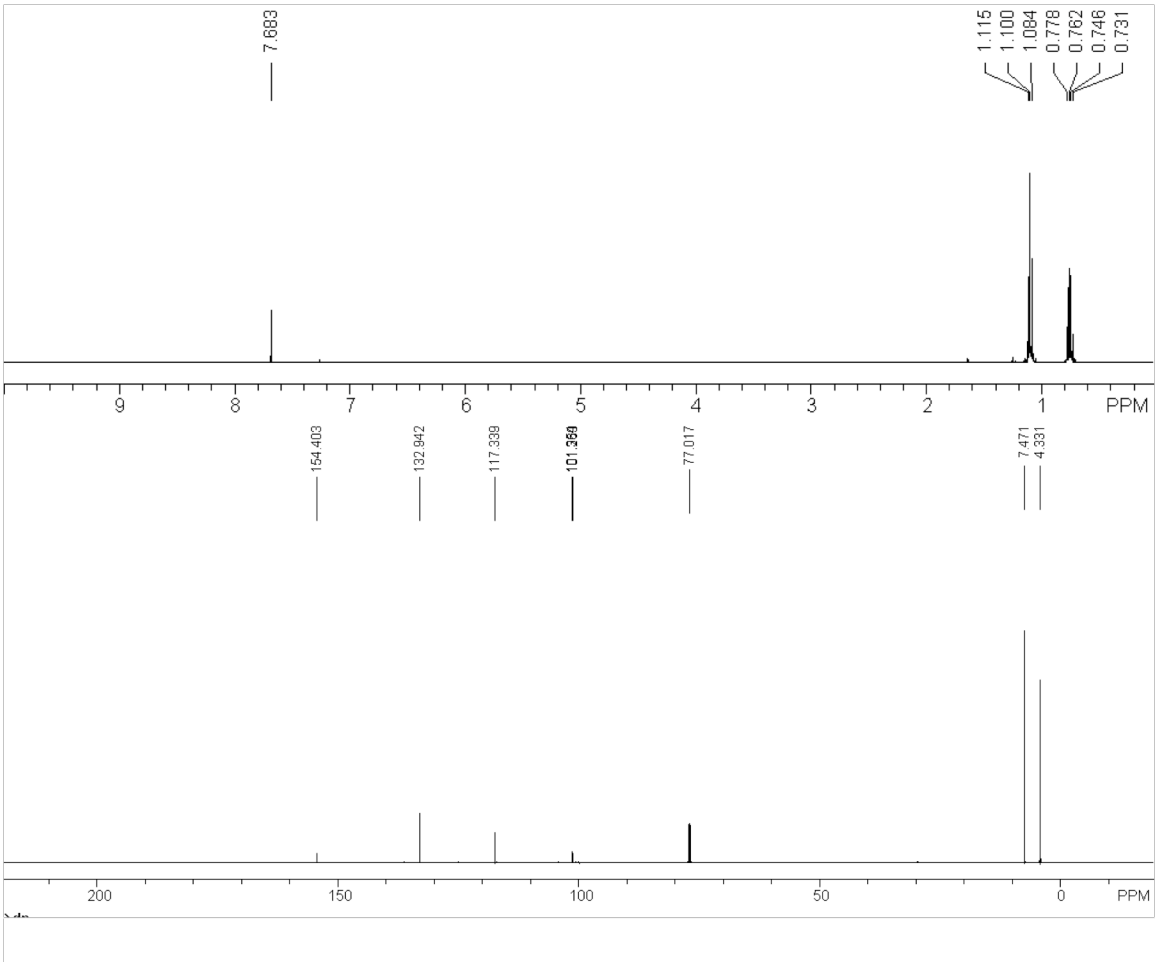

Figure 2.6. ^{1}H NMR (top) and ^{13}C NMR (bottom) of **2.1b**.

2.4.3 4,7-bis((triisopropylsilyl)ethynyl)benzo[c][1,2,5]thiadiazole, 2.1c

In a procedure identical to **2.1a**, **2.1c** was synthesized in 47% yield and isolated as yellow crystals. m.p. = 135 °C. **2.1c**: IR (ATR, cm^{-1}) 3048, 2971, 2950, 2890, 2759, 2718, 2619, 2149, 1880, 1694, 1261, 1168. ^{1}H NMR (δ in $CDCl_3$) 7.677 (s, 2H), 1.196 (m, 42H). ^{13}C NMR (δ in $CDCl_3$) 154.621, 132.647, 117.446, 102.252, 100.205, 18.692, 11.325. Accurate mass for $C_{28}H_{44}N_2SSi_2$: *m/z* = 496.27511 [M^+], calc. *m/z* = 496.27554.

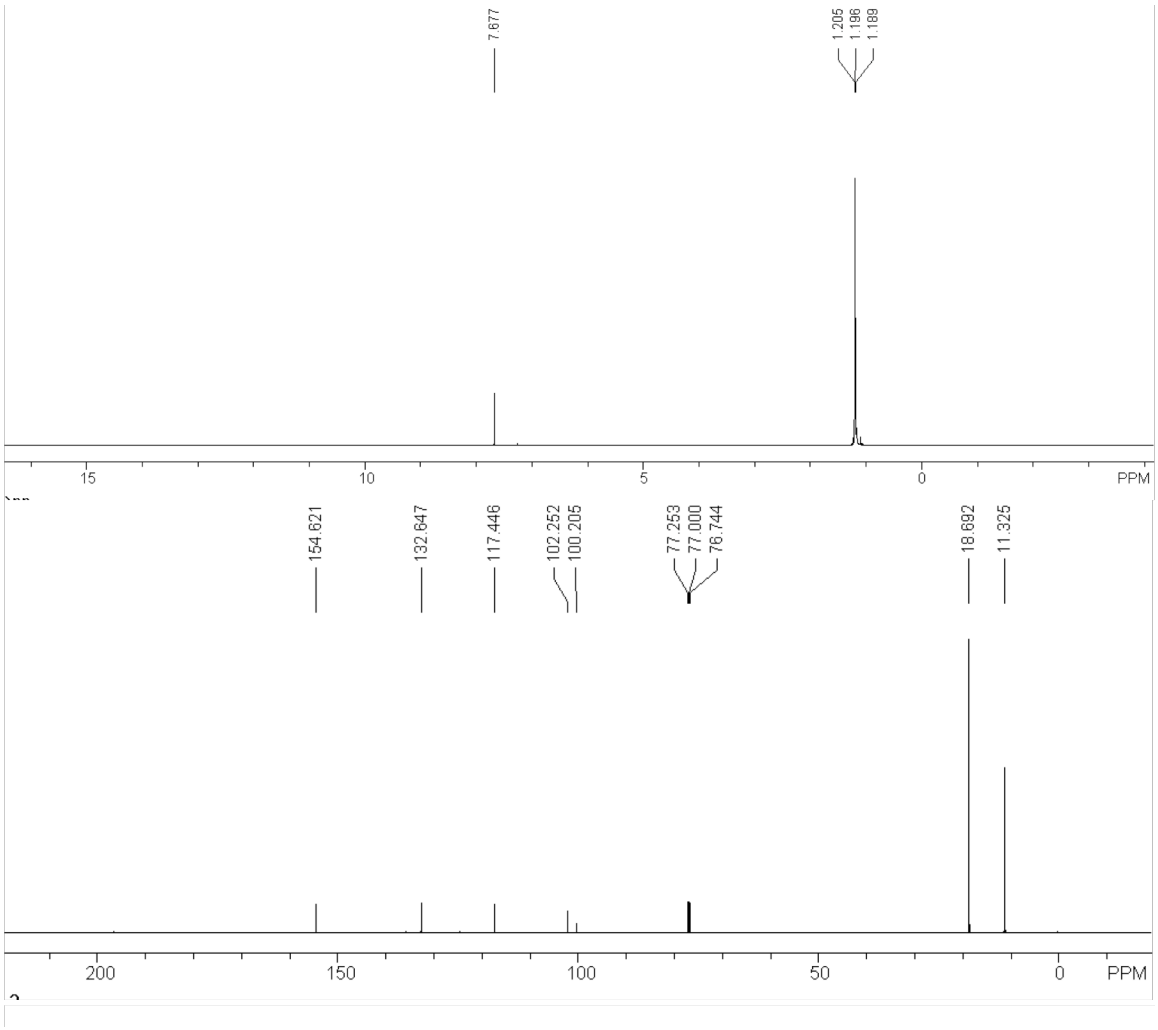

Figure 2.7. ^{1}H NMR (top) and ^{13}C NMR (bottom) of **2.1c**.

2.4.4 4,9-bis(trimethylsilyl)ethynyl)naphtho[2,3-c][1,2,5]thiadiazole, 2.2a

To an oven-dried Schlenk flask was added trimethylsilylacetylene (1.65 mL, 11.6 mmol) and dry THF (10 mL), followed by 1.6 M ^{n}butyllithium in hexane (5.70 mL, 9.12 mmol) at 0 °C. The solution was stirred at room temperature for 1 h, and then compound naphtho[2,3-*c*][1,2,5]thiadiazole-4,9-dione (0.500 g, 2.31 mmol) was added to the solution. The mixture was stirred at ambient temperature for 12 h and then quenched with wet diethyl ether. After evaporation of the solvent, the residue was filtered over silica gel

using hexanes/ethyl acetate (5:1, *v/v*) to yield the corresponding diol. After the solvent was removed *in vacuo*, the crude diol was, without further characterization, suspended in acetic acid (20 mL) and potassium iodide (3.80 g, 22.9 mmol) and NaH_2PO_2 (2.00 g, 22.8 mmol) were added. The mixture was heated to reflux for 1 h. After cooling to room temperature, water (100 mL) was added to the mixture and the aqueous solution was extracted with hexanes (3 x 100 mL). The combined organic layers were dried *in vacuo*. The solids were further purified by chromatography on silica gel using a hexane/CH_2Cl_2 (6:1, *v/v*) solvent mixture. Compound **2.2a** (0.10 g, 11% yield, two steps) was isolated as a red crystalline solid. m.p. = 214-223 °C (Decompose). **2.2a**: IR (ATR, cm^{-1}) 3073, 3037, 2956, 2917, 2914, 2898, 2846, 2785, 2652, 2536, 2475, 2186, 2136, 2009, 1937, 1816, 1538, 1385, 13281279, 1251, 1163, 1142. ^{1}H NMR (δ in $CDCl_3$) 8.498 (AA' of AA'BB', 2H), 7.577 (BB' of AA'BB', 2H), 0.420 (s, 18H). ^{13}C NMR (δ in $CDCl_3$) 152.626, 135.244, 128.101, 127.556, 112.668 110.662, 99.558, 0.073. Accurate mass for $C_{20}H_{22}N_2SSi_2$: *m*/*z* = 378.10601 [M^+], calc. *m*/*z* = 378.10573.

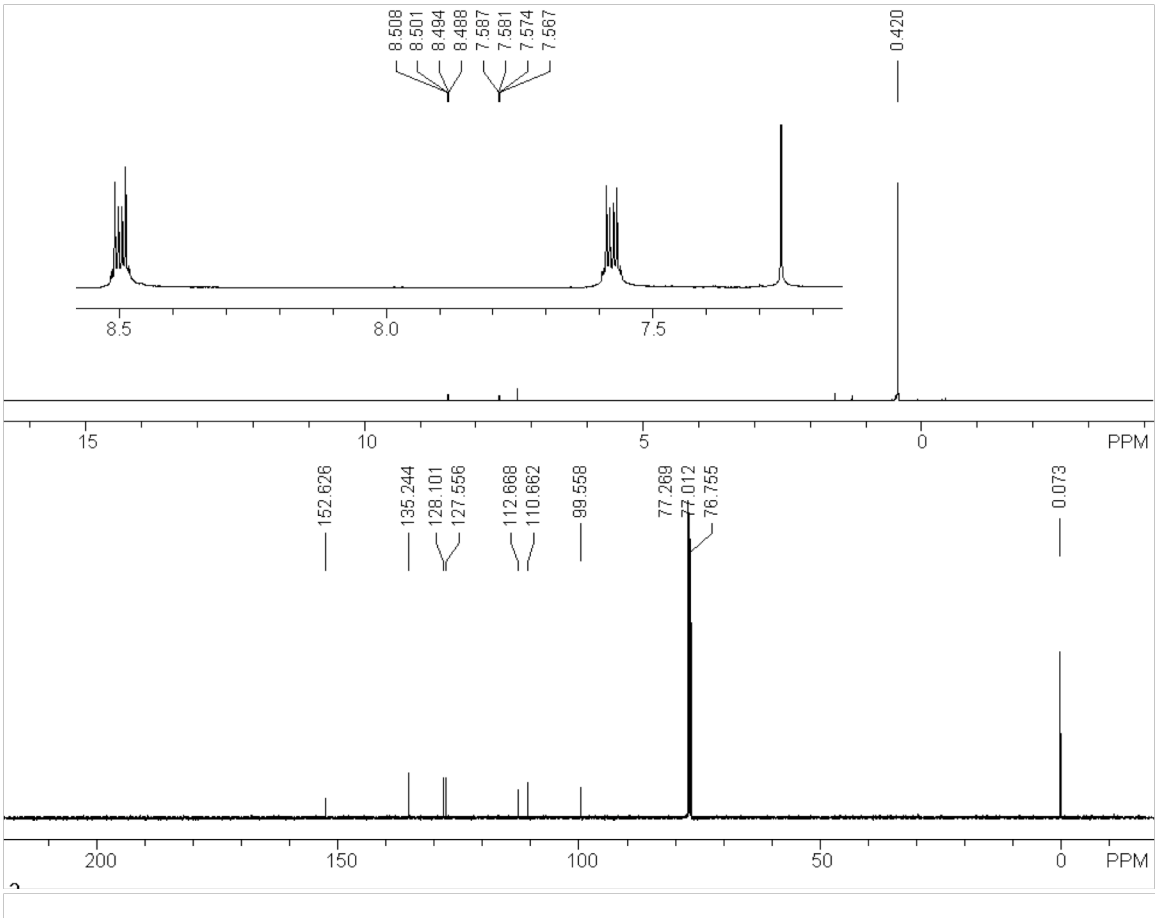

Figure 2.8. ^{1}H NMR (top) and ^{13}C NMR (bottom) of **2.2a**.

2.4.5 4,9-bis(triethylsilyl)ethynyl)naphtho[2,3-c][1,2,5]thiadiazole, 2.2b

Compound **2.2b** has been previously published in reference 12a.

2.4.6 4,9-bis(triisopropylsilyl)ethynyl)naphtho[2,3-c][1,2,5]thiadiazole, 2.2c

Compound **2.2c** has been previously published in reference 12a.

2.4.7 2,3-diaminoanthracene-1,4-dione, 2.8

A mixture of 2,3-dibromo-1,4-anthraquinone **2.6** (14.0 g, 0.0382 mol) and potassium phthalimide **2.7** (14.9 g, 0.0804 mol) in DMF (50 mL) was heated at 120 ºC for 18 h. After cooling to room temperature, water (500 mL) was added to the reaction vessel. The mixture was filtered. The precipitates were washed with water until no color was apparent in the filtrate. The yellowish solid was collected and dried *in vacuo*. The yellowish solid and NH_2NH_2 (15.0 mL) were suspended in water (50 mL) and stirred at 80 ºC for 3 d. The mixture was filtered and the precipitates were washed with water (3 x 100 mL), and dried *in vacuo*. 2,3-Diaminoanthracene-1,4-dione **2.8** was obtained as a dark-brown solid (2.80 g, 31% yield, two steps). ^{1}H NMR (δ in DMSO-d_6): 8.317 (s, 2H), 8.104 (AA' of AA'BB', 2H), 7.630 (BB' of AA'BB', 2H), 5.700 (s, 4H). Due to a lack of solubility, only the ^{1}H NMR was attainable. Accurate mass for $C_{14}H_{10}O_2N_2$: *m/z* = 238.0763 [M+], calc. *m/z* = 238.07423.

2.4.8 Anthra[1,3-c][1,2,5]thiadiazole-4,11-dione, 2.9

A mixture of 2,3-diamino-anthracene-1,4-dione **2.8** (2.40 g, 0.0101 mol) in $SOCl_2$ (15 mL) was refluxed for 12 h. The solvent was removed *in vacuo*. The residue was separated by a column on silica gel using CH_2Cl_2 as the solvent. **2.9** was isolated as a yellow solid (2.10 g, 78%). m.p. = 296–298 ^{o}C. IR (KBr, cm^{-1}) 3633.64, 3355.91, 3062.75, 3020.32, 2688.58, 2538.15, 2410.85, 2183.27, 1974.97, 1874.68, 1685.67, 1616.24, 1585.38, 1411.80, 1234.36, 975.91, 833.19, 775.33, 524.6. ^{1}H NMR (δ in $CDCl_3$): 9.178 (s, 2H), 8.339 (AA' of AA'BB', 2H), 7.979 (BB' of AA'BB', 2H). ^{13}C NMR (δ in $CDCl_3$): 176.35, 157.27, 135.39, 131.77, 130.69, 130.49, 129.66. Accurate mass for $C_{14}H_6N_2O_2S$: *m/z* = 266.01434 [M^+], calc. *m/z* = 266.01500.

2.4.9 4,11-Bis((trimethylsilyl)ethynyl)anthra[2,3-c][1,2,5]thiadiazole, 2.3a

To an oven-dried Schlenk flask was added trimethylsilylacetylene (1.33 mL, 9.39 mmol) and dry THF (10 mL), followed by 1.6 M ^{n}butyllithium in hexanes (4.69 mL, 7.49 mmol) at 0 °C. The solution was stirred at room temperature for 1 h, and then compound **2.9** (0.500 g, 1.89 mmol) was added to the solution. The mixture was stirred at ambient temperature for 12 h and then quenched with wet diethyl ether. After evaporation of the solvent, the residue was filtered over silica gel using hexanes/ethyl acetate (5:1, *v/v*) to yield the corresponding diol. After the solvent was evaporated, the crude diol **2.9a** was, without further characterization, suspended in acetic acid (20 mL) with KI (1.30 g, 7.83 mmol) and NaH_2PO_2 (0.690 g, 7.84 mmol). The mixture was heated to reflux for 30 min. After cooling to room temperature, H_2O (100 mL) was added to the mixture and the aqueous solution was extracted with hexanes (3 x 100 mL). The combined organic layers were dried *in vacuo*. The solids were further purified by chromatography on silica gel using a hexanes/CH_2Cl_2 (10:1. *v/v*) solvent mixture. Compound **2.3a** (0.066 g, 9% yield, two steps) was isolated as dark-blue crystals. **2.3a**: m.p. = 175-180 ^{o}C. IR (KBr, cm^{-1}) 3440, 2959, 2924, 2854, 2357, 2125, 1678, 1647, 1454, 1369, 1246, 1092, 1014, 841, 802, 760, 741, 698. ^{1}H NMR (δ in $CDCl_3$) 9.115 (s, 2H), 7.971 (AA' of AA'BB', 2H), 7.438 (BB' of AA'BB', 2H), 0.495 (s, 18H). ^{13}C NMR (δ in $CDCl_3$) 152.408, 133.126, 132.552, 128.558, 126.954, 126.669, 112.137, 112.109, 100.544, 0.119. Accurate mass for $C_{24}H_{24}N_2SSi_2$: *m*/*z* = 428.11978 [M^+], calc. *m*/*z* = 428.11981.

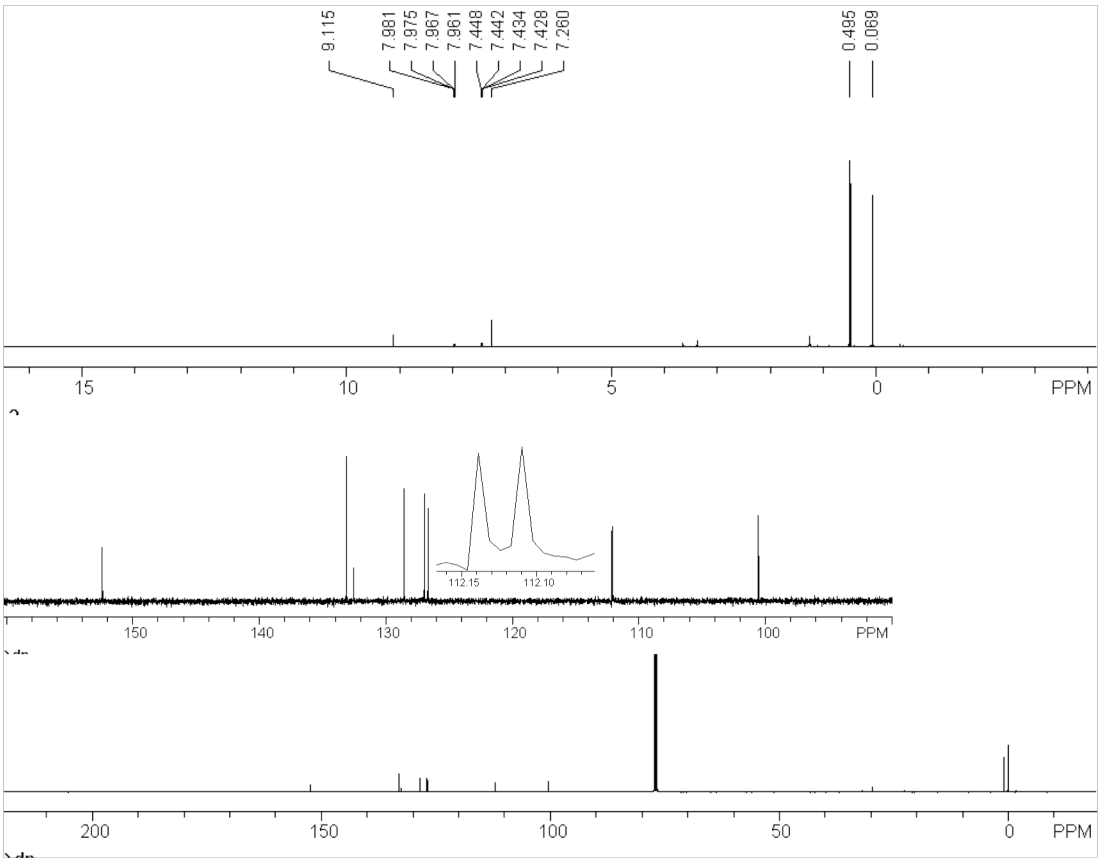

Figure 2.9. ^{1}H NMR (top) and ^{13}C NMR (bottom) of **2.3a**.

2.4.10 4,11-Bis((triethylsilyl)ethynyl)anthra[2,3-c][1,2,5]thiadiazole, 2.3b

In a procedure identical to **2.3a**, **2.3b** was synthesized in 18% yield and isolated as dark-blue crystals. m.p. = 139 °C (decompose). **2.3b**: IR (ATR, cm^{-1}) 3048, 2954, 2878, 2807, 2729, 2691, 2639, 2155, 2117, 1923, 1891, 1787, 1374, 1299, 1267, 1228, 1184, 1148, 1136. ^{1}H NMR (δ in $CDCl_3$): 9.174 (s, 2H), 7.93 (AA' of AA'BB', 2H), 7.413 (BB' of AA'BB', 2H), 1.248 (t, J = 4.5 Hz, 18H), 0.918 (q, J = 4.8 Hz, 12H). ^{13}C NMR (δ in $CDCl_3$): 152.646, 133.069, 132.563, 128.520, 126.850, 126.702, 112.241, 109.858,

101.812, 7.741, 4.588. Accurate mass for $C_{30}H_{36}N_2SSi_2$: *m*/*z* = 512.20859 [M^+], calc. *m*/*z* = 512.20795.

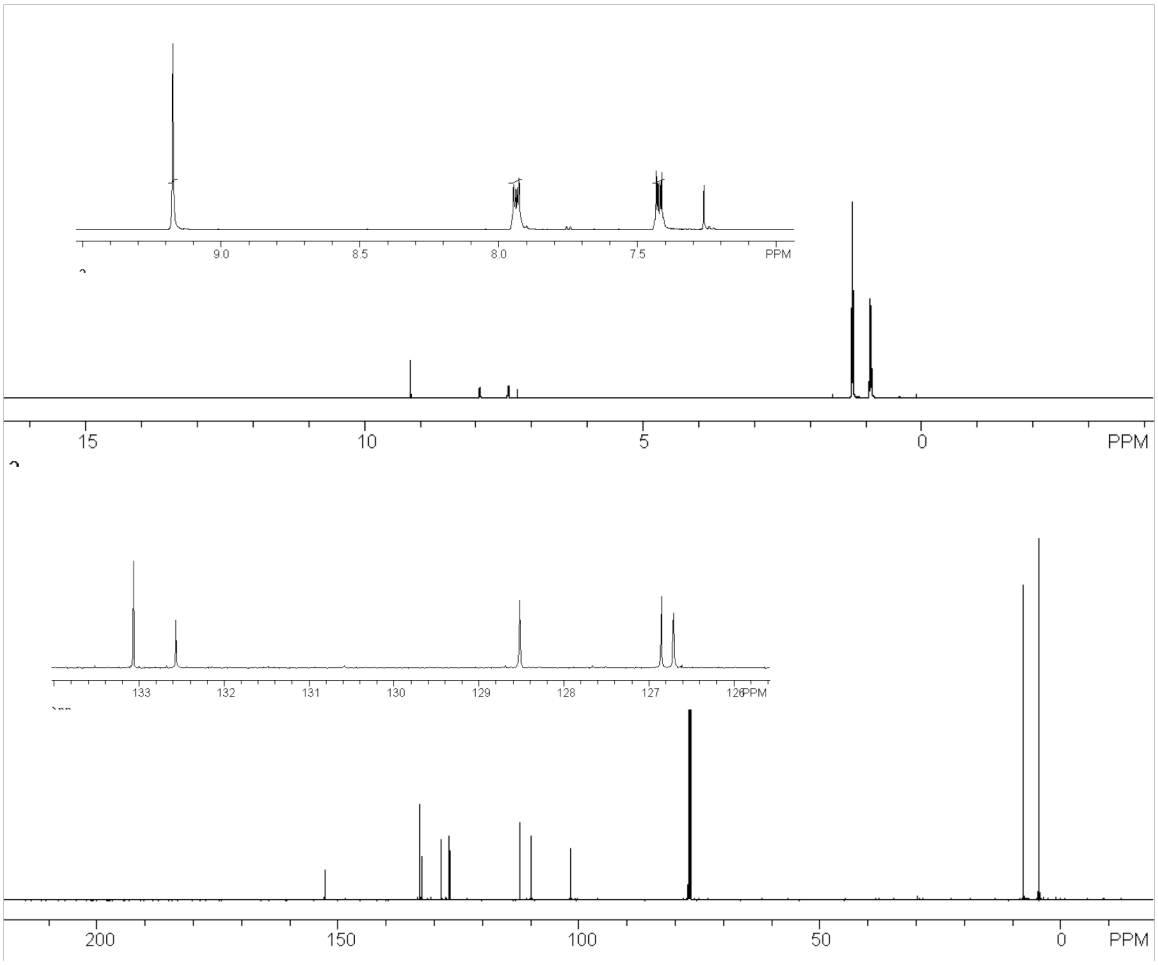

Figure 2.10. ^{1}H NMR (top) and ^{13}C NMR (bottom) of **2.3b**.

2.4.11 4,11-Bis((triisopropylsilyl)ethynyl)anthra[2,3-c][1,2,5]thiadiazole, 2.3c

In a procedure identical to **2.3a**, **2.3c** was synthesized in 92% yield and isolated as dark-blue crystals. m.p. = 172-174 °C (decompose). **2.3c**: IR (KBr, cm^{-1}) 2941, 2863, 2122, 1526, 1462, 1373, 1069, 1013, 993, 879, 734, 672. ^{1}H NMR (δ in $CDCl_3$) 9.23 (s, 2H),

7.925 (AA' of AA'BB', 2H), 7.425 (BB' of AA'BB', 2H), 1.32-1.31 (m, 42H). ^{13}C NMR (δ in $CDCl_3$) 152.93, 133.02, 132.63, 128.54, 126.80, 126.78, 112.34, 108.87, 102.61, 18.90, 11.53. Accurate mass for $C_{36}H_{48}N_2SSi_2$: *m*/*z* = 596.30700 [M^+], calc. *m*/*z* = 596.30768.

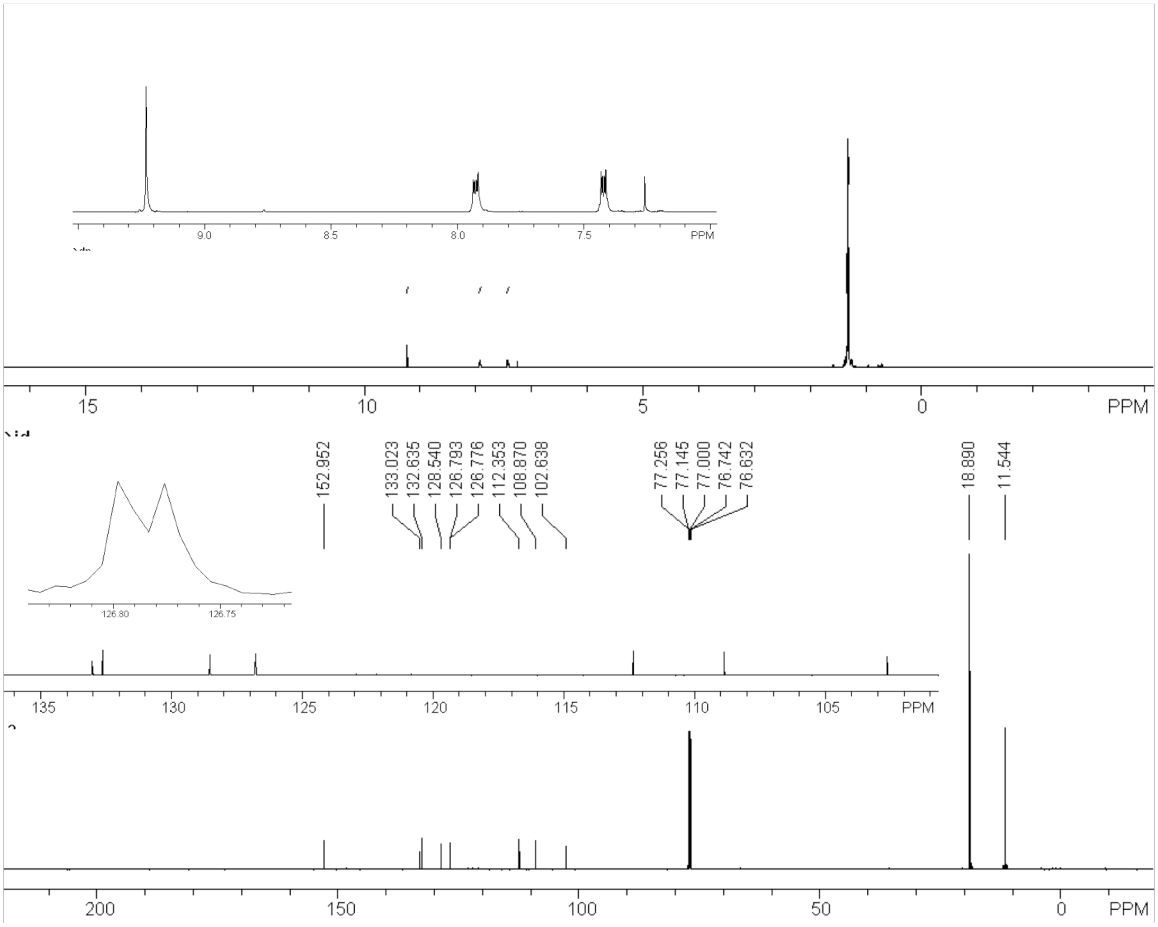

Figure 2.11. ^{1}H NMR (top) and ^{13}C NMR (bottom) of **2.3c**.

2.4.11 UV-vis and emission spectra of 2.1-2.3a-c and tabulated photophysical properties.

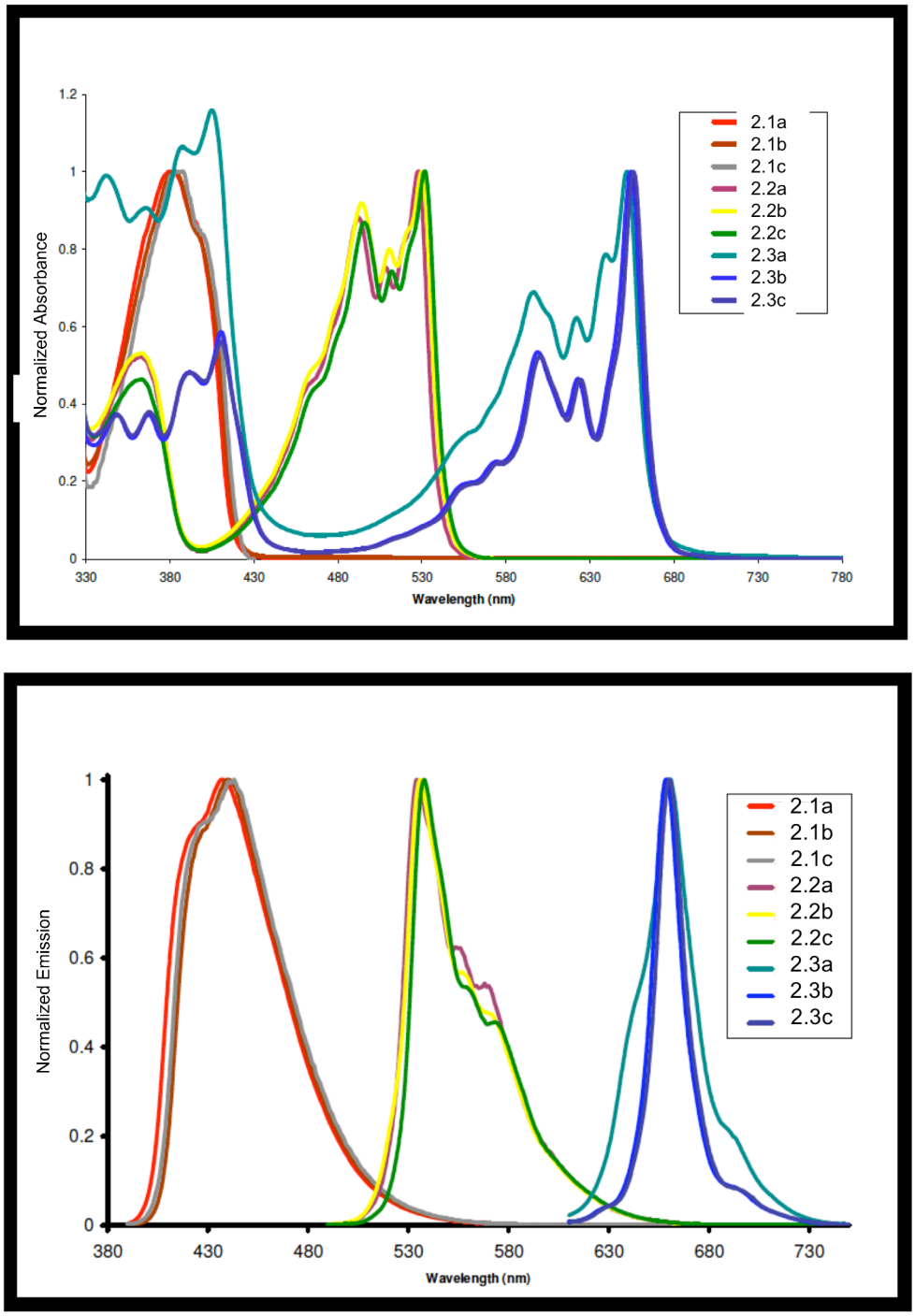

Figure 2.12. Normalized UV-vis absorption (top) and emission (bottom) spectra of **2.1-2.3a-c**.

Table 2.2. Quantum yields (ϕ), molar absorptivities (ε, $M^{-1}cm^{-1}$), and UV-vis low energy λ_{max} (nm) and emission λ_{max} (nm), corresponding to ε and ϕ respectively, of selected acenothiadiazoles. Quinine sulfate in 0.1 M H_2SO_4 (aq.) was used as reference standard for determination of quantum yields. ϕ and ε determined by Scott M. Brombosz.

Compound	**2.1a**	**2.1c**	**2.2b**	**2.2c**	**2.3b**	**2.3c**
ϕ	-	0.94	-	0.28	-	0.01
ε	12950	12282	13240	17600	19830	19570
Abs. λ_{max}	381	385	530	532	654	656
Em. λ_{max}	437	442	536	538	659	660

2.5 References

[1] [a] S.R. Forrest. *Nature* **2004**, *428*, 911. [b] Z. Bao. ACS Symp. Ser. **2004**, *874*, 1.

[2] [a] D. Neher. *Adv. Mater.* **1995**, *7*, 691. [b] M. Gross, D.C. Müller, H.G. Nothofer, U. Scherf, D. Neher, C. Bräuchle, K. Meerholz. *Nature.* **2000**, *405*, 661. [c] A. Kraft, A.C. Grimsdale, A.B. Holmes. *Angew. Chem. Int. Ed. Engl.* **1998**, *37*, 402.

[3] [a] H.E. Katz, Z. Bao, S.L. Gilat. *Acc. Chem. Res.* **2001**, *34*, 359. [b] C.D. Dimitrakopoulos, P.R.L. Malenfant. *Adv. Mater.* **2002**, *14*, 99. [c] X.F. Duan, C.M. Niu, V. Sahi, J. Chen, J.W. Parce, S. Empedocles, J.L. Goldman. *Nature.* **2003**, *425*, 274.

[4] [a] H. Sapnggaard, F.C. Krebs. *Solar Cells.* **2004**, *83*, 125. [b] H. Hoppe, N.S. Sariciftci. *J. Mater. Res.* **2004**, *19*, 1924. [c] S. Gunes, H. Neugebauer, N.S. Sariciftci. *Chem. Rev.* **2007**, *107*, 1324.

[5] [a] J.E. Anthony. *Angew. Chem. Int. Ed.* **2008**, *47*, 452. [b] J.E. Anthony in Functional Organic Materials (T.J.J. Müller and U.H.F. Bunz, Editors), Wiley-VCH, Weinheim **2007**, Chapter 14, pp 511-546. [c] J.E. Anthony. *Chem. Rev.* **2006**, *106*, 5028.

[6] Q. Miao, T.Q. Nguyen, T. Someya, G.B. Blanchet, C. Nuckolls. *J. Am. Chem. Soc.* **2007**, *125*, 10284.

[7] C.R. Swartz, S.R. Parkin, J.E. Bullock, J.E. Anthony, A.C. Mayer, G.G. Malliaras. *Org. Lett.* **2005**, *7*, 3163.

[8] [a] F. Wudl, P.A. Koutentis, A. Weitz, B. Ma, T. Strassner, K.N. Houk, S.I. Kahn. *Pure Appl. Chem.* **1999**, *71*, 295. [b] K. Hutchinson, G. Srdanov, R. Hicks, H.N. Yu, F. Wudl, T. Strassner, M. Nendel, K.N. Houk. *J. Am. Chem. Soc.* **2001**, *120*, 2989. [c] Winkler, K.N. Houk. *J. Am. Chem. Soc.* **2007**, *129*, 1805.

[9] [a] H. Usta, A. Facchetti, T.J. Marks. *J. Am. Chem. Soc.* **2007**, *130*, 8580. [b] Z. Wang, C. Kim, A. Facchetti, T.J. Marks. *J. Am. Chem. Soc.* **2007**, *129*, 13362. [c] M.H. Yoon, A. Facchetti, C.E. Stern, T.J. Marks. *J. Am. Chem. Soc.* **2006**, *128*, 5792. [d] M.H. Yoon, S.A. DiBenedetto, A. Facchetti, T.J. Marks. *J. Am. Chem. Soc.* **2005**, *127*, 1348.

[10] [a] A. Babel, S.A. Jenekhe. *J. Am. Chem. Soc.* **2003**, *125*, 13656. [b] S.A. Jenekhe, S.J. Yi. *Appl. Phys. Lett.* **2000**, *77*, 2635. [c] A. Babel, Y. Zhu, K.F. Cheng, W.C. Chen, S.A. Jenekhe. *Adv. Func. Mater.* **2007**, *17*, 2542.

[11] C.G. Bangcuyo, U. Evans, M.L. Myrick, U.H.F. Bunz. *Macromolecules* **2001**, *34*, 7592.

[12] [a] S. Miao, S.M. Brombosz, P.v.R. Schleyer, J.I. Wu, S. Barlow, S.R. Marder, K.I. Hardcastle, U.H.F. Bunz. *J. Am. Chem. Soc.* **2008**, *130*, 7339. [b] S. Miao, A.L.

Appleton, N.J. Berger, S. Barlow, S.R. Marder, K.I. Hardcastle, U.H.F. Bunz. *Chem. Eur. J.* **2009**, *15*, 4990.

[13] [a] E. Barranco, N. Martin, J.L. Segura, C. Seoane, O. de la Cruz, F. Langa, A. Gonzales, J.M. Pingarron. *Tetrahedron.* **1993**, *49*, 4881. [b] P.V. Bedworth, J.W. Perry, S.R. Marder. *Chem. Comm.* **1997**, 1353.

[14] M.M. Payne, S.A. Odom, S.R. Parkin, J.E. Anthony. *Org. Lett.* **2004**, *6*, 3325.

[15] M. Bendikov, F. Wudl, D.F. Perepichka. *Chem. Rev.* **2004**, *104*, 4891; also ref. 406 within.

[16] R. Schmidt, M.M. Lang, J.H. Oh, M. Winkler, M. Könemann, Z. Bao, F. Würthner. *Adv. Mater.* **2007**, *19*, 3692.

[17] J.K. Politis, F.B. Somoza, J.W. Kampf, M.D. Curtis. *Chem. Mater.* **1999**, *11*, 2274.

CHAPTER 3

WATER-SOLUBLE BENZO- AND NAPHTHOTHIADIAZOLE-BASED BISTRIAZOLES AND THEIR METAL-BINDING PROPERTIES

3.1 Introduction

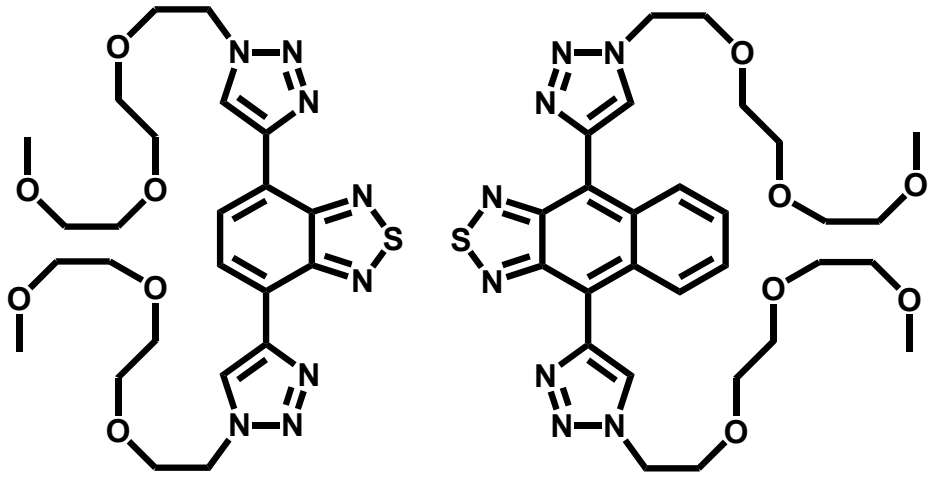

3.4 3.5

Scheme 3.1. Structures of compounds **3.4** and **3.5**.

The 1,3-dipolar cycloaddition of alkynes to azides was first investigated by Szeimies, Huisgen et al.[1] and was later retooled as a copper catalyzed process for the easy access towards 1,4-disubstituted triazoles.[2] While intended by Kolb and Sharpless[3] for the construction of biologically active molecules, the "Click" reaction is now also popular for the construction of polymers and materials.[4]

A generally attractive but less explored aspect of the triazole formation is their incorporation, as functional modules, into fluorophores and/or chromophores; the triazole group could either work as an auxochromic group or a conjugative bridge between two chromophores or π-systems.[5] Herein we report that triazoles are quite powerful auxochromes, i.e. functional groups that bathochromically shift the absorption and emission spectra of acenothiadiazole-types of molecules.

We[6,7] and others[8] are also interested in metallo-responsive fluorophore systems, and we have recently disclosed that a dipolar 1,3-cycloadduct containing a 2-pyridyl residue leads to turn-on fluorescence when exposed to metal cations. Herein we present attractive, novel water-soluble and fluorescent bis-cycloadducts **3.4** and **3.5** that display binding pockets for metal cations.

3.2 Results and Discussion

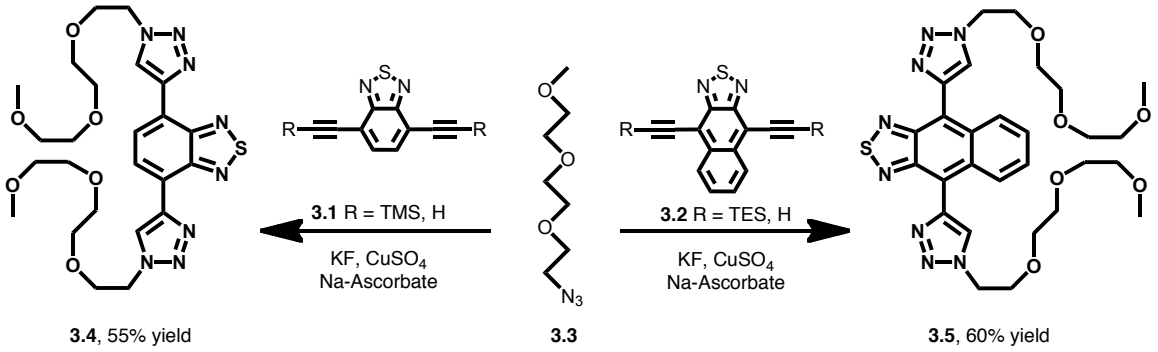

Scheme 3.2. Synthesis of compounds **3.4** and **3.5**.

The TMS-protected diethynylbenzothiadiazole (**3.1**)[9] is deprotected *in situ* by KF; the azide **3.3**, $CuSO_4$ (2.5 eq.) and sodium ascorbate (2.5 eq.) are added to give **3.4** in 55% yield (Scheme 3.2). The same approach works for **3.5**, which is formed analogously

in 60% yield by reaction of **3.2** with **3.3** under identical conditions. The use of a large excess of copper sulfate was necessary to catalyze this reaction, as the products **3.4** and **3.5** were found to bind copper (II) quite efficiently. We selected the oligoethylene glycol azide **3.3** as a substituent as it confers water solubility. Table 3.1 summarizes the relevant photophysical properties of **3.1**, **3.2**, **3.4** and **3.5**, while Figure 3.1 shows the UV-vis and emission spectra of **3.1**, **3.2**, **3.4**, and **3.5**.

Table 3.1. Photophysical properties of compounds **3.1**, **3.2**, **3.4**, and **3.5** in dichloromethane (DCM) and water (H_2O).

Cpd	Abs. λ_{max} (nm)		Emission λ_{max} (nm)		Φ^a		Fluor-escence Lifetime (ns, τ)		Stokes Shift (cm^{-1})		H-L Gap Calcd eV (nm) [b]	FMO positions Calculated (eV)[b]	
	DCM	H_2O	DCM	H_2O	DCM	H_2O	DCM	H_2O	DCM	H_2O		HOMO	LUMO
3.1[c]	386	NA	443	NA	0.85	NA	7.9	NA	3334	NA	3.41 (364)	-6.15	-2.74
3.4	406	385	508	519	0.72	0.13	14.0	7.0	4946	6706	3.10 (399)	-5.64	-2.54
3.2[c]	528	NA	534	NA	0.28	NA	15.2	NA	212	NA	2.50 (496)	-5.55	-3.05
3.5	505	475	610	602	0.09	0.013	18.4	5.3	3409	4442	2.35 (527)	-5.13	-2.78

[a] Quinine sulfate in 0.1 M H_2SO_4 (aq.) used as a reference standard. [b] SPARTAN 08/Windows using the DFT method with the B3LYP functional using the 6-31G**//6-31G** basis set. [c] In the case of **3.1** and **3.2**, the TIPS protected analogue was utilized due to its greater stability than the corresponding TMS or TES analogues.

There are several noteworthy trends. In dichloromethane (DCM) the fluorescence quantum yields of all investigated species (**3.1**, **3.2**, **3.4**, and **3.5**) are high. Generally, the

quantum yields of the precursor alkynes are somewhat higher than those of their 1,3-dipolar azide adducts. As the precursor alkynes do not dissolve in water, only the

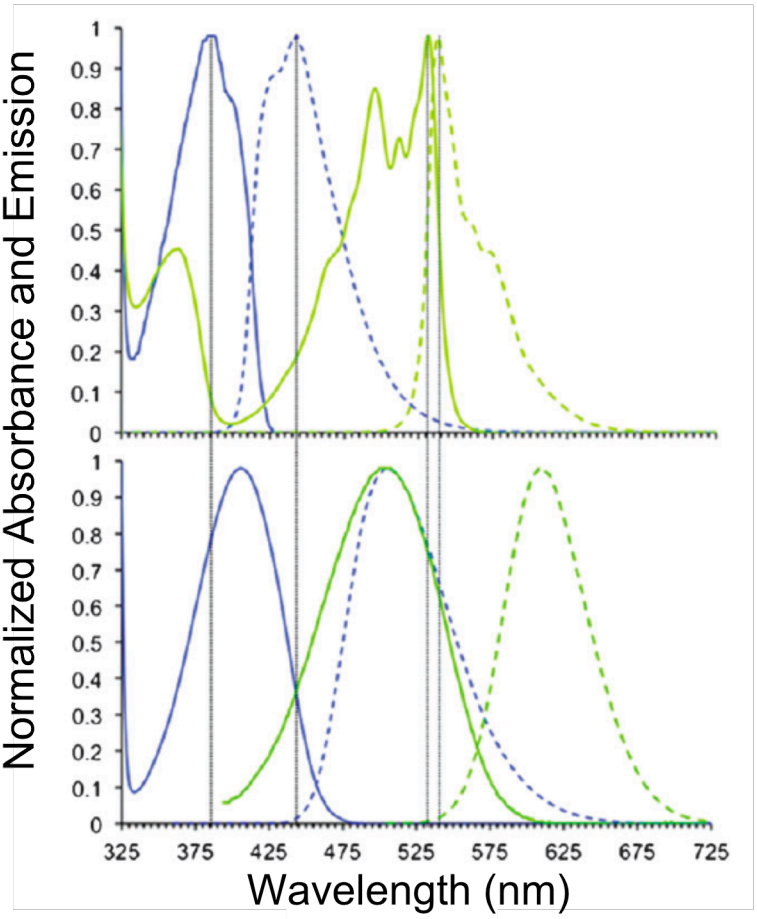

Figure 3.1. Normalized absorption and emission spectra of **3.1** (blue), **3.2** (green, both top), **3.4** (blue) and **3.5** (green, both bottom) in DCM. Solid lines depict absorption spectra while broken lines depict emission spectra. In the case of **3.1** and **3.2**, the TIPS protected analogue was utilized due to its greater stability than the corresponding TMS or TES analogues.

quantum yields of **3.4** and **3.5** were obtained for aqueous solutions. While **3.4** displays quite a robust quantum yield of 13% in water, in the case of **3.5** the quantum yield in water drops to 1.3%. With its emission wavelength of 519 nm and a quantum yield of

13%, **3.4** is a potentially useful fluorophore core as it is stable towards photobleaching. In addition, the fluorescent lifetimes (obtained using a 372 nm laser diode) of **3.4** in DCM (14 ns) and in water (7 ns) are long-lived. The larger congener **3.5** displays similarly long fluorescence lifetimes of 18 ns and 5 ns in DCM and water, respectively. This is testimony to the photophysical properties of the acenothiadiazole core, as the precursor alkynes also display relatively long emissive lifetimes, although not as long as those observed for the 1,3-cycloadducts.

The long fluorescence lifetime of the cycloadduct **3.4** is promising for potential applications as a bio-fluorophore. As complex biological matrices such as cells, serum, etc. are fraught with background fluorescence,[10] displaying an emissive half-life of approximately 3 ns, fluorophores such as **3.4** should still be visible if time-gated detection is used. Quite unusual is that the emission and absorption wavelengths of **3.4** and **3.5** are not very solvent dependent, and that we actually see a slight hypsochromic shift in the absorption features for both **3.4** and **3.5** when going from DCM into water (Table 3.1).

The emission of **3.4** displays a slight bathochromic shift when going from DCM to water, while **3.5** displays a slight hypsochromic shift upon the same solvent change (Table 3.1). The similarity of the spectral properties in water and in DCM suggest that these fluorophores do not exhibit a large degree of charge transfer character in the ground or first excited state; **3.4** and **3.5** are electron poor, as both of their constituent modules (triazoles and acenothiadiazole core) are electron accepting.

Surprising are the quite significant bathochromic shifts in the absorption onset and particularly the emission wavelength of the 1,3-dipolar cycloadducts **3.4** and **3.5** in

comparison to their respective diyne precursors **3.1** and **3.2**.[11] Quantum chemical calculations (obtained by SPARTAN 08/Windows using the B3LYP method with the 6-31G**//6-31G** basis set) support this trend (Table 3.1) and show that the HOMO and the LUMO positions are both destabilized, with the HOMO having the more pronounced destablization than the LUMO when going from alkyne to triazole. The absorption and emission profiles for **3.6a** (λ_{max} abs = 409 nm, λ_{max} emission = 507 nm; in DCM) are very similar to those obtained for **3.4** and the computational studies show the HOMO and LUMO of model compound **3.6b** at -5.69 eV and -2.66 eV, respectively (Scheme 3.3). Consequently, while the triazole unit has a strong auxochrmoic effect, it is poor at transmitting electronic communication between two π-systems.

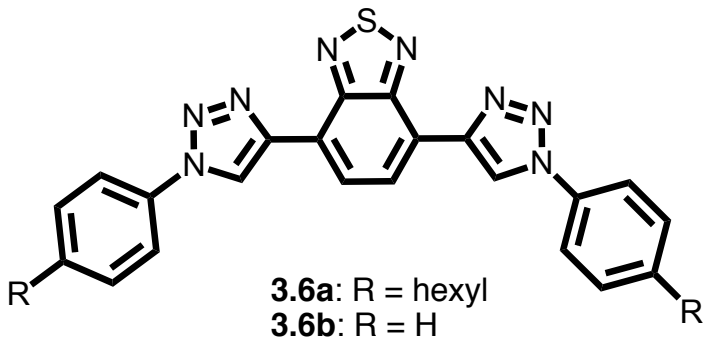

3.6a: R = hexyl
3.6b: R = H

Scheme 3.3. Compound **3.6a** and model compound **3.6b**.

Adducts **3.4** and **3.5** display a binding pocket that should readily bind to metal analytes of appropriate charge and atomic radius as previously demonstrated within our group and be Xie et al. for similar types of 1,3-dipolar cycloadducts, but only in non-aqueous solutions.[6,12]

Our adducts (**3.4** and **3.5**) allow the screening of metal binding in water. Upon addition of the triflate salts of Li^{+}, Na^{+}, K^{+}, Ca^{2+}, Zn^{2+}, Mg^{2+}, and Sn^{2+} to an aqueous solution of **3.4**, no change in the absorption or emission spectra is observed. Upon addition of Hg^{2+} and trifluoroacetic acid (TFA), no change in the absorption spectra is observed, however the emission of **3.4** becomes quenched. Upon the addition of Cu^{2+} or Ni^{2+} the charge transfer band in the absorption spectra bathochromically shifts (~20-30 nm) and the emission becomes quenched (Figures 3.2 and 3.3). Titrations of **3.4** and **3.5** with copper sulfate and **3.4** with nickel sulfate in water were performed to determine the strength of the binding.

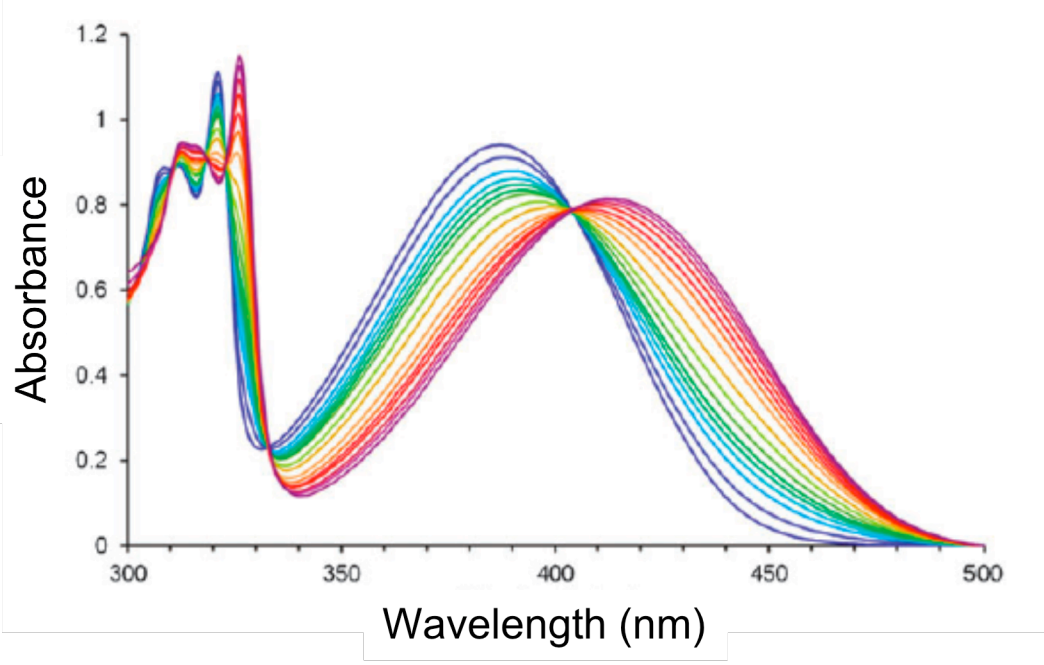

Figure 3.2. Representative absorption titration of **3.4** (blue trace; 151.5 μM) with copper sulfate in water. [Cu^{2+}] ranges from 0-6.26 x 10^{-1} M (red trace is **3.4**-Cu^{2+} complex).

Attempting to plot the fluorescence quenching spectra according to the standard Stern-Volmer equation ($I_o/I_{final} = 1 + K_{SV}[Q]$)[15] resulted in significant deviation from linearity. However, the data were well correlated when Eqn. 3.1 is employed,[12,13] where I_q is the intensity of the fluorescence at a given quencher concentration, I_o is the initial fluorescence intensity of the fluorophore, I_{final} is the final intensity of the fluorescence

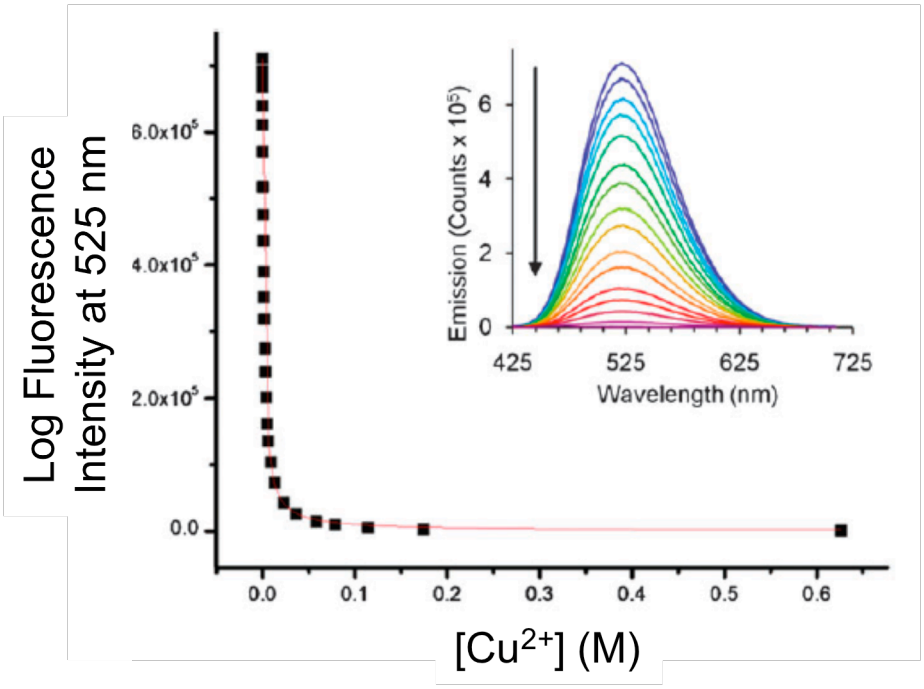

Figure 3.3. Emission data (black dots) of the titration of **3.4** (151.5 μM) with copper sulfate in water. The red line indicates the fitted equation used to determine the binding constant. $[Cu^{2+}]$ ranges from 0-6.26 x 10^{-1} M. Inset: representative emission titration of **3.4** with copper sulfate in water.

of the quenched fluorophore, [Q] is the concentration of the quencher added, [F] is the concentration of the fluorophore, and K_{SV} is the apparent Stern-Volmer constant.

$$I_q = I_o + \frac{I_{final} - I_o}{2} \times \left(1 + \frac{[Q]}{[F]} + \frac{1}{K_{SV}[F]} - \left[\left(1 + \frac{[Q]}{[F]} + \frac{1}{K_{SV}[F]} \right)^2 - 4\frac{[Q]}{[F]} \right]^{1/2} \right) \qquad (3.1)$$

The results of the titrations are summarized in Table 3.2. The binding of **3.4** to Ni(II) in water resulted in a binding constant of log K = 3.17 ± 0.01. The lower binding constant in comparison to Xie's (log K = 4.48 ± 0.03) is expected as the titration was performed in water, which is a more competitive ligating solvent that acetonitrile.[12] The binding constant for Cu(II) in water was slightly smaller in magnitude than that of Ni(II) with log K = 2.70 ± 0.01.

Table 3.2. Binding data of **3.4** and **3.5** with Cu(II) and Ni(II) in water.

Compound	**3.4**	**3.4**	**3.5**
Metal[a]	Cu(II)	Ni(II)	Cu(II)
Log *K* absorption[b]	2.83	3.18	2.96
Log *K* emission[c]	2.70 ± 0.01	3.17 ± 0.01	2.71 ± 0.03

[a] The sulfate salt was used in all cases. [b] Values obtained from the deconvolution of the absorption spectra utilizing Datan software.[14] [c] Values obtained from fitting the quenching of the emission spectra with Eqn. 3.1. Data obtained by Scott M. Brombosz.

The binding constant for the binding of Cu(II) to **3.5** was determined to be log K = 2.71 ± 0.03. This binding constant was nearly identical to that of **3.4**, which demonstrated the independence of the binding upon the size of the aceno portion of the core. Interestingly, the necessity of a stoichiometric amount of copper in the synthesis of **3.4** and **3.5** can be attributed to this high binding constant because once the triazole group

is formed, the effective concentration of free copper available to catalyze the reaction is drastically reduced.

Binding constants were also obtained from the deconvolution of the absorption spectrum from the titration of the metal utilizing Datan software.[14] In all cases, the constants obtained from the absorption spectra were in good to excellent agreement with the values obtained from the modified Stern-Volmer plots of the emission spectra. Assuming a 1:1 complex agrees very well with the obtained data. Apparently upon coordination to one copper ion, the second binding pocket becomes too electron poor to effectively bind another metal ion in aqueous solution.

3.3 Conclusion

In conclusion, we have prepared water-soluble bistriazoles **3.4**, **3.5** and **3.6a**. From the combination of spectroscopic and computational data, we can conclude that the triazole ring has a strong auxochromic effect and leads to the bathochromically shifted spectroscopic features for the connected arene in the 4-position. At the same time, the triazole ring is a poor electronic conduit, as the spectroscopic properties of **3.6a** are almost identical to that of **3.4**. The adducts **3.4** and **3.5** do not show large solvent dependencies of their spectroscopic properties, and **3.4** is fluorescent in water and binds both Cu(II) and Ni(II) in aqueous solution. Overall, the 1,3-dipolar cycloaddition of alkynes to appropriately substituted azides is a superb tool to prepare functional, metallo-responsive fluorophores in aqueous environments.

I was responsible for synthesizing starting materials **3.1** and **3.2**, as well as assisted in the editorial process of the paper. Andrew Zappas synthesized the azide **3.3**. Scott Brombosz was responsible for everything else.

This work has been published in *Chemical Communications*:

Scott M. Brombosz, Anthony Lucas Appleton, Andrew J. Zappas, Uwe H.F. Bunz. *Chemical Communications.* **2010**, *46*, 1419.

3.4 Experimental Information

3.4.1 4,7-Bis(1-(2-(2-(2-methoxyethoxy)ethoxy)ethyl)-1H-1,2,3-triazol-4yl)benzo[c][1,2,5]thiadiazole 3.4.

To a stirring solution of 0.150 g (1.0 eq, 4.57 x 10^{-4} mol) of 4,7-bis((trimethylsilyl) ethynyl)benzo[c][1,2,5]thiadiazole (**3.1**) in 10 mL of 5:1 THF:H_2O was added 0.139 g (4.0 eq, 1.826 x 10^{-3} mol) of KF hydrate was added and the solution was allowed to stir for 30 minutes. After the addition of 0.216 g (2.5 eq, 1.14 x 10^{-3} mol) of **3.3** the solution was freeze-pump-thawed three times to remove any oxygen. While under a flow of N_2, 0.182 g (2.5 eq, 1.14 x 10^{-3} mol) of copper sulfate and 0.226 g (2.5 eq, 1.14 x 10^{-3} mol) of sodium ascorbate was added. After stirring overnight, the crude mixture was filtered through celite with dichloromethane. The solvent was removed under vacuum. The product was filtered through a short silica column with dichloromethane followed by ethyl acetate as the eluent to elute any thiadiazole starting material. The product (**3.4**) was then eluted with acetone. After concentration, the recovered oil was dissolved in water and lyophilized for two days

to yield a yellow/green solid in 55% yield (0.141 g). ^{1}H NMR (500 MHz, $CDCl_3$) 3.30 (s, 6H), 3.46 (m, 4H), 3.59 (m, 4H), 3.65 (m, 8H), 3.98 (t, J = 5 Hz, 4H), 4.68 (t, J = 5 Hz, 4H), 8.63 (s, 2H), 8.85 (s, 2H); ^{13}C NMR (125 MHz, $CDCl_3$) 50.44, 58.95, 69.56, 70.54, 70.73, 71.83, 122.67, 125.02, 125.97, 143.00, 152.25; IR (KBr, cm^{-1}) 3500, 3175, 3113, 2870, 2291, 1946, 1580, 1539, 1456, 1366, 1271, 1227, 1142, 1045, 981, 879, 825, 692, 619, 500; Accurate mass calc. for $C_{24}H_{35}O_6N_8S$ (FAB **3.4** + H) *m/z* = 563.24003, found *m/z* = 563.24070.

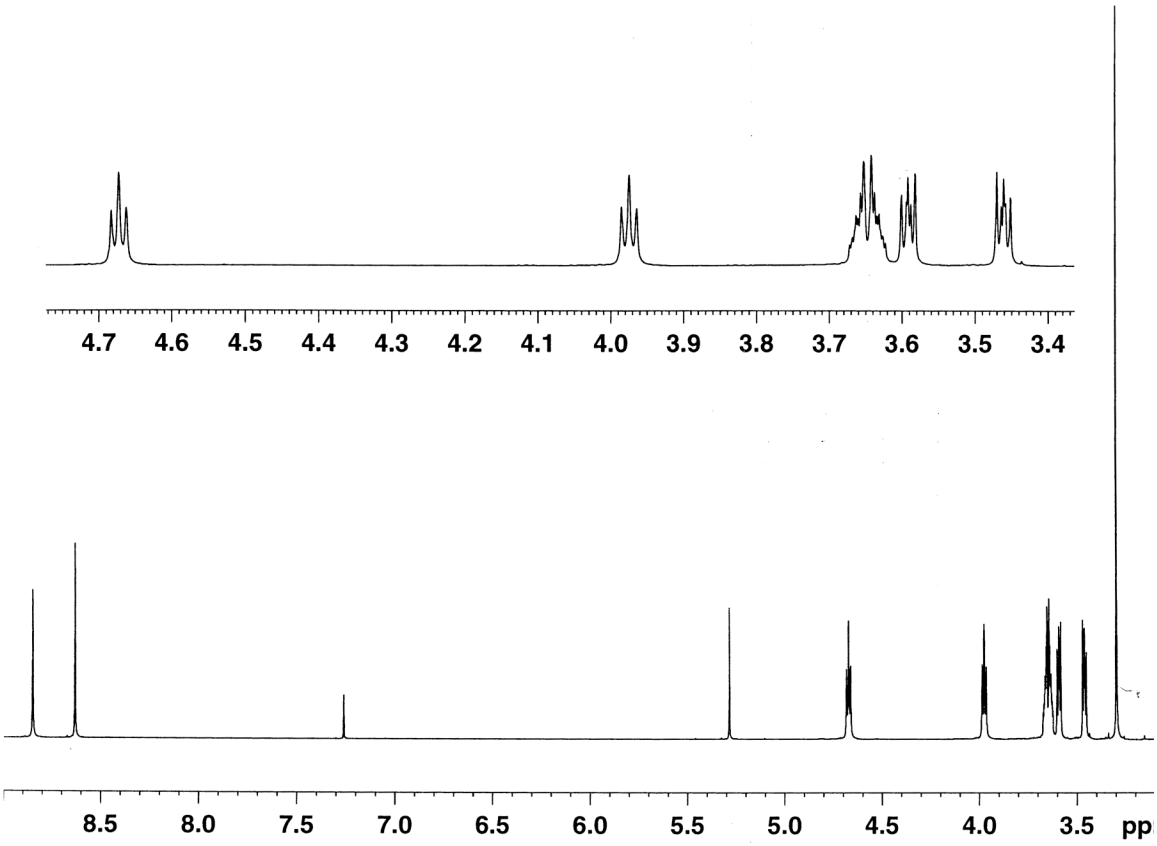

Figure 3.4. ^{1}H NMR spectrum of compound **3.4**.

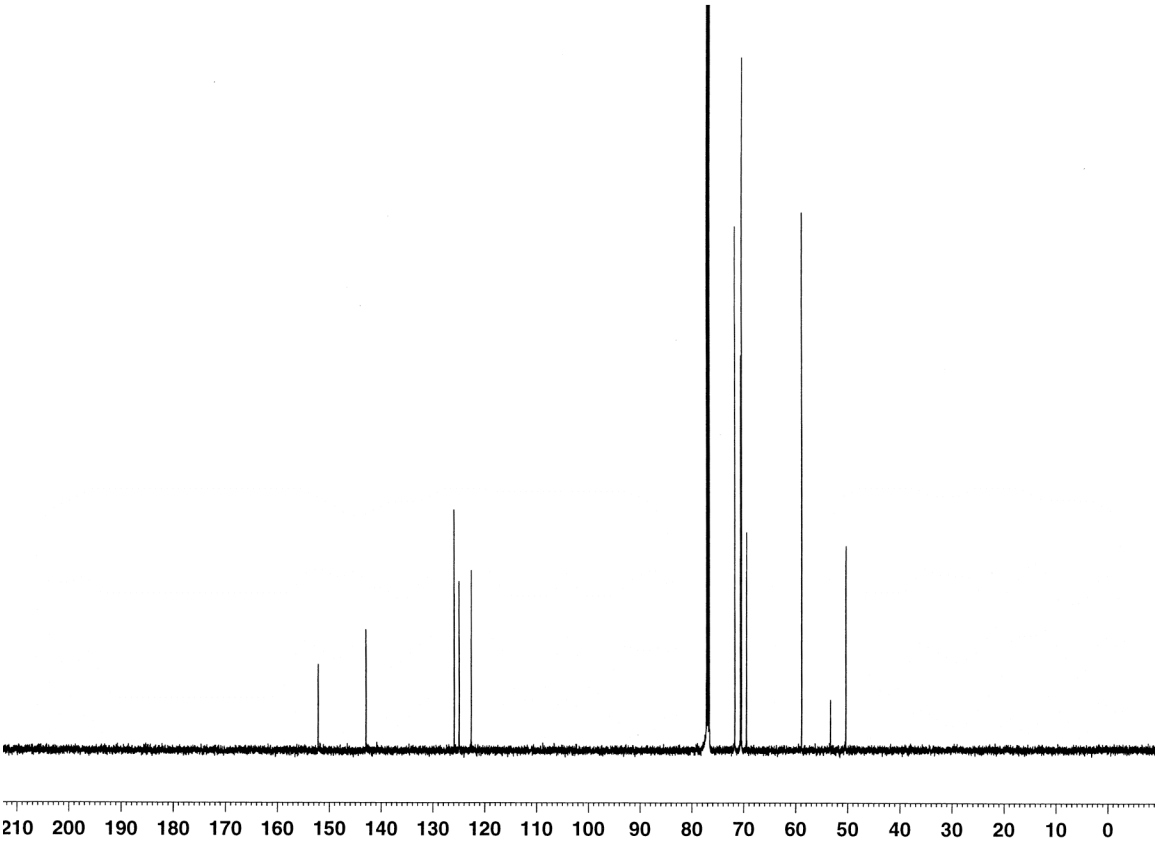

Figure 3.5. ^{13}C NMR spectrum of compound **3.4**.

3.4.2. 4,9-Bis(1-(2-(2-(2-methoxyethoxy)ethoxy)ethyl)-1H-1,2,3-triazol-4-yl)naphtho [c][1,2,5]thiadiazole 3.5.

To a stirring solution of 0.150 g (1.0 eq, $3.24x10^{-4}$ mol) of 4,9-bis((triethylsilyl)ethynyl)-naphtho[2,3-c][1,2,5]thiadiazole (**3.2**) in 10 mL of 5:1 THF:H_2O was added 0.099 g (4.0 eq, $1.3x10^{-3}$ mol) of KF hydrate was added and the solution was allowed to stir for 30 minutes. After the addition of 0.153 g (2.5 eq, $8.10x10^{-4}$ mol) of **3.3** the solution was freeze-pump-thawed three times to remove any oxygen. While under a flow of N_2, 0.129 g (2.5 eq, $8.10x10^{-4}$ mol) of copper sulfate and 0.161 g (2.5 eq, $8.10x10^{-4}$ mol) of sodium

ascorbate was added. After stirring overnight, the crude mixture was filtered through celite with dichloromethane. The solvent was removed *in vacuo*. The product was filtered through a short silica column with dichloromethane followed by ethyl acetate as the eluent to elute any thiadiazole starting material. The product (**3.5**) was then eluted with 20% acetone in ethyl acetate. After concentration, the recovered oil was dissolved in water and lyophilized for two days to yield a red solid in 60% yield (0.119 g). ^{1}H NMR (300 MHz, $CDCl_3$) 3.24 (s, 6H), 3.41 (m, 4H), 3.58 (m, 4H), 3.69 (m, 8H), 4.05 (t, J = 5 Hz, 4H), 4.78 (t, J = 5 Hz, 4H), 7.52 (BB' of AA'BB', 2H), 8.66 (s, 2H), 9.03 (AA' of AA'BB', 2H); ^{13}C NMR (75 Hz, $CDCl_3$) 150.77, 143.03, 132.41, 127.68, 127.55, 127.43, 118.92, 71.79, 70.69, 70.55, 70.52, 69.54, 58.94, 50.52; IR (KBr, cm^{-1}) 3497, 3148, 2870, 1950, 1647, 1533, 1458, 1352, 1259, 1109, 1051, 893, 822, 765, 721, 529; Accurate mass calc. for $C_{28}H_{37}O_6N_8S$ (FAB **3.5** + H) *m/z* = 613.25568, found *m/z* = 613.25273.

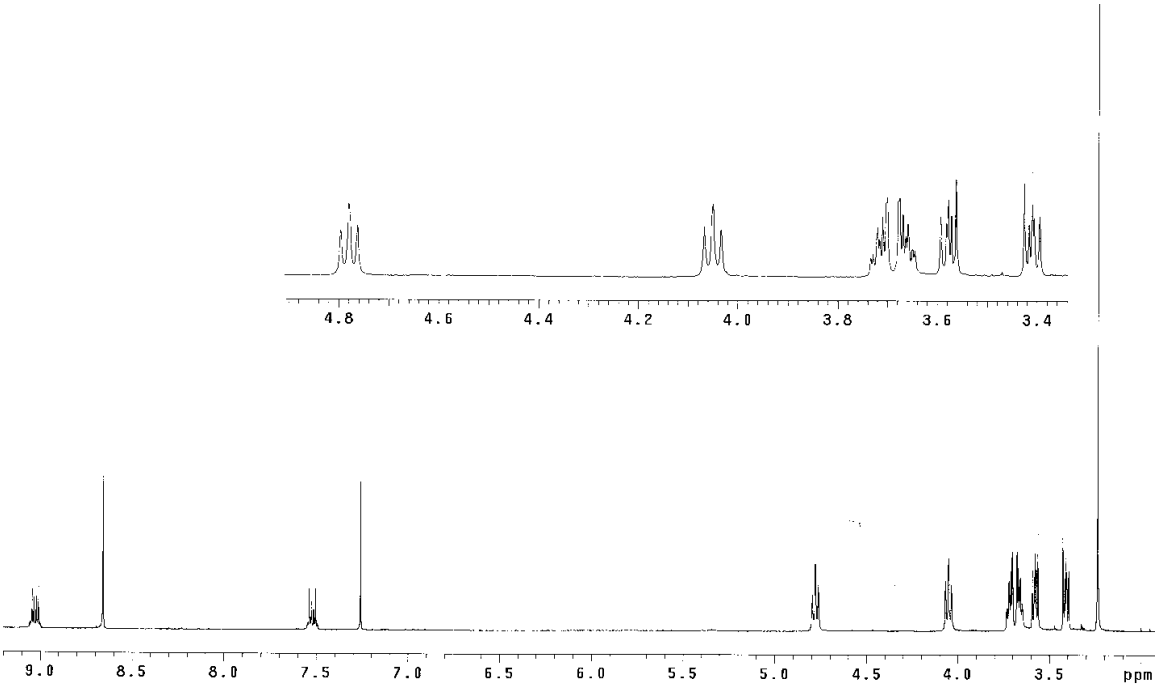

Figure 3.6. ^{1}H NMR spectrum of compound **3.5**.

3.4.3. 4,7-Bis(1-(4-hexylphenyl)-1H-1,2,3-triazol-4-yl)benzo[c][1,2,5]thiadiazole 3.6a.

To a stirring solution of 0.150 g (1.0 eq, $4.57x10^{-4}$ mol) of 4,7-bis((trimethylsilyl) ethynyl)benzo[c][1,2,5]thiadiazole (**3.1**) in 10 mL of 5:1 THF:H_2O was added 0.139 g (4.0 eq, $1.826x10^{-3}$ mol) of KF hydrate was added and the solution was allowed to stir for 30 minutes. After the addition of 0.232 g (2.5 eq, $1.14x10^{-3}$ mol) of **7** the solution was freeze-pump-thawed three times to remove any oxygen. While under a flow of N_2, 0.182 g (2.5 eq, $1.14x10^{-3}$ mol) of copper sulfate and 0.226 g (2.5 eq, $1.14x10^{-3}$ mol) of sodium ascorbate was added. After stirring overnight, the crude mixture was filtered through celite with dichloromethane. The solvent was removed under vacuum. The product was filtered through a short silica column with dichloromethane to elute any thiadiazole starting material. The product (**3.6a**) was then eluted with 5% ethyl acetate in DCM. Concentration under reduced pressure provided **3.6a** as a yellow solid (0.070 g, 26% yield). ^{1}H NMR (300 MHz, $CDCl_3$) 0.89 (t, 6H), 1.32 (m, 12H), 1.63 (m, 4H), 2.65 (t, 4H), 7.29 (d, J = 5 Hz, 4H), 7.68 (d, J = 5 Hz, 4H), 8.59 (s, 2H), 9.00 (s, 2H); ^{13}C NMR (125 MHz, $CDCl_3$) 14.41, 22.85, 29.14, 31.54, 31.92, 35.73, 120.44, 121.77, 122.49, 126.13, 129.76, 134.91, 143.54, 144.08, 152.16; IR (KBr, cm^{-1}) 3167, 3051, 2955, 2924, 2853, 2280, 1909, 1728, 1580, 1517, 1466, 1410, 1240, 1177, 1040, 989, 885, 837, 802, 519; Accurate mass calc. for $C_{34}H_{38}N_8S$ (EI **3.6b** + H) calc. *m/z* = 590.2940, found *m/z* = 590.2925.

3.4.4. Spectroscopic Response Data of 3.4 in Water

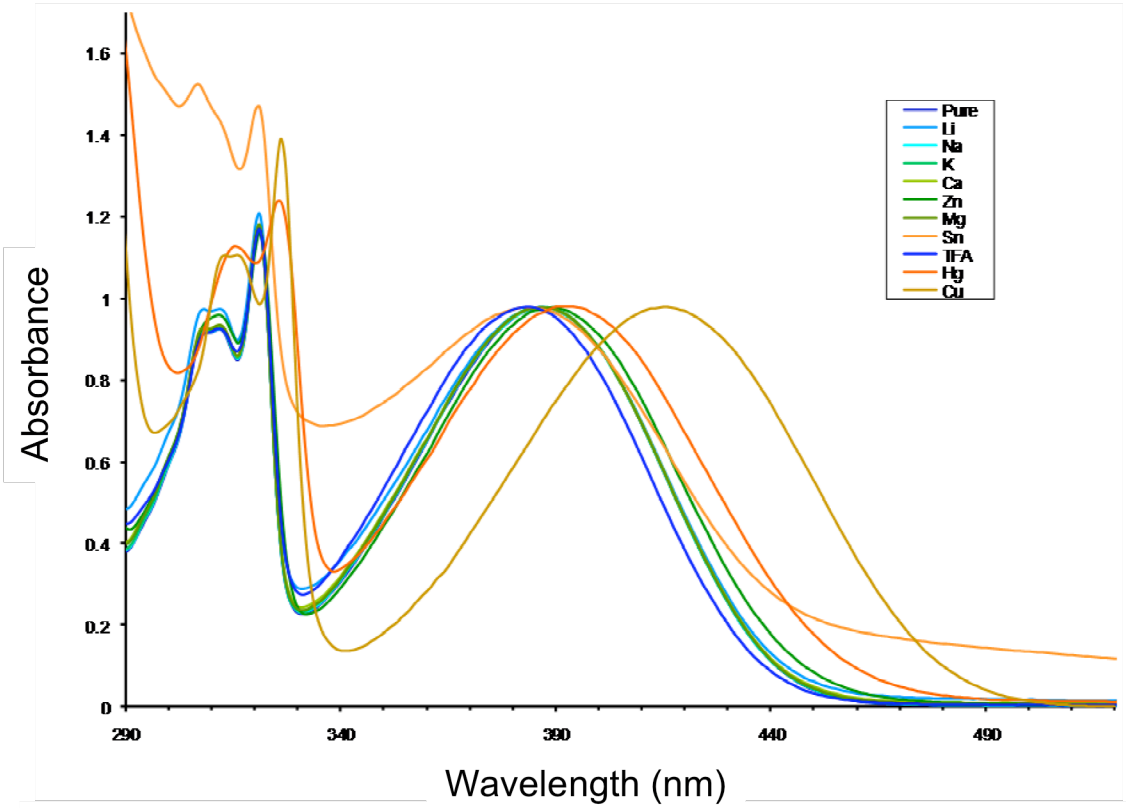

Figure 3.7. Absorption spectra of **3.4** before and after the addition of metal triflates and TFA in water. All fluorophore concentrations were at 89 μM.

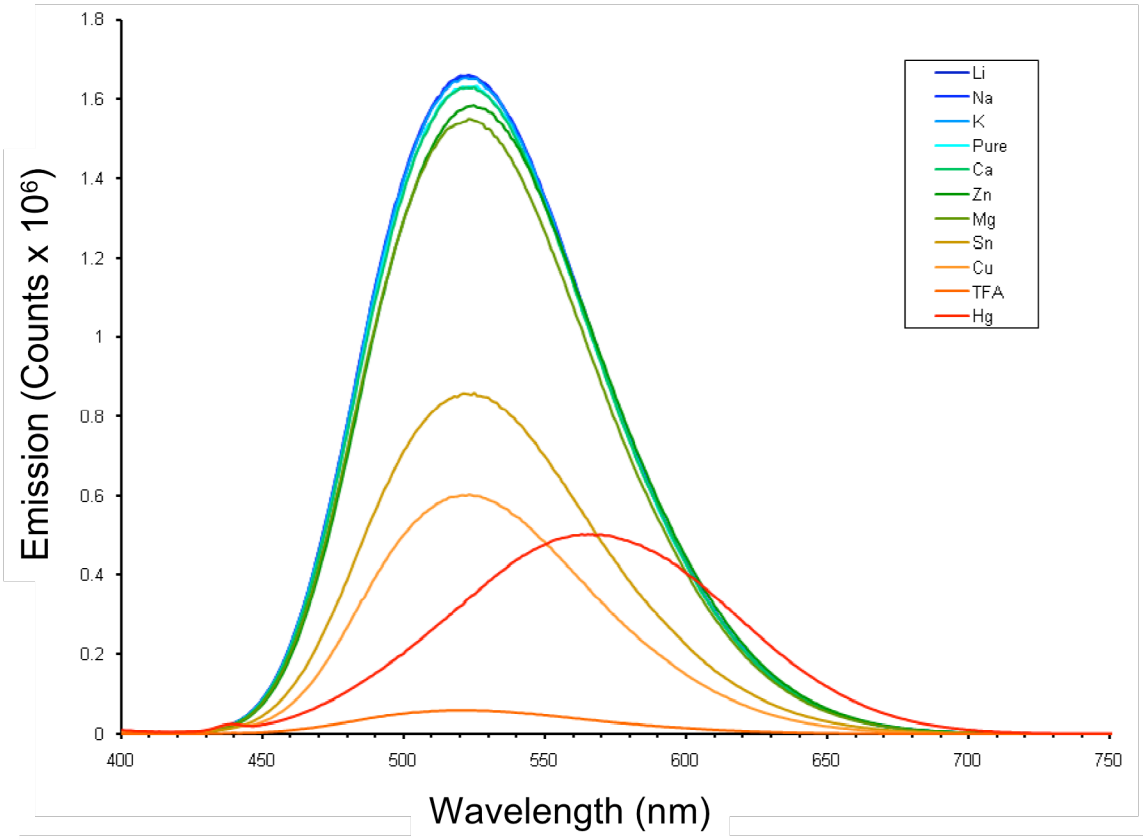

Figure 3.8. Emission spectra of **3.4** before and after the addition of metal triflates and TFA in water. All fluorophore concentrations were at 89 μM.

3.4.5 Stern-Volmer Plots of 3.4 and 3.5

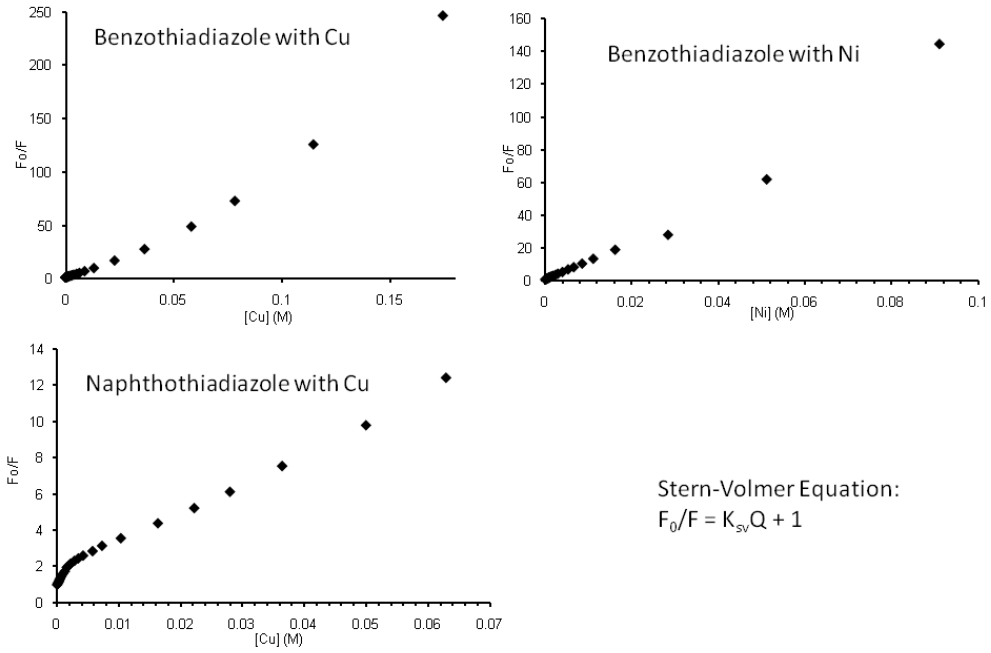

Figure 3.9. Emission quenching data plotted according to the standard Stern-Volmer equation showing the non-linear behavior of the quenching. Compound **3.4** with Cu(II) (Top Left), compound **3.4** with Ni (II) (Top Right), **3.5** with Cu(II) (Bottom Left).

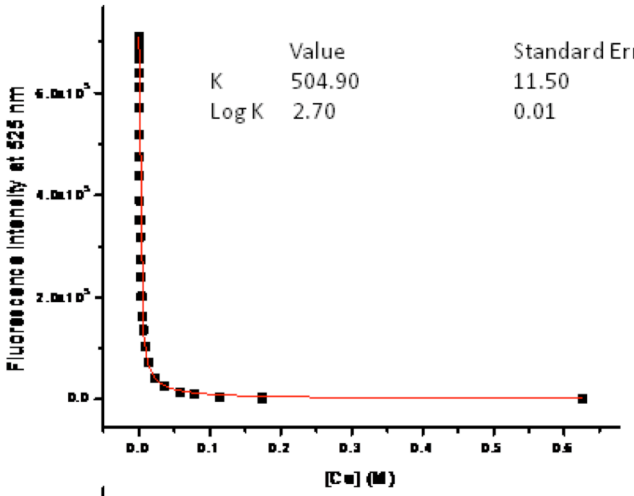

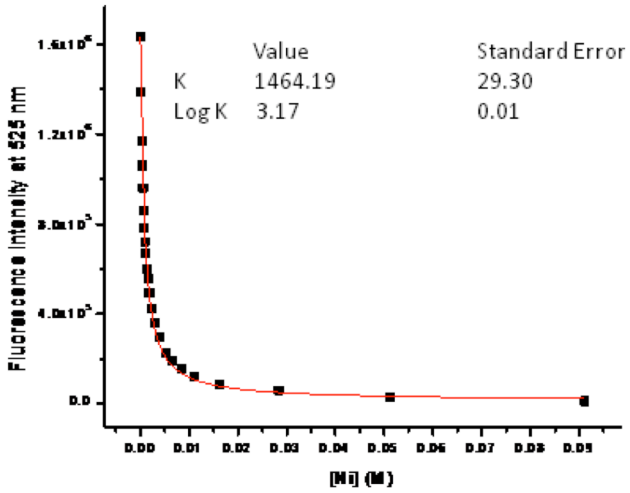

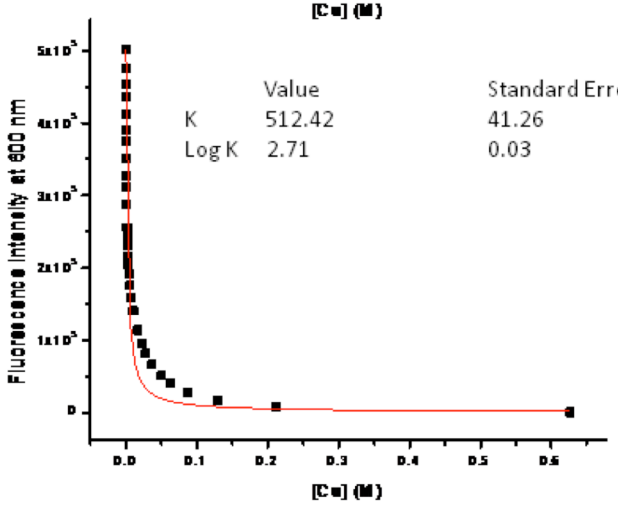

Modified Stern-Volmer Equation:

$$I_g = I_o + \frac{I_{final} - I_o}{2} * \left\{ 1 + \frac{[Q]}{[F]} + \frac{1}{K_{sv}[F]} - \left[\left(1 + \frac{[Q]}{[F]} + \frac{1}{K_{sv}[F]} \right)^2 - 4\frac{[Q]}{[F]} \right]^{\frac{1}{2}} \right\}$$

Figure 3.10. Emission quenching data plotted according to the modified Stern-Volmer equation. Compound **3.4** with Cu(II) (Top Left), compound **3.4** with Ni(II) (Top Right), **3.5** with Cu(II) (Bottom Left).

3.4.6 Absorption and Emission Titrations of 3.4 and 3.5.

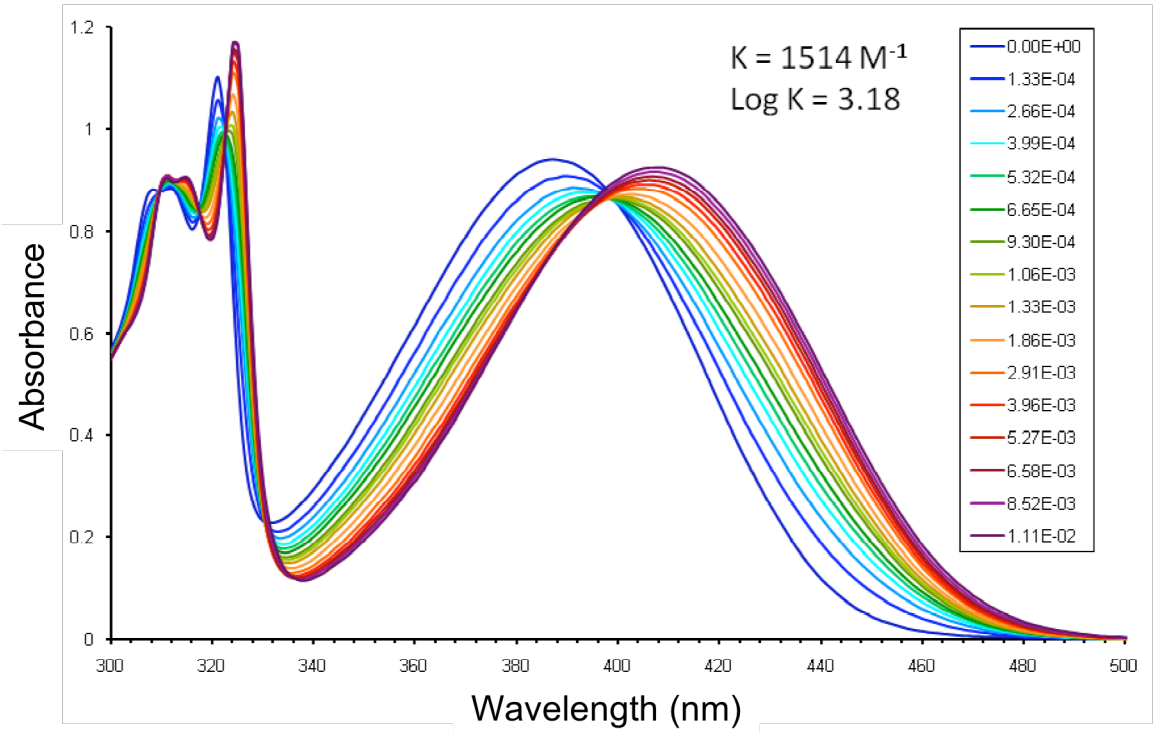

Figure 3.11. Absorption spectra of the titration of **3.4** (151 μM) with $NiSO_4$ in water.

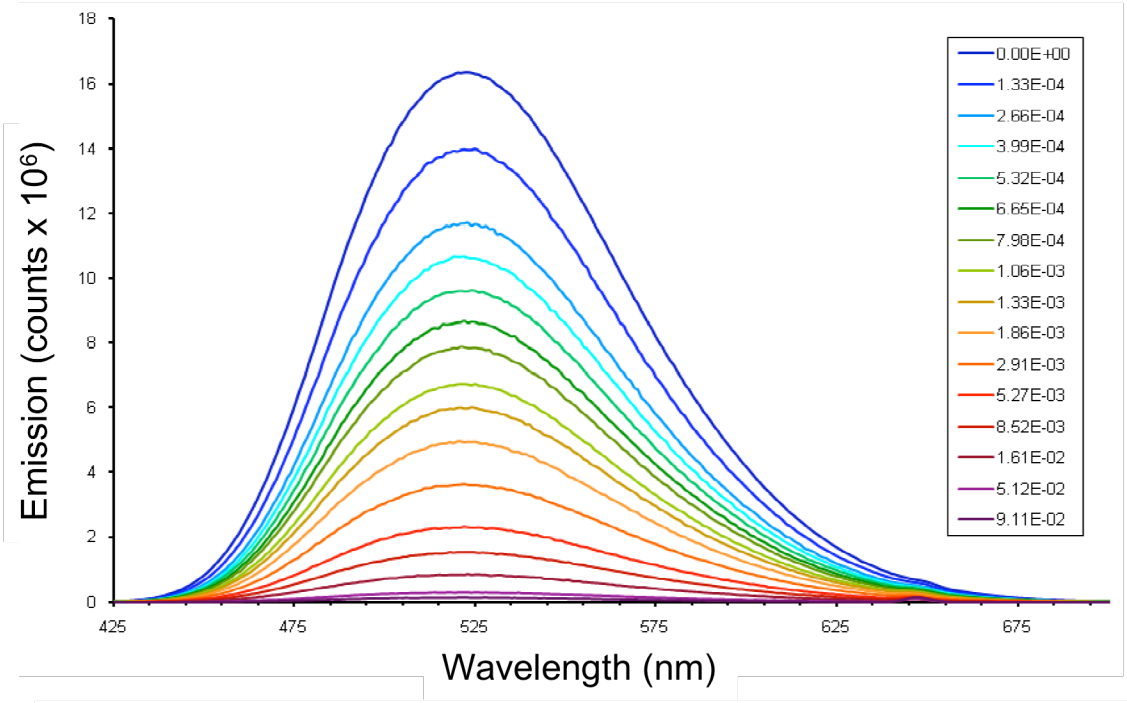

Figure 3.12. Emission spectra of the titration of **3.4** (151 μM) with $NiSO_4$ in water.

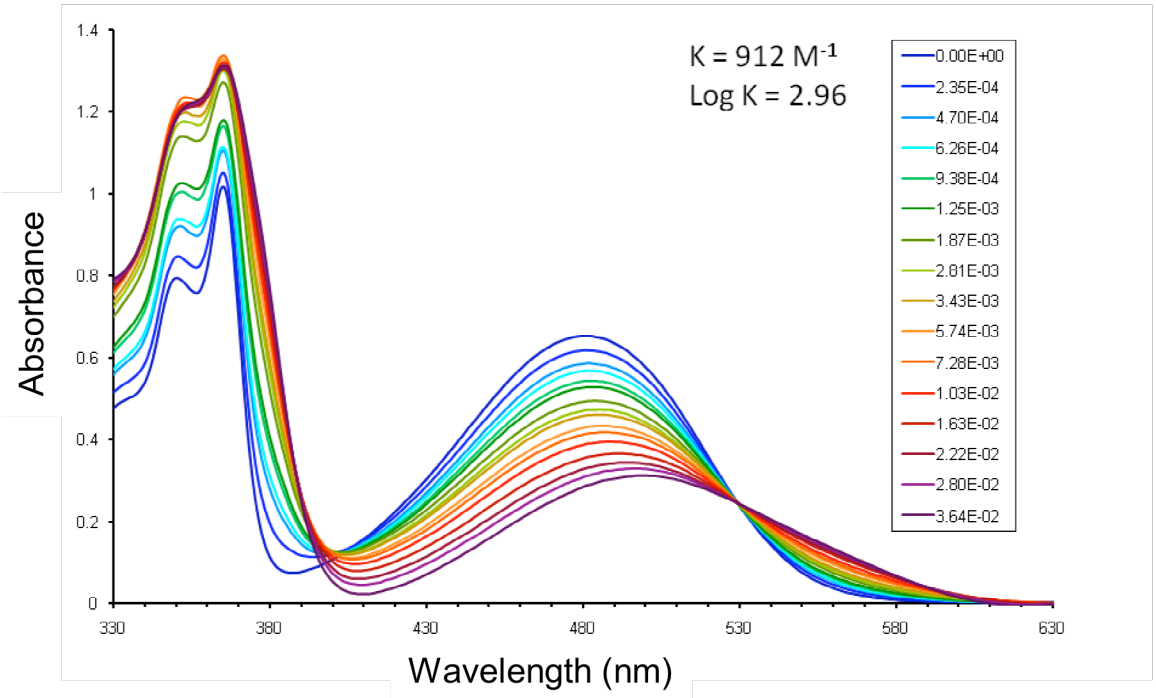

Figure 3.13. Absorption spectra of the titration of **3.5** (166 μM) with $CuSO_4$ in water.

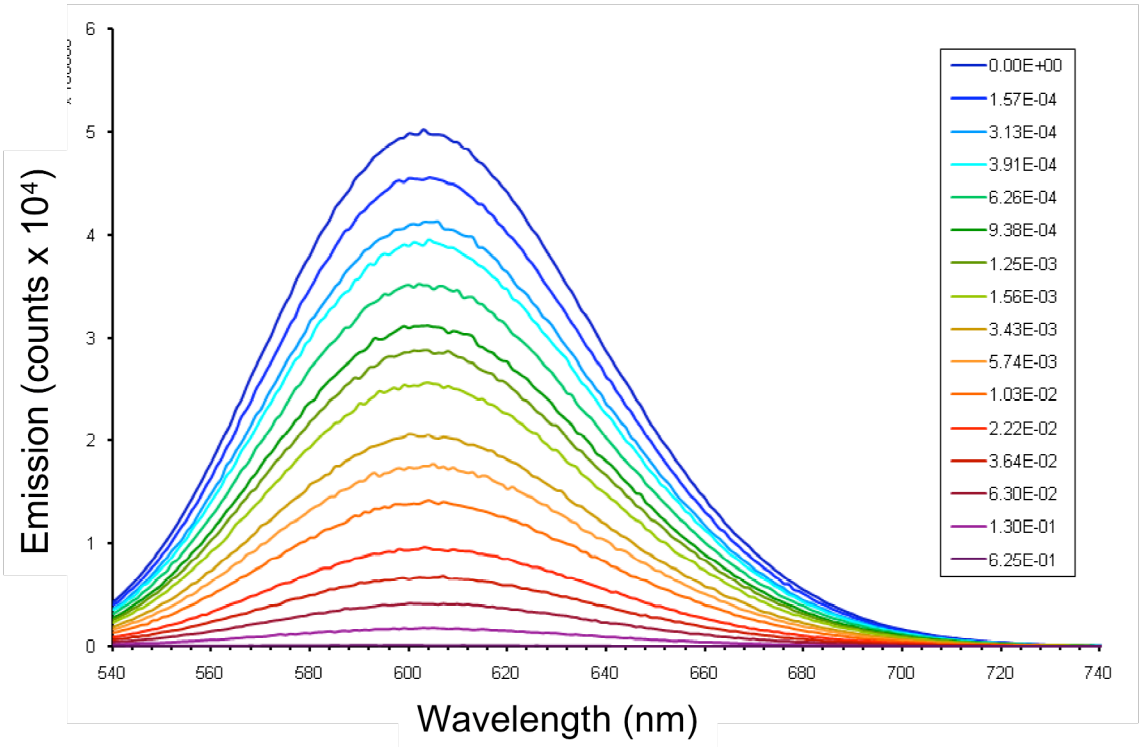

Figure 3.14. Emission spectra of the titration of **3.5** (166 μM) with $CuSO_4$ in water.

3.5 References

[1] [a] R. Huisgen, G. Szeimies, L. Moebius. *Chem. Ber.* **1967**, *100*, 2494. [b] R. Huisgen, R. Knorr, L. Moebius, G. Szeimies. *Chem. Ber.* **1965**, *98*, 4014.

[2] J.F. Lutz. *Angew. Chem.* **2007**, *46*, 1018. [b] W.H. Binder, R. Sachsenhofer. *Macromolecules Rapid Comm.* **2007**, *28*, 15. [c] M. Meldal, C.W. Tornoe. *Chem. Rev.* **2008**, *108*, 2952.

[3] [a] H.C. Kolb, K.B. Sharpless. *Drug Discovery Today.* **2003**, *8*, 1128. [b] R.L. Phillips, I.B. Kim, L.M. Tolbert, U.H.F. Bunz. *J. Am. Chem. Soc.* **2008**, *130*, 6952. [c] R.L. Phillips, I.B. Kim, B.E. Carson, B. Tidbeck, Y. Bai, T.L. Lowary, L.M. Tolbert, U.H.F. Bunz. *Macromolecules.* **2004**, *126*, 3678.

[4] [a] B.C. Engert, S. Bakbak, U.H.F. Bunz. *Macromolecules*. **2005**, *38*, 5868. [b] S. Bakbak, P.J. Leech, B.E. Carson, S. Saxena, W.P. King, U.H.F. Bunz. *Macromolecules.* **2006**, *39*, 6793. [c] B. Erdogan, L.L. Song, J.N. Wilson, J.O. Park, M. Srinivasaro, U.H.F. Bunz. *J. Am. Chem. Soc.* **2004**, *126*, 3678.

[5] J.A. Opsteen, J.C.M. van Hest. *Chem. Comm.* **2005**, 57.

[6] D. Schweinfurth, K.I. Hardcastle, U.H.F. Bunz. *Chem. Comm.* **2008**, 2203.

[7] [a] J.N. Wilson, U.H.F. Bunz. *J. Am. Chem. Soc.* **2005**, *127*, 4124. [b] A.J. Zucchero, J.N. Wilson, U.H.F. Bunz. *J. Am. Chem. Soc.* **2006**, *128*, 11872. [c] J. Tolosa, A.J. Zucchero, U.H.F. Bunz. *J. Am. Chem. Soc.* **2008**, *132*, 6498.

[8] [a] X.Y. Wang, A. Kimyonok, M. Weck. *Chem. Comm.* **2006**, 3933. [b] B. Happ, C. Friebe, A. Winter, M.D. Hager, R. Hoogenboom, U.S. Schubert. *Chem. Asian J.* **2009**, *4*, 154.

[9] C.G. Bungcuyo, U. Evans, M.L. Myrick, U.H.F. Bunz. *Macromolecules*. **2001**, *34*, 7592.

[10] J.R. Lakowicz. Principles of Fluorescence Spectroscopy. Springer, New York, NY, 3rd Edition, 2006, 11.

[11] J.A. Gonzalez, E. Lukovi, B. Imperiali. *J. Org. Chem.* **2009**, *74*, 7309.

[12] S. Maisonneuve, Q. Fang, J. Xie. *Tetrahedron.* **2008**, *64*, 8716.

[13] R.L. Phillips, O.R. Miranda, D.E. Mortenson, C. Subramani, V.M. Rotello, U.H.F. Bunz. *Soft Matter.* **2009**, *5*, 5042.

[14] http://www.iss.com/products/components/datan/.

[15] IUPAC Compendium of Chemical Terminology 2nd Edition, 1997. Accessed on the web October 28, 2010.

CHAPTER 4

6,13-DIETHYNYL-5,7,12,14-TETRAAZAPENTACENE

4.1 Introduction

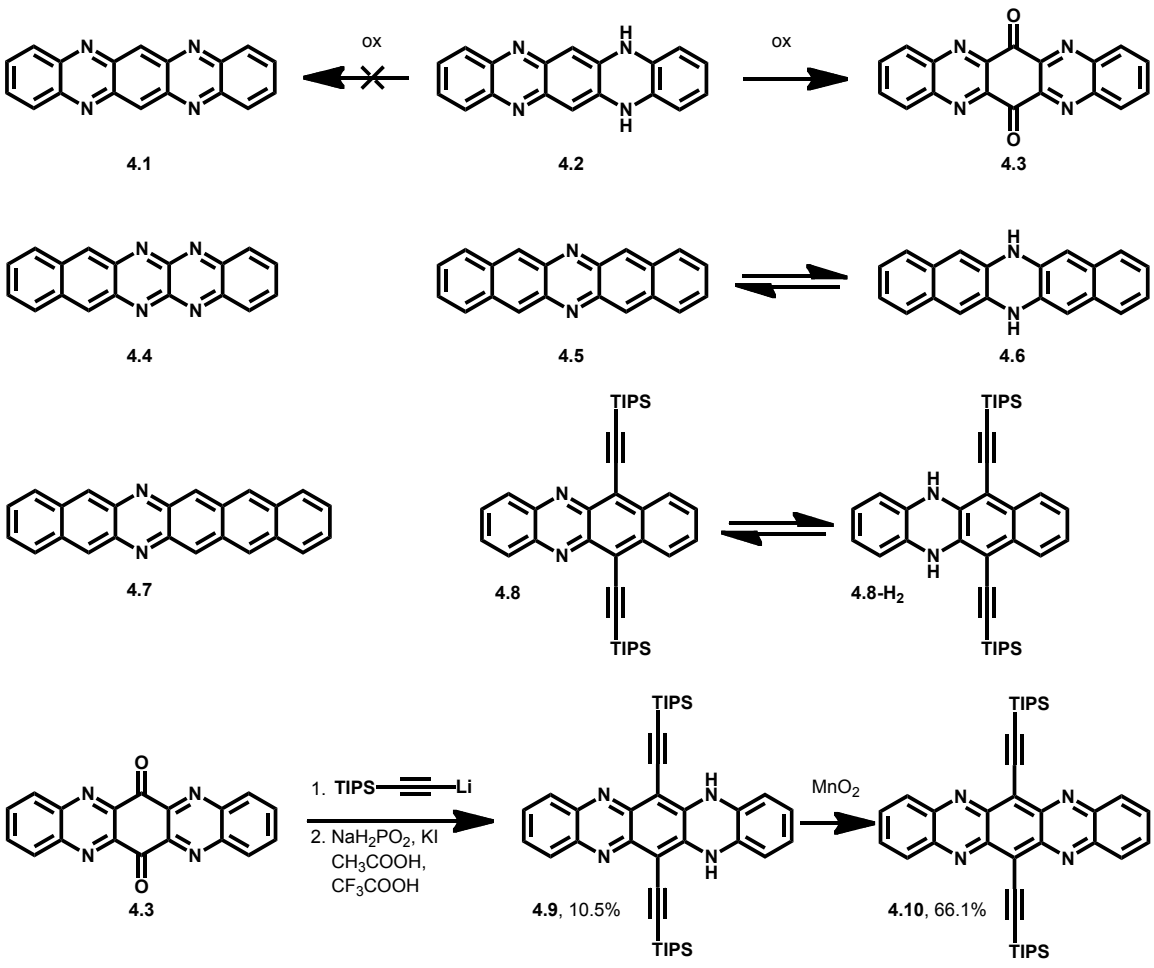

Scheme 4.1. Historical molecules of the azaacene family and synthesis of **4.9** and **4.10**.

We report the synthesis and properties of the first soluble, solution-processible and stable tetraazapentacene (**4.10**). The larger acenes are important in organic

electronics and pentacene has shown excellent hole mobility values, widely used in organic thin-film transistors.[1] As of July 2010, around 3500 scientific articles cover the topic of "pentacene."[2] Studies of morphology, film formation, charge-carrier mobility, and use in organic electronic devices are prevalent. Most investigations have focused on unsubstituted pentacene. However, protection of the 6 and 13 positions prevents oxidation and leads to air-stable pentacenes; suitable substituents in these two positions can also provide soluble derivatives, as shown by Anthony et al. who have reported the synthesis of doubly trialkylsilylethynyl-substituted tetracenes, pentacenes, hexacenes, and heptacenes.[3] While the chemistry and physics of pentacene and its derivatives have received much attention, and some thia-[4] and dioxane-type annelated representatives have been produced,[5] the chemistry and application of aza-pentacenes is essentially unexplored,[6] despite the fact that this class of molecules could be potentially attractive as electron-transporting materials in organic electronic devices.[7]

To understand the dearth of aza-pentacene derivatives, a glimpse into history is instructive. In 1901, Hinsberg (and before him Hepp and Fischer) described fluoroindine (**4.2**).[8] Attempts to oxidize **4.2** were unsuccessful (Scheme 4.1), but Dutt claimed that the condensation of 2,3-diamnophenazine with 1,2-benzoquinone gave **4.1**.[9] However, Dutt had, in fact, obtained **4.3** instead of **4.1**, as demonstrated by the independent synthesis of **4.3** via oxidation of **4.2** by Petit and Badger.[10] Kummer and Zimmermann described the oxidation of the NH precursors of **4.4** and **4.5** by either *o*-chloranil or by a lead dioxide slurry.[11] While **4.4** and **4.5** appear stable, the authors only reported electronic spectra that showed a structured absorption around 625-677 nm. Fluorescence was not observed, but the limited solubility of **4.4** and **4.5** was mentioned as they were recrystallized from

pyridine. The synthesis of larger diazaacenes (i.e. diazahexacene, **4.7**) was unsuccessful by this method.

The presence of electronegative nitrogen atoms in **4.1**, **4.4** and **4.5** should allow for increased ionization potentials and electron affinities relative to pentacene, while their isoelectronic π-systems suggest the possibility of similar solid-state intermolecular interactions promoting charge-carrier mobilities. Indeed, these materials may potentially function as electron-transport analogues of pentacene, which would be of great interest for applications in organic electronics.[12] Nuckolls described the successful use of the dihydro compound **4.6** as a hole-transport material for the fabrication of field-effect transistors with large on/off ratios but low (10^{-4} $cm^2V^{-1}s^{-1}$) hole mobility values; **4.6** is instrinsically electron-rich, as it is a diarylamine-derivative.[13]

4.2 Results and Discussion

To obtain soluble (and thus characterizable and potentially solution-processible) derivatives of **4.1**, we reacted the dione **4.3**[8] with the anion of TIPS-acetylene. The intermediate diol was then, without further purification, dissolved in acetic acid and trifluoroacetic acid to which NaH_2PO_2 and KI were added (Scheme 4.1). Workup and chromatography furnished **4.9** in 22% yield, which forms bright orange solutions that fluoresce green-yellow. In its IR spectrum, a prominent NH stretch appears at 3380 cm^{-1}. The ^1H NMR spectrum of **4.9** displays two sets of AA'BB' systems for the two inequivalent terminal aromatic rings and a broad singlet for the NH protons, all in agreement with the proposed structure and inconsistent with other tautomers.

Oxidation of **4.9** to **4.10** proceeds smoothly if manganese dioxide is used, and the tetraazapentacene **4.10** is isolated as dark blue crystalline material in 60% yield.

Solutions of **4.10** are blue-green and display a faint, deep-red fluorescence. Upon oxidation, the NH stretch of **4.9** disappears (Figure 4.1). Additional structural evidence comes from the ^{1}H NMR spectrum, where the signal from the NH protons of **4.9** (7.1 ppm) are no longer observed upon formation of **4.10** and the remaining aromatic signals are downfield shifted relative to the aromatic peaks in **4.9** (Figure 4.2).

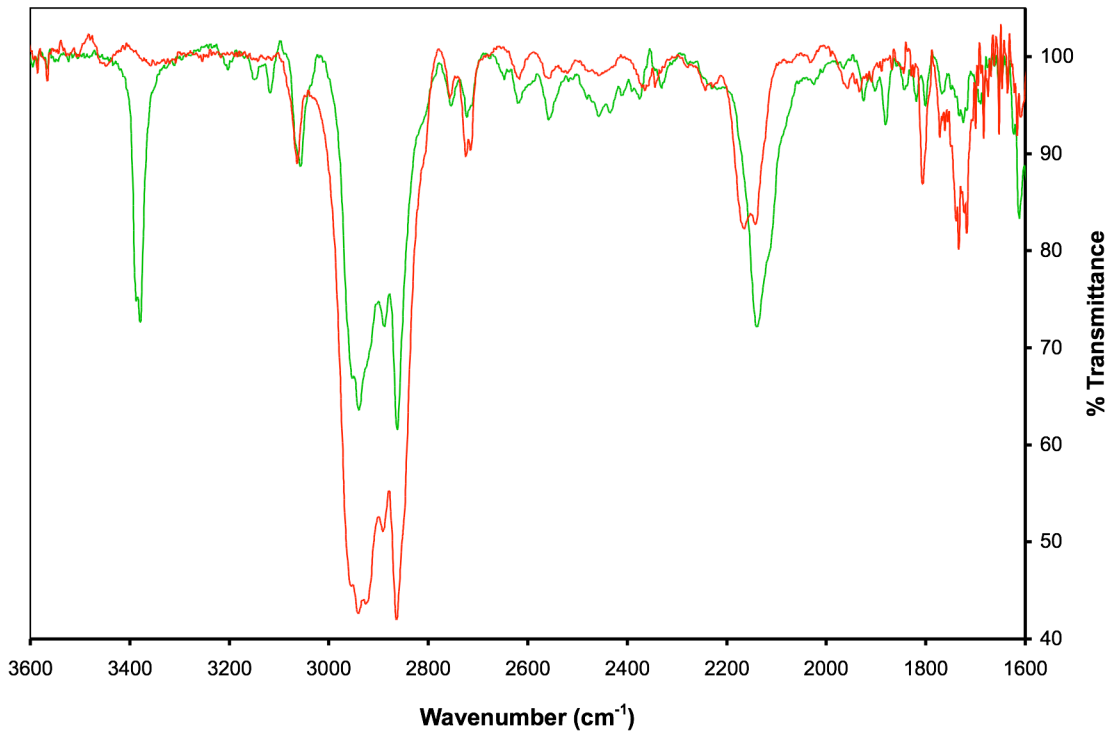

Figure 4.1. IR spectra of **4.9** (green) and **4.10** (red).

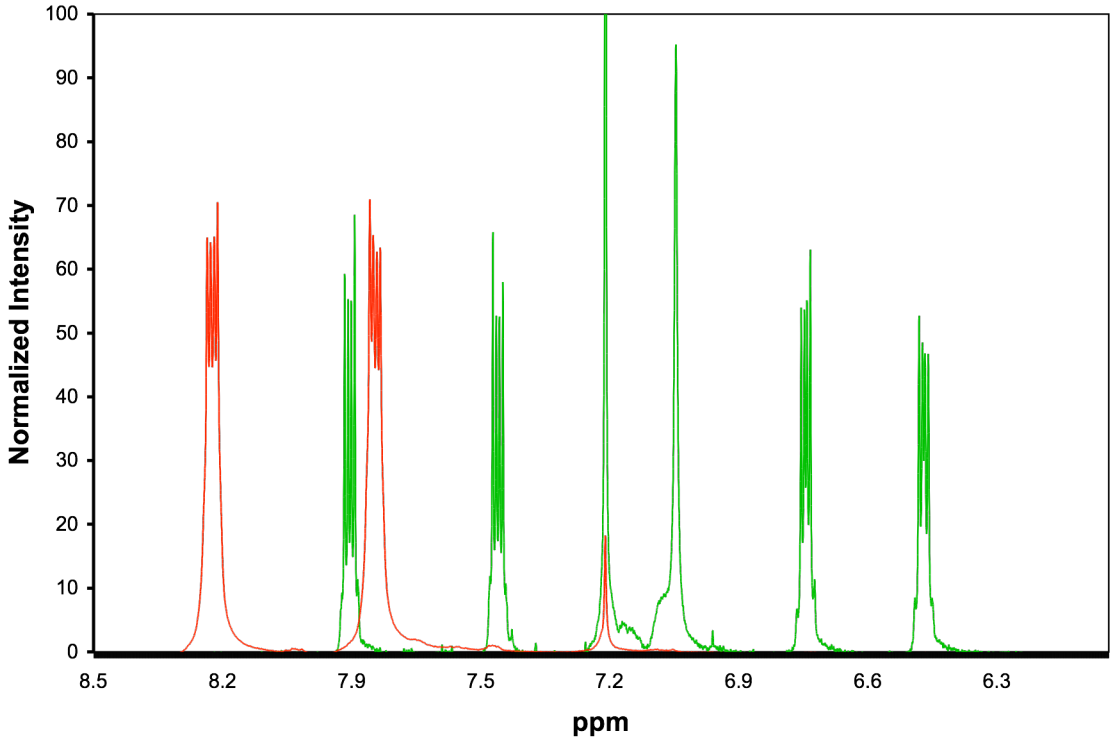

Figure 4.2. Aromatic region of the ^{1}H NMR spectra of **4.9** (green) and **4.10** (red).

Upon oxidation of **4.9** into **4.10**, a bathochromic shift of the absorption from 521 nm to 681 nm results (160 nm, 4500 cm^{-1}), while the emission also shows a bathochromic shift from 525 nm to 694 nm (169 nm, 4600 cm^{-1}) (Figure 4.3). The Stokes shifts are small in both cases, a testament of the rigid character of **4.9** and **4.10**. Quantum chemical calculations were performed by DFT using the B3LYP method with the 6-31G**//6-31G** basis set on model compounds **4.9a** and **4.10a** (Table 4.1) by Prof. Bunz. The computational results are consistent with the optical H-L gaps determined by spectroscopy.

To put these values in perspective with currently utilized molecules, we also performed calculations on compound **4.11** and pentacene (Table 4.1). Compound **4.10a**

has stabilized HOMO and LUMO energies as compared to the analogous pentacene derivative **4.11**. For computational reasons, we substituted trimethylsilyl (TMS) groups

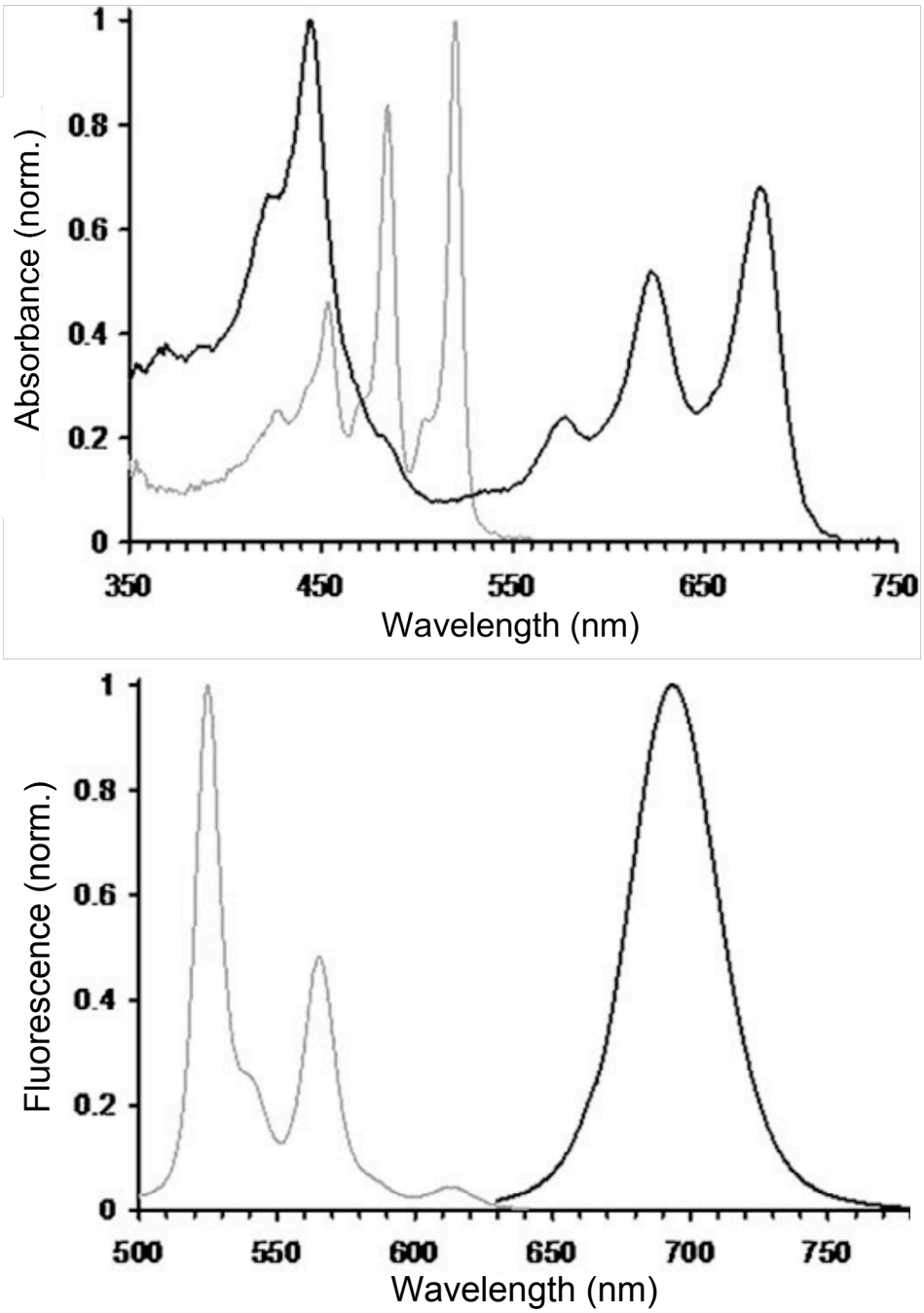

Figure 4.3. UV-vis (top) and fluorescence (bottom) of **4.9** (grey) and **4.10** (black); both spectra have been normalized.

Table 4.1. Quantum chemical calculations were performed using SPARTAN 08/Windows by DFT method using the B3LYP functional with the 6-31G**//6-31G** basis set on model compounds **4.9a**, **4.10a**, **4.11**, and pentacene (Prof. Bunz). [a] calculated from λ_{max} of absorption. [b] J.E. Anthony et al. *J. Am. Chem. Soc.* **2001**, *123*, 9482. [c] N. Nijegorodov et al. *Spectrochim. Acta Part A.* **1997**, *53*, 1813.

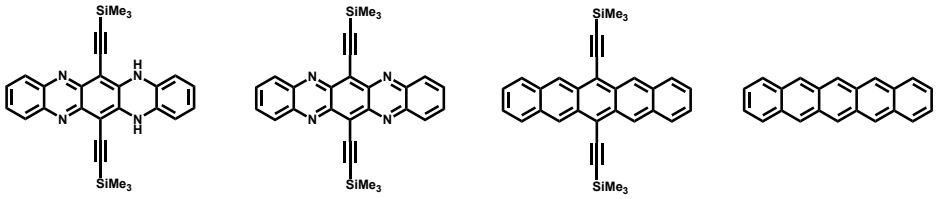

Compound	**4.9a**	**4.10a**	**4.11**	pentacene
HOMO (eV)	-4.93	-5.29	-4.61	-4.60
LUMO (eV)	-2.14	-3.43	-2.71	-2.39
H-L Gap (eV)	2.79	1.86	1.90	2.21
Optical Gap (eV)	2.37[a]	1.82[a]	1.92[b]	2.11[c]

for triisopropylsilyl (TIPS) groups, which should not have any effect on the electronic character of these species. The calculated HOMO and LUMO energies and HOMO-LUMO gap are shown in Table 4.1, along with experimental optical gaps. The acenes **4.10** and **4.11** display almost an identical HOMO-LUMO gap and optical gap, but the positions of the frontier molecular orbitals (FMO) are approximately 0.7 eV lower in **4.10a** than in **4.11**. The formally antiaromatic **4.9a** displays a HOMO energy that is positioned between that of **4.10a** and **4.11** according to the calculations, while its LUMO energy is even higher than that calculated for **4.11** leading to a larger calculated HOMO-LUMO gap and significant hypsochromic shift in its λ_{max} compared to **4.10** and **4.11**.

The calculations suggest that **4.10** could be a potential electron-transporting version of **4.11**. To obtain more information, Dr. Steve Barlow performed cyclic voltammetry (Figure 4.4) in deoxygenated THF / 0.1 M $^{n}Bu_4NPF_6$ solutions using ferrocene as an internal reference. Compound **4.10** undergoes two successive reductions:

a reversible reduction at a half-wave potential, $E_{1/2}$, of -0.79 V followed by a less reversible reduction characterized by a peak potential, E_{red}, of -1.23 V. Voltammograms of **4.10** are qualitatively similar to those of the related azaacene, **4.8**;[14] however, each reduction occurs at considerably less reducing potential than the corresponding reductions of **4.8** ($E_{1/2,0/-1}$ = -1.23 V and $E_{1/2,-1/-2}$ = -1.78 V). This reflects the roles of both the larger π-system and the presence of additional electronegative nitrogen atoms lowering the energy of the LUMO. Compound **4.9** undergoes an irreversible oxidation (E_{ox} = +0.32 V) at slightly more oxidizing potential than the similar irreversible oxidation of the related dihydroazaacene **4.8-H$_2$** (E_{ox} = +0.19 V), also a result of the additional electronegative nitrogen atoms. However, while no reduction processes could be detected for **4.8-H$_2$**, **4.9** shows an irreversible reduction at E_{red} = -1.82 V. The difference between the reduction potentials of **4.9** and **4.10** are consistent with the LUMO energy differences as suggested by the computational data.

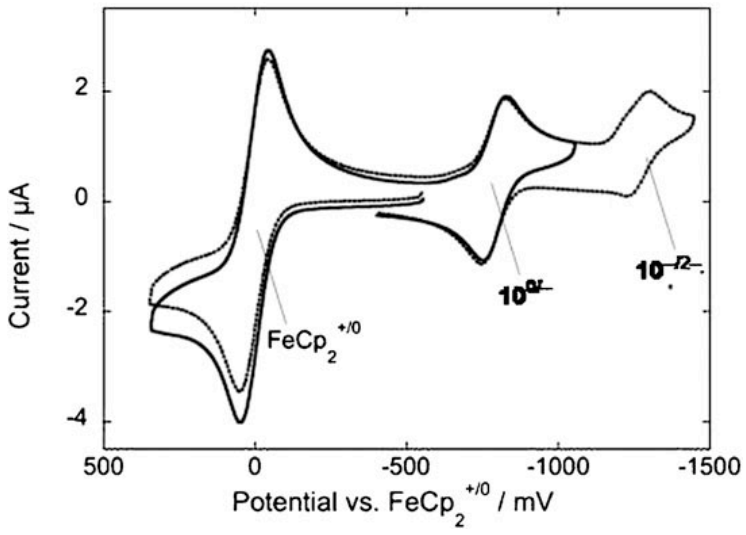

Figure 4.4. Cyclic voltammogram of **4.10**.

The X-ray single-crystal structure (Figure 4.5) of **4.10** displays a brick wall-type packing motif. The unit cell of **4.10** is very similar to that of TIPS-pent published by Anthony et al.[3c] However, the distance between the planes of stacked molecules of **4.10** is only 3.3 Å, 0.1 Å closer than that found for TIPS-pent. This is a testament to the reduced repulsive interactions in electron-poor acenes, which has also been observed in related fluorinated species.[5]

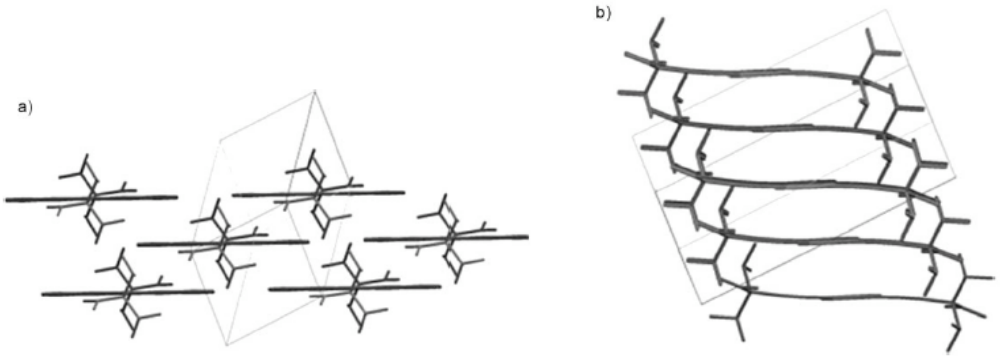

Figure 4.5. Crystal structure of tetraazapentacene **4.10**. a) View of the packing along the *b* and *c* axes (left). b) View of the packing along the "vertical" axis, which does not correspond to any crystallographic axis (right).

4.3 Conclusions

In conclusion tetraazapentacene **4.10**, was synthesized and isolated as an ambiently stable, organosoluble material. While the solid-state structure of **4.10** is similar to that of TIPS-pent, its electrochemistry shows facile reducibility due to a stabilized LUMO according to computational studies, which suggests that it could be utilized in organic devices as an electron-transporting material.

Dr. Shaobin Miao began the synthesis for this project, but I took over when he left for Augusta State. I was in charge of all characterization except where noted

This work has been published in *Chemistry A European Journal*:

Shaobin Miao, Anthony Lucas Appleton, Nancy Berger, Stephen Barlow, Seth R. Marder, Kenneth I. Hardcastle, Uwe H.F. Bunz. *Chem. Eur. J.* **2009**, *15*, 4990.

This work has been highlighted in Synfacts:

Timothy M. Swager, Trisha L. Andrew. *Synfacts.* **2009**, *8*, 0857.

4.4 Experimental Information

4.4.1 6,13-bis(triisopropylsilylethynyl)-5,14-dihydroquinoxalino[2,3-*b*]phenazine 4.9. To an oven-dried Schlenk flask was added triisopropylsilylacetylene (0.60 mL, 2.67 mmol) and dry THF (10 mL), followed by *n*-butyllithium (1.20 mL, 1.6 M in hexanes, 1.92 mmol), at 0 °C. The solution was stirred at room temperature for 1 h, and then compound **4.3**[10] (0.200 g, 0.640 mmol) was added. The mixture was allowed to stir for 12 h and then quenched with wet ethyl ether. After the solvent was removed *in vacuo*, the residue was filtered over silica gel using hexane/ethyl acetate (5:1 *v/v*) to yield the corresponding diol. After the solvent was removed *in vacuo*, the crude diol was, without further characterization, suspended in acetic acid (20 mL) with KI (1.00 g, 6.02 mmol) and NaH_2PO_2 (0.530 g, 6.02 mmol) with 1 mL of trifluoroacetic acid. The mixture was heated to reflux for 45 min. After cooling to room temperature, water (100 mL) and triethylamine (2.0 mL) were added to the mixture, which was extracted with dichloromethane (3 x 100mL). The combined organic layers were dried *in vacuo*. The solids were purified by column chromatography on silica gel using hexane/dichloromethane (1:1 *v/v*) solvent mixture. Compound **4.9** (43.2 mg, 22%, 10.5% yield over two steps, starting from **4.3**) was isolated as red-orange crystals. m.p. = 280 °C; ^{1}H NMR (400 MHz, δ in $CDCl_3$) 7.90 (AA' of AA'BB', 2H), 7.52 (BB' of AA'BB', 2H), 7.80 (s, 2H), 6.77 (BB" of AA"BB", 2H), 6.49 (AA" of AA"BB", 2H), 1.255 ppm (m, broad 42H); ^{13}C NMR (100 MHz, δ in $CDCl_3$) 143.6, 142.0, 139.7, 128.9, 128.2, 128.1, 123.3, 113.8, 104.5, 99.5, 96.8, 18.9, 11.4 ppm; IR (KBr, cm^{-1}) 3380, 2939, 2862, 2140, 1576, 1451, 1311, 1226, 1015, 881, 749, 723; Accurate mass calcd for $C_{40}H_{52}N_4Si_2$: *m/z* = 644.37305, found: *m/z* = 644.37270 [M+].

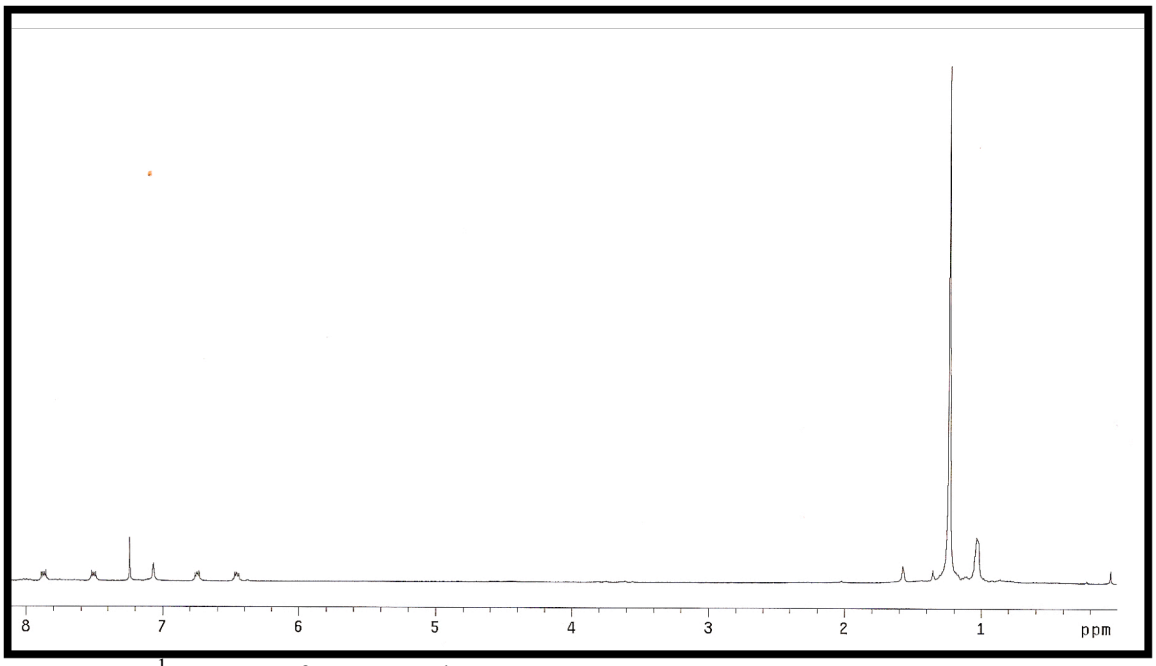

Figure 4.6. ^{1}H NMR of compound **4.9**.

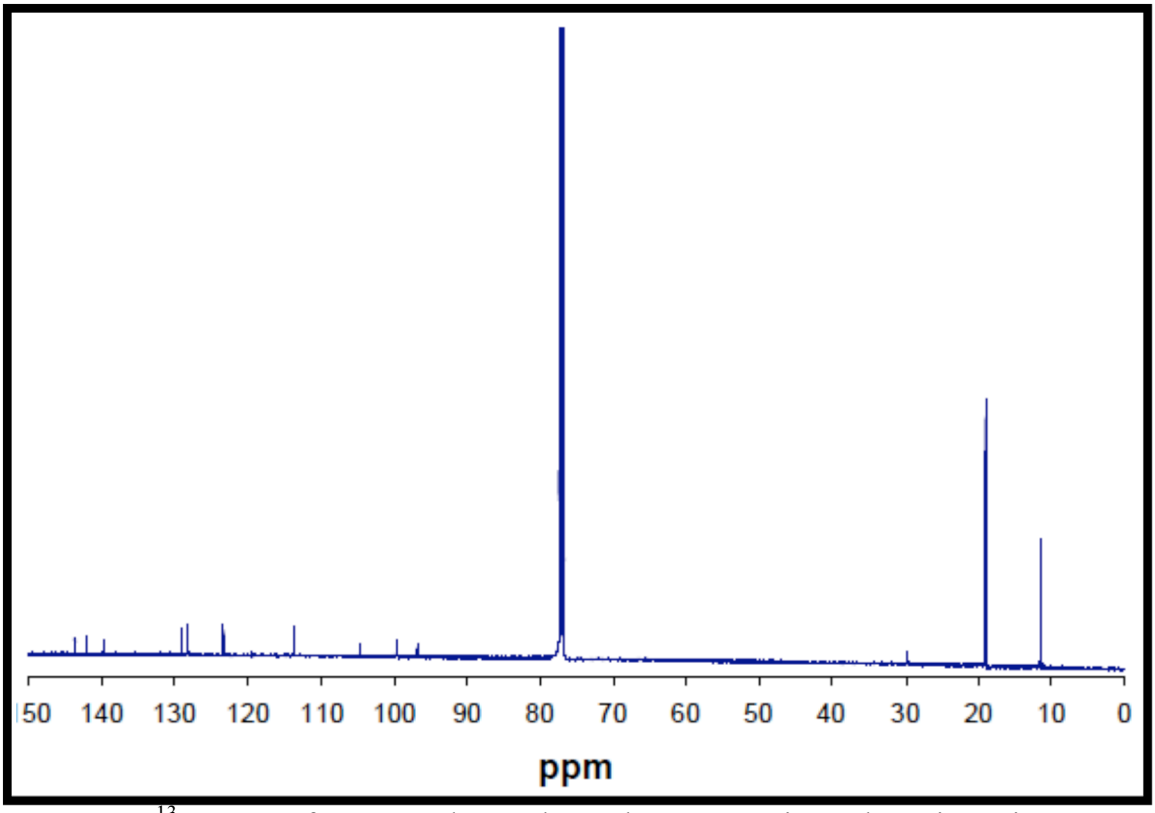

Figure 4.7. ^{13}C NMR of compound **4.9**. The peak at 30 ppm is a solvent impurity.

4.4.2 6,13-bis(triisopropylsilylethynyl)quinoxalino[2,3-b]phenazine 4.10.

In a 100 mL flask, 4.9 (90 mg) was dissolved in dichloromethane (30 mL) and MnO_2 was added in excess (2.0 g). The solution was allowed to stir at ambient conditions for 4 h. After the MnO_2 was filtered off, the solvent was removed *in vacuo*. The solids were purified by column chromatography on silica gel using hexane/dichloromethane (1:1 *v/v*) solvent micture. Compound **4.10** (59.3 mg, 66.1%) was isolated as dark blue crystals. m.p. = 222-224 °C (decompose). ^{1}H NMR (400 MHz, δ in $CDCl_3$) 8.22 (AA' of AA'BB', 4H), 7.8 (BB' of AA'BB', 4H), 1.365 (m, broad, 42H); ^{13}C NMR (100 MHz, δ in $CDCl_3$) 145.5, 142.8, 132.0, 131.1, 122.9, 112.5, 103.0, 18.9, 11.7 ppm; IR (KBr, cm^{-1}) 2941, 1864, 2164, 1806, 1463, 1382, 1248, 1134, 996, 882, 839, 761, 677; Accurate mass calcd for $C_{40}H_{50}N_4Si_2$: *m/z* = 642.35740, found: *m/z* = 642.35637 [M+].

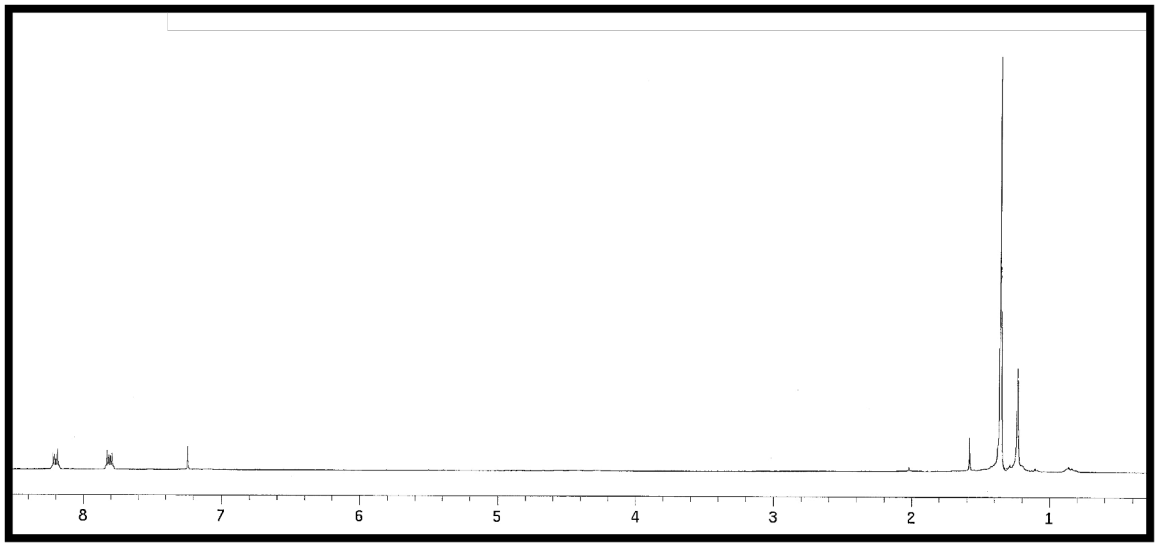

Figure 4.8. ^{1}H NMR of compound **4.10**.

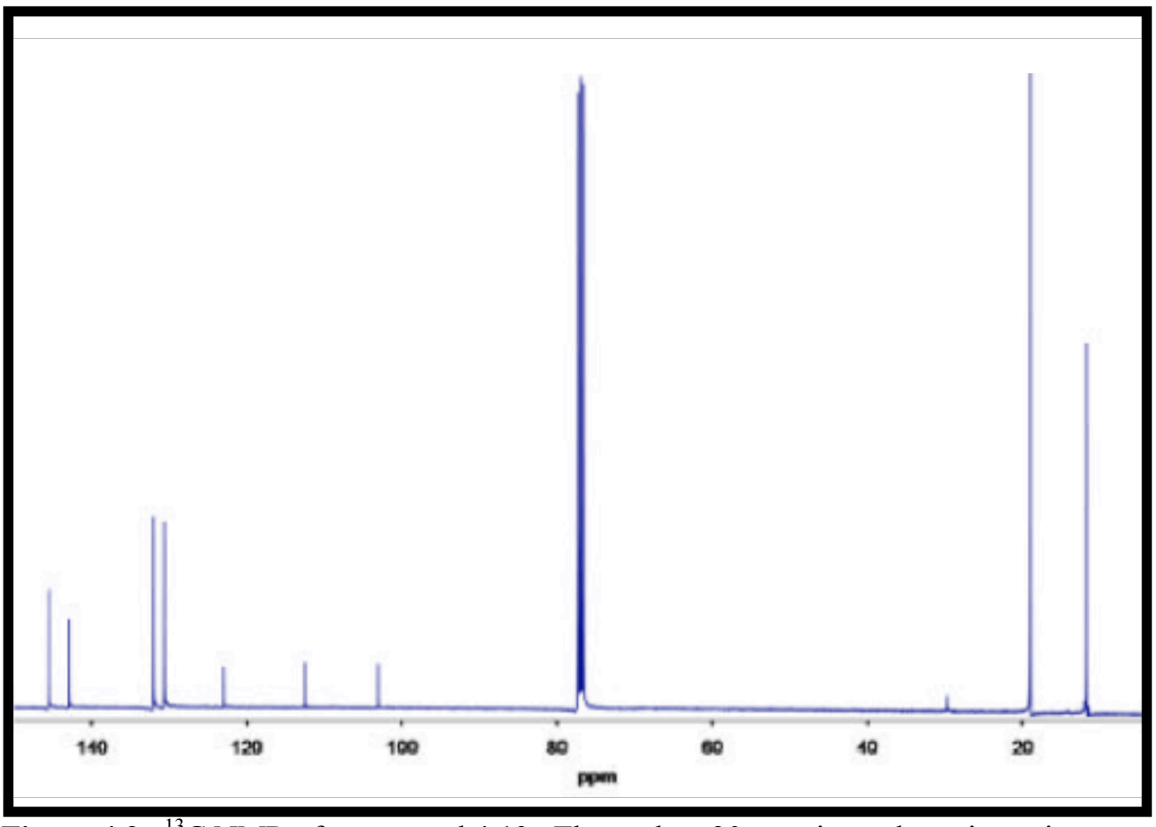

Figure 4.9. ^{13}C NMR of compound **4.10**. The peak at 30 ppm is a solvent impurity.

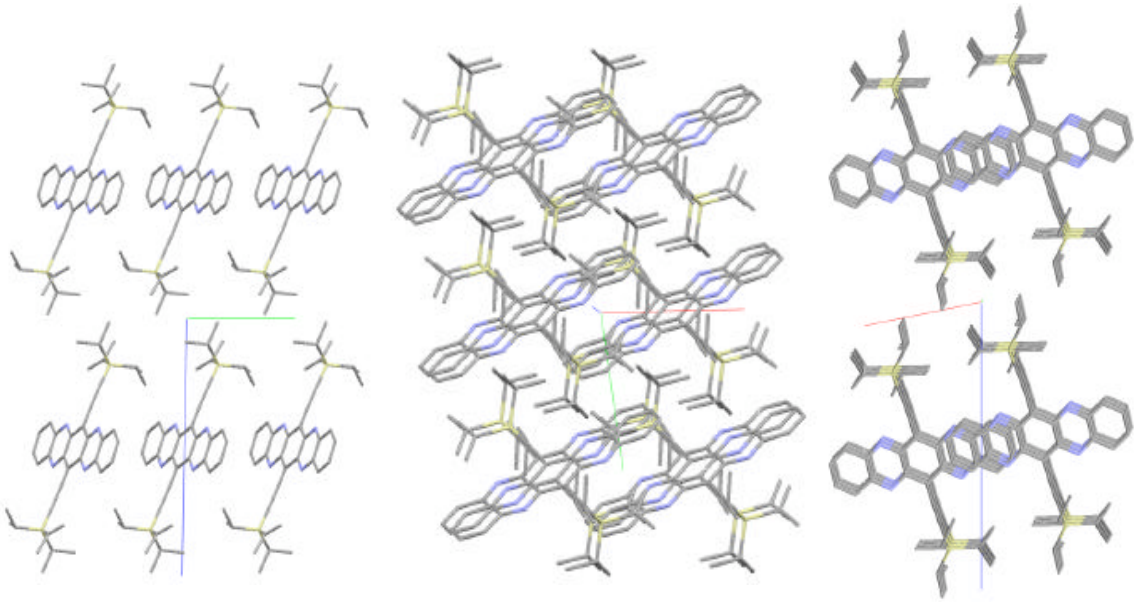

Figure 4.10. X-ray crystal structures of **4.10** along the *a* axis (left), *b* axis (middle), and *c* axis (right).

4.5 References

[1] [a] C.D. Dimitrakopolous, P.R.L. Malenfant. *Adv. Mater.* **2002**, *14*, 99. [b] S.F. Nelson, Y.Y. Lin, D.J. Gundlach, T.N. Jackson. *Appl. Phys. Lett.* **1998**, *72*, 1854. [c] H. Klauk, M. Halik, U. Zschieschang, G. Schmid, W. Ralik, W. Weber. *J. Appl. Phys.* **2002**, *92*, 5259. [d] H.E. Katz, Z. Bao. *J. Phys. Chem. B*. **2000**, *104*, 671. [e] S. Yoo, B. Domercq, B. Kippelen. *Appl. Phys. Lett.* **2004**, *85*, 5427. [f] A.L. Briseno, S.C.B. Mannsfeld. M.M. Ling, S.H. Liu, R.J. Tseng, C. Reese, M.E. Roberts, Y. Yang, F. Wudl, Z. Bao. *Nature.* **2006**, *444*, 913. [g] M. Bendikov, F. Wudl, D.F. Perepichka. *Chem. Rev.* **2004**, *104*, 4891. [h] L.B. Roberson, J. Kowalik, L.M. Tolbert, C. Kloc, R. Zeis, X.L. Chi, R. Fleming, C. Wilkins. *J. Am. Chem. Soc.* **2005**, *127*, 3069.

[2] ISI Web of Knowledge, Thomson Reuters, 2010.

[3] [a] J.E. Anthony. *Angew. Chem.* **2008**, *120*, 460; *Angew. Chem. Int. Ed.* **2008**, *47*, 452. [b] J.E. Anthony. *Chem. Rev.* **2006**, *106*, 5028. [c] J.E. Anthony, J.S. Brooks, E.L. Eaton, S.R. Parkin. *J. Am. Chem. Soc.* **2001**, *123*, 9482. [d] M.M. Payne, S.R. Parkin, J.E. Anthony. *J. Am. Chem. Soc.* **2005**, *127*, 8028. [e] M.M. Payne, S.A. Odom, S.R. Parkin, J.E. Anthony. *Org. Lett.* **2004**, *6*, 3325.

[4] A.L. Briseno, Q. Miao, M.M. Ling, C. Reese, H. Meng, Z. Bao, F. Wudl. *J. Am. Chem. Soc.* **2006**, *128*, 15576.

[5] M.M. Payne, J.H. Delcamp, S.R. Parkin, J.E. Anthony. *Org. Lett.* **2004**, *6*, 1609.

[6] C. Nuckolls, personal communication.

[7] M. Winkler, K.N. Houk. *J. Am. Chem. Soc.* **2007**, *129*, 1805.

[8] [a] O. Fischer, E. Hepp. *Chem. Ber.* **1890**, *23*, 2789. [b] O. Fischer, E. Hepp. *Chem. Ber.* **1900**, *33*, 1485. [c] F. Kehrmann. Chem. Ber. 1890, 23, 2446. [d] O. Hinsberg. *Liebigs Ann. Chem.* **1901**, *319*, 257.

[9] S. Dutt. *J. Chem. Soc.* **1926**, *129*, 1171.

[10] G.M. Badger, R. Petit. *J. Chem. Soc.* **1951**, 3211.

[11] F. Kummer, H. Zimmermann. *Ber. Bensenges. Phys. Chem.* **1967**, *71*, 1119.

[12] [a] F. Wudl, P.A. Koutentis, A. Weitz, B. Ma, T. Strassner, K.N. Houk, S.I. Khan. *Pure Appl. Chem.* **1999**, *71*, 295. [b] A.E. Riley, G.W. Mitchell, P.A. Koutentis, M. Bendikov, P. Kaszynki, F. Wudl, S.H. Tolbert. *Adv. Func. Mater.* **2003**, *13*, 531.

[13] Q. Miao, T.Q. Nguyen, T. Someya, G.B. Blanchet, C. Nuckolls. *J. Am. Chem. Soc.* **2003**, *125*, 10284.

[14] S. Miao, S.M. Brombosz, P.v.R. Schleyer, J.I. Wu, S. Barlow, S.R. Marder, K.I. Hardcastle, U.H.F. Bunz. *J. Am. Chem. Soc.* **2008**, *130*, 7339.

CHAPTER 5

FROM ACENES TO DIAZAACENES:

ENABLING ELECTRONEGATIVE SUBSTITUTION

AS A TOOL FOR ENGINEERING

OPTICAL AND ELECTRONIC PROPERTIES

5.1 Introduction

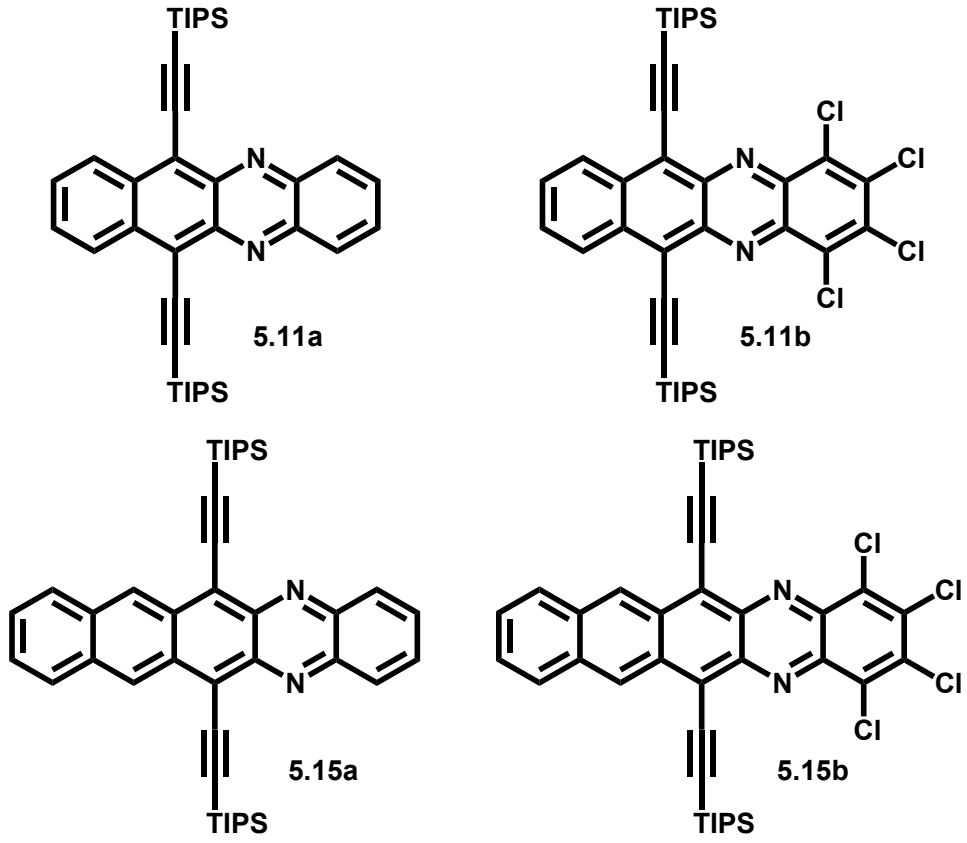

Scheme 5.1 Compounds **5.11a,b** and **5.15a,b**.

The larger acene cores provide an attractive framework for the design of molecules with tunable properties that can be useful for application in organic electronic devices. Pentacenes such as **5.1** or **5.5**, but also **5.2** (first prepared by Hinsberg in 1901[1]), are of interest as hole-transport materials in thin-film transistors[2,3] and have high charge-carrier mobilities due to their favorable solid-state packing and small reorganization energies;[3,4,5] pentacene is also a component of reference systems in the development of small-molecule organic solar cells.[6] While Houk suggested that larger *N*-heteroacenes

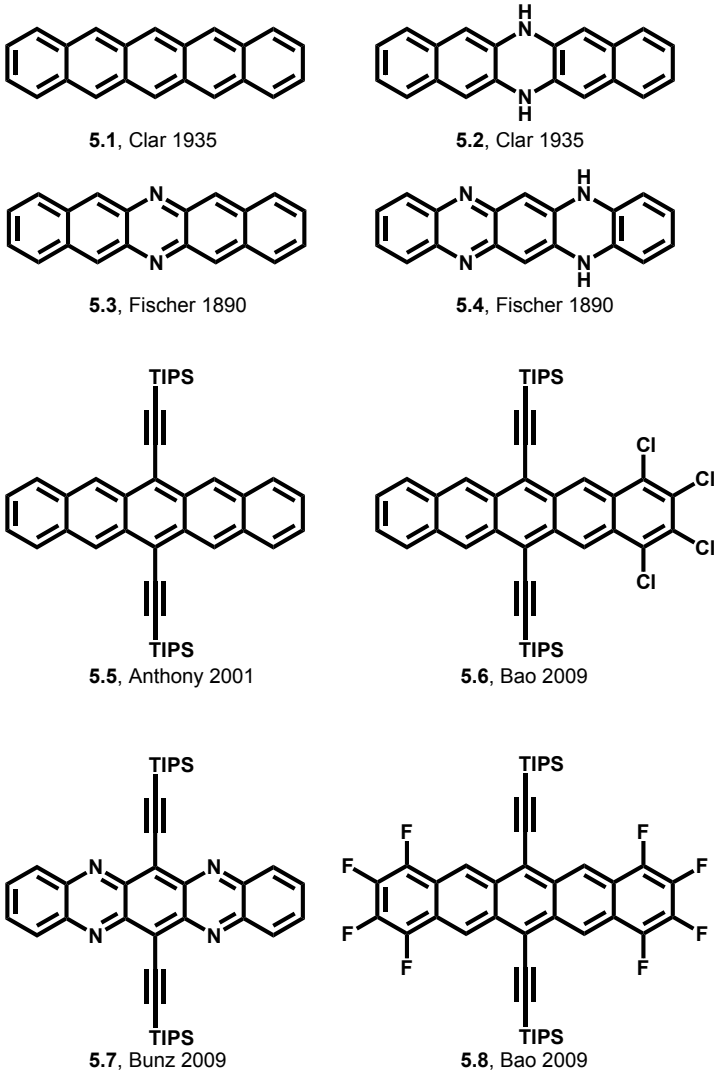

Scheme 5.2. Historical molecules of the acene and heteroacene families.

could behave as electron-transport materials when suitably substituted,[7] to date acenes have generally functioned as hole-transport materials (see section **1.2**). Only a few acenes have exhibited appreciable electron mobilities.[8-11] To realize the full potential of acenes and heteroacenes, it is essential to expand the scope of materials that are available. Scheme 5.2 shows recent and historical members in the pentacene family.[12,13] Chlorinated pentacenes such as **5.6** were processed into a field-effect transistor that showed ambipolar behavior under an inert atmosphere. Chlorination lowers both HOMO and LUMO energies, but with the former effect insufficient to preclude hole-injection, while the latter effect facilitated electron-injection; however, the optical gap does not change to any appreciable extent as both, HOMO and LUMO, are almost equally stabilized.[14] The tetrachloro substitution only led to a slight bathochromic shift in the absorption maximum going from 643 nm for **5.5**[15] to 654 nm for **5.6** in solution, suggesting that chlorine substitution had comparable impact on both the ground and first excited state.[16-19] Lowering the energy required for an electronic transition can be useful in the context of organic solar cells when looking for acene derivatives displaying absorption into the near-IR as observed in Anthony's hexacenes and heptacenes.[20,21]

We report here the synthesis of novel *N*-heteroacenes, i.e. diazapentacene **5.15a**, the tetrahalogenated diazatetracene **5.11b** and the tetrahalogenated diazapentacenes **5.15b,c**. Electronegative substitution, i.e. the transformation of **5.11a** to **5.11b** and **5.15a** to **5.15b,c**, causes significant bathochromic shifts in absorption, in addition to improved reducibility, expected to originate from the greater stabilization of the LUMO as compared to the HOMO of each molecule upon halogenation.[22]

5.2 Results and Discussion

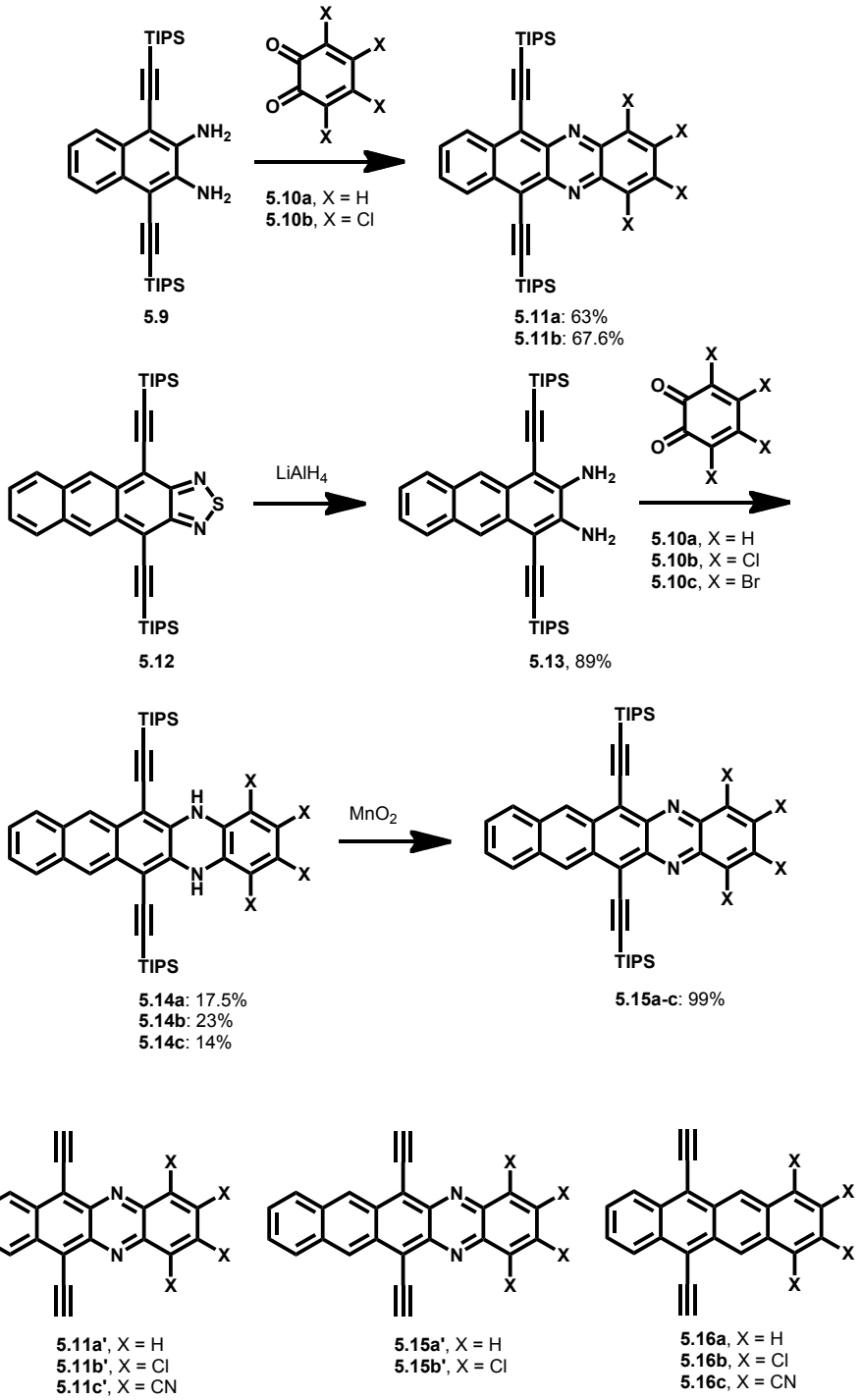

Scheme 5.3. Synthesis of **5.11a,b**, **5.14a-c**, and **5.15a-c**. Depiction of model compounds **5.11a',b'**, **5.15a'-c'**, and **5.16a-c** utilized in the computational studies in order to reduce computing time.

Condensation of **5.9** (Scheme 5.3) with **5.10b** gave tetrachlorodiazatetracene **5.11b** in 68% yield after chromatography. For comparison purposes, we also re-synthesized **5.11a**.[23] The *o*-diamine **5.13** is obtained by lithium aluminum hydride reduction of **5.12**[24] and was reacted with **5.10a-c** to furnish the *N,N*-dihydrodiaza-pentacenes **5.14a-c** in 14-23% yields. It has been noted in the past that the formation of the formally antiaromatic **5.14a-c** (diazapentacene series) occurs, but the same is not observed in the diazatetracene series (**5.11**).[1,25,26] The intermediates **5.14a-c** are oxidized by manganese dioxide to give **5.15a-c** after chromatography as green-black, environmentally stable materials in near quantitative yield.

Figure 5.1 shows the UV-vis absorption spectra in terms of the molar absorption coefficients of compounds **5.11a,b** and **5.15a-c**. The significant bathochromic shift observed when going from **5.11a** to **5.11b** and from **5.15a** to **5.15b,c** is evident in Figure 5.1. While bathochromic shifts have precedence upon substitution of molecules with electronegative groups, the magnitude of the shift of the pairs **5.11a**/**5.11b** (49 nm, 0.17 eV) and **5.15a**/**5.15b,c** (67 nm, 0.16 eV) was unanticipated given the results of Bao et al. upon chlorination of **5.5** to generate **5.6** (11 nm, 0.032 eV).[14] Also of importance, if utilized in an OPV, is how well the azaacene series absorbs light compared to the acenes, which have showed success in organic devices. For the long wavelength λ_{max}, Anthony et al. reported ε = 20,000 (**5.5**), 15,400 (**5.5-F$_4$**), 13,100 (**5.8**) $cm^{-1}M^{-1}$.[15] Comparatively, we found that ε = 22,694 (**5.11a**), 17,227 (**5.11b**), 19,092 (**5.15a**), 12,863 (**5.15b**), 10,249 (**5.15c**) $cm^{-1}M^{-1}$. There is no significant difference in molar absorptivity when comparing analogous structures of the heteroacene versus acene series using their absorption λ_{max}.

By change of substituent/size of the acene framework, an absorption range of 571-761 nm (1.63-2.17 eV) can be "tuned in" across the series **5.11a,b** to **5.15a-c**. Vibronic fine structure is observed for all compounds. To gain a full understanding of the electronic behavior of these compounds, we conducted cyclic voltammetry

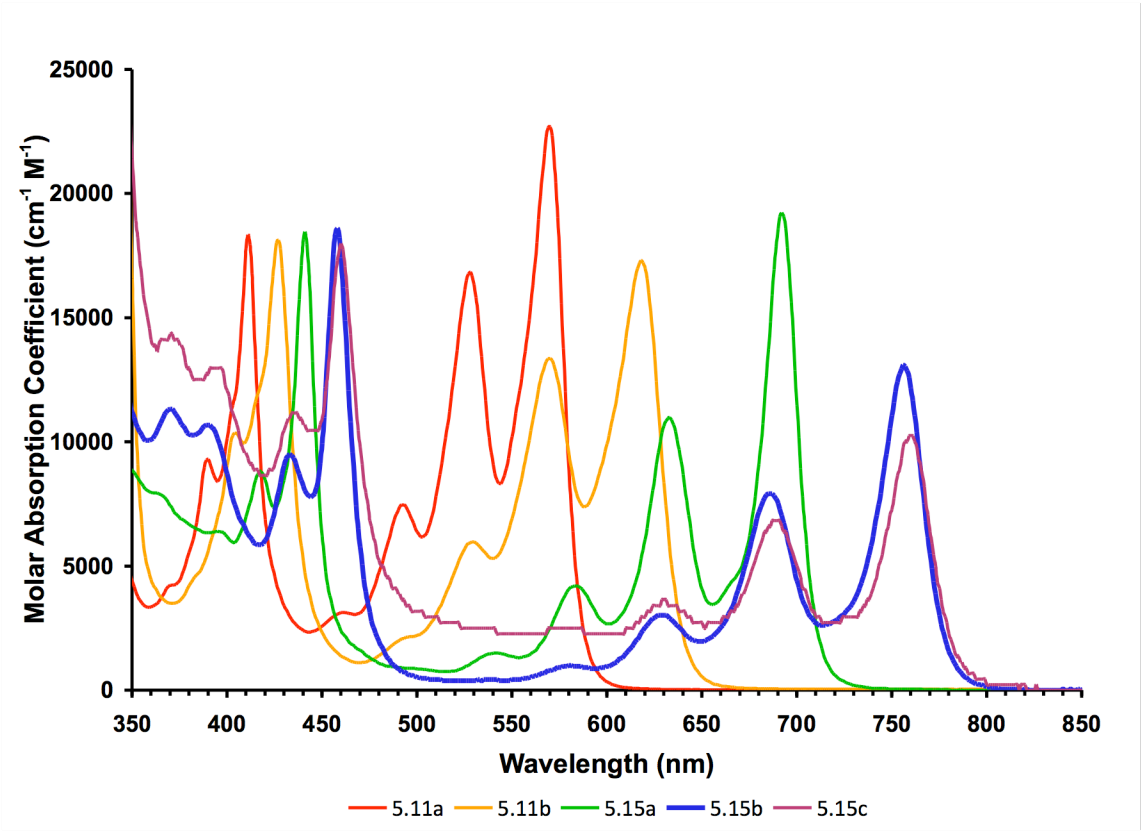

Figure 5.1. Molar absorptivity profile of compounds **5.11a,b** and **5.15a-c** in terms of their molar absorption coefficient at a given wavelength.

experiments (Dr. Steve Barlow) and performed Time-Dependent Density Functional Theory (TD-DFT) quantum chemical calculations at the B3LYP/6-311+G* level of theory (Dr. John S. Sears). All data is summarized in Table 5.1. Due to the spectroscopic and cyclic voltammetry similarity of the bromo (**5.15c**) and chloro (**5.15b**)

derivatives of diazapentacene (**5.15a**), computational results include only parent and chloro model compounds (**5.11a'**, **5.11b'**, **5.15a'**, and **5.15b'**). This is consistent with the similar inductive and mesomeric properties of these two halogens (Br: F = +0.45, R = -0.22; Cl: F = +0.42, R = -0.19; F = field effect parameter, R = resonance parameter) as both act as moderately inductive (σ) electron-withdrawing groups and as weak π-donors as indicated by the Swain-Lupton parameters quantifying these two effects.[27]

Table 5.1. Data summary of the investigated compounds.

Compound	**5.11a**	**5.11b**	**5.11c'**	**5.15a**	**5.15b**	**5.15c**	**5.16a**	**5.16b**	**5.16c**
λ_{max} abs (nm)	571	620	-	693	759	761	-	-	-
$E_{1/2}^{0/-}$(V)[b]	-1.19	-0.92	-	-1.05	-0.79	-0.79	-	-	-
$E_{1/2}^{0/+}$ (V)[b]	+0.99	+1.11	-	+0.68	+0.83	+0.80	-	-	-
elchem. gap (V)	2.18	2.03	-	1.73	1.62	1.59	-	-	-
opt. gap (eV) [a]	2.17	2.01	-	1.79	1.64	1.63	-	-	-
S_1^{vert} [c]	2.07	1.91	1.38	1.58	1.44	nd	2.16	2.13	1.61
calcd. H-L gap (eV)[d]	2.37	2.25	1.81	1.87	1.77	nd	2.41	2.39	2.00
HOMO (eV)[d]	-5.72	-6.03	-6.30	-5.37	-5.66	nd	-5.28	-5.68	-6.38
LUMO (eV)[d]	-3.35	-3.78	-4.49	-3.50	-3.89	nd	-2.87	-3.30	-4.38

a) From absorption maxima. *b)* In a 1:1 *v/v* mixture of a 0.1 M acetonitrile:toluene solution of $^{n}Bu_4NPF_6$ and toluene, vs. $FeCp_2^{+/0}$. *c)* Time-Dependent Density Functional Theory (TD-DFT) calculations at the B3LYP/6-311+G* level of theory. The transitions are all one-electron transitions with a > 80% HOMO-LUMO contribution. *d)* The desilylated model compounds **5.11a'**, **5.11b'**, **5.15a'** and **5.15b'** were used for the calculations to reduce the computation time.

TD-DFT results of the vertical transition energies (S_1^{vert}) for the lowest-lying singlet excited states of model compounds **5.11a'**, **5.11b'**, **5.15a'**, **5.15b'** reproduce the trends observed in the experimental data of **5.11a,b** and **5.15a,b**; the calculations for the

tetracenes **5.16a** and **5.16b** predict only a small bathochromic shift in the absorption as a result of chlorination, which is also consistent with the experimental data for the corresponsing homologous pentacenes, **5.5** and **5.6**. Moreover, the computational results indicate in all cases that the transitions are predominantly HOMO-to-LUMO in character, > 80%. The trends observed in the electrochemical gaps between the half-wave potentials corresponding to molecular oxidation and reduction correlate well with the experimental and TD-DFT optical transition energies and the DFT HOMO-LUMO gaps.[28] Accordingly, we examined the FMOs of model compounds in order to better understand the origin of the large bathochromic shifts observed in the spectra of the azaacenes upon halogenation (**5.11a'** to **5.11b'**) in comparison to their homologous acenes (**5.16a** to **5.16b**).

Figure 5.2 displays the FMOs (energy in eV) of **5.11a'**/**5.11b'** and **5.16a**/**5.16b**. In both pairs, stabilization of the LUMO results when attaching four chlorine substituents to positions 1, 2, 3, and 4 (right side, ring 1 [numbered right to left]). The stabilization is 0.43 eV in both **5.11b'** and **5.16b**. More importantly, upon going from **5.11a'** to **5.11b'** the HOMO is only stabilized by 0.31 eV, while in the case of **5.16a**/**5.16b** the HOMO stabilization is 0.40 eV, only 0.03 eV less stabilization than the LUMO. This is a possible reason for the increased bathochromic shift of the absorption in the heteroacene (**5.11a'**/**5.11b'**) vs acene (**5.16a**/**5.16b**) molecules upon halogenation. This can also be seen by inspection of the geometric orbital densities on each pair of molecules. The LUMOs of all four compounds are strikingly similar to each other in shape and density. In contrast, the HOMOs differ between the two pairs of molecules: **5.11a'**/**5.11b'** display smaller orbital coefficients on rings 1 and 2, while in the pair **5.16a**/**5.16b** the HOMOs

have almost the same coefficients on all rings (Figure 5.2). The smaller HOMO coefficients on rings 1 and 2 in **5.11b'** lead to its reduced stabilization by the four chlorine substituents when compared to the pair **5.16a**/**5.16b**, in which the coefficients

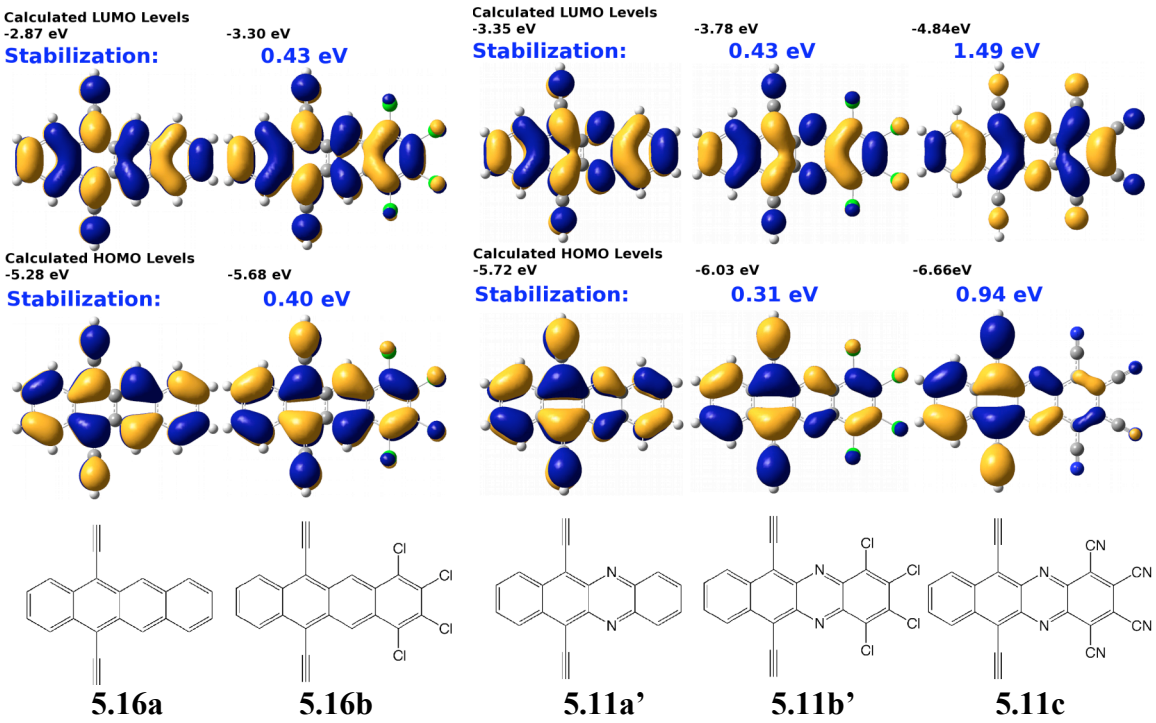

Figure 5.2. Frontier molecular orbitals (HOMO, middle, LUMO, top) of investigated compounds. The bottom shows the structural formulae. The numbering of the rings is from right (1) to left (4). The LUMOs of the four compounds are very similar to each other. Both **5.11b'** and **5.16b** experience a stabilization of 0.43 eV through the chlorine substitution. The HOMOs of **5.11a'** and **5.11b'** and **5.16a** and **5.16b** resemble each other qualitatively but are pair wise (**5.11**/**5.16**) different. The differences are pronounced in rings 1 and 2 as particularly in the HOMO of **5.11a'** the orbital coefficients (see Section 5.4) on the rings 1 and 2 are reduced; as a consequence the chlorine substituents are less effective in stabilizing the HOMO (going from **5.11a'** to **5.11b'**), mirroring the optical behavior seen in compound **5.11b**. Also, frontier molecular orbitals (HOMO -6.66 eV, middle right, LUMO -4.84 eV, top right, gap = 1.82 eV) of tetracyanodiazaacene **5.11c**. Calculated by DFT using B3LYP/6-311+G* basis sets. Compared to **5.11a** calculated on the same level of theory, the optical band gap (S_0-S_1 transition) shrinks from 2.07eV to 1.38 eV.

are larger on these rings. Based upon the computational results, the contribution (sum of the squared orbital coefficients) from rings 1 and 2 is about three times as large in **5.16a** as in the heteroacene **5.11b'**. The reduced delocalization of the HOMO when going from **5.11a'** to **5.11b'** is the reason for the larger induced bathochromic shift of the diazatetracenes upon halogenation at positions 1, 2, 3, and 4 compared to the acene series (**5.16**). The same effect is also operative for the larger diazapentacenes (**5.15a** and **5.15b**) where identical effects are observed according to computational results, electrochemistry, and optical spectroscopy (Table 5.1).

If such an explanation is correct, stronger electron withdrawing substituents at positions 1, 2, 3, and 4 such as cyano should have an increased effect and reduce the energy of the first optical transition even further. In such compounds, the HOMO should have reduced coefficients on rings 1 and 2 compared to **5.11a'/b'**. To test this hypothesis, we performed quantum chemical computational studies on model compound **5.11c** (Figure 5.2). The HOMO of **5.11c** is predominantly localized on rings 3 and 4, while the LUMO is delocalized across all rings. This leads to an increased stabilization of the LUMO as compared to the HOMO even more so than **5.11a'/b'**, resulting in a calculated vertical transistion (S_1) of 1.38 eV for **5.11c**. When compared to the model parent compound's (**5.11a'**) estimated H-L gap, compound **5.11c** displays a decrease of 0.55 eV. A disjoint orbital structure,[13] i.e. spatially separated frontier molecular orbitals, with the orbital separation further amplified by electronegative substituents at the appropriate positions decreases the optical transition energies of diazaacenes, an effect not observed in acenes which have more equally distributed HOMO and LUMO frontier molecular orbitals.

5.3 Conclusion

The disjoint frontier molecular orbitals of diazaacenes is one of their defining features and opens the door to amplified substiuent effects in the engineering of electronic and optical properties of organic electronic materials. In conclusion, we have prepared the first solution processible diazapentacene derivative **5.15a**, as well as the halogenated congeners **5.11b** and **5.15b,c**; which we observe to have significantly lower energy optoelectronic transitions compared to nonhalogenated compounds **5.11a** and **5.15a**. Significant bathochromic shifts upon halogenation are not observed in the analogous acene series, indicating that the pyrazine moiety and electron withdrawing substitution at appropriate positions is a necessary ingredient for this engineering of optical properties. Quantum chemical computational studies reveal that this difference in behavior can be attributed to the substituent-induced disjoint HOMO frontier molecular orbitals of the azaacenes. The interplay between the pyrazine moiety and the electronegative substituents serves as a uniquely useful tool to indepently manipulate the optical and electrochemical properties of *N*-heteroacenes. This effect could enhance the rational design and tuning ability of acene-type materials for application in organic electronic devices.

This work has been published in *Nature Communications*:

"From Acenes to Diazaacenes: Enabling Electronegative Substitution as a Tool for Engineering Optical and Electronic properties." Anthony Lucas Appleton, Scott M. Brombosz, Stephen Barlow, John S. Sears, Jean-Luc Brédas, Seth R. Marder, Uwe H.F. Bunz. *Nature Comm*, 2010, 1:90. DOI: 10.1038/ncomms1088.

Provisional Patents:

"Chlorinated and Non-chlorinated Heteroacenes." GTRC ID 5101. Serial Number 61/329,343.

5.4 Experimental Information

^{1}H NMR and ^{13}C NMR were recorded on a Bruker 400 operating at 400 MHz and 100 MHz, respectively.

5.4.1 6,11-bis((triisopropylsilyl)ethynyl)benzo[*b*]phenazine, 5.11a

Prepared according to literature procedures.[23]

5.4.2 1,2,3,4-tetrachloro-6,11-bis((triisopropylsilyl)ethynyl)benzo[*b*]phenazine, 5.11b

To a dry 50 mL round bottom flask was added compund **5.9**[23] (0.200 g, 3.85 x 10^{-4} mol, 1 eq.), compound **5.10b** (0.0950 g, 3.85 x 10^{-4} mol, 1 eq.), ethanol (10 mL) and acetic acid (3 mL). The solution was brought to reflux and stirred overnight. The reaction was cooled on an ice bath and quenched with water. The precipitate was filtered with water, washed with cold methanol (10 mL) and allowed to dry in ambient. The product was purified by column chromatography on silica gel using hexanes/dichloromethane (10:1 *v/v*). Compound **5.11b** was isolated as green-black crystals (0.190 g, 67.6% yield). m.p. = 179 ºC (decompose). IR (KBr, cm^{-1}) 3116, 3062, 2939, 2889, 2862, 2754, 2723, 2360, 2129, 1461, 1438, 1388, 1361, 1238, 1180. ^{1}H NMR (δ in $CDCl_3$) 8.76 (AA' of AA'BB', 2H), 7.70 (BB' of AA'BB', 2H), 1.28 (m, broad, 42H). ^{13}C NMR (δ in $CDCl_3$) 140.52, 139.27, 136.58, 134.60, 132.26, 129.03, 127.82, 121.35, 109.68, 101.90, 18.94, 11.56. Accurate mass for $C_{38}H_{46}Cl_4N_2Si_2$: *m/z* = 726.19656 [M+], calc. *m/z* = 726.19537. Elemental analysis for $C_{38}H_{46}Cl_4N_2Si_2$: [C] = 62.69, calc. [C] = 62.63; [H] = 6.44, calc. [H] = 6.36; [Cl] = 19.7, calc. [Cl] = 19.5; [N] = 3.81, calc. [N] = 3.84.

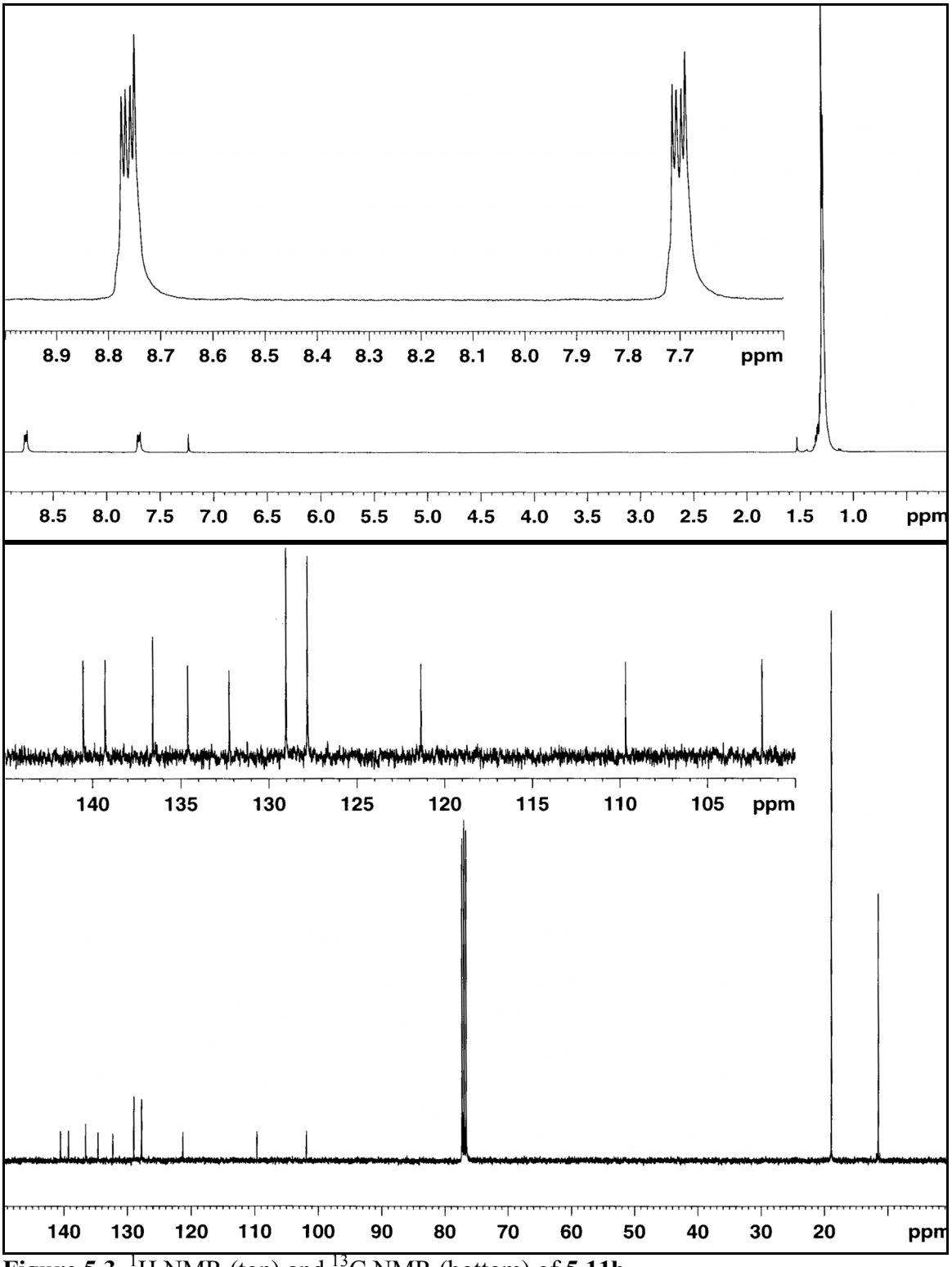

Figure 5.3. ^{1}H NMR (top) and ^{13}C NMR (bottom) of **5.11b**.

5.4.3 1,4-bis((triisopropylsilyl)ethynyl)anthracene-2,3-diamine, 5.13

To an oven dried 1 L Schlenk flask was added **5.12**[24] (5.20 g, 8.71 x 10^{-2} mol) and dry THF (100 mL). The solution was purged with nitrogen for 5 min and cooled on an ice bath to 0 °C. Lithium aluminum hydride (3.31 g, 8.71 x 10^{-2} mol, 10 eq.) was added slowly. The reaction mixture was purged once more with nitrogen for 5 min, sealed from the atmosphere with a bubbler, and stirred for 12 h while the ice bath was allowed to come to room temperature. The reaction was quenched with aqueous ammonium chloride solution and extracted with diethyl ether (5 x 150 mL). The organic layer was dried with sodium sulfate, filtered, and the solvent was removed *in vacuo*. The product was purified by column chromatography on silica gel using hexanes/dichloromethane (3:1 *v/v*). Compound **5.13** was obtained as a golden solid (4.41 g, 89% yield). m.p. = stable to 250 °C. IR (KBr, cm^{-1}) 3448, 3355, 3228, 3163, 3047, 2962, 2862, 2719, 2136, 1932, 1913, 1620, 1550, 1539, 1454, 1392, 1307, 1238, 1180. ^{1}H NMR (δ in $CDCl_3$) 8.60 (s, 2H), 7.91 (AA' of AA'BB', 2H), 7.39 (BB' of AA'BB', 2H), 4.49 (s, 4H) 1.25 (s, 42H). ^{13}C NMR (δ in $CDCl_3$) 139.67, 130.93, 127.82, 127.53, 124.57, 122.81, 102.75, 102.13, 101.74, 18.70, 11.28. Accurate mass for $C_{36}H_{52}N_2Si_2$: *m/z* = 568.36863 [M+], calc. *m/z* = 568.36691.

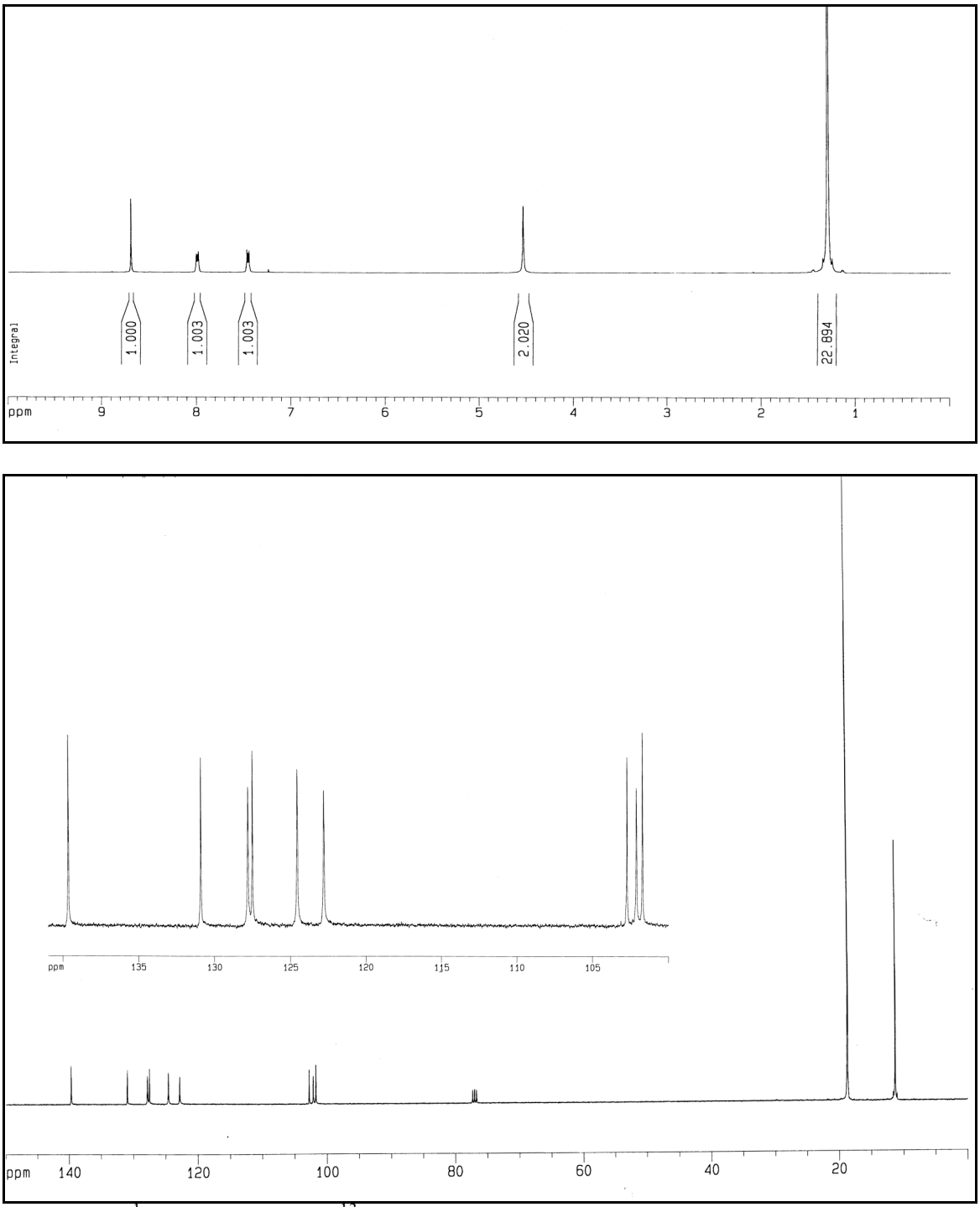

Figure 5.4. ^{1}H NMR (top) and ^{13}C NMR (bottom) of **5.13**.

5.4.4 6,13-bis((triisopropylsilyl)ethynyl)-5,14-dihydronaphtho[2,3-b]phenazine, 5.14a

Compound **5.13** (0.435 g, 7.65 x 10^{-4} mol) and **5.10a**[23] (0.245 g, 2.29 x 10^{-3} mol, 3 eq.) were heated to reflux in dichloromethane (50 mL) and acetic acid (3 mL) and stirred for 12 h. The reaction mixture was washed with water (2 x 250 mL); the organic layer was dried with sodium sulfate, filtered, and the solvent removed *in vacuo*. The product was purified by column chromatography on silica gel using pure hexanes. Compound **5.14a** was obtained as a metallic red-green solid (0.0853 g, 17.5% yield). m.p. = 263 ºC (decompose). IR (KBr, cm^{-1}) 3488, 3400, 3199, 3147, 3120, 3055, 3028, 2956, 2923, 2864, 2752, 2721, 2360, 2198, 2135, 2030, 1870, 1737, 1589, 1461, 1315, 1261, 1182. ^{1}H NMR (δ in $CDCl_3$) 8.169 (s, 2H), 7.75 (AA' of AA'BB', 2H), 7.31 (BB' of AA'BB', 2H), 6.64 (BB" of AA"BB", 2H), 6.33 (AA" of AA"BB", 2H), 6.61 (s, 2H), 1.25 (s, 42H). ^{13}C NMR (δ in $CDCl_3$) 136.25, 131.55, 129.07, 128.46, 127.66, 124.82, 122.15, 122.13, 112.98, 103.52, 100.93, 96.01, 18.90, 11.41. Accurate mass for $C_{42}H_{54}N_2Si_2$: *m/z* = 642.3849 [M+], calc. *m/z* = 642.3826.

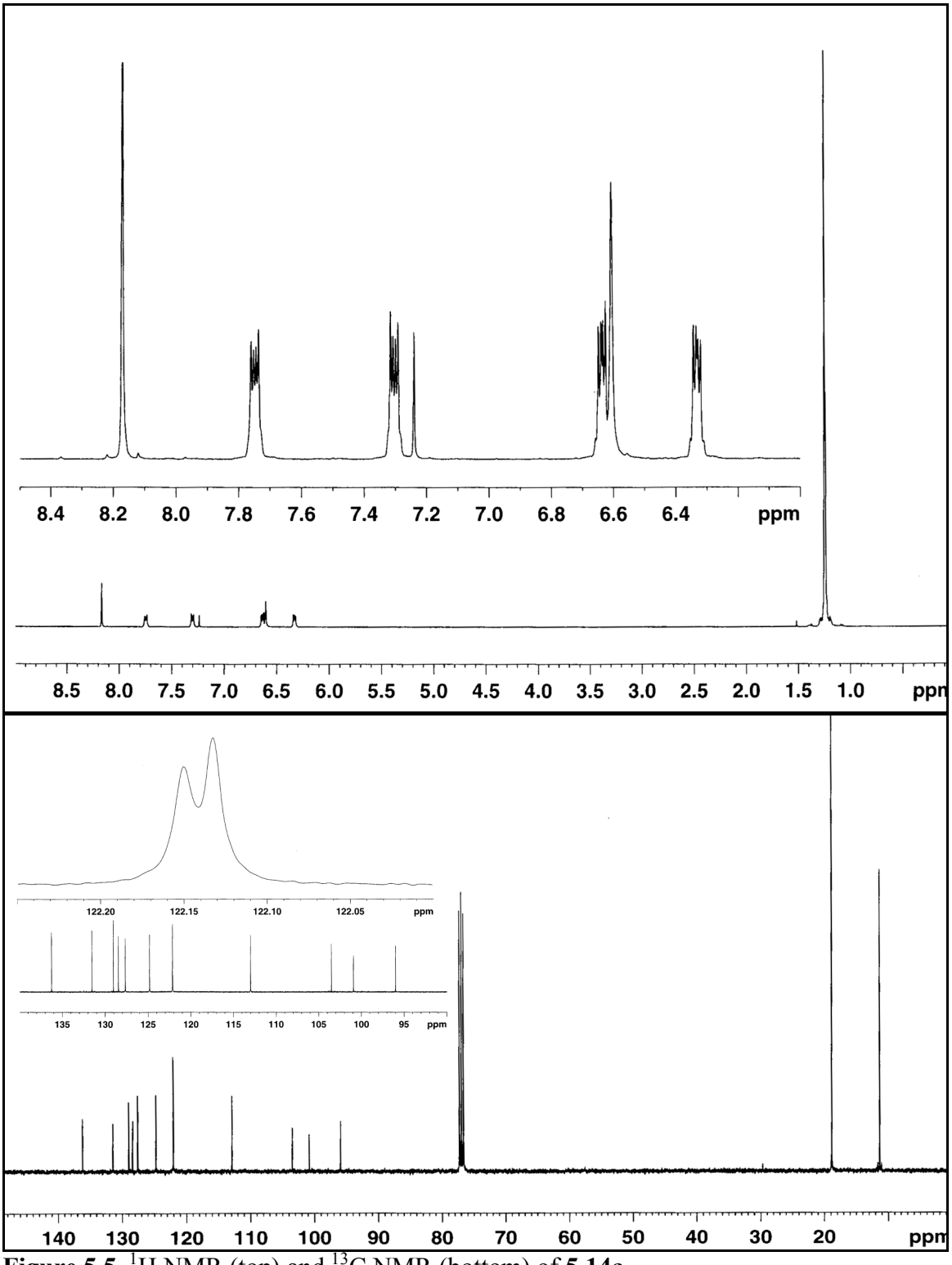

Figure 5.5. ^{1}H NMR (top) and ^{13}C NMR (bottom) of **5.14a**.

5.4.5 6,13-bis((triisopropylsilyl)ethynyl)naphtho[2,3-b]phenazine 5.15a.

Compound **5.14a** (0.100 g, 1.56 x 10^{-4} mol) was dissolved in dichloromethane (25 mL) and stirred for 4 h with an excess of MnO_2 (1.0 g). The solvent was removed *in vacuo*. The product was purified by column chromatography on silica gel using hexanes/dichloromethane (3:1 *v/v*). Compound **5.15a** was obtained as a green crystals (0.0995 g, 99% yield). m.p. = 265 °C (decompose). IR (KBr, cm^{-1}) 3145, 3118, 3047, 3024, 2956, 2939, 2923, 2862, 2752, 2721, 2136, 2111, 1731, 1600, 1521, 1461, 1377, 1259, 1103. ^{1}H NMR (δ in $CDCl_3$) 9.41 (s, 2H), 8.16 (AA' of AA'BB', 2H), 8.02 (AA" of AA"BB", 2H), 7.75 (BB" of AA"BB", 2H), 7.46 (BB' of AA'BB', 2H), 1.35 (m, broad, 42H). ^{13}C NMR (δ in $CDCl_3$) 145.01, 140.98, 132.92, 132.57, 131.21, 130.48, 128.71, 126.80, 126.75, 120.75, 109.52, 103.81, 18.98, 11.69. Accurate mass for $C_{42}H_{52}N_2Si_2$: *m/z* = 640.3674 [M+], calc. *m/z* = 640.3669. Elemental analysis for $C_{42}H_{52}N_2Si_2$: [C] = 78.11, calc. [C] = 78.69; [H] = 8.14, calc. [H] = 8.18; [N] = 4.20, calc. [N] = 4.37.

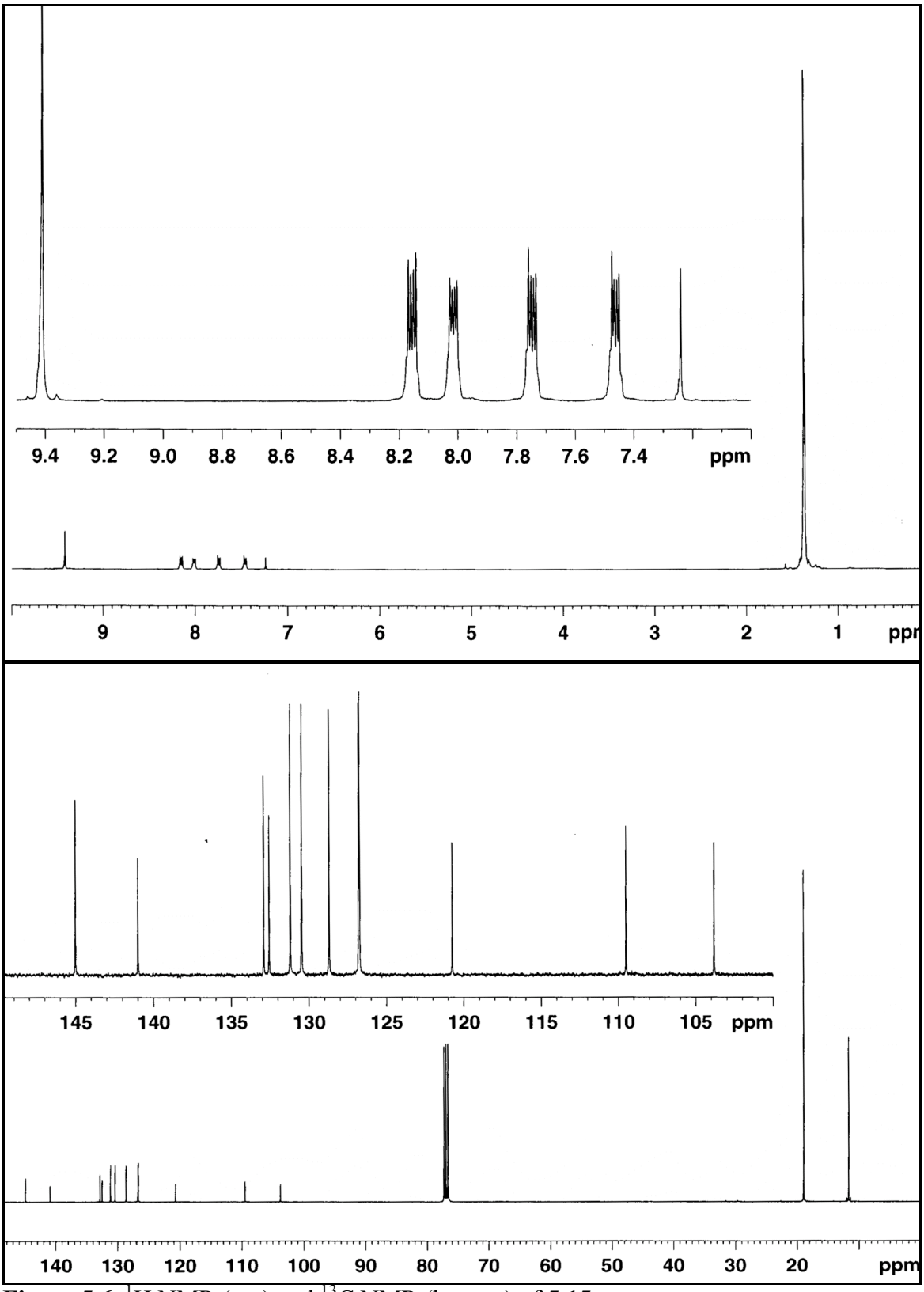

Figure 5.6. ^{1}H NMR (top) and ^{13}C NMR (bottom) of **5.15a**.

5.4.6 1,2,3,4-tetrachloro-6,13-bis((triisopropylsilyl)ethynyl)-5,14-dihydronaphtho[2,3-b]phenazine 5.14b.

Compound **5.13** (0.200 g, 3.52 x 10^{-4} mol) and 5.10b (0.0864 g, 5.52 x 10^{-4}, 1 eq.) were dissolved in a mixture of ethanol (3 mL) and acetic acid (1.5 mL) and reacted under microwave irradiation at 120 °C for 40 min. The reaction mixture was extracted with dichloromethane (50 mL) and washed with water (2 x 25 mL). The organic layer was dried with sodium sulfate and the solvent was removed *in vacuo*. The product was purified by column chromatography on silica gel using hexanes/dichloromethane (9:1 *v/v*) to give **5.14b** as a metallic red-green solid (0.0631 g, 23% yield). m.p. = stable up to 350 °C. IR (KBr, cm^{-1}): 3382, 3186, 3168, 3155, 3048, 2927, 2918, 2891, 2863, 2853, 2722, 2554, 2129, 1928, 1888, 1797, 1750, 1579, 1553, 1488, 1463, 1429, 1421, 1387, 1365, 1313, 1275, 1180, 1144. ^{1}H NMR (δ in $CDCl_3$) 8.34 (s, 2H), 7.81 (AA' of AA'BB', 2H), 7.39 (BB' of AA'BB', 2H), 7.18 (s, 2H), 1.26 (m, broad, 42H). ^{13}C NMR (δ in $CDCl_3$) 133.29, 131.86, 128.34, 127.84, 126.89, 125.49, 123.57, 123.21, 114.93, 105.40, 99.52, 99.13, 18.86, 11.35. Accurate mass for $C_{42}H_{50}N_2Si_2Cl_4$: *m/z* = 778.22852 [M+], calc. *m/z* = 778.22667.

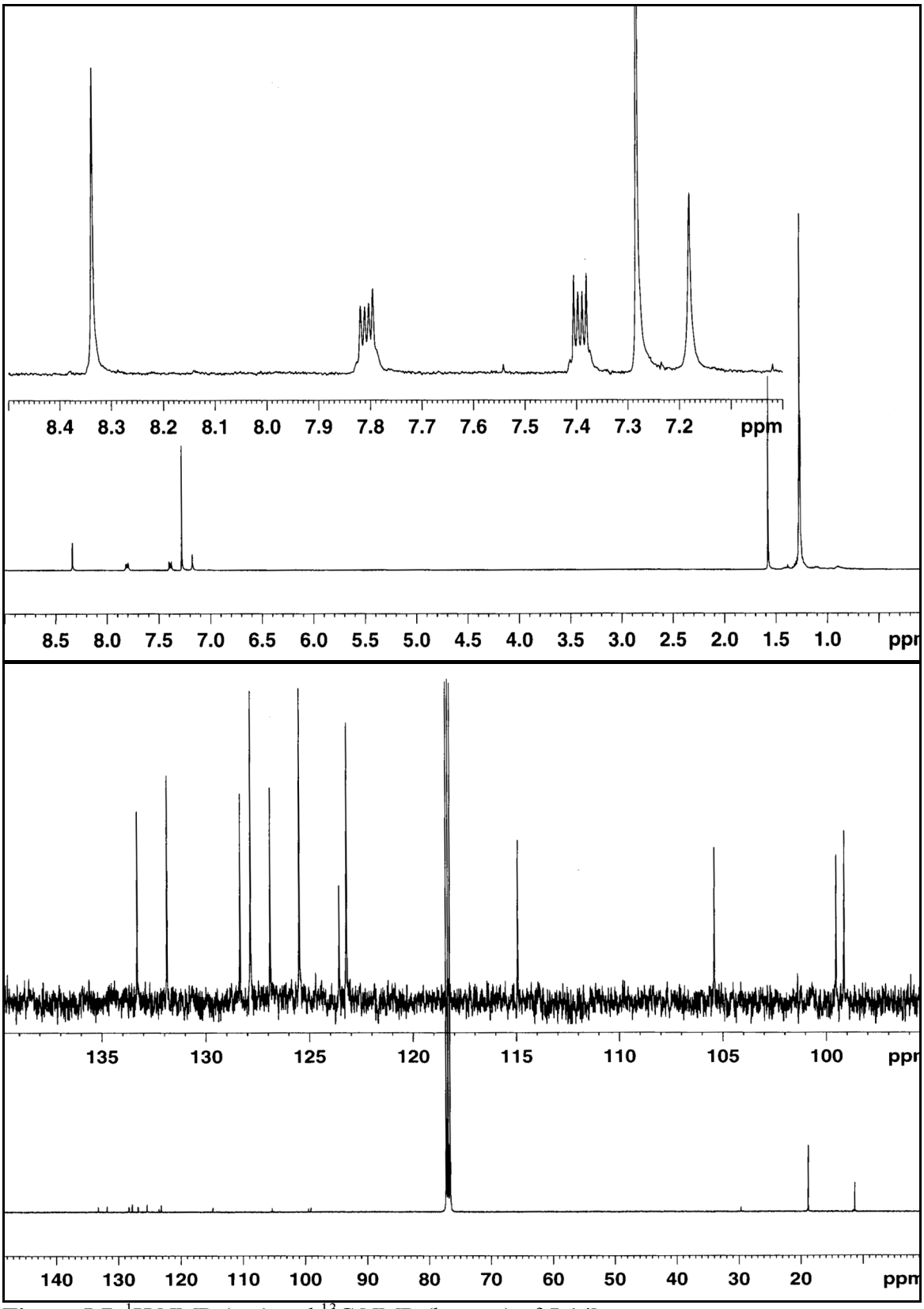

Figure 5.7. ^{1}H NMR (top) and ^{13}C NMR (bottom) of **5.14b**.

5.4.7 1,2,3,4-tetrachloro-6,13-bis((triisoprypyleilyl)ethynyl)naphtho[2,3-b]phenazine 5.15b.

Compound **5.14b** (0.0631 g, 8.08 x 10^{-5} mol) was dissolved in dichloromethane (25 mL) and stirred for four h with an excess of MnO_2 (1.0 g). The solvent was removed *in vacuo*. The product was purified by column chromatography on silica gel using hexanes/dichloromethane (3:1 *v/v*) to give **5.15b** (0.061 g, 99% yield) as a dark green solid. m.p. = 243 °C. IR (KBr, cm^{-1}) 3068, 3045, 2953, 2940, 2926, 2920, 2889, 2863, 2756, 2722, 2136, 1538, 1462, 1437, 1374, 1355, 1110. ^{1}H NMR (δ in $CDCl_3$) 9.45 (s, 2H), 8.05 (AA' of AA'BB', 2H), 7.56 (BB' of AA'BB', 2H), 1.34 (m, broad, 42H). ^{13}C NMR (δ in $CDCl_3$) 139.93, 139.42, 134.59, 133.52, 133.45, 132.27, 128.73, 127.42, 127.23, 121.43, 111.14, 102.91, 18.95, 11.61. Accurate mass for $C_{42}H_{48}N_2Si_2Cl_4$: *m/z* = 776.21004, calc. *m/z* = 776.21102. Elemental analysis for $C_{42}H_{48}N_2Si_2Cl_4$: [C] = 64.56, calc. [C] = 64.77; [H] = 6.55, calc. [H] = 6.21; [N] = 3.09, calc. [N] = 3.60; [Cl] = 14.2, calc. [Cl] = 18.21.

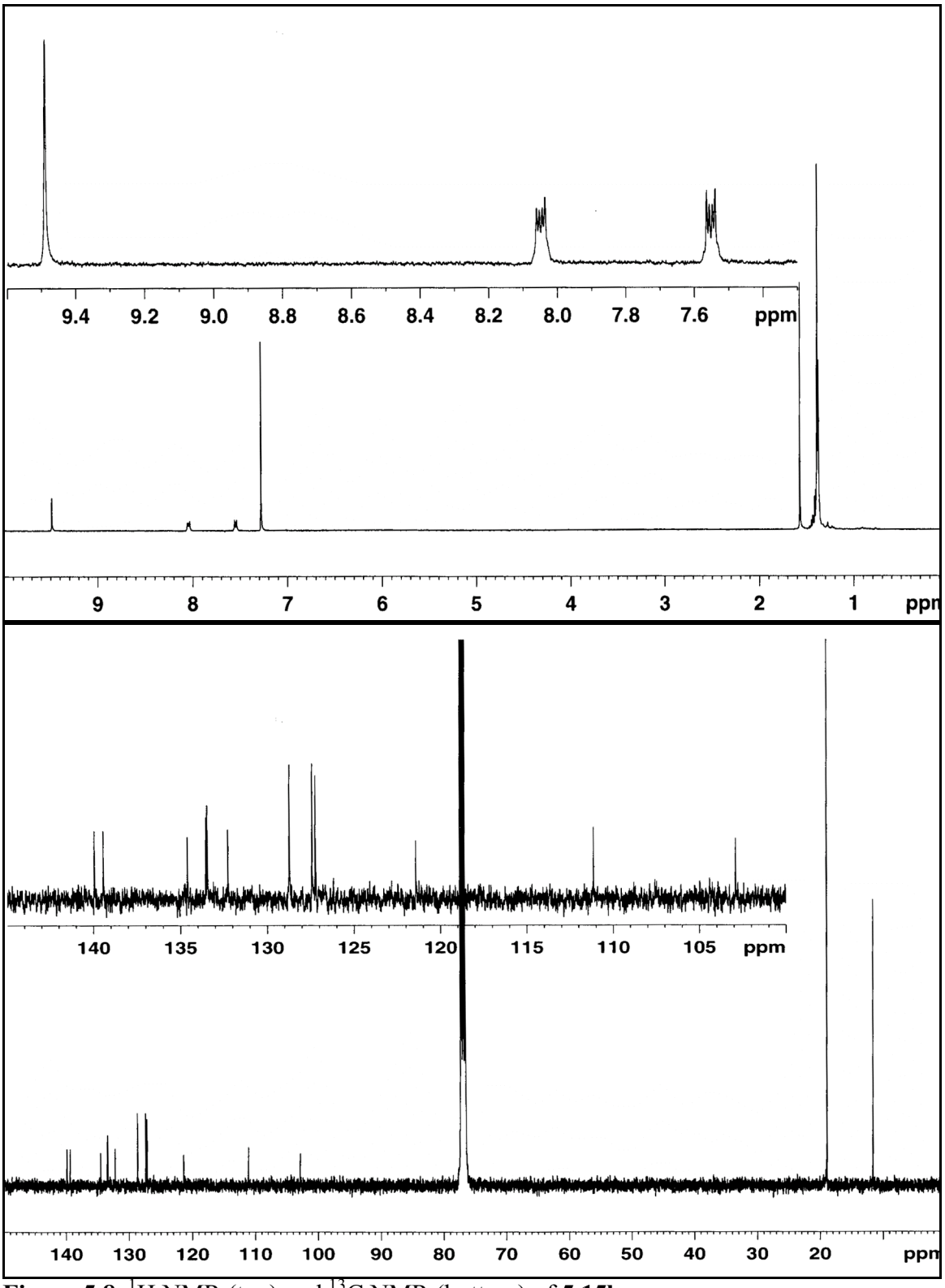

Figure 5.8. ^{1}H NMR (top) and ^{13}C NMR (bottom) of **5.15b**.

5.4.8 1,2,3,4-tetrabromo-6,13-bis((triisopropylsilyl)ethynyl)-5,14-dihydronaphtho[2,3-*b*]phenazine 5.14c.

Compound **5.13** (0.0730 g, 1.28 x 10^{-4} mol) and compound **5.10c** (0.0544 g, 1.28 x 10^{-4} mol, 1 eq.) were dissolved in ethanol (5 mL) and acetic acid (1.5 mL) and heated to reflux for 12 h. The reaction was extracted with dichloromethane (50 mL) and washed with water (2 x 25 mL). The organic layer was dried with sodium sulfate and the solvent was removed *in vacuo*. The product was purified by column chromatography on silica gel using pure hexanes. Compound **5.14c** was obtained as a dark red-green solid (0.0172 g, 14% yield). m.p. = 275 °C. IR (KBr, cm^{-1}) 3361, 3045, 2939, 2926, 2920, 2887, 2862, 2721, 2534, 2360, 2143, 2127, 1580, 1556, 1485, 1462, 1455, 1431, 1421, 1389, 1361, 1311, 1265, 1229, 1181, 1143. ^{1}H NMR (δ in $CDCl_3$) 8.30 (s, 2H), 7.75 (AA' of AA'BB', 2H), 7.34 (BB' of AA'BB', 2H), 7.27 (s, 2H), 1.22 (m, broad, 42H). ^{13}C NMR (δ in $CDCl_3$) 133.79, 131.87, 128.82, 128.45, 127.83, 125.47, 123.21, 118.41, 109.09, 105.42, 99.64, 98.93, 18.91, 11.41. Accurate mass for $C_{42}H_{50}N_2Si_2Br_4$: *m/z* = 954.02184, calc. *m/z* = 954.02460.

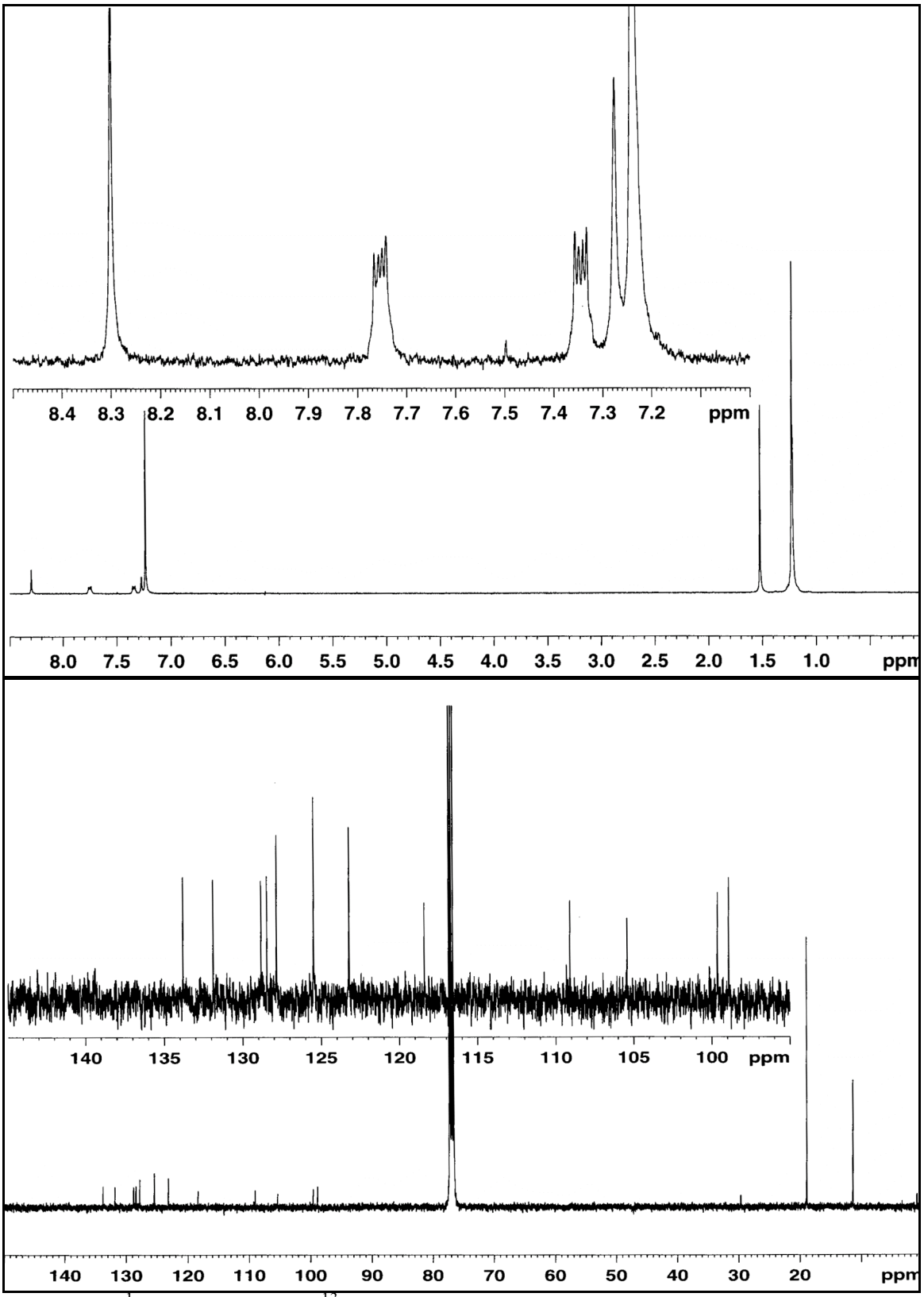

Figure 5.9. ^{1}H NMR (top) and ^{13}C NMR (bottom) of **5.14c**.

5.4.9 1,2,3,4-tetrabromo-6,13-bis((triisopropylsilyl)ethynyl)naphtho[2,3-b]phenazine 5.15c.

Compound **5.14c** (0.0172 g, 1.79 x 10^{-5} mol) was dissolved in dichloromethane (25 mL) and stirred for 4 h with an excess of MnO_2 (1.0 g). The solvent was removed *in vacuo*. The product was purified by column chromatography on silica gel using hexanes/dichloromethane (3:1 *v/v*). Compound **5.15c** was obtained as a dark green solid (0.0171 g, 99% yield). m.p. = 275 °C (decompose). IR (KBr, cm^{-1}) 3045, 2954, 2939, 2925, 2889, 2861, 2753, 2722, 2143, 2125, 1531, 1486, 1463, 1433, 1422, 1407, 1375, 1359, 1344, 1163, 1137, 1108. ^{1}H NMR (δ in $CDCl_3$) 9.46 (s, 2H), 7.99 (AA' of AA'BB', 2H), 7.50 (BB' of AA'BB', 2H), 1.34-1.33 (m, broad, 42H). ^{13}C NMR (δ in $CDCl_3$) 140.52, 140.48, 133.63, 133.55, 131.68, 128.96, 128.75, 127.45, 127.29, 121.27, 111.11, 103.11, 19.04, 11.69. Mass spectra analysis (ESI) for $C_{42}H_{48}N_2Si_2Br_4$: *m/z* = 952 [M+], calc. *m/z* = 952. Due to poor ionization, accurate mass could not be determined. However, the isotopic splitting pattern was consistent with a tetrabrominated derivative.

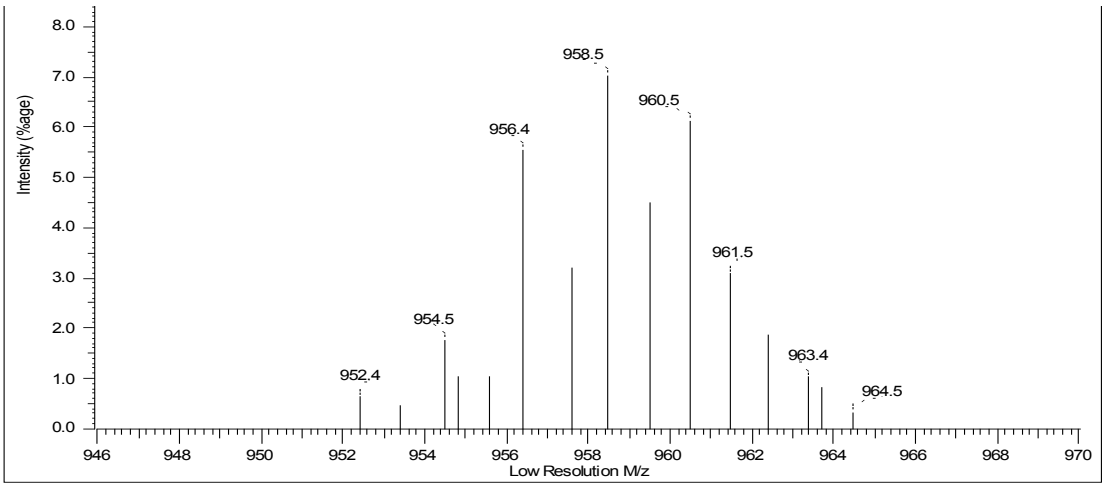

Figure 5.10. Isotopic splitting pattern for compound **5.15c**.

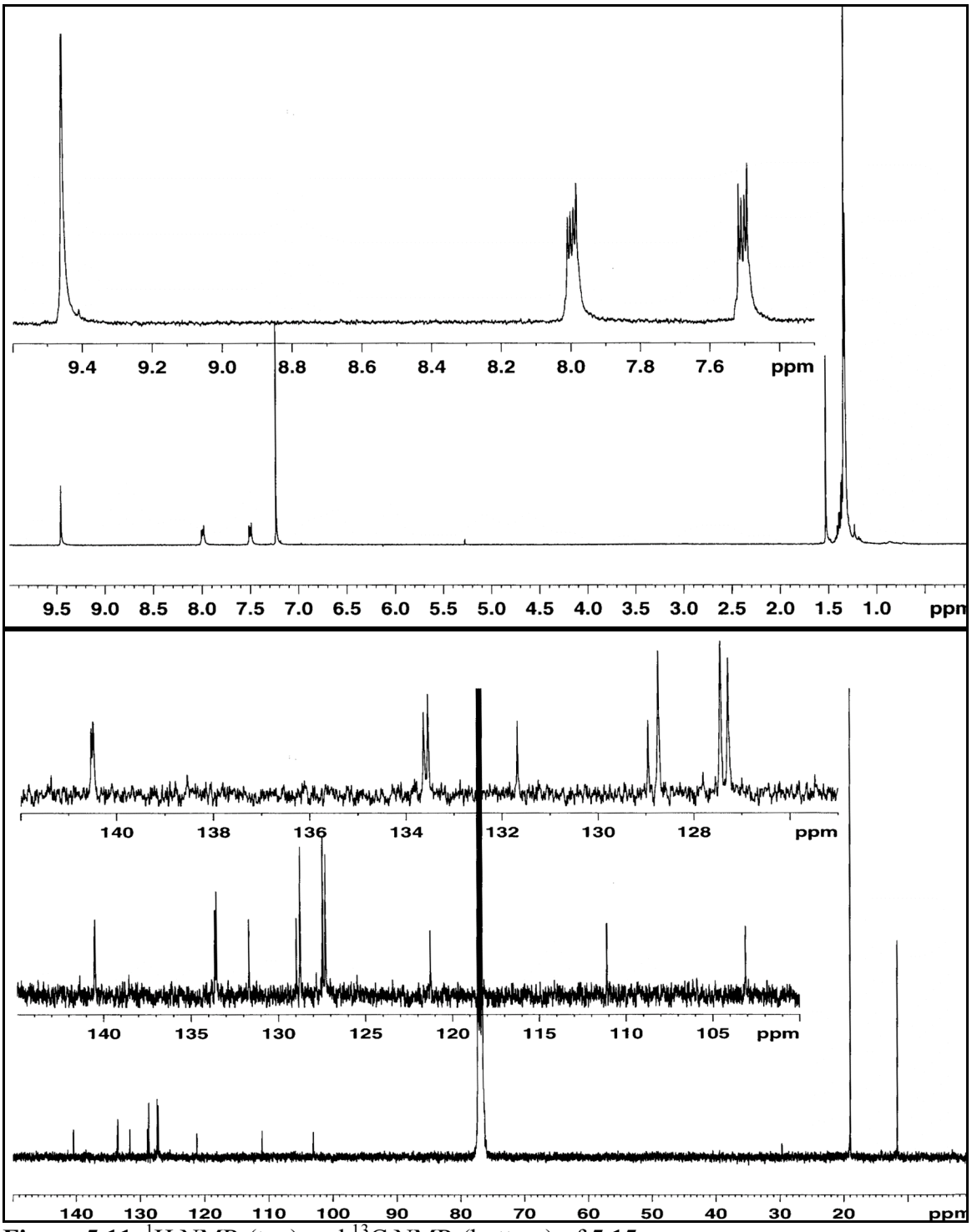

Figure 5.11. ^{1}H NMR (top) and ^{13}C NMR (bottom) of **5.15c**.

5.4.10 Selected IR Spectra

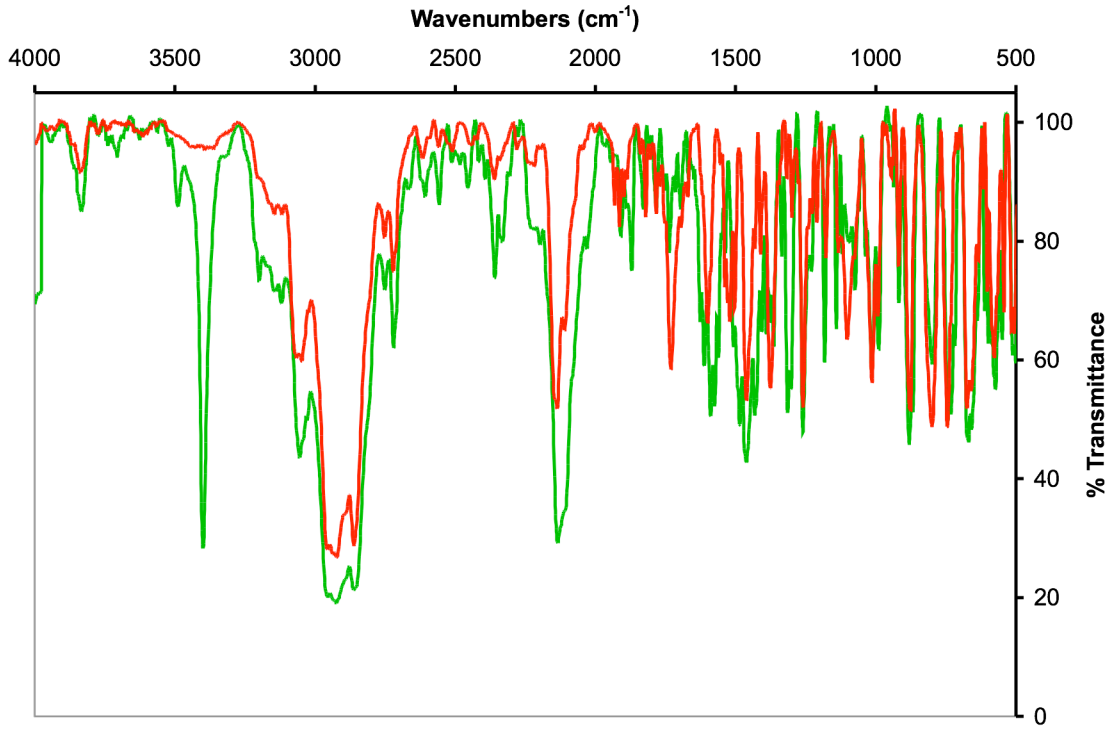

Figure 5.12. IR spectra of compounds **5.14a** (green) and **5.15a** (red).

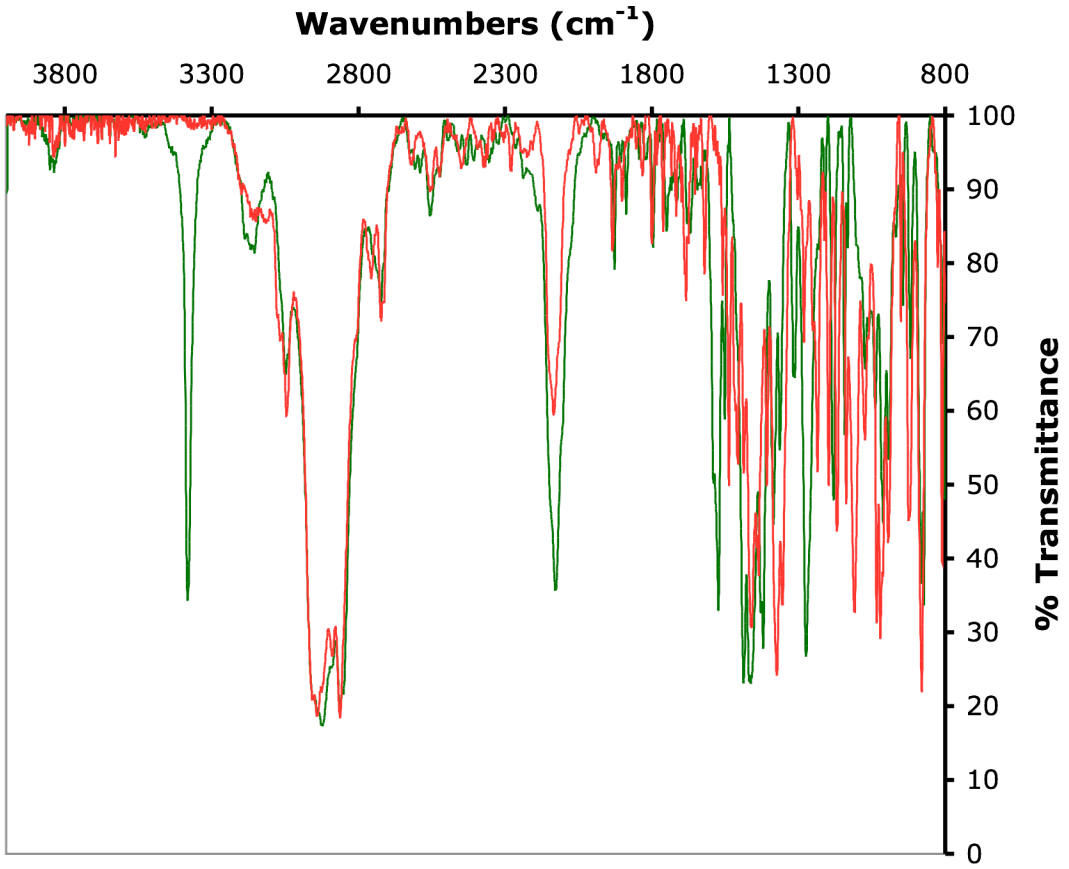

Figure 5.13. IR spectra of compounds **5.14b** (green) and **5.15b** (red).

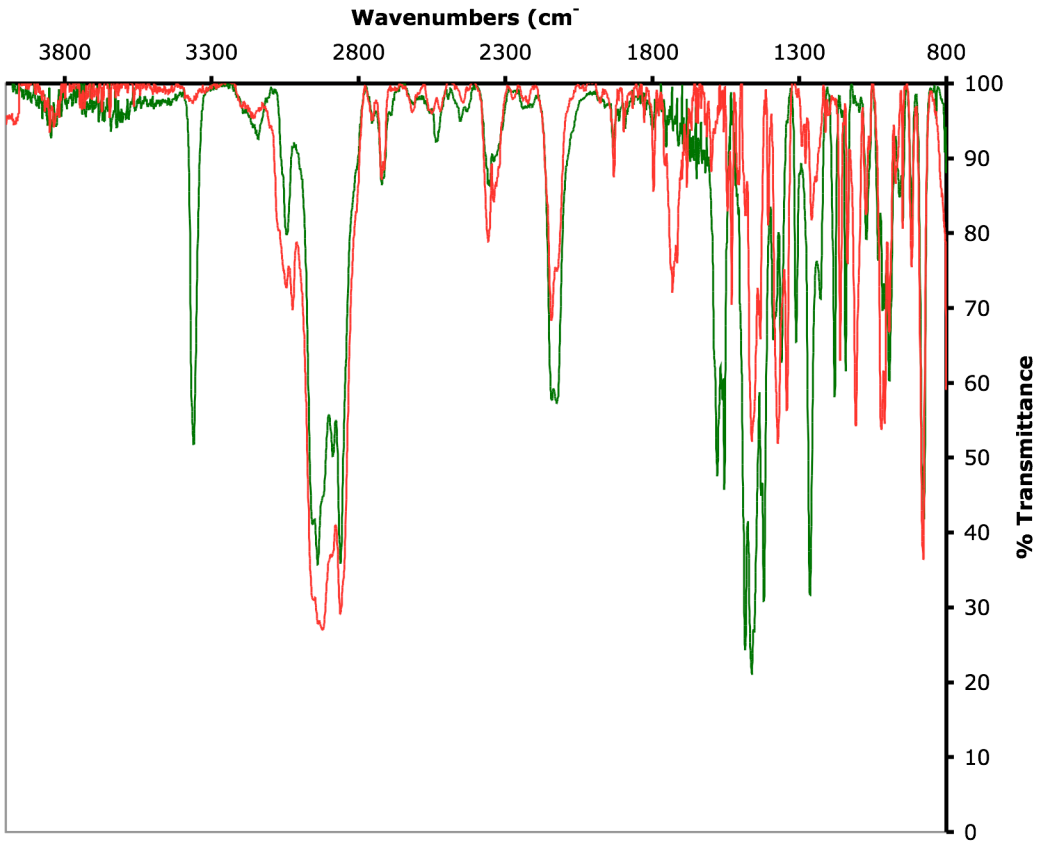

Figure 5.14. IR spectra of compounds **5.14c** (green) and **5.15c** (red)**.**

5.4.11 UV-vis and Emission Spectra

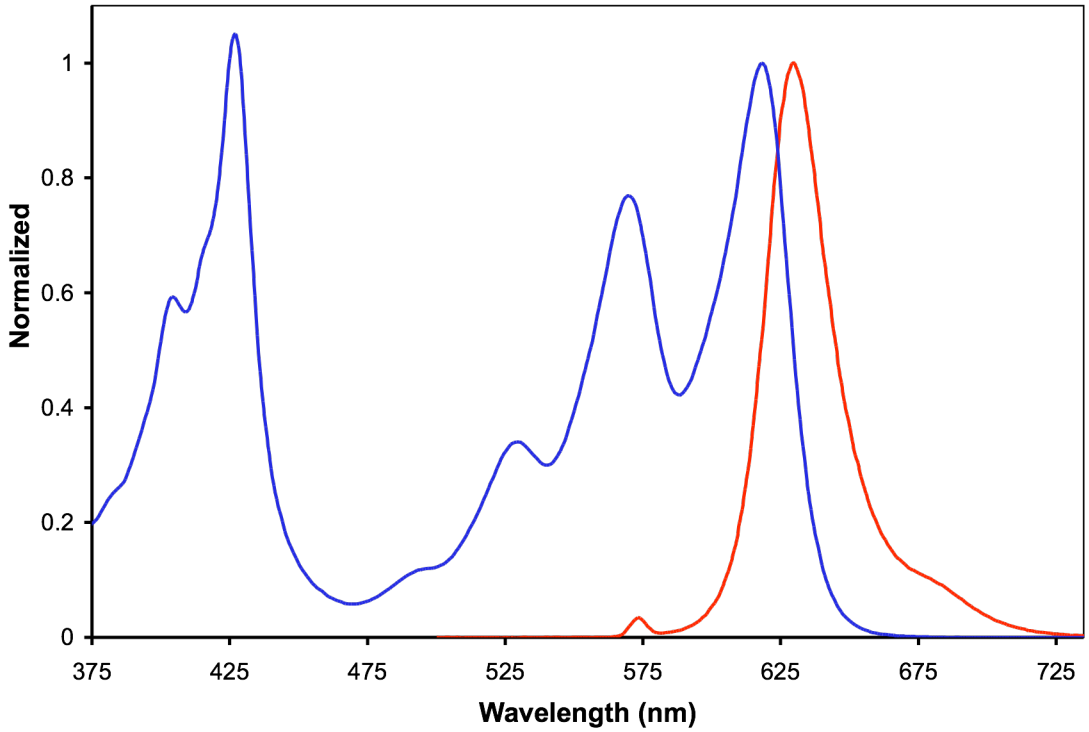

Figure 5.15. Normalized UV-vis absorption (blue) and emission (red) spectra of **5.11b**.

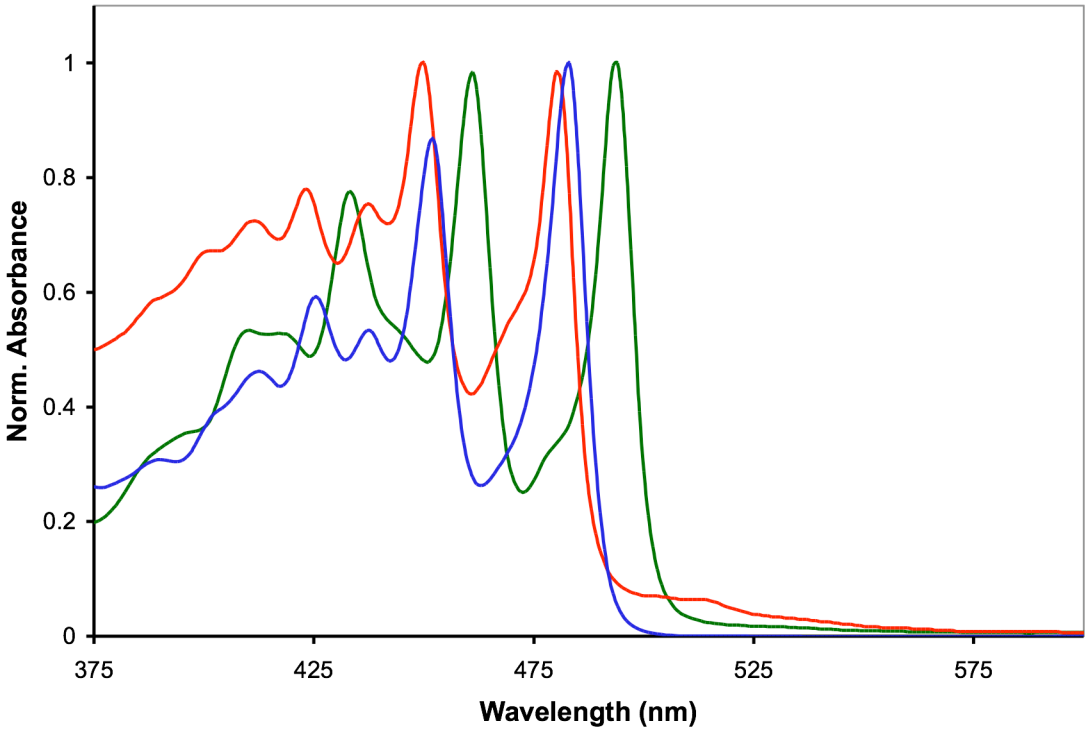

Figure 5.16. Normalized UV-vis absorption spectra of **5.14a-c** (green, red, blue, respectively).

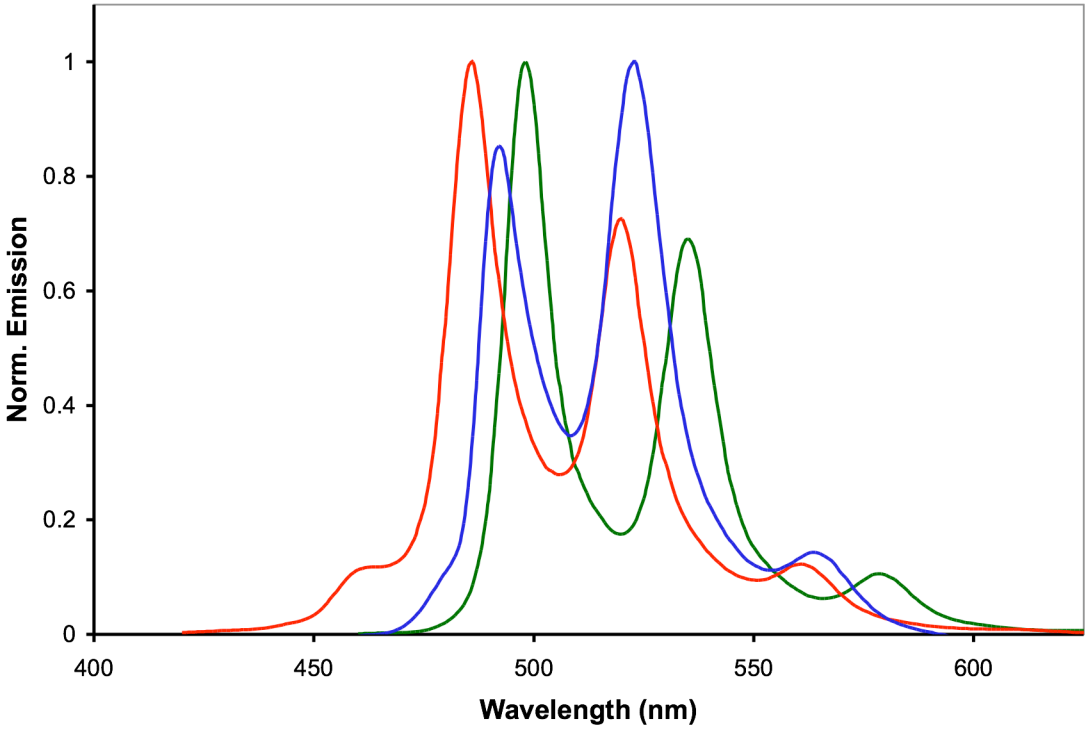

Figure 5.17. Normalized emission spectra of **5.14a-c** (green, red, blue, respectively).

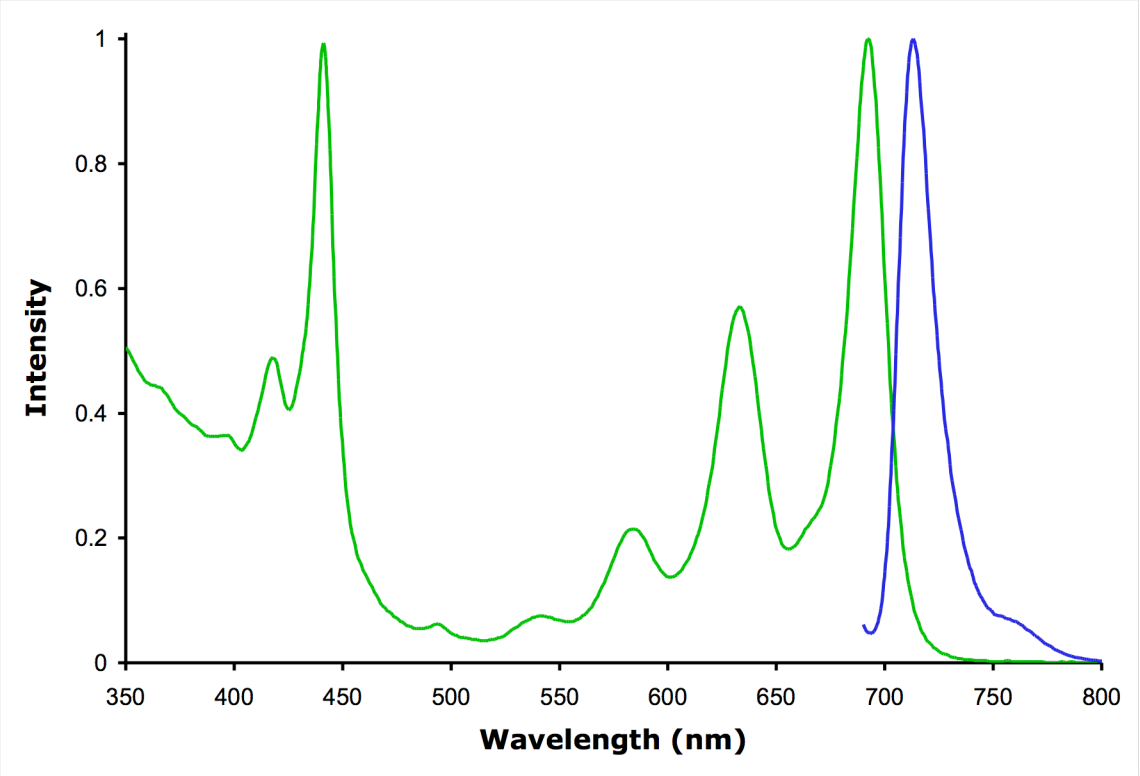

Figure 5.18. Normalized UV-vis absorption (green) and emission (blue) spectra of **5.15a**.

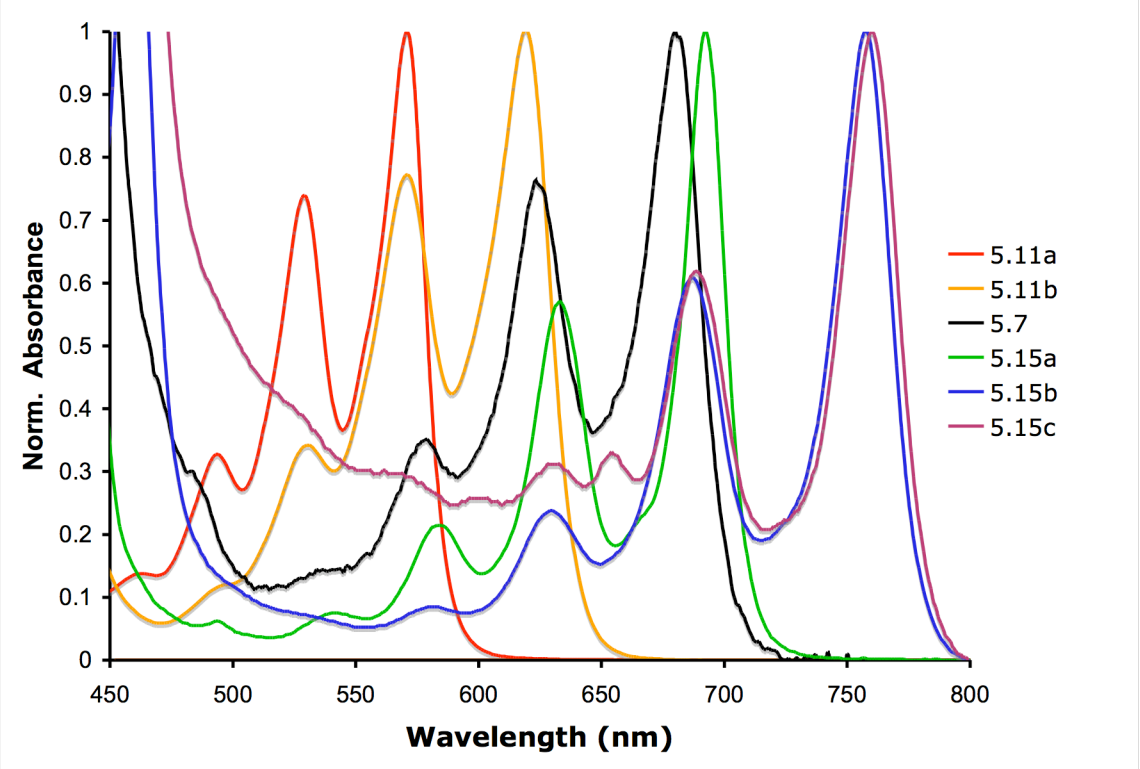

Figure 5.19. Normalized long wavelength UV-vis absorption of **5.11a,b**, **5.7**, and **5.15a-c**.

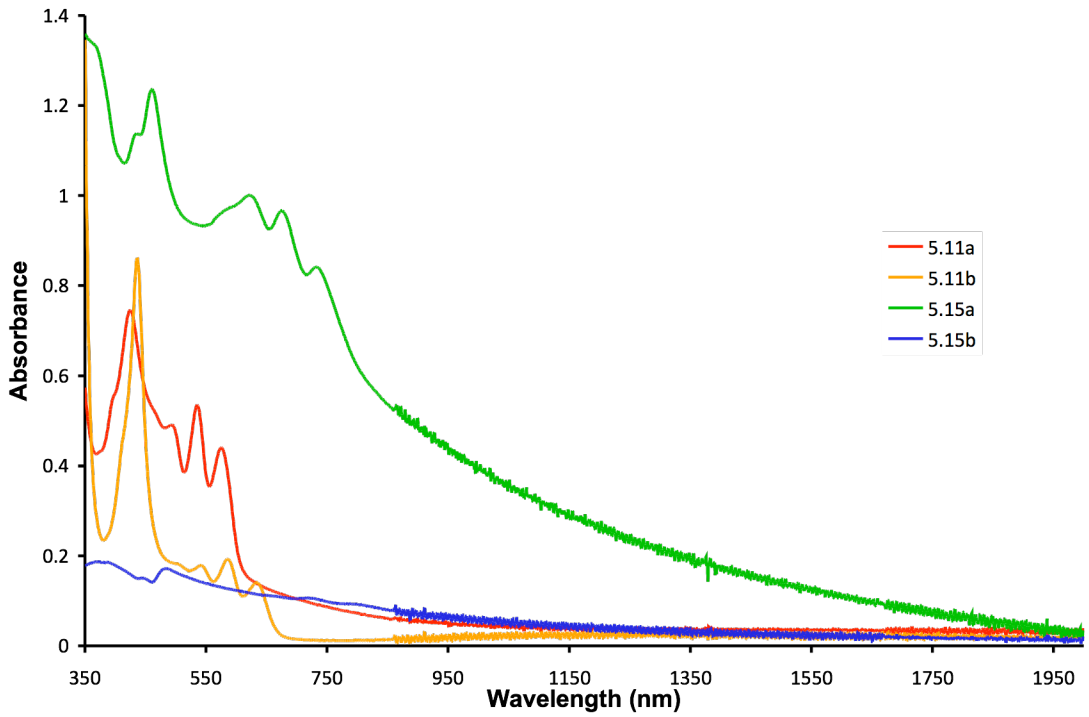

Figure 5.20. Thin-film absorption spectra of **5.11a**,**b** and **5.15a**,**b**.

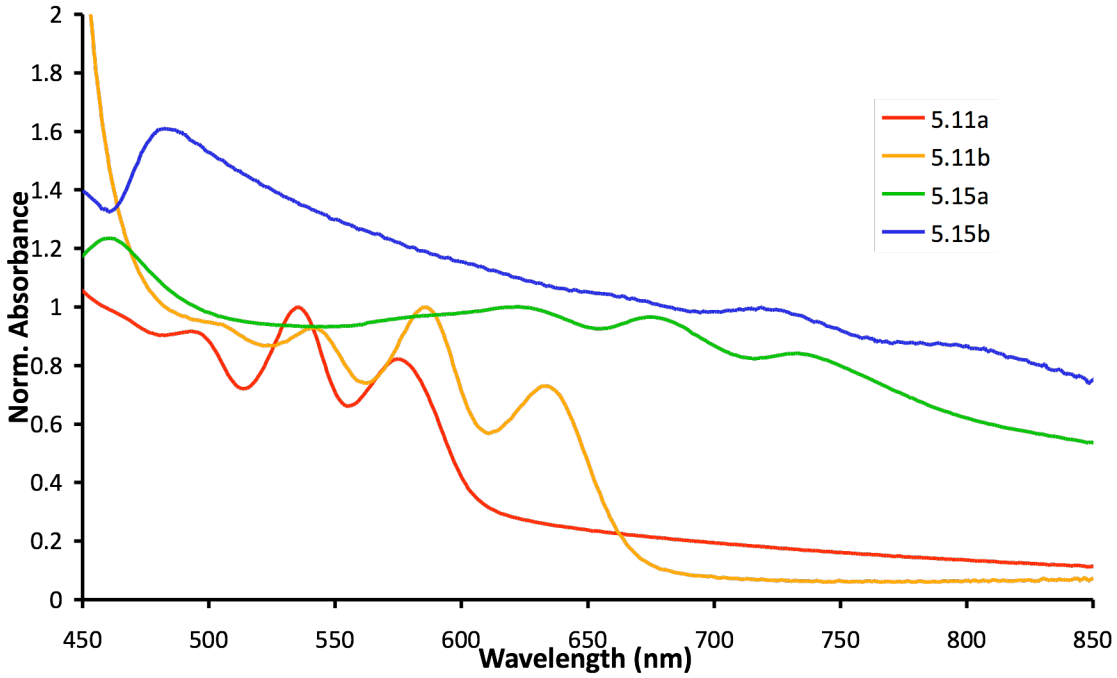

Figure 5.21. Normalized thin-film absorption (450-850 nm) spectra of **5.11a**,**b** and **5.15a**,**b**.

5.4.12 Electrochemical Data

Table 5.2. Summary of cyclic voltammetry experiments by Dr. Steve Barlow.

cpd	solvent	$E_{1/2}^{+/0}$ / V[a]	$E_{1/2}^{0/-}$ / V	$E_{1/2}^{-/2-}$ / V	E_{gap} / V
5.11a	CH_2Cl_2	+0.95[a]	–1.21[a]	–1.68[a]	2.16
	THF	–	–1.23[a]	–1.78[ab]	–
	1:4 tol/MeCN	+0.99	–1.15	–1.67[b]	2.14
	1:1 tol/MeCN	+0.99	–1.19	–1.73	2.18
5.11b	THF		–0.92	–1.50	
	1:4 tol/MeCN	+1.12[b]	–0.85	–1.40[b]	1.97
	1:1 tol/MeCN	+1.11[b]	–0.92	–1.51	2.03
5.15a	THF	+0.82[d]	–1.08	–1.59	–
	1:4 tol/MeCN	+0.70[b]	–0.99	–1.50	1.69
	1:1 tol/MeCN	+0.68	–1.05	–1.51	1.73
5.15b	THF	–	–0.80	–1.32[d]	–
	1:1 tol/MeCN	+0.83[b]	–0.79	–1.32	1.62
5.15c	THF	–	–0.80	–1.30[b]	–
	1:1 tol/MeCN	+0.80[b]	–0.79	–1.23	1.59

[a]Data from ref 23. [b]Not fully chemically reversible at 50 mVs^{-1} (i.e., $I_{ox}<I_{red}$ for molecular reductions and vice versa for oxidation processes). [c]Complex and irreversible at Pt working electrode; the value given in 1:1 *v/v* tol/MeCN was determined by additional experiments with a glassy-carbon working electrode, at which this reduction appears reversible. [d]Irreversible; peak potential given.

Table 5.3. HOMO and LUMO orbital energies, HOMO-LUMO gap, vertical and adiabatic ionization potentials, electron affinities, and excitation energies (all in eV), and ground-state dipole moments (Debye) computed at the B3LYP/6-311+G* level of theory computed by Dr. John S. Sears. S_1 was calculated using Time Dependent Density Function Theory (TD-DFT) using the same method and basis set.

	HOMO /LUMO	$\Delta_{HOMO-LUMO}$	IP^{VERT} /$IP^{ADIABATIC}$	EA^{VERT} /$EA^{ADIABATIC}$	$S_1{}^{VERT}$ /$S_1{}^{ADIABATIC}$	**μ**
5.11a'	-5.72	2.37	7.05	2.02	2.07	0.17
	-3.35		6.99	2.10	1.91	
5.11b'	-6.03	2.25	7.29	2.53	1.91	3.69
	-3.78		7.23	2.62	1.75	
5.11c'	-6.66	1.81	7.16	4.39	1.38	11.52
	-4.84		7.08	4.46	0.46	
5.15a'	-5.37	1.87	6.61	2.27	1.58	0.24
	-3.50		6.56	2.34	1.45	
5.15b'	-5.66	1.77	6.85	2.72	1.44	4.44
	-3.89		6.79	2.80	1.31	
5.16a'	-5.28	2.41	6.60	1.57	2.16	0.22
	-2.87		6.55	1.65	2.02	
5.16b'	-5.68	2.39	6.92	2.07	2.13	3.81
	-3.30		6.86	2.15	1.99	
5.16c'	-6.38	2.00	7.62	3.17	1.61	11.74
	-4.38		7.57	3.23	1.48	

5.5 References

[1] O. Hinsberg. *Liebigs Ann. Chem.* **1901**, *319*, 257.

[2] Q. Miao, T.Q. Nguyen, T. Someya, G.B. Blanchet, C. Nuckolls. *J. Am. Chem. Soc.* **2003**, *125*, 10284.

[3] J.E. Anthony. *Angew. Chem. Int. Ed.* **2008**, *47*, 452.

[4] J.E. Anthony. *Chem. Rev.* **2006**, *106*, 5028.

[5] V. Coropceanu, M. Malagoli, D.A. da Silva Filho, N.E. Gruhn, T.G. Bill, J-L Brédas. *Phys. Rev. Lett.* **2002**, *89*, 275503.

[6] S. Yoo, B. Domerq, B. Kippelen. *Appl. Phys. Lett.* **2004**, *85*, 5427.

[7] M. Winkler, K.N. Houk. *J. Am. Chem. Soc.* **2007**, *129*, 1805.

[8] Y. Sakamoto, T. Suzuki, M. Kobayashi, Y. Gao, Y. Fukai, Y. Inoue, F. Sato, S. Tokito. *J. Am. Chem. Soc.* **2004**, *126*, 8138.

[9] M.C.R. Delgado, K.R. Pigg, D. Filho, N.E. Gruhn, Y. Sakamoto, T. Suzuki, R.M. Osuna, J. Casado, V. Hernandez, J.T.L. Navarette, N.G. Martinelli, J. Cornil, R.S. Sanchez-Carrera, V. Coropceanu, J-L. Brédas. *J. Am. Chem. Soc.* **2009**, *131*, 1502.

[10] Z.H. Chen, P. Muller, T.M. Swager. *Org. Lett.* **2006**, *8*, 273.

[11] S. Salman, M.C.R. Delgado, V. Coropceanu, J-L. Brédas. *Chem. Mater.* **2009**, *21*, 3593.

[12] S. Miao, A.L. Appleton, N. Berger, S. Barlow, S.R. Marder, K.I. Hardcastle, U.H.F. Bunz. *Chem. Eur. J.* **2009**, *15*, 4990.

[13] U.H.F. Bunz. *Chem. Eur. J.* **2009**, *15*, 6780.

[14] M.L. Tang, J.H. Oh, A.D. Reichardt, Z. Bao. *J. Am. Chem. Soc.* **2009**, *131*, 3733.

[15] J.E. Anthony, J.S. Brooks, D.L. Eaton, S.R. Parkin. *J. Am. Chem. Soc.* **2001**, *123*, 9482.

[16] Electronegative substitution on π-systems can lead to either hypsochromic or bathochromic shift or an almost unchanged absorption spectra, and chlorination for example induces bathochromic shifts in 9,10-dichloroanthracene and some chlorinated nitro-aminodiazobenzene derivatives of disperse red. Such effects due to electronegativity occur if either the HOMO or the LUMO is particularly stabilized or not;

they are especially pronounced in molecules with disjoint orbital structures, where HOMO and LUMO are localized on different parts of a molecule.

[17] V.S. Pavlovich. *J. Appl. Spectroscopy.* **2007**, *74*, 180.

[18] L. De Boni, J.J. Rodrigues, D.S. de Santos, C. Silva, D.T. Balogh, O.N. Oliveira, S.C. Zilio, L. Misoguti, C.R. Mendonca. *Chem. Phys. Lett.* **2002**, *361*, 209.

[19] A.J. Zucchero, P.L. McGrier, U.H.F. Bunz. *Acc. Chem. Res.* **2010**, *43*, ASAP Article.

[20] *Acc. Chem. Res. 42*, Thematic Issue *11*, Organic Photovoltaics **2009**.

[21] M.M. Payne, S.R. Parkin, J.E. Anthony. *J. Am. Chem. Soc.* **2005**, *127*, 8028.

[22] F. Kummer, H. Zimmermann. *Ber. Bunsenges.* **1967**, *71*, 1119.

[23] S. Miao, S.M. Brombosz, P.v.R. Schleyer, J.I. Wu, S. Barlow, S.R. Marder, K.I. Hardcastle, U.H.F. Bunz. *J. Am. Chem. Soc.* **2008**, *130*, 7339.

[24] A.L. Appleton, S. Miao, S.M. Brombosz, N.J. Berger, S. Barlow, S.R. Marder, B.M. Lawrence, K.I. Hardcastle, U.H.F. Bunz. *Org. Lett.* **2009**, *11*, 5222.

[25] The stabilization of the formally antiaromatic **5.14a-c** results from the interplay of energetically advantageous enamine groups and the presence of two Clar sextets instead of one for the heteroacenes **5.15a-c**. In the case of the diazatetracenes (**5.11**), this delicate energetic balance is such that the overall aromaticity drives the formation of the diazaacenes, and the significantly more antiaromatic NH-compounds are not observed as already shown by Hinsberg for the parent diazatetracene in 1901; see refs 1 and 26.

[26] J.I. Wu, C.S. Wannere, Y.R. Mo, P.v.R. Schleyer, U.H.F. Bunz. *J. Org. Chem.* **2009**, *74*, 4343.

[27] C. Hansch, A. Leo, R.W. Taft. *Chem. Rev.* **1991**, *91*, 165.

[28] The very close correspondence between the values of the experimental optical and electrochemical gaps (rather than merely trends in these values) is not necessarily to be expected, and presumably arises from a fortuitous balancing of the exciton binding energy stabilizing the excited state and strong solvation of the relatively small ions formed upon oxidation or reduction.

CHAPTER 6

AMPHIPHILIC PHENAZINE BISTRIAZOLES AND THEIR METAL-BINDING PROPERTIES

6.1 Introduction

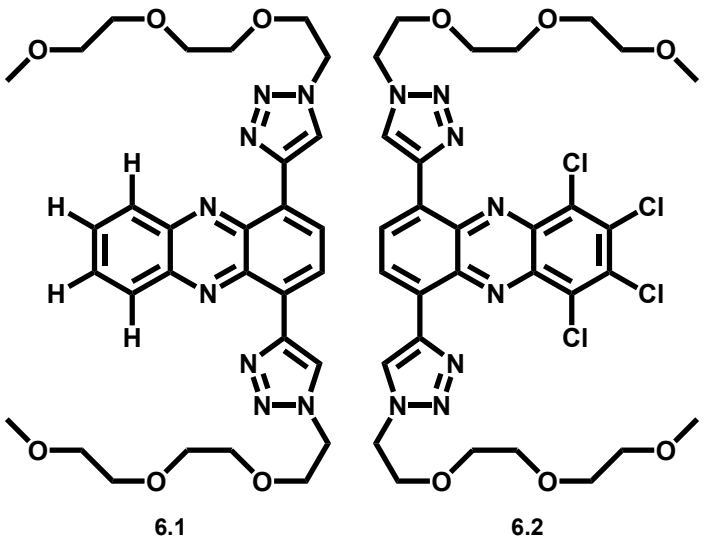

Scheme 6.1. Structures of compounds **6.1** and **6.2**.

Herein we expand on our "Click" products first described in Chapter 3 by changing the size and electronic character of the metal-binding pocket by using bistriazole-phenazine derivatives **6.1** and **6.2**. We explore their optoelectronic and metallo-responsive binding properties in DCM, water, and in one case a water : methanol mix. Finally, we compare all compounds (**6.1**, **6.2**, **3.4**, **3.5**) and their responses to metal cations in aqueous environments.

Since the 1,3-dipolar cycloaddition of terminal alkynes to azides was developed by Huisgen and Szeimies,[1] and was later promoted by Sharpless[2] as a tool for the construction of biologically active molecules, the Click reaction is utilized in many areas of science.[3] Although the Click reaction can join two molecular pieces together, it can also be used to create novel compounds with useful properties. A quite attractive, but less developed aspect of the triazole formation is their incorporation as functional modules into fluorophores to form a recognition site utilized as fluorescent probes.[4]

Our group has previously reported benzo- and naphthothiadiazole bistriazoles and their metal-binding properties in water.[5] Here, we present two novel non-halogenated and halogenated fluorescent bis-cycloadducts **6.1** and **6.2**, which possess binding pockets for metal cations. An interesting difference between the work presented here and the work in Chapter 3 is that in this case, we were able to isolate the terminal alkyne after deprotection and then perform the Click reaction. Isolated terminal alkynes are very useful synthetic building blocks.[6]

6.2 Results and Discussion

The TMS-protected diethynyl *o*-phenylene diamine (**6.4**) is formed smoothly from the corresponding benzothiadiazole by lithium aluminum hydride reduction in 91% yield (Scheme 6.2). The phenazine derivatives (**6.6a-c**) are synthesized by condensation of **6.4** with the appropriate *o*-benzoquinone (**6.5a-b**) in moderate to good yields. The deprotected alkynyl forms (**6.7a-b**) are easily obtained by stirring in a basic solution of methanol and THF. Now that we have a stable terminal alkyne (**6.7a-b**), we are ready to perform the click reaction with the oligoethyleneglycol azide (**6.8**) to furnish bistriazole phenazine derivatives **6.1** and **6.2** in 61 and 46% yield, respectively. Due to the heavy

atom effect of bromine, the fluorescence of **6.6c** is completely quenched, and so was not utilized further due to the desired property of fluorescence needed for detection of metal cations by fluorescence quenching. The azide **6.8** was chosen because it is neutral and increases water solubility.[5]

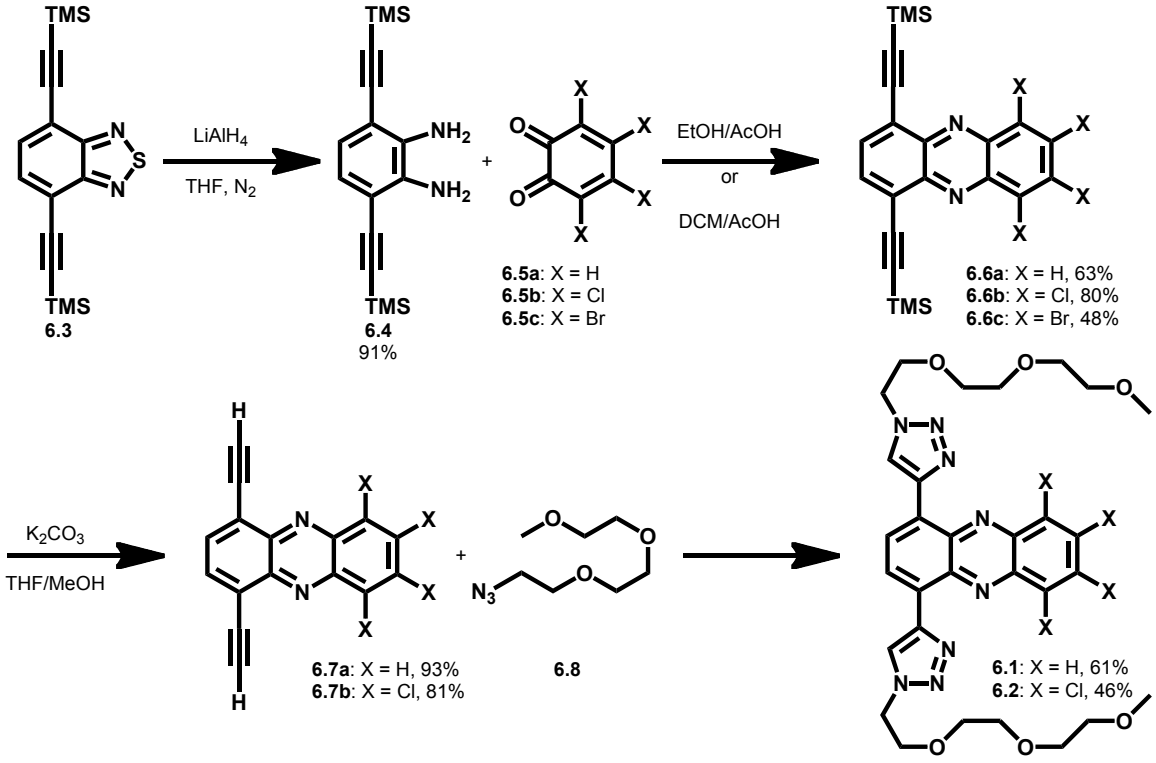

Scheme 6.2. Synthetic pathway to compounds **6.1** and **6.2**.

Spectroscopic studies of **6.6** and **6.7** were carried out in DCM due to their insolubility in water, **6.1** in water, and **6.2** in a water : methanol (1:1 *v*/*v*) solution (Table 6.1). The solubility of **6.2** is very poor in water, an effect we attribute to the halogenation of the phenazine core. There are interesting trends between **6.6**, **6.7**, **6.1**, and **6.2**. First, there is a bathochromic shift observed in the absorption onset for compounds **6.6b** and **6.6c** as compared to **6.6a**. In a similar manner to the shift observed in the absorption

Table 6.1. Photophysical properties of compounds **6.6**, **6.7**, **6.1**, and **6.2**. a: Quinine sulfate in 0.1 M H_2SO_4 used as a reference standard. b: **6.2** aqueous measurements were done in a water : methanol (1:1 *v/v*) solution. Determined by Yexiang Zhang.

	ABS (nm)		EMS (nm)		Quantum Yield[a]		Fluorescence Lifetime (ns)	
Cpd	DCM	H_2O	DCM	H_2O	DCM	H_2O	DCM	H_2O
6.6a	373	NA	487	NA	0.015	NA	NA	NA
6.6b	388	NA	532	NA	0.042	NA	NA	NA
6.6c	391	NA	NA	NA	NA	NA	NA	NA
6.7a	371	NA	462	NA	0.005	NA	NA	NA
6.7b	388	NA	496	NA	0.011	NA	NA	NA
6.1	451	435	553	559	0.24	0.01	29.73	3.52
6.2[b]	492	488	610	619	0.06	0.0026	4.39	2.2

spectra, a bathochromic shift is also observed in the emission maximum of **6.6b** (recall, **6.6c** has no emission). The probable explanation for the observed bathochromic shift upon halogenation is due to the same effect previously seen in non-halogenated and halogenated diazatetracene and diazapentacene derivatives as observed by our group in Chapter 5.[7] This is attributed to a greater stabilization of the LUMO as compared to the HOMO upon tetrahalogen substitution on the periphery directly adjacent to the pyrazine moiety. The absorbance profiles of **6.6a** versus **6.7a** are nearly identical, as they both possess the same core structure. The same trend is observed in the chlorinated derivatives as well. However, the emission after deprotection (**6.6** → **6.7**) is hypsochromically shifted. This is probably due to the removal of the TMS group, which increased the relaxation of the excited state molecule after absorption of light down to the lowest excited state due to additional degrees of freedom through the sp^3 carbons of TMS, thus giving a longer wavelength, lower energy emission before deprotection. Stated another way, the rigidity of the molecule increased upon deprotection.

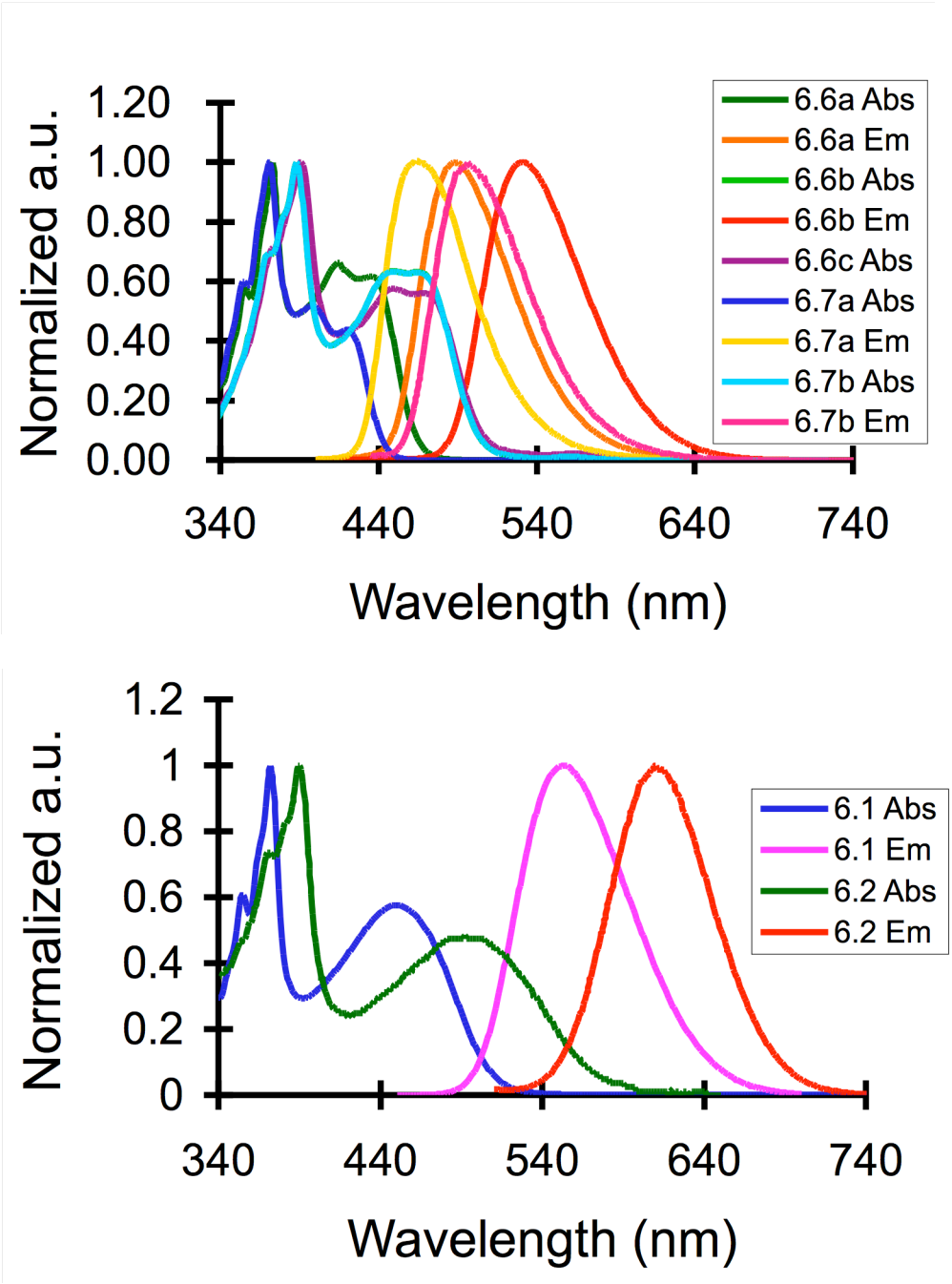

Figure 6.1. Normalized absorption and emission spectra of **6.1**, **6.2**, **6.6a,b**, and **6.7a,b** in DCM.

The absorption and emission wavelengths for the 1,3-dipolar azide adducts (**6.1** and **6.2**) are bathochromically shifted compared to their precursors. However, a change

of solvent from DCM to water produces a hypsochromic shift of the absorption maxima in compounds **6.1** and **6.2**, but a bathochromic shift is observed in their emission maxima. These changes are slight, less than 0.012 eV in all cases. The similarity of the spectral properties in DCM and water suggests that this series of fluorophores do not show strong intermolecular charge transfer in the ground or first-excited state.

We also found that the quantum yields increased after the Click reaction to form **6.1** and **6.2**. The quantum yields, did however, decrease upon changing the solvent from DCM to water to 1% or less. Also, important to certain applications is the fluorescence lifetime, as it may allow for time-gated fluorescence imaging of cells.[8] Unfortunately, although compound **6.1** has a fluorescence lifetime of 30 ns in DCM, the lifetime of both **6.1** and **6.2** decreases to less than 4 ns in water, a discouraging result for application in cell imaging because the background fluorescence of a cellular matrix is ~3 ns.[12]

Adducts **6.1** and **6.2** display a similar binding pocket for metal cations, but show differential responses to the binding of selected metals in solution (Figure 6.2). First, we determined the response of **6.1** towards different metal cations in pure water. We have found no change in the fluorescence upon adding Li^+, Na^+, K^+, Mg^{2+}, Zn^{2+}, and only a slight quenching effect from Ni^{2+}. Upon the addition of Cu^{2+} and Ag^+, the absorption spectra shows no change and a hypsochromic shift, respectively; both cause quenching of the emission. On the other hand, **6.2** shows very different responses to the same metal cations. Adding Li^+, Na^+, K^+, Mg^{2+}, Zn^{2+}, and Ni^{2+} will not change the absorption and emission at all, but interestingly Cu^{2+} and Ag^+ only decrease the emission 5% and 20%, respectively, with no change in the absorption profile. The different spectral responses of

6.1 and **6.2** can be attributed to the effect of halogenation on the size and electronic character of the binding pocket for metal cations.

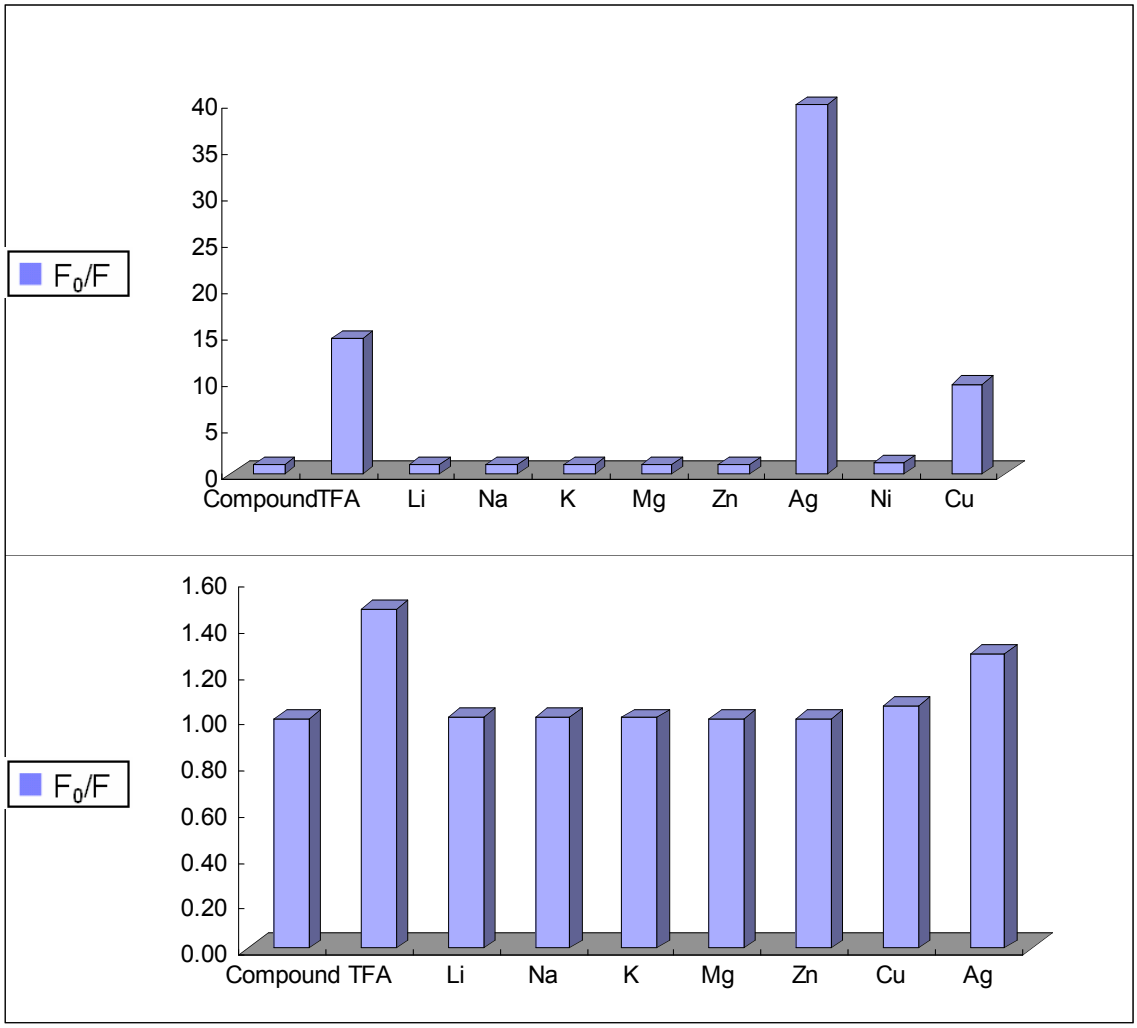

Figure 6.2. Fluorescence response of **6.1** (top) in H_2O and **6.2** (bottom) in the H_2O:MeOH solution to different metal cations. F_0 and F are the initial fluorescence intensity and final fluorescence intensity, respectively, at the λ_{max} of emission.

Furthermore, we would like to determine the strength of the binding between the metal cation(s) and the fluorophore **6.1**. The standard Stern-Volmer equation ($I_o/I_{final} = 1 + K_{SV}[Q]$)[13] resulted in deviations from linearity, however the data were well correlated when Equation (1) is employed from our previous work[5,9]:

$$I_q = I_o + \frac{I_{final} - I_o}{2} \times \left(1 + \frac{[Q]}{[F]} + \frac{1}{K_{SV}[F]} - \left[\left(1 + \frac{[Q]}{[F]} + \frac{1}{K_{SV}[F]} \right)^2 - 4\frac{[Q]}{[F]} \right]^{1/2} \right) \quad (3.1)$$

where I_q is the intensity of the fluorescence at a given quencher concentration, I_o is the initial fluorescence intensity of the fluorophore, I_f is the final intensity of the fluorescence of the quenched fluorophore, [Q] is the concentration of the quencher added, [F] is the concentration of the fluorophore, and K_{SV} is the apparent Stern-Volmer constant. This equation fits the data well, which assumes a 1:1 metal:fluorophore ratio, despite the presence of two binding pockets. We have previously attributed this to a loss of electron density of the second triazole ring upon coordination of a metal to the first triazole ring.[5]

The results of the titrations of compound **6.1** (Figure 6.3) are summarized in Table 6.2, together with compound **3.4** for comparison.[5] The binding of **6.1** to Cu^{2+} in water resulted in a binding constant of log K = 1.59 ± 0.01, which is lower than **3.4**'s binding with Cu^{2+} (log K = 2.70 ± 0.01). **6.1** only shows minimal quenching when Ni^{2+} is added, while **3.4** shows strong binding with Ni^{2+}. On the other hand, **3.4** showed no binding towards Ag^+, while the binding constant of **6.1** with Ag^+ is log K = 4.00 ± 0.03. Due to the greater attention gained by the negative impact of silver on the environment and the human body due to its widespread use, **6.1** could be very useful in its detection in aqueous environments.[10] Also, few sensors for silver cations are used in pure water, which would be ideal for detection and practical applications.[11]

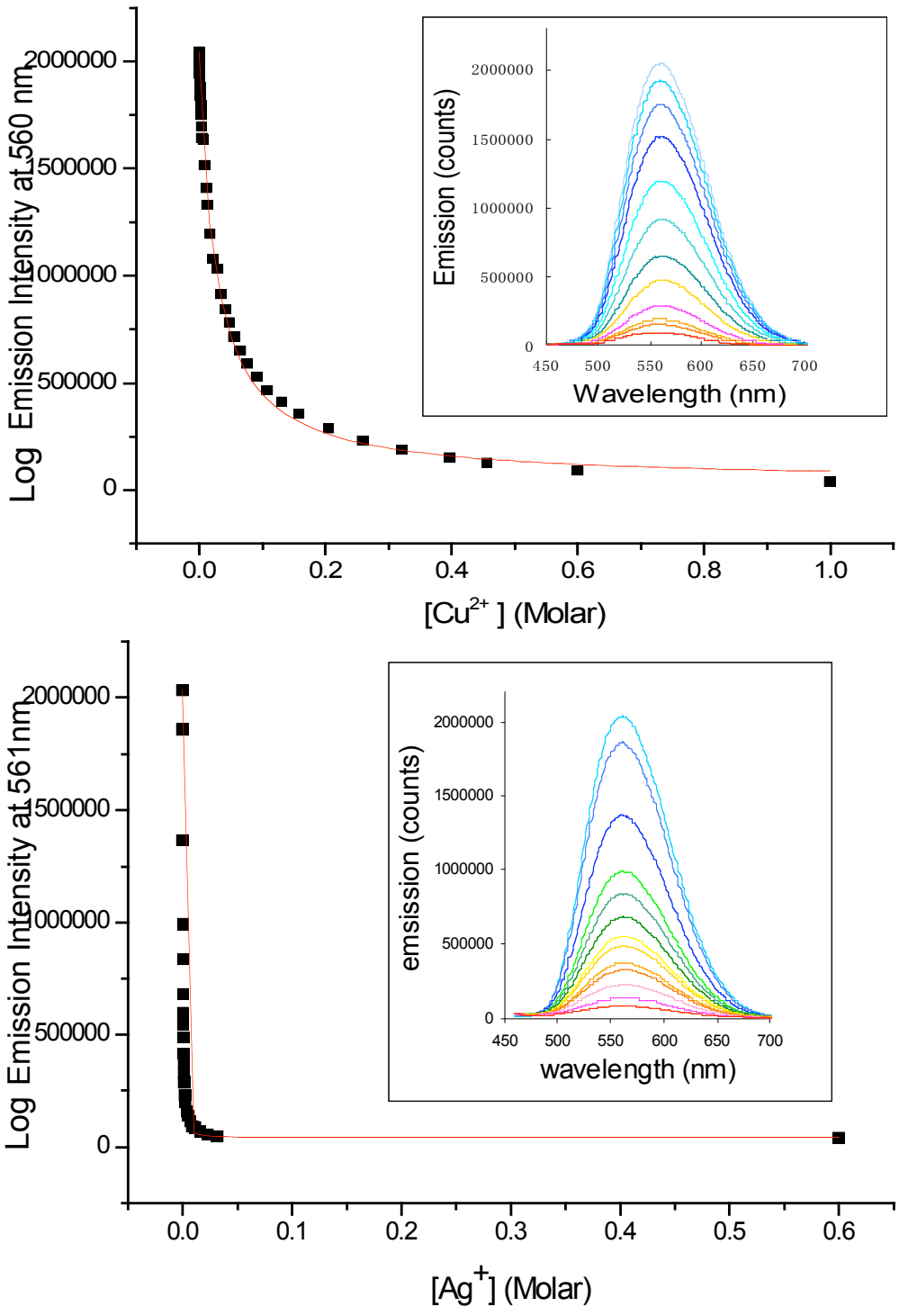

Figure 6.3. TOP: Representative titration of **6.1** (197 μM) with $CuSO_4$ in water. The red line indicates the fitting of Eqn 1 used to determine the binding constant. [Cu^{2+}] ranges from 0-1.0 M. Inset: the actual decrease of fluorescence intensity observed upon the addition of Cu^{2+}. BOTTOM: Representative titration of **6.1** (200 μM) with AgOTf in

(continued caption from Figure 6.3) water. [Ag^+] ranges from 0-0.6 M. Inset: the actual decrease of fluorescence intensity observed upon the addition of Ag^+.

Table 6.2. Summary of the binding data for **6.1** and **3.4**.

Compound	**6.1**	**6.1**	**3.4**	**3.4**
Metal	Cu^{2+}	Ag^+	Cu^{2+}	Ni^{2+}
Log K	1.59 ±0.01	4.00 ±0.03	2.70 ±0.01	3.71 ±0.01

6.3 Conclusion

In conclusion, we have prepared halogenated and non-halogenated phenazine derivatives (**6.6**) and their isolable terminal alkyne forms (**6.7**). The halogen substitution causes bathochromic shifts in the absorption and emission spectra. Derivatives of **6.7** were further functionalized to the previously unknown bistriazole derivatives **6.1** and **6.2**, which display binding towards certain metal cations in pure water and aqueous environments, respectively. The metal binding is negatively affected by halogenation, which caused a change in the optoelectronic properties and the character of the binding pocket. The bistriazoles do not show significant solvent dependencies of their spectroscopic properties. Finally, compound **6.1** shows strong responses to both copper and silver, indicating in conjunction with our previous work, that a library of similar compounds could provide for differential responses to different metal analytes in aqueous environments.

I was responsible for synthesizing the starting materials and co-authoring the paper with Yexiang Zhang.

This work has been submitted to *Chemical Communications*:

Yexiang Zhang, Anthony Lucas Appleton, Scott M. Brombosz, Andrew J. Zappas II, Xuhong Qian, Uwe H.F. Bunz. "Amphiphilic phenazine- and halogenated phenazine-bistriazoles and their metal-binding properties." *Chem. Comm.* **Submitted**.

6.4 Experimental Information

6.4.1 1,4-bis((trimethylsilyl)ethynyl)benzene-1,2-diamine 6.4

To an oven dried 500 mL Schlenck flask was added 4,7-bis((trimethylsilyl)ethynyl)benzo [c][1,2,5]thiadiazole (**6.3**) (5.2 g, 0.0158 mol) and dry THF (50 mL), which was purged with N_2 for five minutes and brought to 0 ºC on an ice bath. Lithium aluminum hydride (5.98 g, 0.158 mol, 10 eq.) was added slowly over 30 min. The reaction was sealed with a bubbler and stirred for 12 h while the ice melted. The reaction was then cooled again to 0 ºC on an ice bath before quenching with aqueous ammonium chloride. The product was extracted with ether (3 x 200 mL), dried with magnesium sulfate, filtered, and the solvent removed *in vacuo*. Compound **6.4** was obtained as a light yellow solid (4.31g, 0.0144mol, 91% yield). m.p. = 129 ºC; IR (KBr, cm^{-1}) 3425, 3420, 3335, 3075, 2956, 2897, 2788, 2142, 1616, 1608, 1451, 1411, 1247, 1245, 1184, 1123; ^{1}H NMR (δ in $CDCl_3$) 6.767 (s, 2H), 3.941 (s, 4H), 0.255 (s, 42H); ^{13}C NMR (δ in $CDCl_3$) 136.53, 122.06, 109.58, 101.79, 100.92, 0.13; accurate mass for $C_{16}H_{24}N_2Si_2$: *m/e* = 300.1472 [M+], calc. *m/e* = 300.1478.

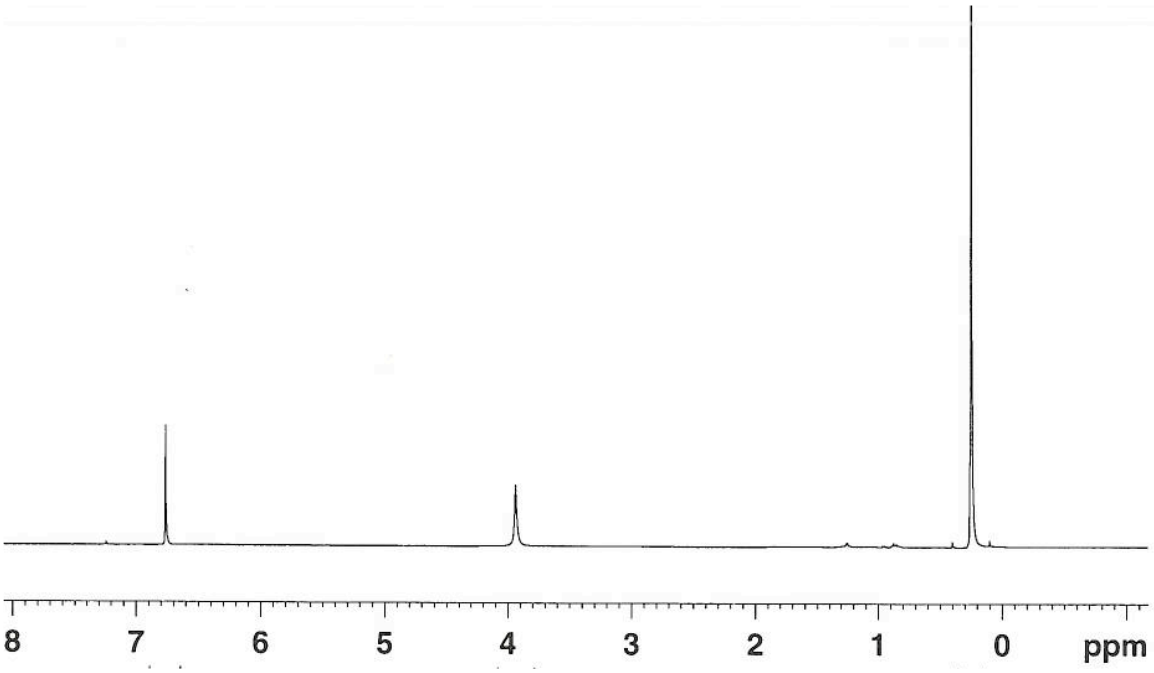

Figure 6.4. ^{1}H NMR of **6.4**.

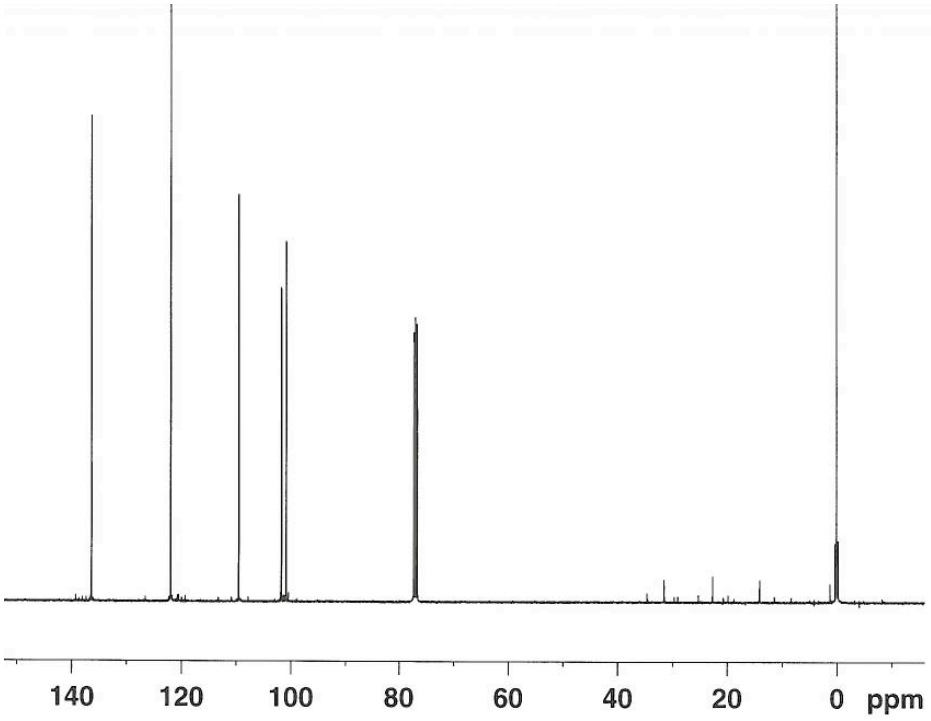

Figure 6.5. ^{13}C NMR of **6.4**.

6.4.2 1,4-bis((trimethylsilyl)ethynyl)phenazine 6.6a

1,4-bis((trimethylsilyl)ethynyl)benzene-1,2-diamine (**6.4**) (1.00 g, 3.3x 10^{-3} mol) and cyclohexa-3,5-diene-1,2-dione (**6.5a**) (1.07g, 9.9x 10^{-3} mol, 3 eq.) were heated to 40 ºC in stirring DCM (50 mL) and acetic acid (3 mL) for 12 h. The organic layer was washed with H_2O (2 x 250 mL), dried with Na_2SO_4, filtered, and the solvent removed *in vacuo*. The product was purified by column chromatography on silica gel using a 3:1 (hexanes : dichloromethane, *v/v*) solution. Compound **6.6a** was isolated as a yellow solid (0.78 g, 63.1 % yield). m.p. = 167 ºC; IR (KBr, cm^{-1}) 3089, 3040, 2963, 2954, 2897, 2152, 1919, 1518, 1473, 1406, 1281, 1138, 1118, 1025; ^{1}H NMR (δ in $CDCl_3$) 8.298 (AA' of AA'BB', 2H), 7.950 (s, 2H), 7.834 (BB' of AA'BB', 2H), 0.353 (s, 18H); ^{13}C NMR (δ in $CDCl_3$) 143.64, 142.99, 134.37, 131.15, 130.31, 124. 33, 104.21, 101.59, 0.13; accurate mass for $C_{22}H_{20}N_2Si_2$: *m/z* = 372.1488 [M+], calc. *m/z* = 372.1478.

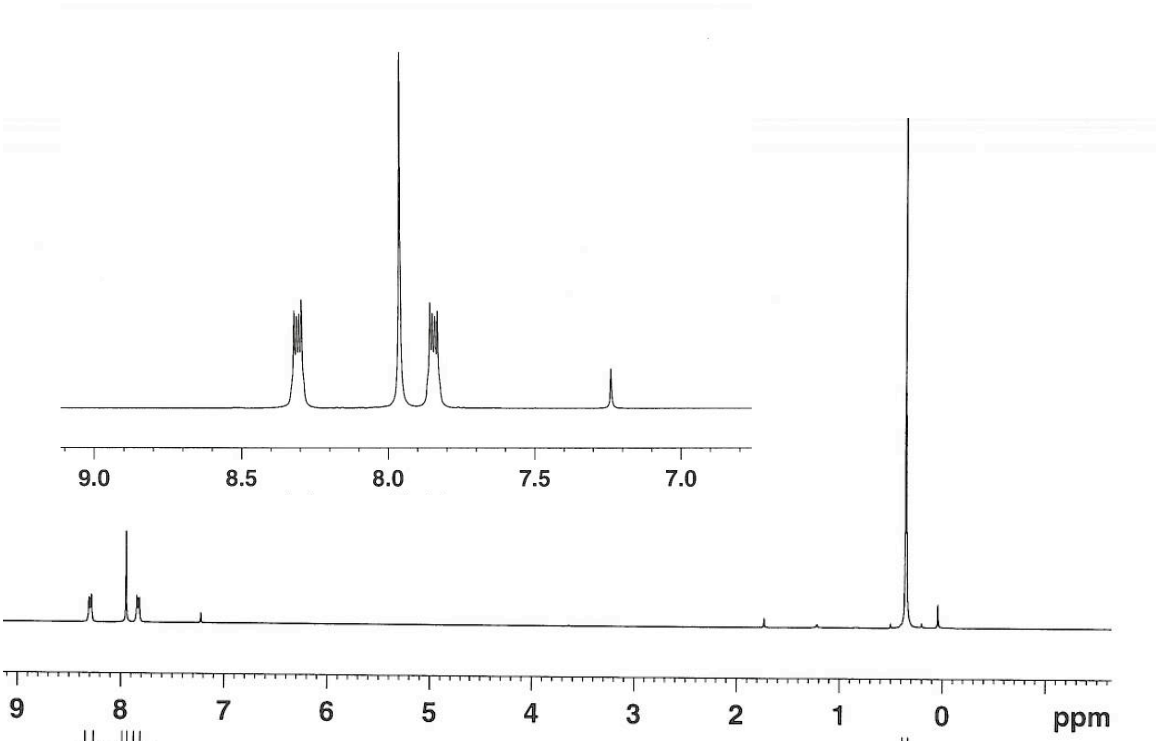

Figure 6.6. ^{1}H NMR of **6.6a**.

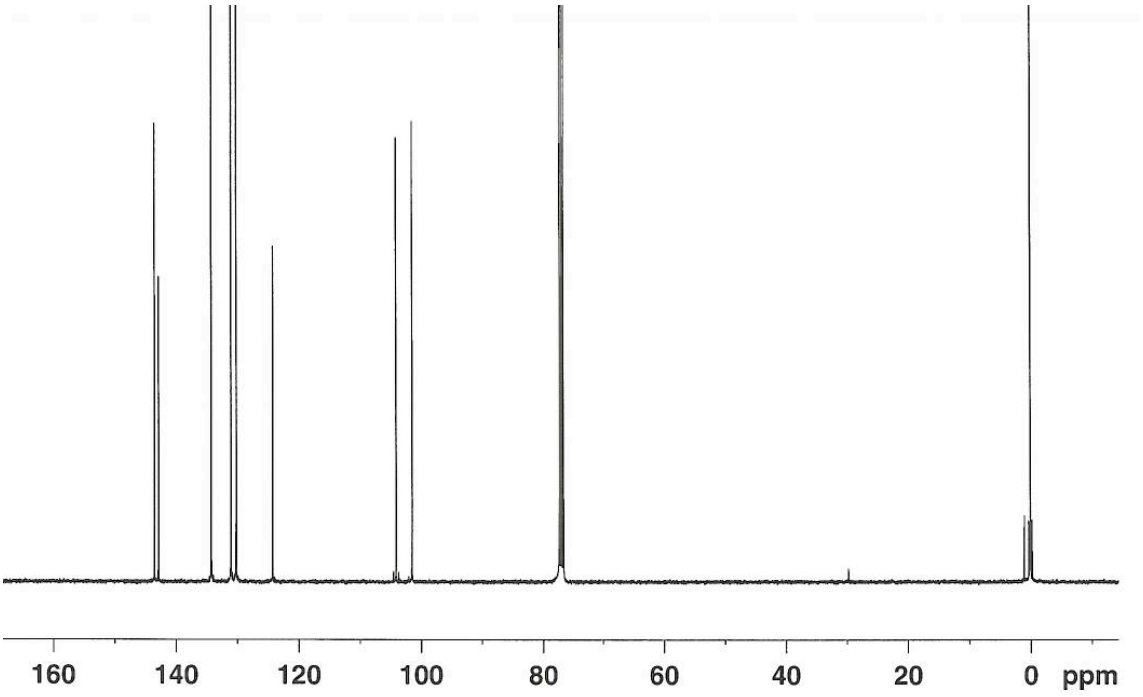

Figure 6.7. ^{13}C NMR of **6.6a**.

6.4.3 1,2,3,4-tetrachloro-6,9-bis((trimethylsilyl)ethynyl)phenazine 6.6b

1,4-bis((trimethylsilyl)ethynyl)benzene-1,2-diamine (**6.4**) (0.600 g, 2 x 10^{-3} mol) and 3,4,5,6-tetrachlorocyclohexa-3,5-diene-1,2-dione (**6.5b**) (0.984 g, 4 x 10^{-3} mol) were dissolved in ethanol (7 mL) and acetic acid (3 mL) and were stirred for 12 h at 40 ºC. The product mixture was poured into H_2O (250 mL), extracted with dichloromethane (3 x 50 mL), dried with sodium sulfate, filtered, and the solvent was removed *in vacuo*. The mixture was separated by column chromatography on silica gel using a 20:1 (hexanes : dichloromethane, *v/v*) solution. Compound **1b** was isolated as a yellow solid (819.1mg, 80.3 % yield). m.p. = 202 ºC; IR (KBr, cm^{-1}) 2958, 899, 2152, 1573, 1551, 1488, 1454, 1371, 1245, 1132, 1050; ^{1}H NMR (δ in $CDCl_3$) 8.021 (s, 2H), 0.364 (s, 18H); ^{13}C NMR (δ in $CDCl_3$) 143.26, 138.67, 135.35, 135.08, 132.20, 124.27, 105.82, 100.21, -0.13; accurate mass for $C_{22}H_{20}Cl_4N_2Si_2$: *m/z* = 507.9918 [M+], calc. *m/z* = 507.9919.

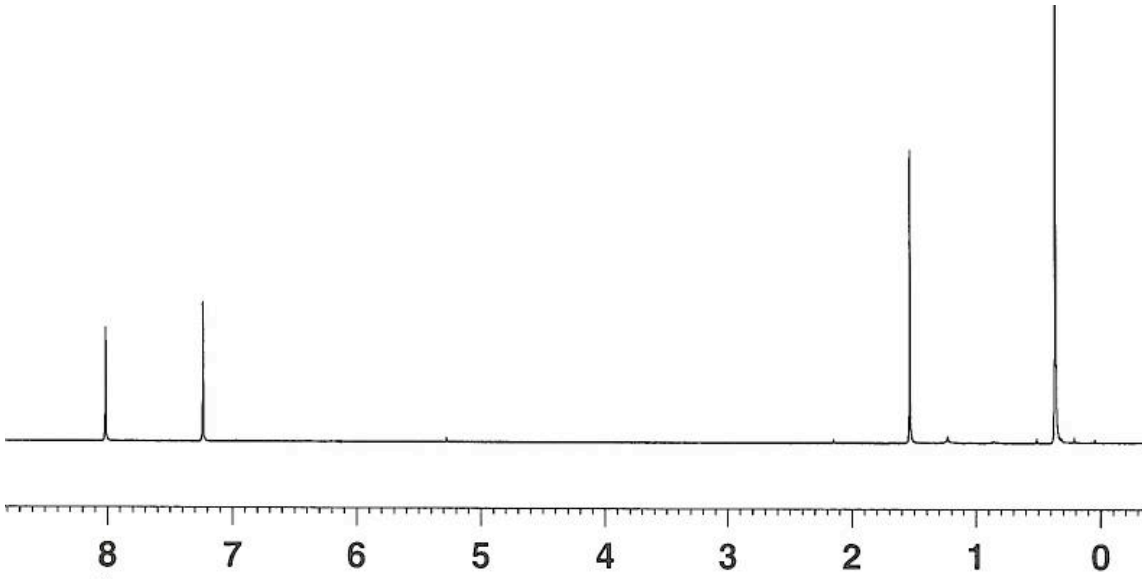

Figure 6.8. ^{1}H NMR of **6.6b**.

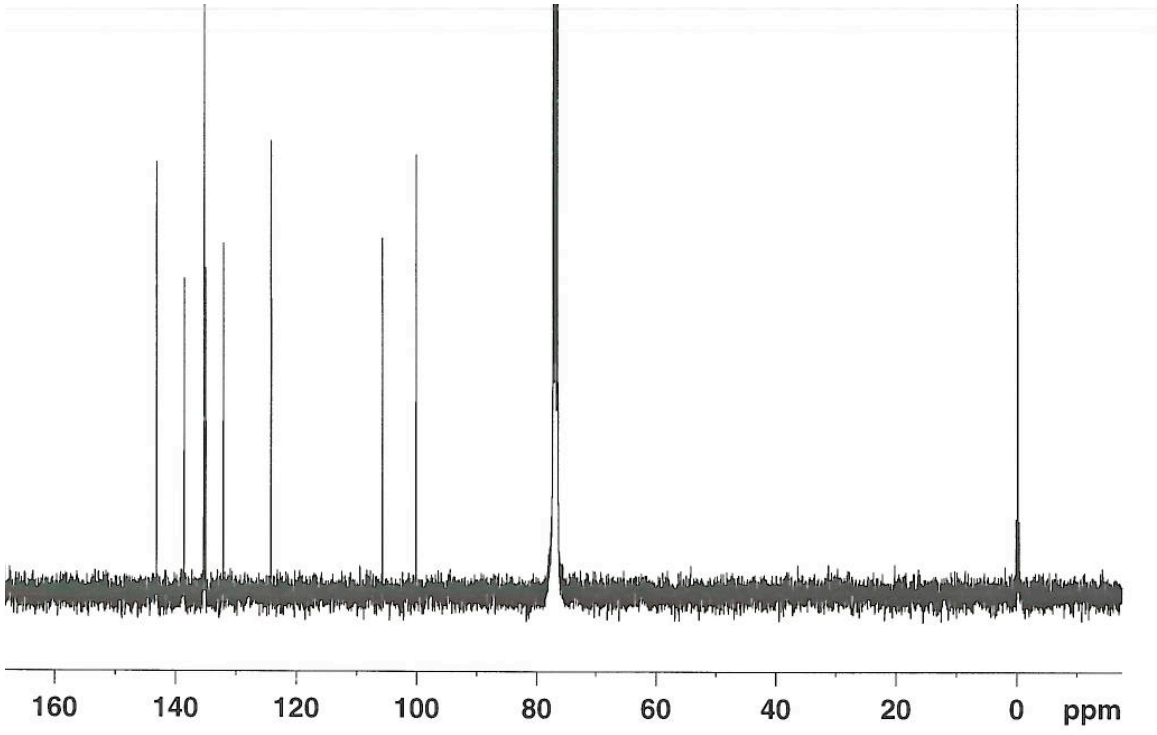

Figure 6.9. ^{13}C NMR of **6.6b**.

6.4.4 1,2,3,4-tetrabromo-6,9-bis(trimethylsilyl)ethynyl)phenazine 6.6c

1,4-bis((trimethylsilyl)ethynyl)benzene-1,2-diamine (**6.4**) (0.300 g, 1 x 10^{-3} mol) and 3,4,5,6-tetrabromocyclohexa-3,5-diene-1,2-dione (**6.5c**) (0.85 g, 2 x 10^{-3} mol) were dissolved in ethanol (10 mL) and acetic acid (3 mL) and were stirred for 12 h at 40 ºC. The product mixture was poured in H_2O (250 mL), extracted with dichloromethane (3 x 50 mL), dried with sodium sulfate, filtered, and the solvent removed *in vacuo*. The mixture was separated by column chromatography on silica gel using pure hexanes as solvent. Compound **6.6c** was isolated as a yellow solid (303.4 mg, 48% yield). m.p. = 137 ºC (decompose); IR (KBr, cm^{-1}) 2958, 2925, 2899, 2852, 2153, 1893, 1573, 1446, 1359, 1254, 1247, 1099, 1044; ^{1}H NMR (δ in $CDCl_3$) 8.037 (s, 2H), 0.376 (s, 18H); ^{13}C NMR (δ in $CDCl_3$) 148.95, 145.03, 140.54, 137.12, 133.88, 129.25, 110.76, 105.47, 5.07; accurate mass for $C_{22}H_{20}Br_4N_2Si_2$: *m/z* = 683.7895 [M+], calc. *m/z* = 683.7899.

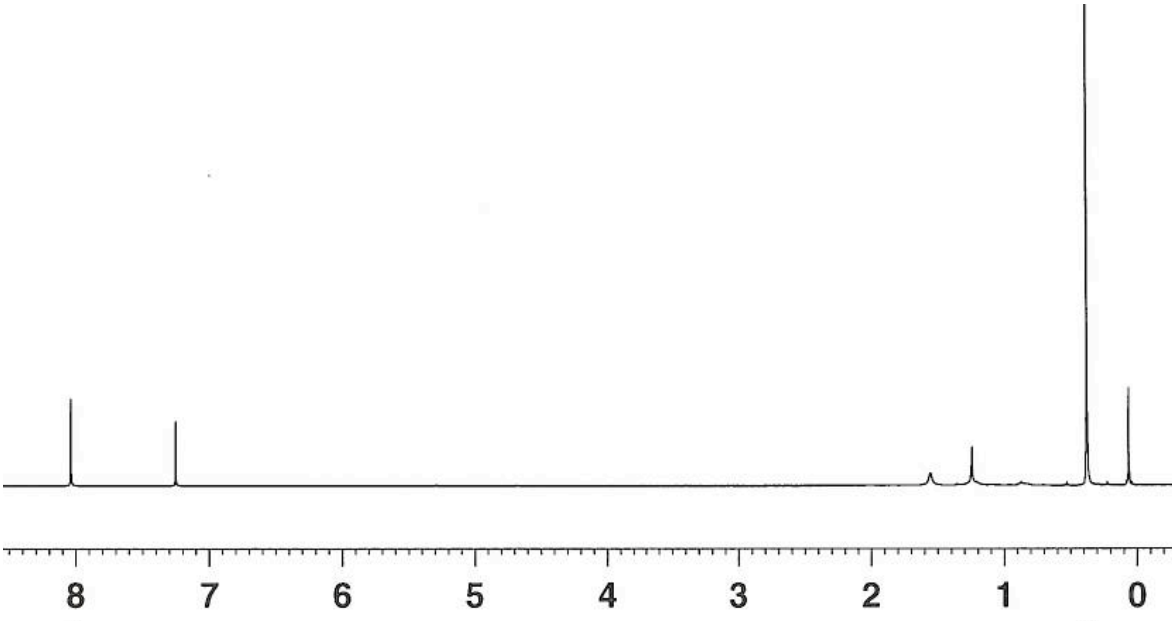

Figure 6.10. ^{1}H NMR of **6.6c**.

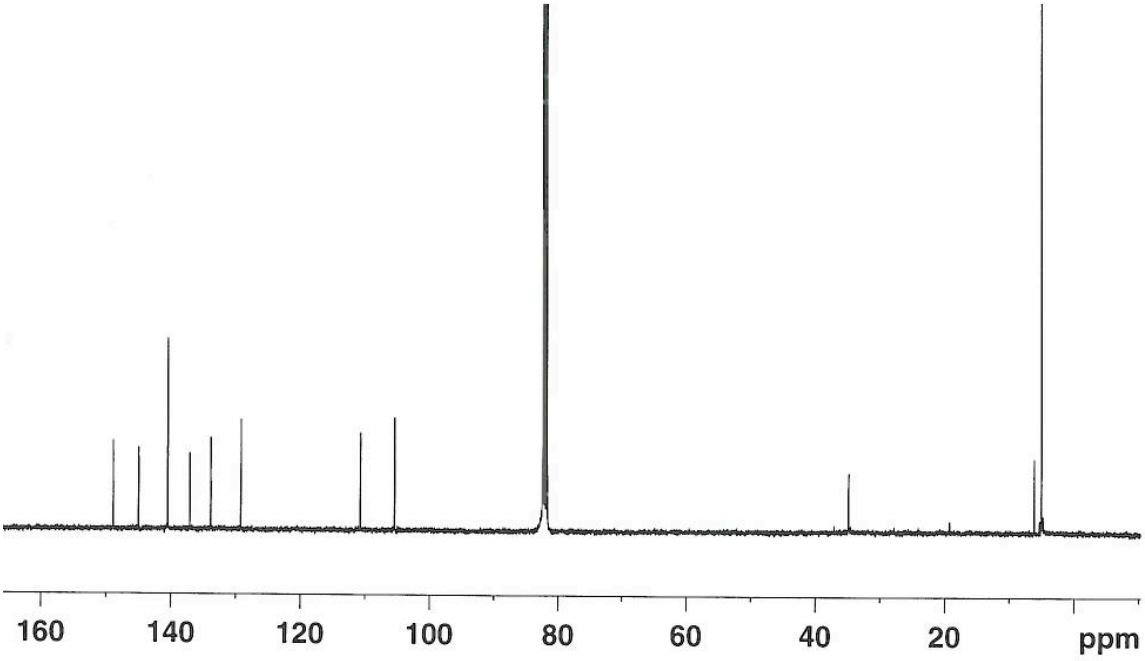

Figure 6.11. ^{13}C NMR of **6.6c**.

6.4.5 1,4-diethynylphenazine 6.7a

1,4-bis((trimethylsilyl)ethynyl)phenazine (**6.6a**) (186 mg, 5 x 10^{-4}mol) was dissolved in the THF : methanol (1:1 *v/v*) solution. K_2CO_3 (69 mg, 5 x 10^{-4} mol) was added then stirred for 20 min at room temperature. The product mixture was poured in H_2O (250 mL), extracted with dichloromethane (3 x 50 mL), dried with sodium sulfate, filtered, and the solvent removed *in vacuo*. The mixture was separated by column chromatography on silica gel using pure hexanes as solvent. Compound **6.7a** was isolated as a yellow solid (105.4 mg, 92.5% yield). m.p. = 80 ºC (decompose); IR (KBr, cm^{-1}) 3298, 3270, 3232, 3205, 2101,1521,1473,1334, 1112, 1034; ^{1}H NMR (δ in $CDCl_3$) 8.379 (AA' of AA'BB', 2H), 8.021 (s, 2H), 7.884 (BB' of AA'BB', 2H), 3.757 (s,2H); ^{13}C NMR (δ in $CDCl_3$) 143.69, 142.89, 134.61, 131.46, 130.07, 123.69, 85.78, 80.24; accurate mass for $C_{16}H_8N_2$: *m/z* = 228.0690 [M+], calc. *m/z* = 228.0687

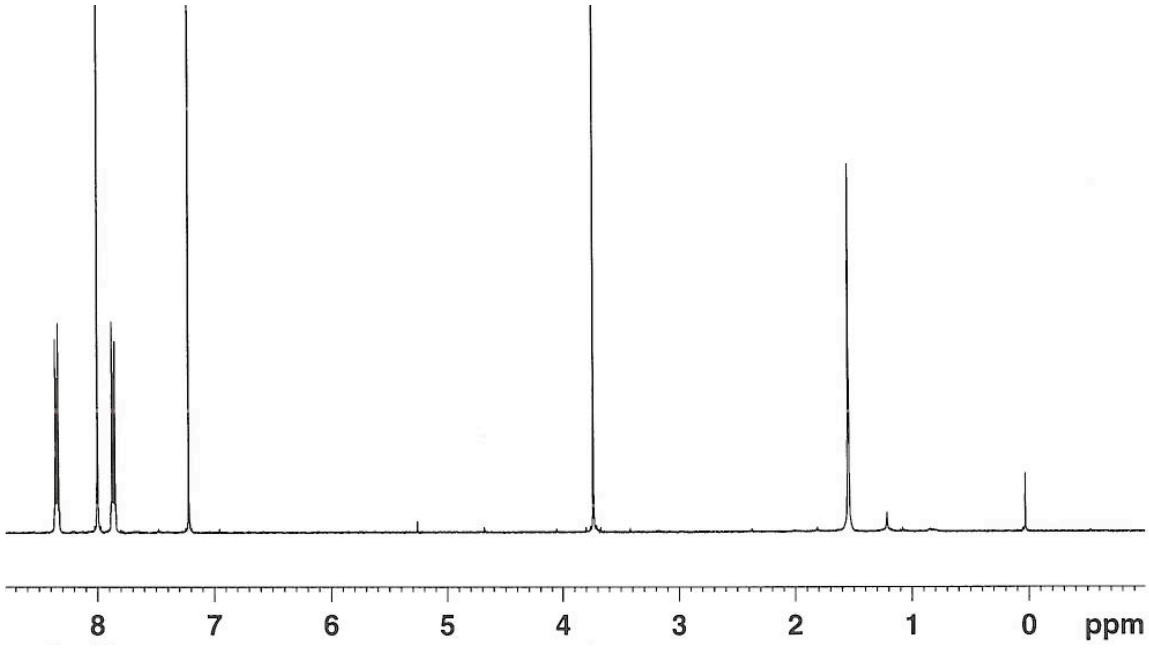

Figure 6.12. ^{1}H NMR of **6.7a**.

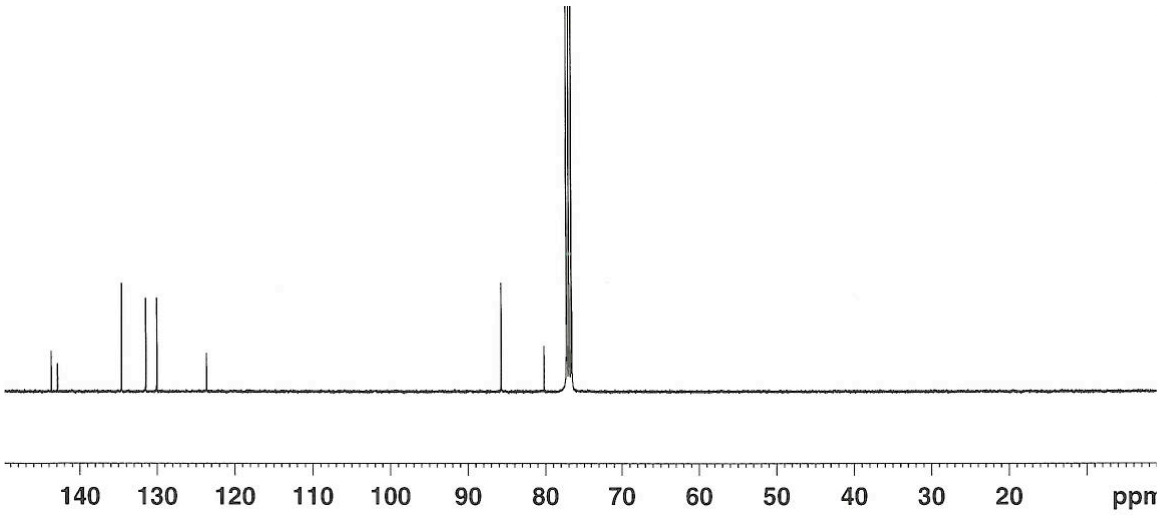

Figure 6.13. ^{13}C NMR of **6.7a**.

6.4.6 1,2,3,4-tetrachloro-6,9-diethynylphenazine 6.7b

1,2,3,4-tetrachloro-6,9-bis((trimethylsilyl)ethynyl)phenazine (**6.6b**) (200 mg, 4 x 10^{-4} mol) was dissolved in the THF : methanol (1:1, *v/v*)solution. K_2CO_3 (55 mg, 4 x 10^{-4} mol) was added then stirred for 20 min at room temperature. The product mixture was poured in H_2O (250 mL), extracted with dichloromethane (3 x 50 mL), dried with sodium sulfate, filtered, and the solvent removed *in vacuo*. The mixture was separated by column chromatography on silica gel using pure hexanes as solvent. Compound **6.6b** was isolated as a yellow solid (119.3 mg, 81.1% yield). m.p. = 40 ºC (decompose) IR (KBr, cm^{-1}) 3269, 2958, 2954, 2924, 2109, 1727, 1549, 1454, 1368, 1287, 1247, 1051, 1039; ^{1}H NMR (δ in $CDCl_3$) 8.087 (s, 2H), 3.766 (s, 2H); ^{13}C NMR (δ in $CDCl_3$) 143.08, 138.86, 136.12, 135.40, 132.12, 123.97, 86.83, 79.17; accurate mass for $C_{16}H_4Cl_4N_2$: *m/z* = 363.9133 [M+], calc. *m/z* =363.9129.

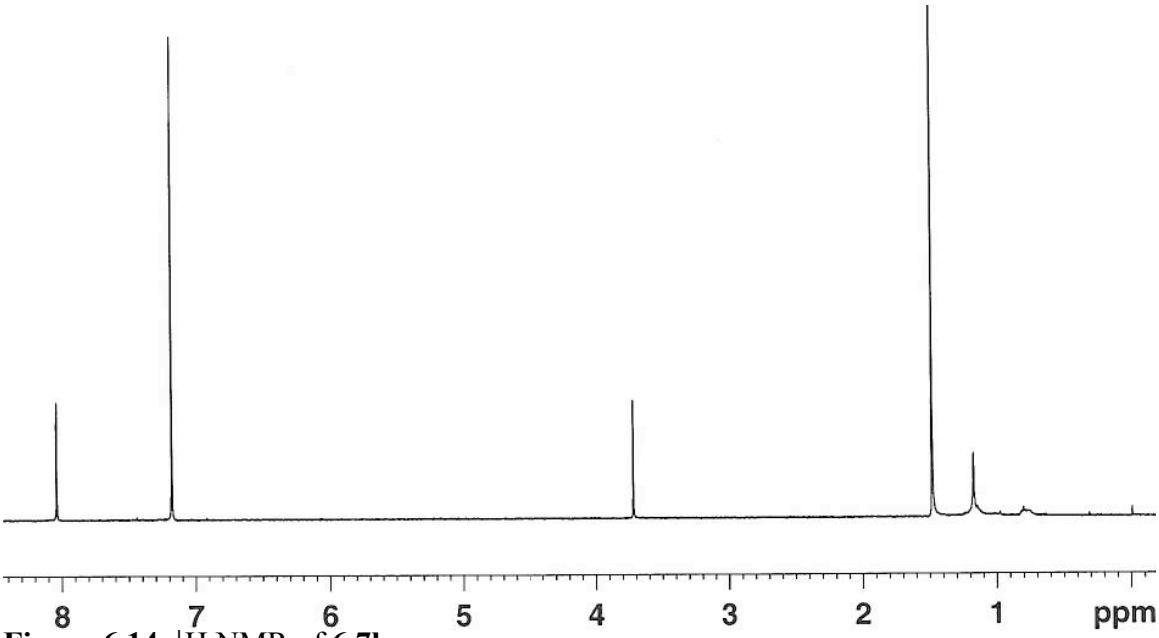

Figure 6.14. ^{1}H NMR of **6.7b**.

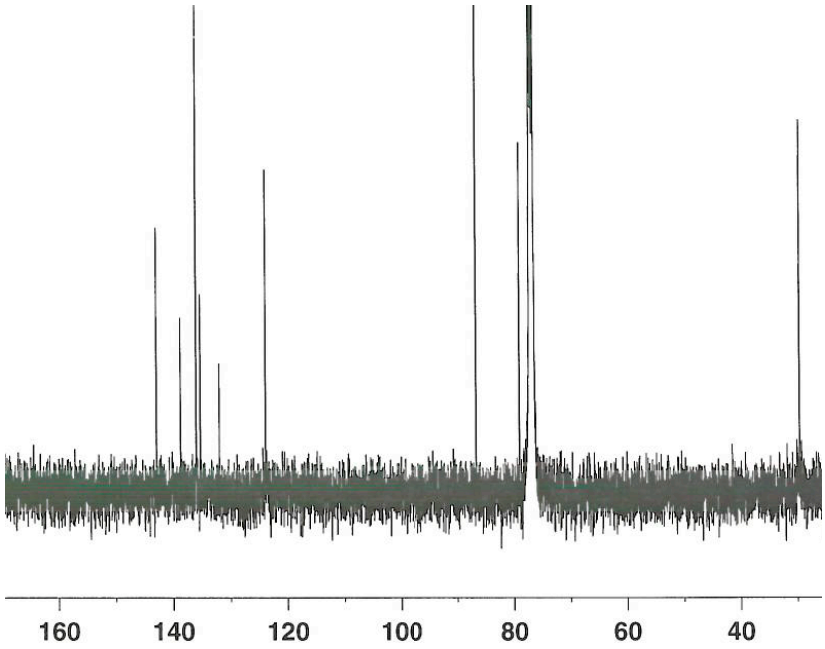

Figure 6.15. ^{13}C NMR of **6.7b**.

6.4.7 1,4-bis(1-(2-(2-(2-methoxyethoxy)ethoxy)ethyl)1H-1,2,3-triazol-4-yl)phenazine 6.1

1,4-diethynylphenazine (**6.7a**) (0.300 g, 1.316 x 10^{-3} mol) and 1-azido-2-(2-(2-methoxy-ethoxy)ethoxy)ethane (**6.8**) (0.750 g, 3.29 x 10^{-3} mol) were dissolved into a THF: H_2O (5:1 *v/v*) solution (20 mL) and freeze-pumped-thawed three times to remove oxygen. While under a flow of N_2, 0.525 g (2.5 eq, 3.29 x 10^{-3} mol) of copper sulfate and 0.651 g (2.5 eq, 3.29 mol) of sodium ascorbate was added. After stirring overnight, the crude mixture was filtered through celite with dichloromethane. The solvent was removed *in vacuo*. The product was filtered through a short silica column with dichloromethane followed by ethyl acetate as the eluent. The product **6.1** was isolated as orange oil (0.487g, 0.803 x 10^{-3} mol, 61% yield). IR (KBr, cm^{-1}) 2942, 2921, 2871, 2783, 2772, 2739, 2739, 1751, 1653, 1647, 1558, 1447, 1430, 1352, 1332, 1229, 1108, 1098, 1064, 1030; ^{1}H NMR (δ in $CDCl_3$) 9.136 (s, 2H), 8.892 (s, 2H), 8.206 (AA' of AA'BB', 2H), 8.813 (BB' of AA'BB', 2H), 4.699 (t, J = 5 Hz, 2H), 3.999 (t, J = 5 Hz, 2H), 3.670 (m, 2H), 3.622 (m, 2H), 3.532 (m, 2H), 3.373 (m, 2H), 3.206 (s, 3H); ^{13}C NMR (δ in $CDCl_3$) 143.12, 141.99, 140.16, 130.52, 129.61, 128.57, 128.04, 126.38, 71.78, 70.77, 70.53, 70.50, 69.74, 58.91, 50.38; accurate mass for $C_{32}H_{38}N_8O_6$: *m/z* = 606.2903 [M+], calc. *m/z* =606.2914.

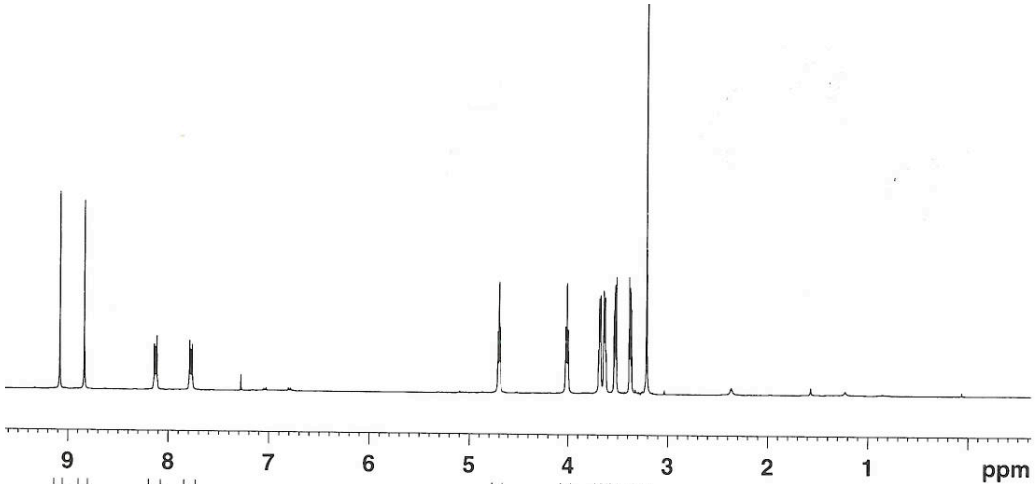

Figure 6.16. ^{1}H NMR of **6.1**.

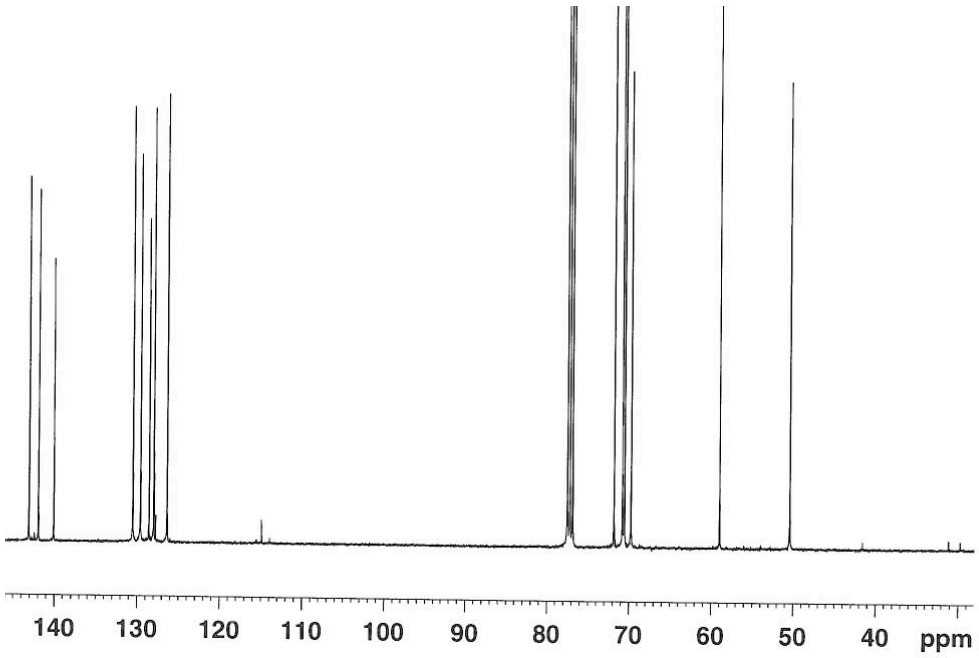

Figure 6.17. ^{13}C NMR of **6.1**.

6.4.8 1,2,3,4-tetrachloro-6,9-bis(1-(2-(2-(2-methoxyethoxy)ethoxy)ethyl)-1H-1,2,3-triazol-4-yl)phenazine 6.2

1,2,3,4-tetrachloro-6,9-diethynylphenazine (**6.7b**) (0.080 g, 0.219 x 10^{-3} mol) and 1-azido-2-(2-(2-methoxyethoxy)ethoxy)ethane (**6.8**) (0.750 g, 0.546 x 10^{-3} mol) were dissolved into a THF: H_2O (5:1 *v/v*) solution (20 mL) and freeze-pumped-thawed three times to remove oxygen. While under a flow of N_2, 0.088 g (2.5 eq, 0.546 x 10^{-3} mol) of copper sulfate and 0.108 g (2.5 eq, 0.546 x 10^{-3} mol) of sodium ascorbate were added. After stirring overnight, the crude mixture was filtered through celite with dichloromethane. The solvent was removed *in vacuo*. The product was filtered through a short silica column with dichloromethane followed by ethyl acetate. The product of **6.2** was isolated as red oil stuff (0.075g, 0.101 x 10^{-3} mol, 46% yield). IR (KBr, cm^{-1}) 2904, 2883, 2869, 2854, 1734, 1653, 1558, 1457, 1374, 1252, 1108, 1099; ^{1}H NMR (δ in $CDCl_3$) 9.154 (s, 2H), 8.976 (s, 2H), 4.699 (t, J = 5 Hz, 2H), 3.999 (t, J = 5 Hz, 2H), 3.670 (m, 2H), 3.622 (m, 2H), 3.532 (m, 2H), 3.373 (m, 2H), 3.206 (s, 3H); ^{13}C NMR (δ in $CDCl_3$) 141.75, 138.86, 136.38, 134.33, 131.44, 129,52, 128,20, 126.34, 71.86, 70.77, 70.56, 69.58, 58.99, 50.51; accurate mass for $C_{30}H_{34}Cl_4N_8O_6$: *m/z* = 742.1333 [M+], calc. *m/z* = 742.1355.

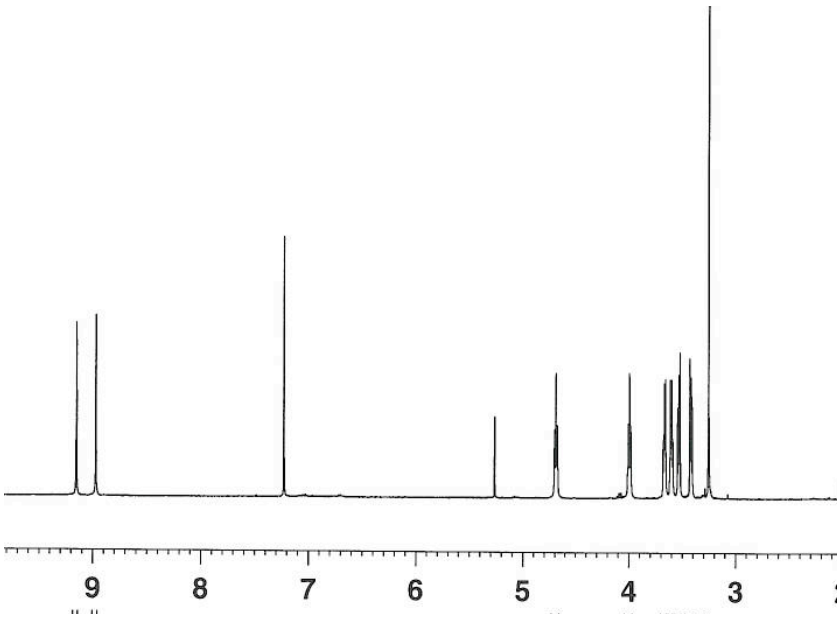

Figure 6.18. ^{1}H NMR of **6.2**.

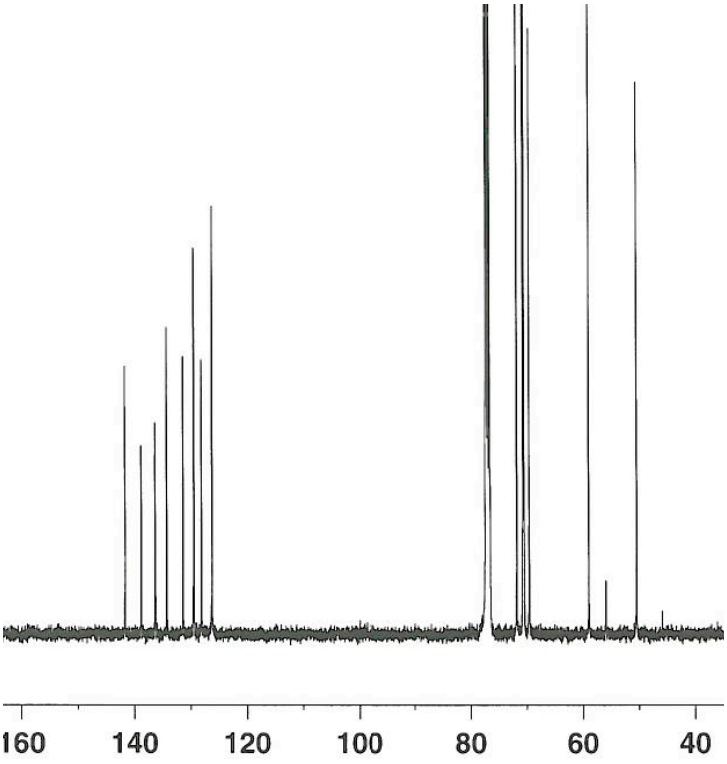

Figure 6.19. ^{13}C NMR of **6.2**.

6.4.9 Spectra of the addition of metal salts to 6.1 and 6.2.

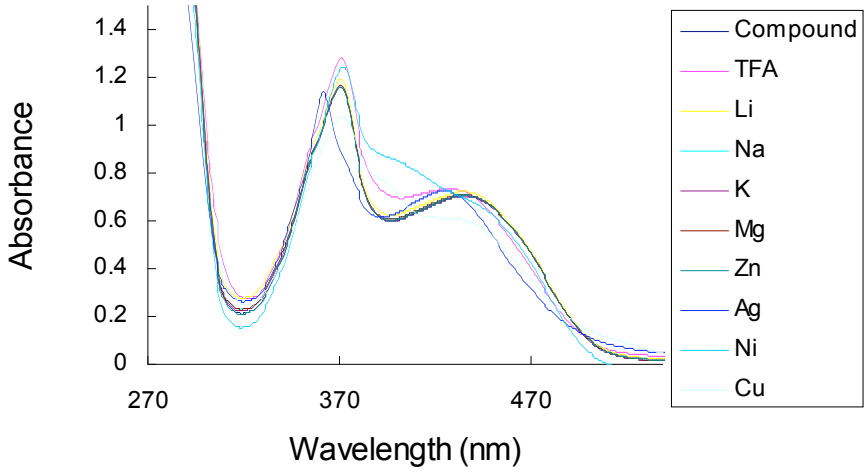

Figure 6.20. Absorption spectra of **6.1** (197 μM) before and after the addition of selected metals and TFA in water.

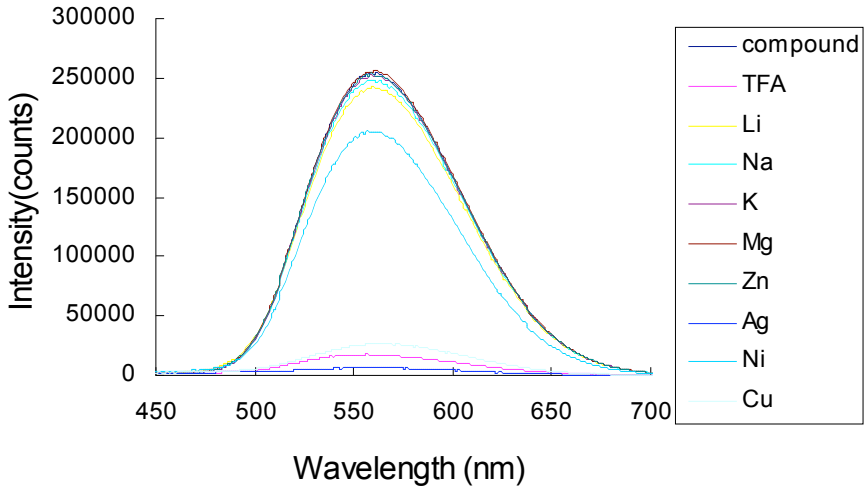

Figure 6.21. Emission spectra of **6.1** (197 μM) before and after the addition of selected metals and TFA in water.

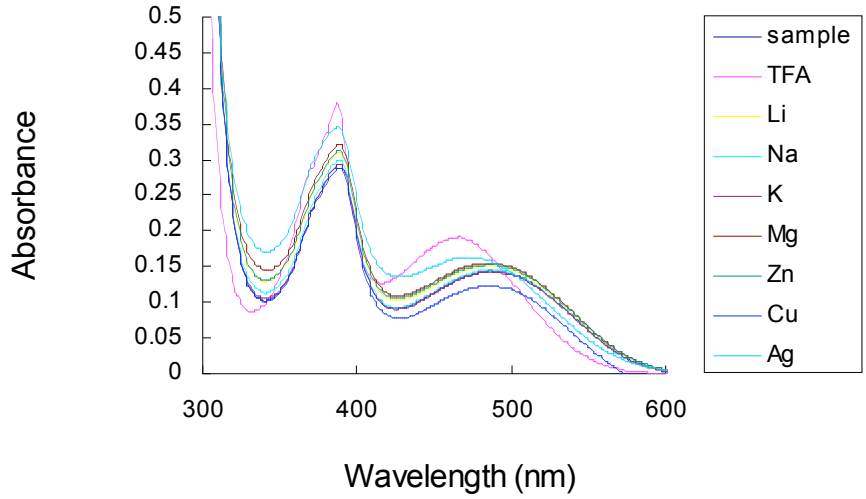

Figure 6.22. Absorption spectra of **6.2** (200 μM) before and after the addition of selected metals and TFA in water/methanol (1:1 *v/v*) solution.

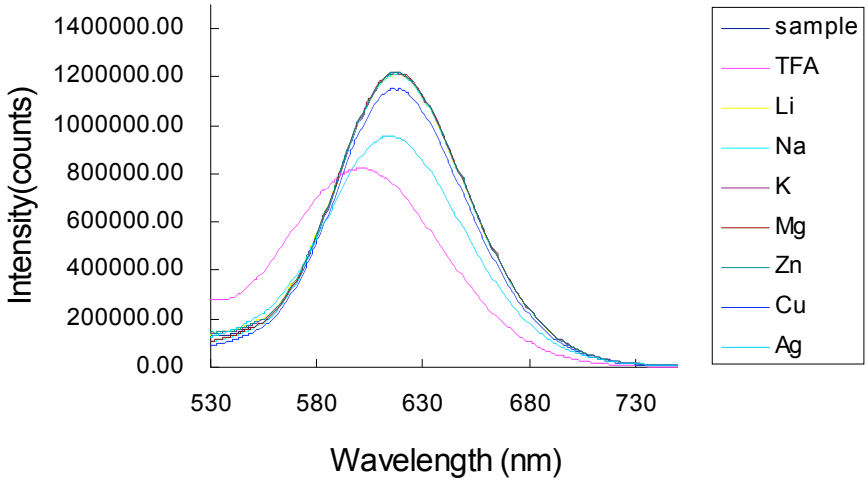

Figure 6.23. Emission spectra of **6.2** (200 μM) before and after the addition of selected metals and TFA in water/methanol (1:1 *v/v*) solution.

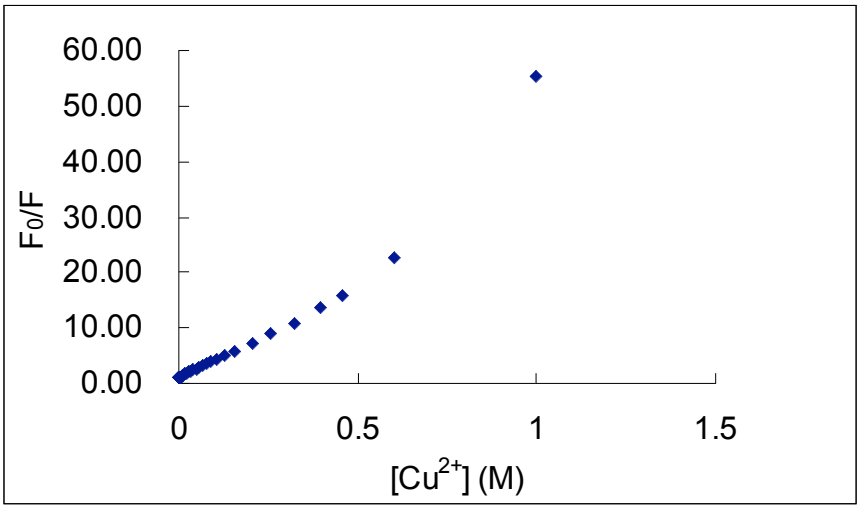

Figure 6.24. Plotting of the emission spectra during the titration of **6.1** with copper(II) according to the standard Stern-Volmer equation. The nonlinear behavior is apparent.

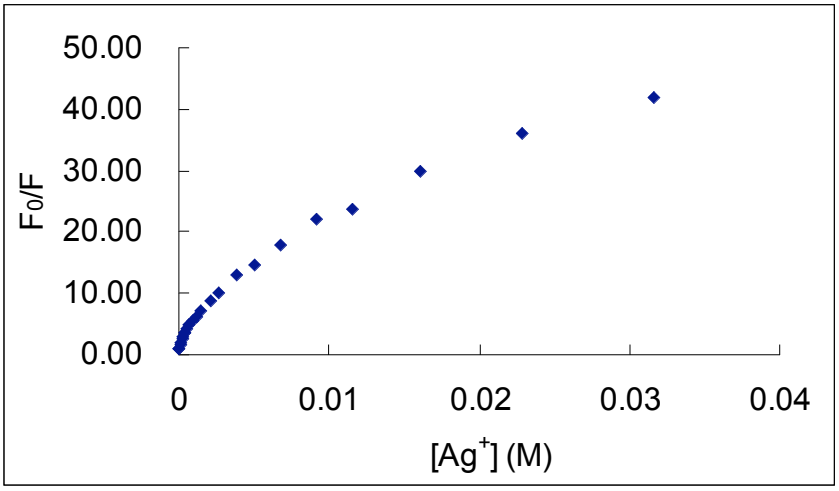

Figure 6.25. Plotting of the emission spectra during the titration of **6.1** with silver(I) according to the standard Stern-Volmer equation. The nonlinear behavior is apparent.

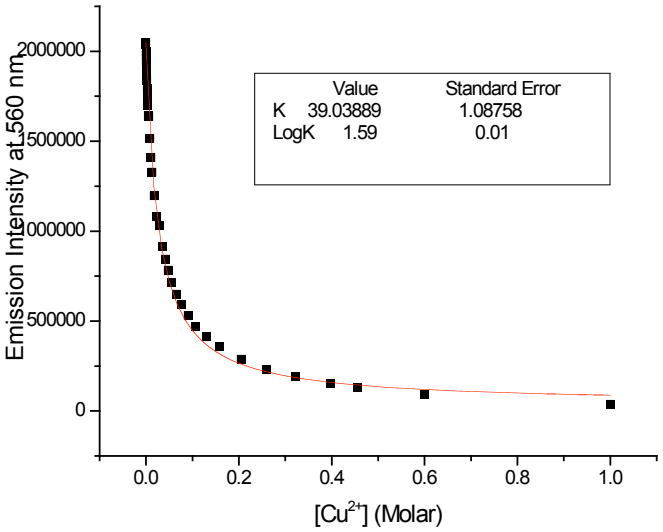

Figure 6.26. Plotting of the emission spectra during the titration of **6.1** with copper(II) according to the modified Stern-Volmer equation (Eqn 1).

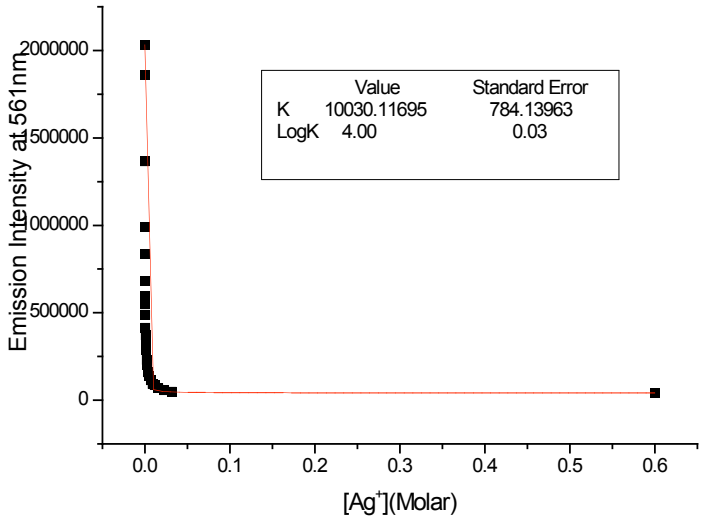

Figure 6.27. Plotting of the emission spectra during the titration of **6.1** with silver(I) according to the modified Stern-Volmer equation (Eqn 1).

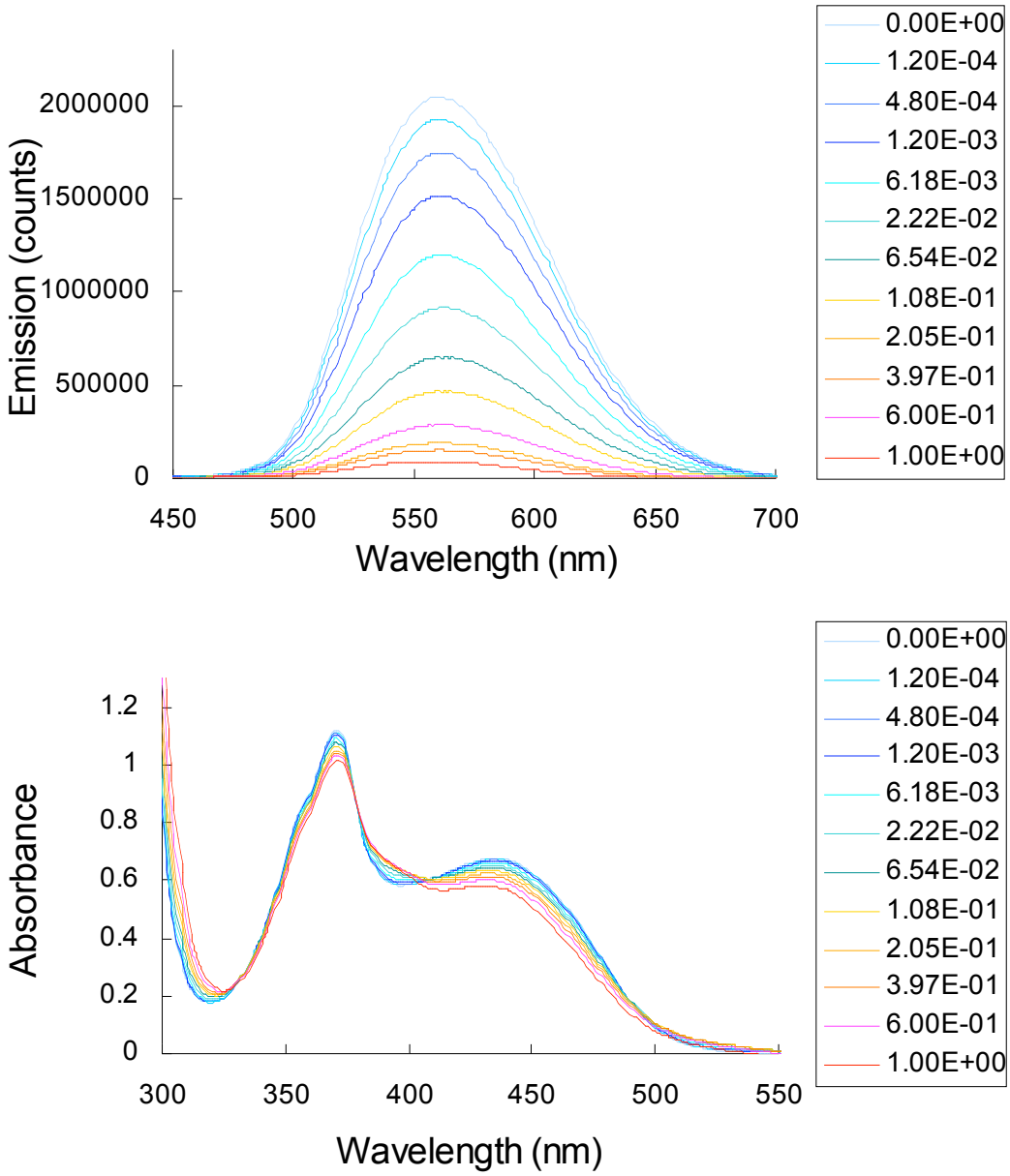

Figure 6.28. Absorption (top) and emission (bottom) spectra of the titration of **6.1** (197 μM) with $CuSO_4$ in water.

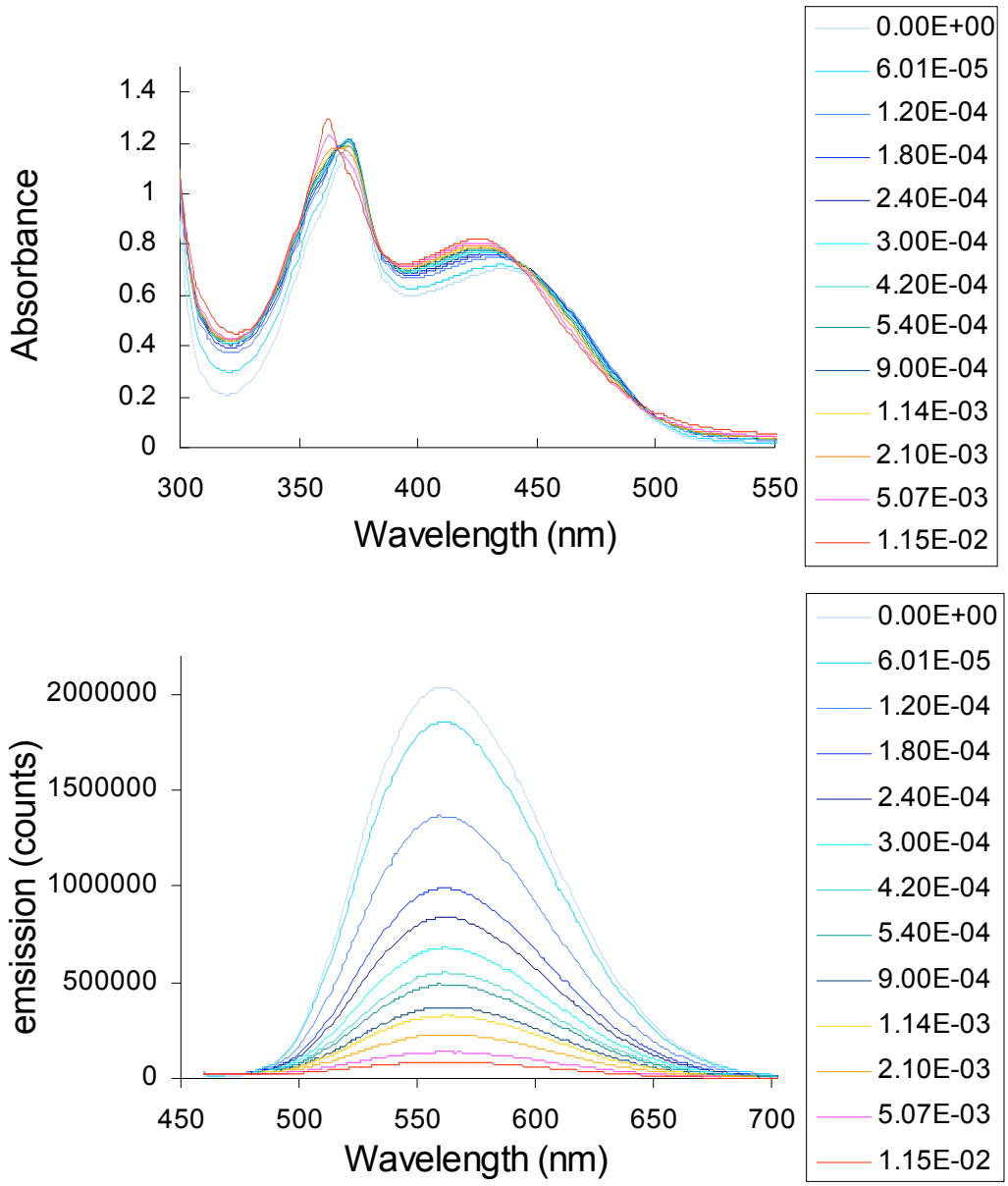

Figure 6.29. Absorption (top) and emission (bottom) spectra of the titration of **6.1** (200 μM) with AgOTf in water.

6.5 References

[1] [a] R. Huisgen, G. Szeimies, L. Moebius. *Chem. Ber.* **1967**, *100*, 2494. [b] R. Huisgen, R. Knorr, L. Moebius. G. Szeimies. *Chem. Ber.* **1965**, *98*, 4014.

[2] H.C. Kolb, K.B. Sharpless. *Drug Discovery Today*. **2003**, *8*, 1128.

[3] M.G. Finn, V. Fokin. *Chem. Soc. Rev.* **2010**, *39*, 1231.

[4] J.A. Opsteen, J.C.M. van Hest. *Chem. Comm.* **2005**, *1*, 57.

[5] S.M. Brombosz, A.L. Appleton, A.J. Zappas, U.H.F. Bunz. *Chem. Comm.* **2010**, *46*, 1419.

[6] [a] G. Franc, A.K. Kakkar. *Chem. Soc. Rev.* **2010**, *39*, 1536. [b] U.H.F. Bunz. *Macromol. Rapid Commun*. **2009**, *30*, 772.

[7] A.L. Appleton, S.M. Brombosz, Stephen Barlow, John S. Sears, Jean-Luc Brédas, Seth R. Marder, Uwe H.F. Bunz. *Nature Comm*. **2010**, 1:90.

[8] A. Almutairi, S.J. Guillaudeu, M.Y. Berezin, S. Achilefu, J.M. Frechet. *J. Am. Chem. Soc.* **2008**, *130*, 444.

[9] [a] R.L. Phillips, O.R. Miranda, D.E. Mortenson, C. Subramani, V.M. Rotello, U.H.F. Bunz. *Soft Mater.* **2009**, *5*, 5042. [b] S. Maisonneuve, Q. Fang, J. Xie. *Tetrahedron.* **2008**, *64*, 8716.

[10] H. Wang, L. Xue, Y. Qian, H. Jiang. *Org. Lett.* **2010**, *12*, 292.

[11] [a] Y. Wen, F. Xing, S. He, S. Song, L. Wang, Y. Long, D. Li, C. Fan. *Chem. Comm.* **2010**, *46*, 2596. [b] S. Iyoshi, M. Taki, Y. Yamamoto. *Inorganic Chemistry.* **2008**, *47*, 3946.

[12] J.R. Lakowicz. Principles of Fluorescence Spectroscopy. Springer, New York, NY, 3rd Edition, 2006, 11.

[13] IUPAC Compendium of Chemical Terminology 2nd Edition, 1997. Accessed on the web October 28, 2010.

CHAPTER 7

THE THIADIAZOLOPHENAZINES

7.1 Introduction

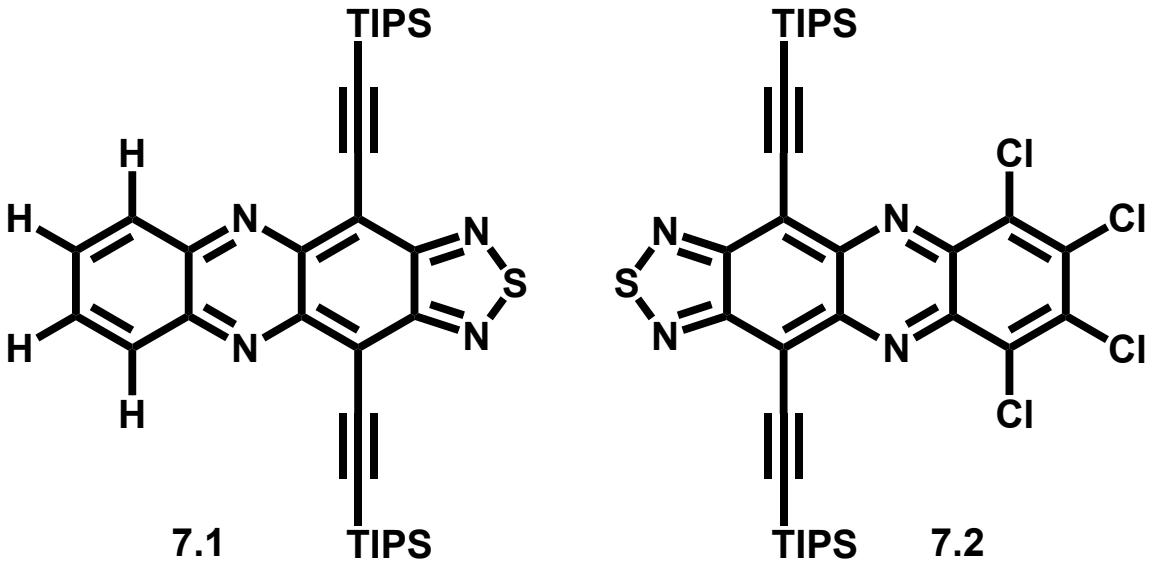

Scheme 7.1. Structures of compounds **7.1**-**7.2**.

Attempting to be presented by the work within this Thesis is the synthesis of a solution-processible, electron-transporting small molecule that can operate under ambient conditions. Synthetic chemistry provides the means to expand the lexicon of available materials for engineers and attempts to understand the properties that give rise to stable electron-transport via computational studies and experimental results. Herein we further explore the thiadiazoles by pyrazine substitution at the 5 and 10 positions, as well as peripheral chlorination around the edge at positions 6, 7, 8, and 9. The goal was to synthesize the most electron deficient small molecule of all the series presented so far in

this Thesis. What we have found is that we have achieved the lowest record (within our series of molecules) for the first reduction potential, as well as have been able to show that the single-crystal X-ray parameters associated with R = TIPS do not necessarily dominate the solid-state optical properties observed upon thin-film formation (i.e. Ch 2).

7.2 Results and Discussion

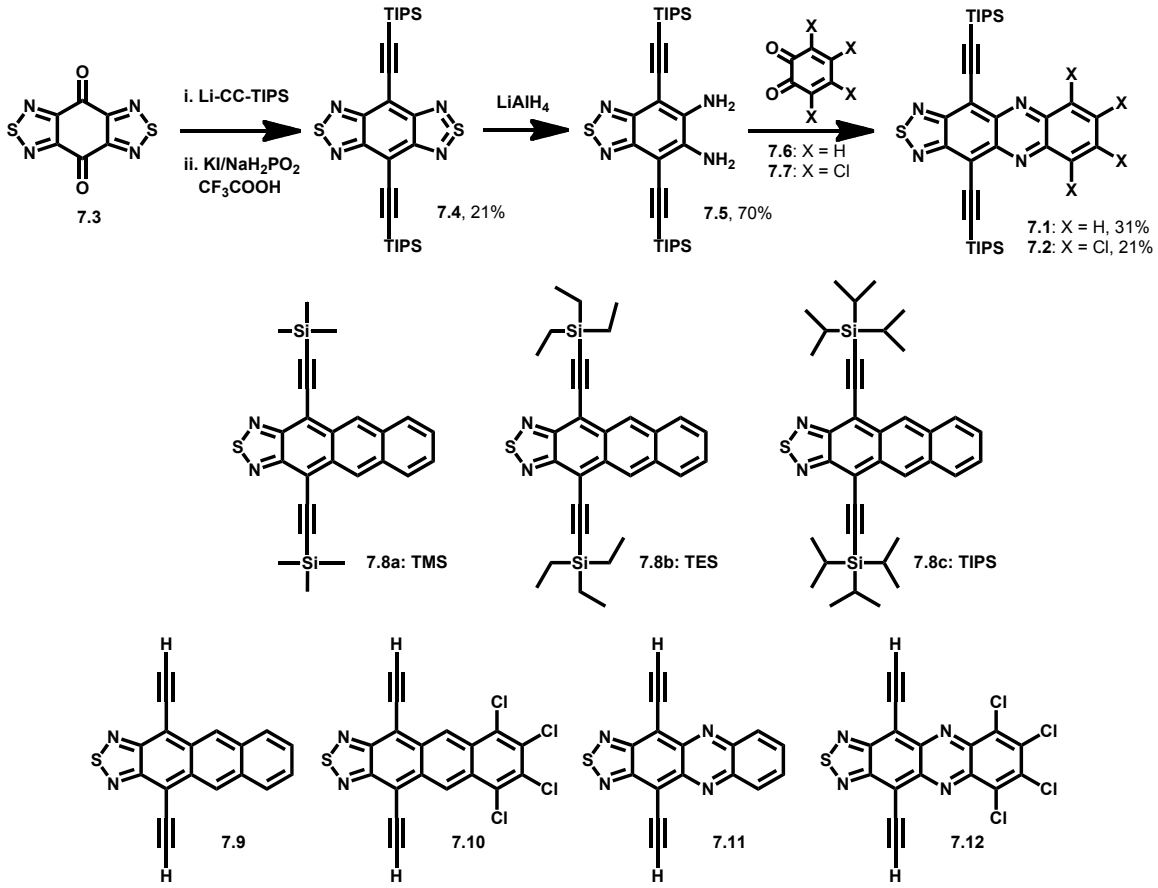

Scheme 7.2. Synthesis of thiadiazolophenazine derivatives **7.1** and **7.2** (top). Structures of compounds **7.8** (middle) for comparison and compounds **7.9**-**7.12** (bottom) utilized in our computational studies.

We started with the known benzo-bisthiadiazole-dione[1] (**7.3**, Scheme 7.2) and performed a modification of our acetylide reaction with a dione[2] in order to obtain **7.4** in

21% overall yield in two steps. The *o*-diamine (**7.5**) was formed by reaction of **7.4** with lithium aluminum hydride (LAH) to reduce a thiadiazole ring. Interestingly, even up to twenty equivalents of LAH did not generate the bis-*o*-diamine form. Finally, condensation of the *o*-dione of choice (**7.6** or **7.7**) with **7.5** furnished the thiadiazolophenazine derivatives **7.1** and **7.2** in 21-31% yield, respectively.

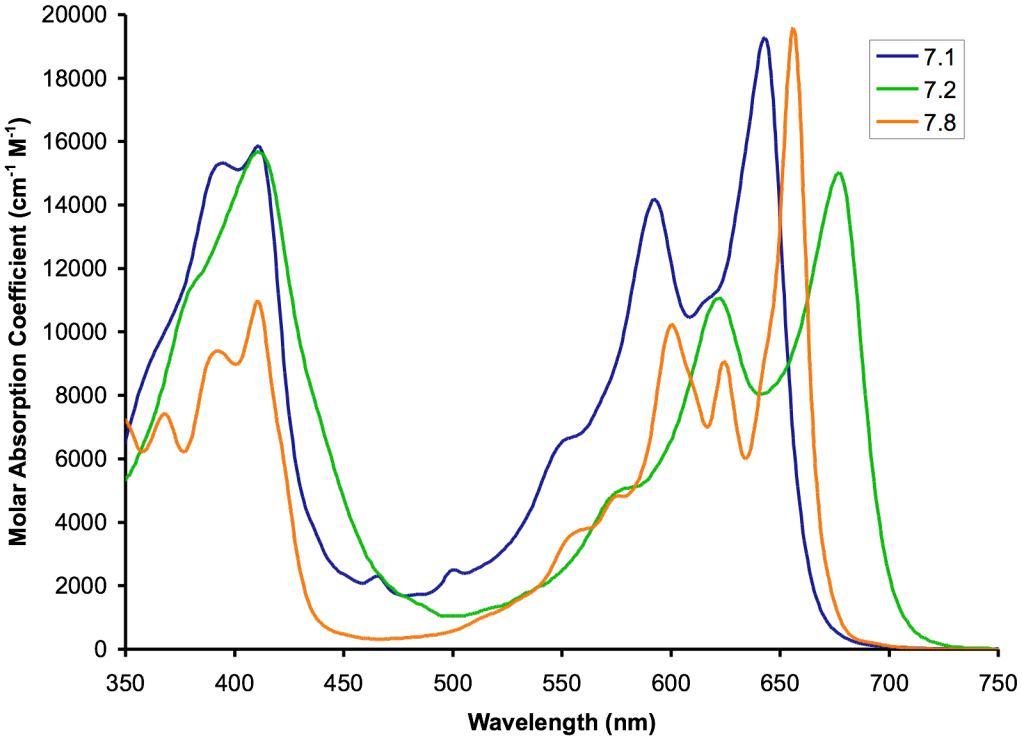

Figure 7.1. Molar absorptivity profile of compounds **7.1**, **7.2**, and **7.8**. It has been previously shown that **7.8a-c** behave similarly in solution (see Chapter 2). All spectra were taken in hexanes.

Figure 7.1 shows the absorption profiles of **7.1**, **7.2**, and **7.8c**[3] in terms of their molar absorption coefficients and Table 7.1 summarizes the optical measurements and electrochemistry. The λ_{max} of absorption does not change significantly upon addition of a pyrazine moiety to **7.8c** (**7.8c** → **7.1**), as shown by only a 1.5% drop in absorbance efficiency and a slight hypsochromic shift of 13 nm. If we add four chlorine atoms to **7.1**

(**7.1** → **7.2**), we observe a drop in absorbance of 23% and a bathochromic shift of 34 nm. We have previously observed a hypsochromic shift of our tetrazapentacene[4] derivative relative to our diazapentacene[5] derivative, and also bathochromic shifts accompanied with a reduction in molar absorptivity upon halogenation of diazaacene derivatives.[5] The cyclic voiltammetry experiments (Dr. Steve Barlow) were carried out in deoxygenated THF or DCM / 0.1 M ^{n}BuNPF$_6$ solutions. The results indicate that these compounds behave similarly in both solvents. We have achieved our lowest first reduction potential to date of -0.57 V for compound **7.2**, while **7.1**'s first reduction occurs at -0.82 V which is similar to some of our previous work (compounds **4.10**, **5.11b**, **5.15b**, **5.15c**). Due to the inability to observe an oxidation potential for **7.2** in either solvent, we were unable to determine the transport gap by electrochemistry. On the other hand, we were able to obtain such results for **7.1** and **7.8c**, which show good correlation with the HOMO-LUMO gap calculated from CV and the position of the long wavelength λ_{max} of absorption.

Table 7.1. Compiled data experimentally determined in solution of compounds **7.1**, **7.2**, **7.8c**. a: THF, b: DCM, c: irreversible. All CV data were performed in 0.1M solvent with ^{n}BuNPF$_6$ using ferrocene as an internal reference using CH Instruments 620D potentiostat. Opt.: optical; Trans.: transport.

Compound	**7.1**	**7.2**	**7.8c**
Abs. λ_{max} (nm)	643	677	656
ε at λ_{max} ($cm^{-1}M^{-1}$)	19278	15022	19567
$E_{1/2}$ (0/-)[a] (V)	-0.82	-0.57	-1.18
$E_{1/2}$ (0/-2)[a] (V)	-1.41	-1.16	-1.80
E_{ox} (0/+)[a] (V)	ND	ND	+0.86
$E_{1/2}$ (0/-)[b] (V)	-0.84	-0.62	-1.18
$E_{1/2}$ (0/-2)[b] (V)	-1.41	-1.18	-1.78
E_{ox} (0/+)[b] (V)	+1.17[c]	ND	+0.74
Opt. gap (λ_{max}) (eV)	1.93	1.83	1.89
Trans. gap CV (V)	2.01	ND	1.92[a], 2.04[b]

In order to better understand the effects observed in the absorption profiles and cyclic voltammetery experiments, Dr. John S. Sears performed computational studies

using DFT with the B3LYP functional and the 6-311+G* basis set on model compounds **7.9**-**7.12** (Figure 7.2, left to right), which represent the stepwise progression of peripheral halogenation and core insertion of the pyrazine moiety beginning from the parent compound. Interestingly, either pyrazine introduction (**7.9** → **7.10**) or peripheral chlorination (**7.9** → **7.11**) leads to the same effect: the HOMO is stabilized by 0.5 eV and the LUMO is stabilized by 0.3 eV. This would imply that either pyrazine introduction or chlorination would lead to similar optoelectronic properties (unfortunately, we have been unable to synthesize derivatives of **7.11** to date). Why is the HOMO stabilized to a greater extent than the LUMO, an opposite trend observed in Chapter 5? The answer comes from the orbital structures of **7.9**, which show a partially disjoint HOMO frontier molecular orbital that has much larger coefficients on the anthracene portion of the molecule (right side) than the thiadiazole moiety (left side), while the LUMO appears delocalized across the structure. Upon either peripheral halogen substitution or pyrazine insertion, the HOMO becomes overall less disjoint and is thus stabilized to a greater extent than the already fully delocalized LUMO. This indicates that derivatives of model compound **7.10**, would display a hypsochromic shift in their absorption profile. This is indeed the case of **7.1** (analogous to **7.10**), as can been seen in Figure 7.1, however the shift is much smaller than the computational results indicate by 0.16 eV. The computational results also indicate that when both pyrazine insertion and halogen substitution are performed (**7.9** → **7.12**, analogously **7.8** → **7.2**), a hypsochromic shift in the absorption profile would also occur. This is not the case, as can be seen in Figure 7.1. The experimental UV-vis absorption data show a bathochromic shift of the λ_{max} of **7.2** of 21 nm (0.06 eV) compared to the parent

compound **7.8**. However, the experimental results are within the acceptable error of the computational results, overall less than a few tenths of an eV difference.[8] The trend in LUMO stabilization is in agreement with the observed first reduction potentials of **7.8**, **7.1**, and **7.2** as they decrease across the series.

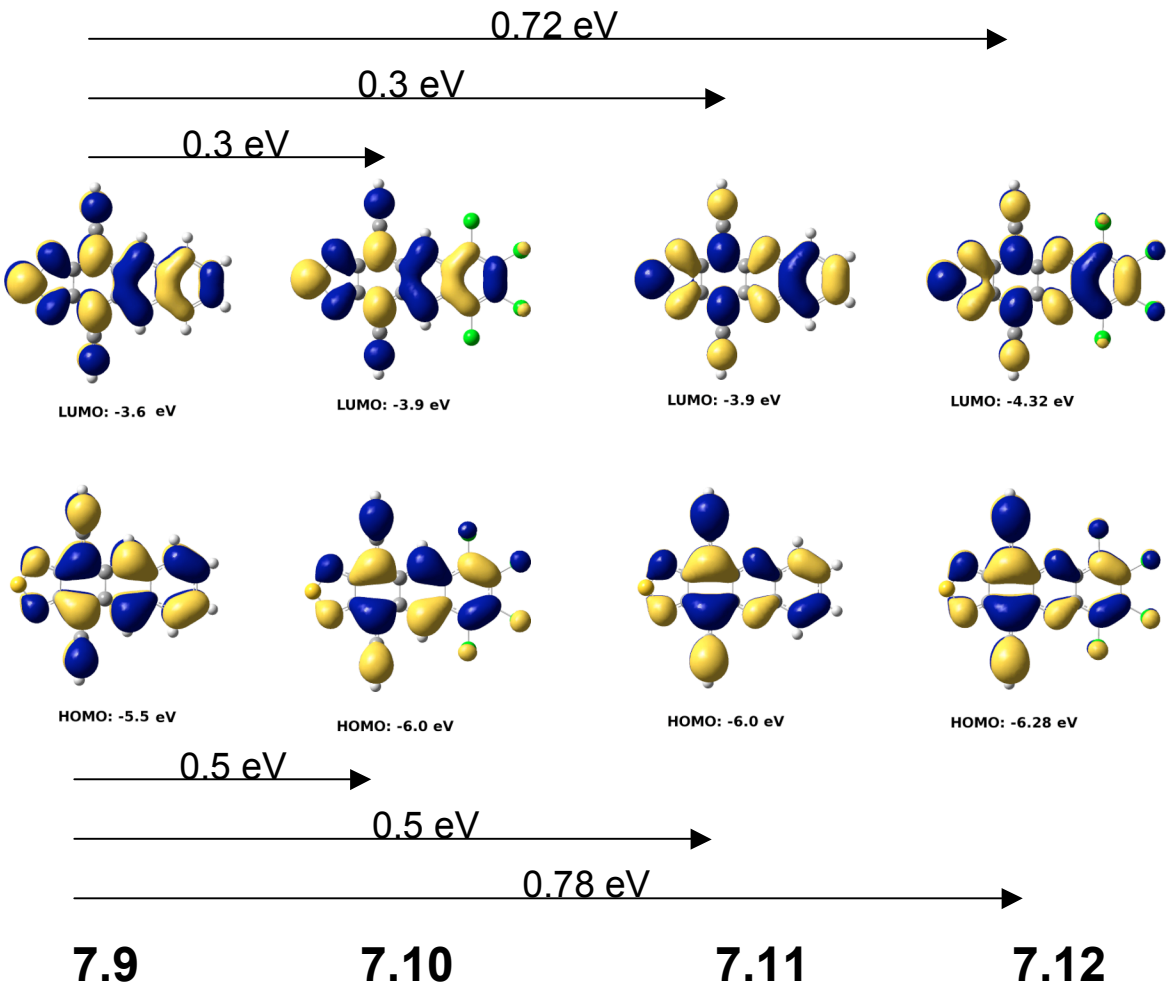

Figure 7.2. Frontier molecular orbiatls (LUMO: top, HOMO: bottom) of investigated model compounds 7.9-7.12 calculated by DFT computational studies using the B3LYP functional and the 6-311+G* basis set. The arrows indicate the amount of stabilization (eV) from the model parent compound (**7.9**, left) to other models compounds (**7.10**-**7.12**) upon peripheral chlorination, pyrazine insertion, and both, respectively. (Dr. John S. Sears)

Table 7.2. Single-crystal X-ray parameters of compounds **7.1**, **7.2**, and **7.8a-c**.

Compound R-group	**7.1** TIPS	**7.2** TIPS	**7.8a** TMS	**7.8b** TES	**7.8c** TIPS
a axis (Å)	8.8986(5)	7.825(6)	11.170(9)	6.954	8.1657(8)
b axis (Å)	12.5110(6)	14.279(12)	31.42(2)	34.474	13.1305(12)
c axis (Å)	16.6041(9)	17.162(14)	6.923(5)	11.839	17.1500(16)
α	71.327(4)	83.187(12)	90	90	78.272(2)
β	82.100(3)	80.733(12)	103.83(3)	90.2	81.704(2)
γ	80.699(3)	81.494(12)	90	90	80.618(2)
System	Triclinic	Triclinic	Monoclinic	Orthorhombic	Triclinic
Space Group	P -1	P -1	P_2 1/c	P 1	P -1

The solid-state packing properties of these materials were evaluated by single-crystal X-ray diffraction and solution cast thin-film absorbance. Table 7.2 is a compilation of the single-crystal data for **7.1**, **7.2**, and **7.8a-c**. The parameters are strikingly similar for the compounds possessing the same R-group (**7.8c**, **7.1**, and **7.2**), even though their core structure is very different in terms of electron density due to the pyrazine insertion and peripheral chlorination. Figure 7.3 shows the thin-film absorption profiles of all compounds for comparison purposes. Interestingly, the thin-film behavior of **7.1** and **7.2** resembles that of **7.8a**, even though their crystal packing parameters in Table 7.2 are significantly different. This may not be entirely unexpected, as the single crystals were grown from hexanes solution in a silicate vial and the thin-films were spin coated or drop-cast from chloroform solution onto a quartz slide. Importantly, the behavior of **7.1** and **7.2** in their thin-film polymorph observed here is indicative of π-π interactions,[7] which is a necessity for application in optoelectronic devices. This can be seen from the bathochromic shift in the long wavelength λ_{max} (11 nm and 16 nm for **7.1** and **7.2**, respectively) and spectral broadening, which was previously thought to arise

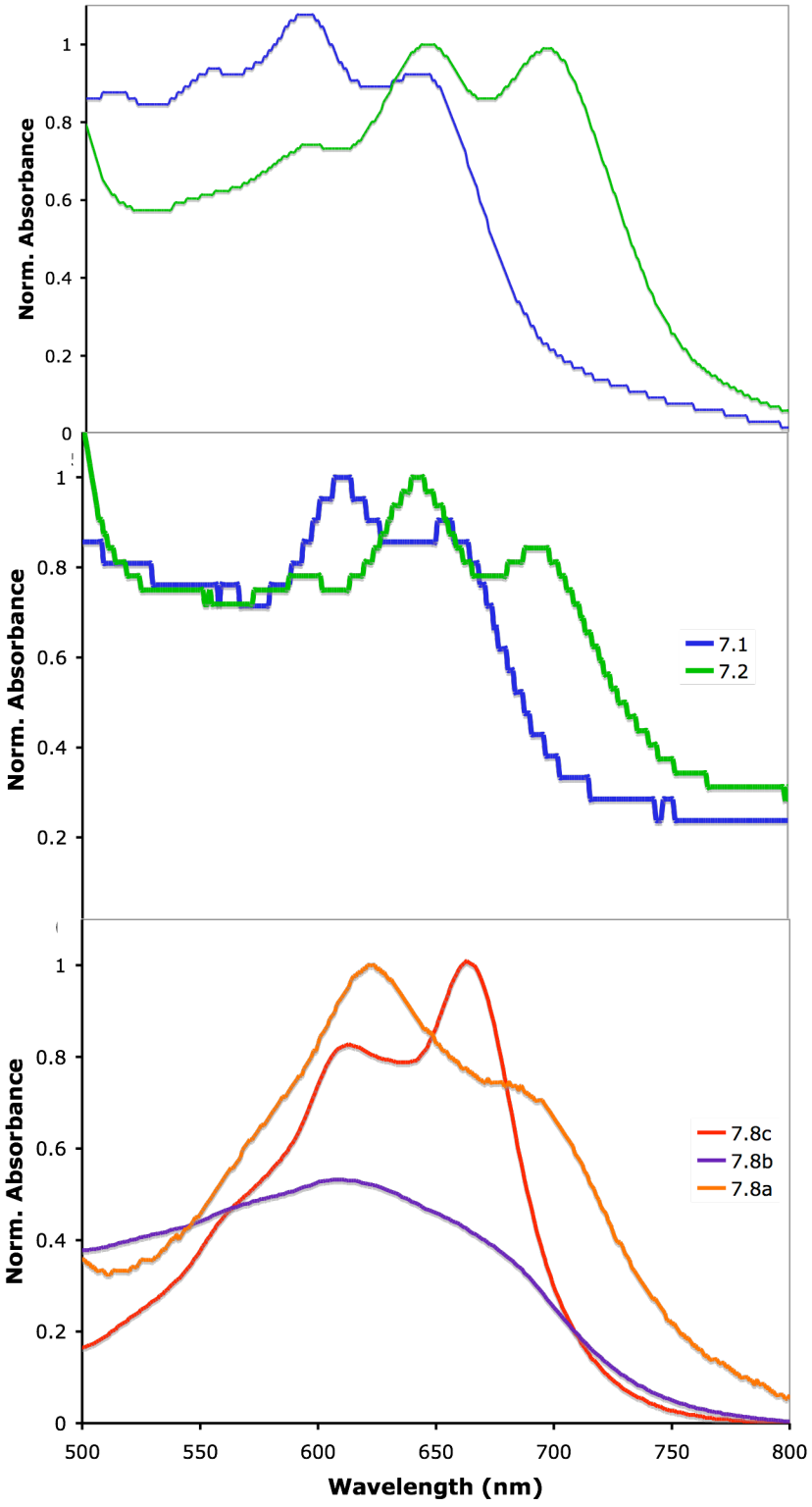

Figure 7.3. Normalized thin-film absorption profiles of compounds **7.1**, **7.2** (Top: drop-cast onto quartz from dichloromethane solution; Middle: spin-coated onto quartz from chloroform solution) and **7.8a-c** (Bottom: drop-cast from dichloromethane).

from the fact that **7.8a** and **7.8b** form microcrystalline films, while **7.8c** forms amorphous films.[5]

7.3 Conclusion

In conclusion, we continue to expand the library of small molecules for their potential application in organic optoelectronic devices, but no such devices have been fabricated to date. However, these materials possess promising properties towards such applications. We have achieved HOMO and LUMO levels as stabilized as -6.28 eV and -4.32 eV, respectively, according to our computational results, which when compared to Bao et al's[6] paper of energy level correllation to charge-carrier type indicate the real possibility that these molecules should behave as electron-transporting small molecules. In fact, these orbital energies are below those for perfluroropentacene.[6] Although the single-crystal structural determination of **7.1** and **7.2** indicate the packing structure to be very similar to **7.8c**, which does not show π-π interactions in its solution-cast thin-film, their solution cast thin-films do show a bathochromic shift in the long wavelength absorption maximum and spectral broadening more closely resembling **7.8a**. Also, we have been able to further reduce the first reduction potential to -0.57 V (**7.2**), a new minimum among all of our molecules synthesized to date, which indicates the ease of electron injection into this material. Synthetically we continue to explore new molecules and their properties, but still have been unable to prepare functional devices. We have ideas (molecules) that may work and at least establish useful trends in optoelectronic properties, but have yet to produce any meaningful solutions (devices) to problems in the area of organic electronics.

7.4 Experimental Information

7.4.1 benzo[1,2-c:4,5-c']-4,8-bis((triisopropylsilyl)ethynyl)bis([1,2,5]thiadiazole) 7.4

To an oven dried Schlenk tube cooled under nitrogen was added freshly distilled THF (50 mL) and was freeze, pump, thawed x 3. Then the Schlenk tube was purged with nitrogen for 5 min and sealed with a rubber septum. The solution was brought to 0 °C on an ice bath and TIPS-acetylene (4.88 g, 2.7 x 10^{-2} mol, 3.0 eq.) was added. Then n-butyllithium (10.0 mL of 2.5 M solution, 2.5 x 10^{-2} mol, 2.8 eq.) was added and the solution was stirred for 30 min at 0 °C, the ice bath was removed and the solution was allowed to stir for 30 min at ambient temperature. Compound **7.3** (2.0 g, 8.9 x 10^{-3} mol) was added to the solution, and the reaction mixture was purged with nitrogen for 5 min. The reaction was then sealed again and allowed to stir for 12 h. The reaction was quenched in wet ethyl ether and the solvent removed *in vacuo*. The intermediate diol was collected by column chromatography over silica gel using pure ethyl acetate (4.26 g, 81%). Without further characterization, the residue was suspended in trifluoroacetic acid and the salts KI (8.4 g, 5 x 10^{-2} mol, 7 eq.) and NaH_2PO_2 (4.45 g, 5 x 10^{-2} mol, 7 eq.) were added to the solution. After stirring for 90 min, the reaction was quenched in water (100 mL) and extracted with dichloromethane (4 x 100 mL). The organic layer was washed with copious amounts of water to remove the acid, chemically dried with anhydrous sodium sulfate, and the solvent was removed *in vacuo*. The crude product was purified by column chromatography on silica gel using hexanes/dichloromethane (10:3 *v/v*). Compound **7.4** was collected as a purple solid (1.05 g, 21% yield). m.p. = 175 °C (decomposition); IR (KBr, cm^{-1}) 3838, 3166, 2943, 2893, 1862, 2758, 2723, 2553, 2241, 2221, 2129, 1944, 1901, 1774, 1465, 1384, 1357, 1288, 1234, 1068, 1010; ^1H NMR (400

MHz, δ in $CDCl_3$) 1.23 (m, broad, 42 H); ^{13}C NMR (100 MHz, $CDCl_3$) 155.28, 110.92, 106.10, 100.87, 18.76, 11.40; accurate mass for $C_{28}H_{42}N_4S_2Si_2$: *m/z* = 554.23688 [M+], calc. *m/z* = 554.23895.

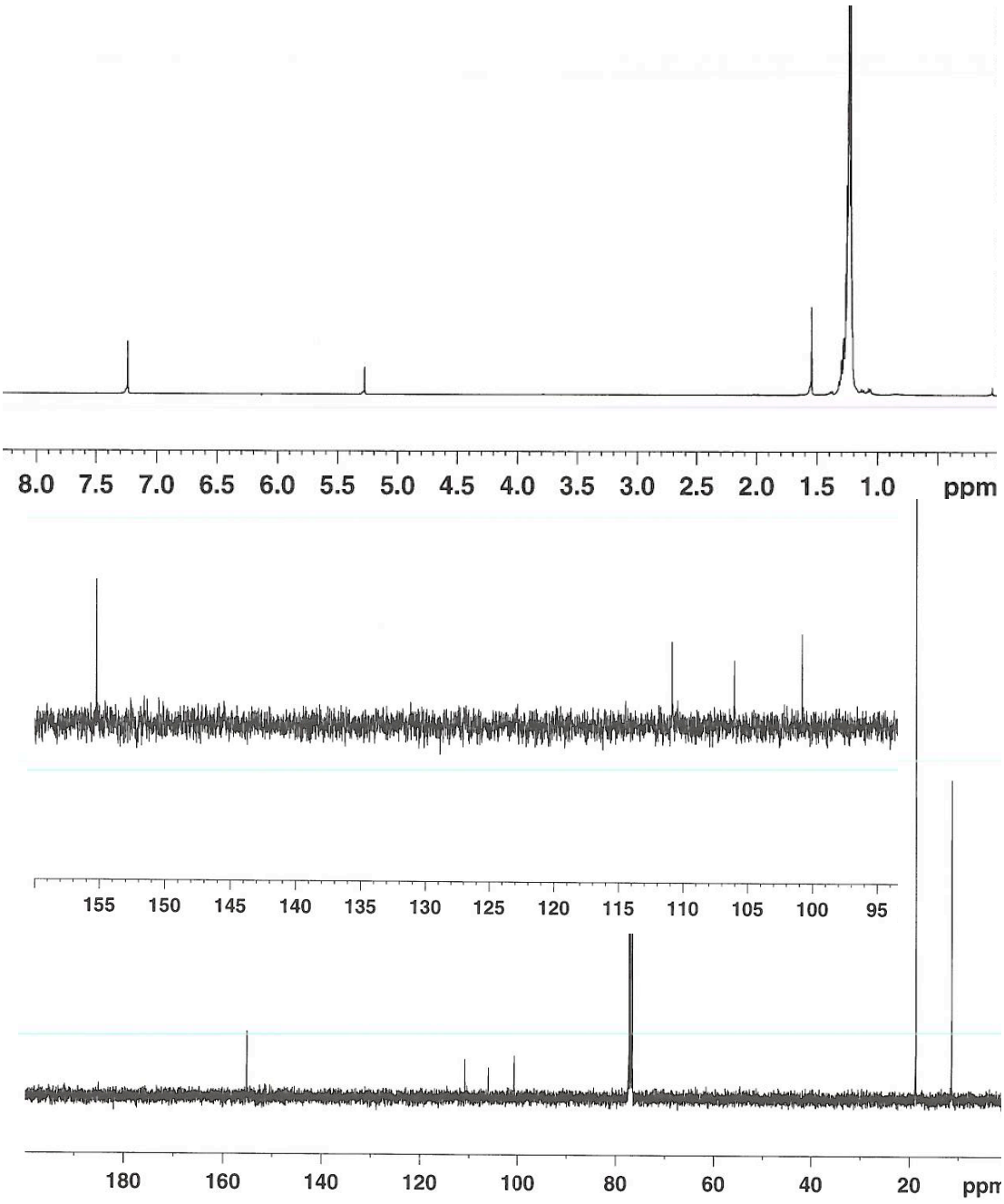

Figure 7.4. ^1H NMR (top) and ^{13}C NMR (bottom) of **7.4**.

7.4.2 4,7-bis((triisopropylsilyl)ethynyl)benzo[c][1,2,5]thiadiazole-5,6-diamine 7.5

To an oven dried Schlenk flask, cooled under nitrogen, was added compound **7.4** (1.80 g, 3.2 x 10^{-3} mol) and freshly distilled THF (75 mL). The solution was purged with nitrogen for 5 min and placed on an ice bath. Then lithium aluminum hydride (1.23 g, 3.2 x 10^{-2}, 10 eq.) was slowly added over thirty minutes and the reaction mixture was sealed with a bubbler and stirred for 12 h while the ice bath came to ambient temperature. After 12 h, the reaction was placed back on an ice bath and very slowly quenched with saturated aqueous ammonium chloride (100 mL) and extracted with ethyl ether (3 x 150 mL) and the solvent was removed i*n vacuo*. The residue was resuspended in dichloromethane, dried with anhydrous sodium sulfate, and the solvent removed *in vacuo*. The crude reaction mixture was separated by column chromatography on silica gel using hexanes/dichloromethane (2:1 *v/v*). The product was recrystallized from hot hexanes. Compound **7.5** was obtained as a bright yellow solid (1.280 g, 76%). m.p. = 206-208 °C; IR (KBr, cm^{-1}) 3455, 3370, 3275, 3247, 3225, 3162, 3045, 2956, 2943, 2937, 2926, 2887, 2863, 2770, 2753, 2721, 2622, 2358, 2145, 2129, 1650, 1646, 1618, 1529, 1497, 1462, 1455, 1446, 1385, 1265, 1359, 1316, 1250, 1126, 1074, 1016; ^{1}H NMR (400 MHz, δ in $CDCl_3$) 4.58 (s, 4H), 1.17 (m, broad, 42H); ^{13}C NMR (100 MHz, δ in $CDCl_3$) 150.40, 143.40, 103.31, 99.53, 97.13, 18.80, 11.30; accurate mass for $C_{28}H_{46}N_4SSi_2$: *m/z* = 526.29419 [M+], calc. *m/z* = 526.29818.

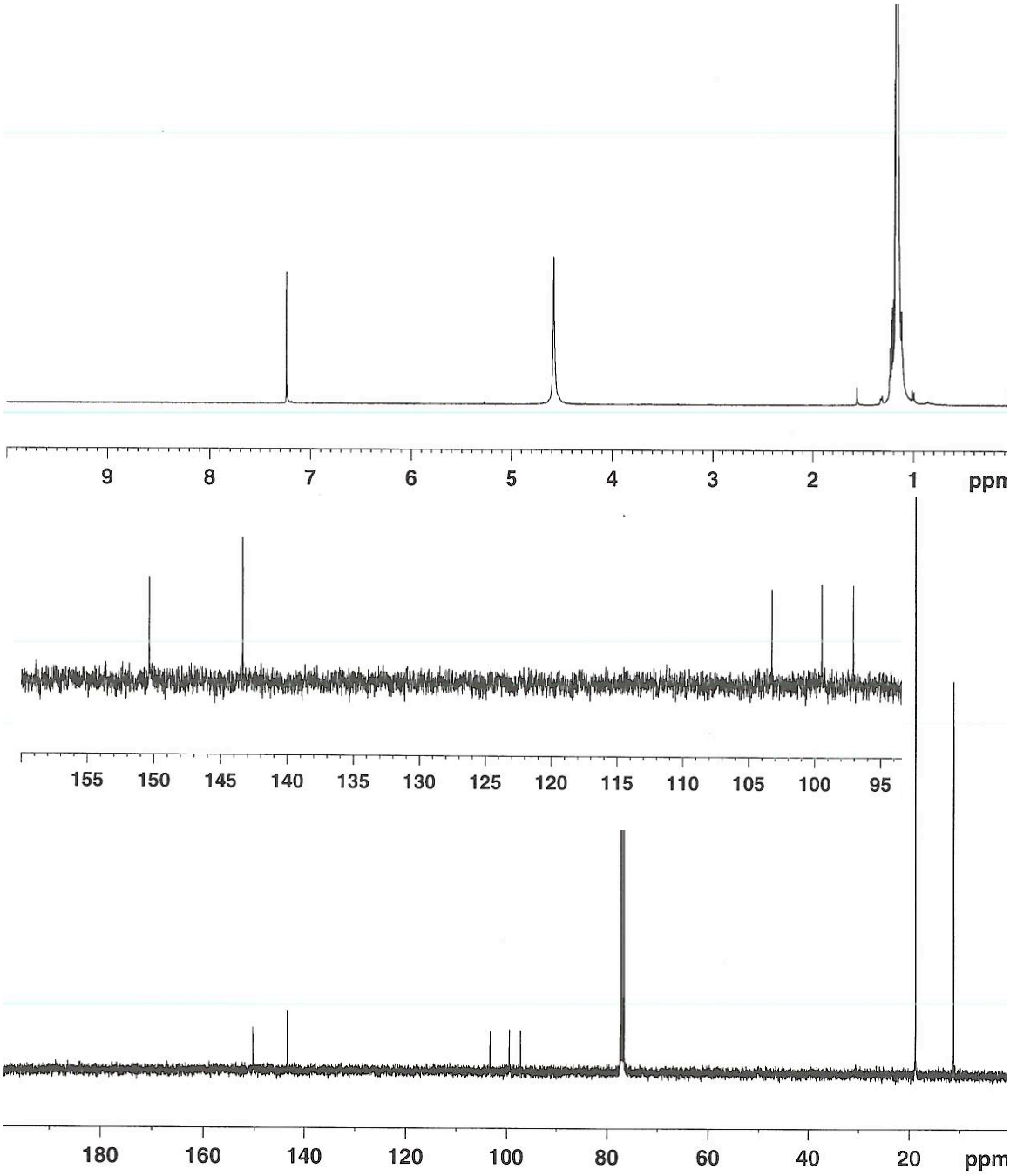

Figure 7.5. ^{1}H NMR (top) and ^{13}C NMR (bottom) of **7.5**.

7.4.3 4,11-bis((triisopropylsilyl)ethynyl)-[1,2,5]thiadiazolo[3,4-*b*]phenazine 7.1

In a 50 mL round bottom flask was added compound **7.5** (0.086 g, 1.6 x 10^{-4} mol) and placed in an oil bath at 50 °C, whereupon compound **7.6** (0.053 g, 4.9 x 10^{-3} mol, 3 eq., dissolved in 25 mL dichloromethane) was added slowly over two hours. The reaction mixture was allowed to stir for an additional hour at 50 °C. The reaction mixture was quenched in water and extracted with dichloromethane (3 x 25 mL). The organic layer was dried with anhydrous sodium sulfate and the solvent removed *in vacuo*. The crude reaction mixture was purified by column chromatography on silica gel using hexane/dichloromethane (2:1 *v/v*) to yield compound **7.1** as dark blue-purple crystals (0.030 g, 31% yield). m.p. = 184-185 °C; IR (KBr, cm^{-1}) 3066, 2938, 2923, 2918, 2889, 2862, 2752, 2723, 2132, 1824, 1696, 1522, 1485, 1381, 1022; ^{1}H NMR (400 MHz, δ in $CDCl_3$) 8.10 (AA' of AA'BB', 2H), 7.77 (BB' of AA'BB', 2H), 1.30 (m, broad, 42H); ^{13}C NMR (100 MHz, δ in $CDCl_3$) 154.58, 145.55, 142.67, 132.18, 130.40, 114.45, 111.77, 102.08, 18.88, 11.58; accurate mass for $C_{34}H_{46}N_4SSi_2$: *m/z* = 598.2963 [M+], calc. *m/z* = 598.2982.

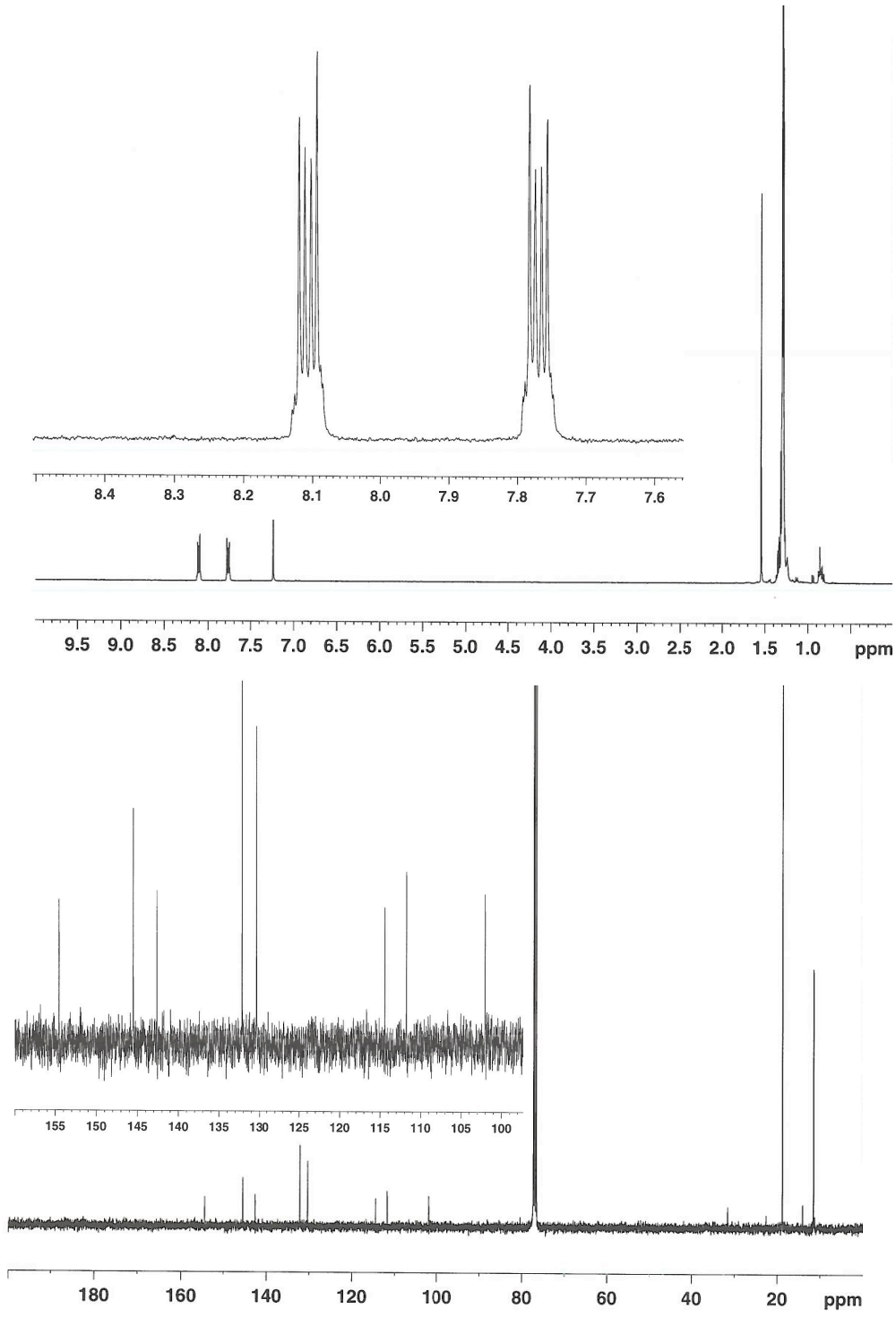

Figure 7.6. ^{1}H NMR (top) and ^{13}C NMR (bottom) of **7.1**.

7.4.4 6,7,8,9-tetrachloro-4,11-bis((triisopropylsilyl)ethynyl)-[1,2,5]thiadiazolo[3,4-*b*]phenazine 7.2

Compound **7.5** (0.166 g, 3.2 x 10^{-4} mol) and **7.7** (0.077 g, 3.2 x 10^{-4} mol, 1 eq.) were dissolved in ethanol (7 mL) and acetic acid (2 mL), heated to 85 °C and stirred for 12 h. The crude reaction was extracted with dichloromethane (3 x 25 mL). The organic layer was dried with anhydrous sodium sulfate and the solvent removed *in vacuo*. The crude product was purified by column chromatography on silica gel using hexanes/dichloromethane (2:1, *v/v*) to yield compound **7.2** as dark blue-purple crystals (0.050 g, 21% yield). m.p. = 284-286 °C; IR (KBr, cm^{-1}) 2957, 2939, 2920, 2889, 2863, 2756, 2723, 1558, 1457, 1447, 1419, 1366, 1351, 1180, 1134, 1070, 1053, 1036, 1018; ^{1}H NMR (400 MHz δ in $CDCl_3$) 1.26 (m, broad, 42H); ^{13}C NMR (100 MHz δ in $CDCl_3$) 155.67, 141.68, 140.03, 135.75, 132.25, 115.17, 113.17, 101.32, 18.83, 11.51; accurate mass for $C_{34}H_{42}Cl_4N_4SSi_2$: *m/z* = 734.1418, calc. *m/z* = 734.1425.

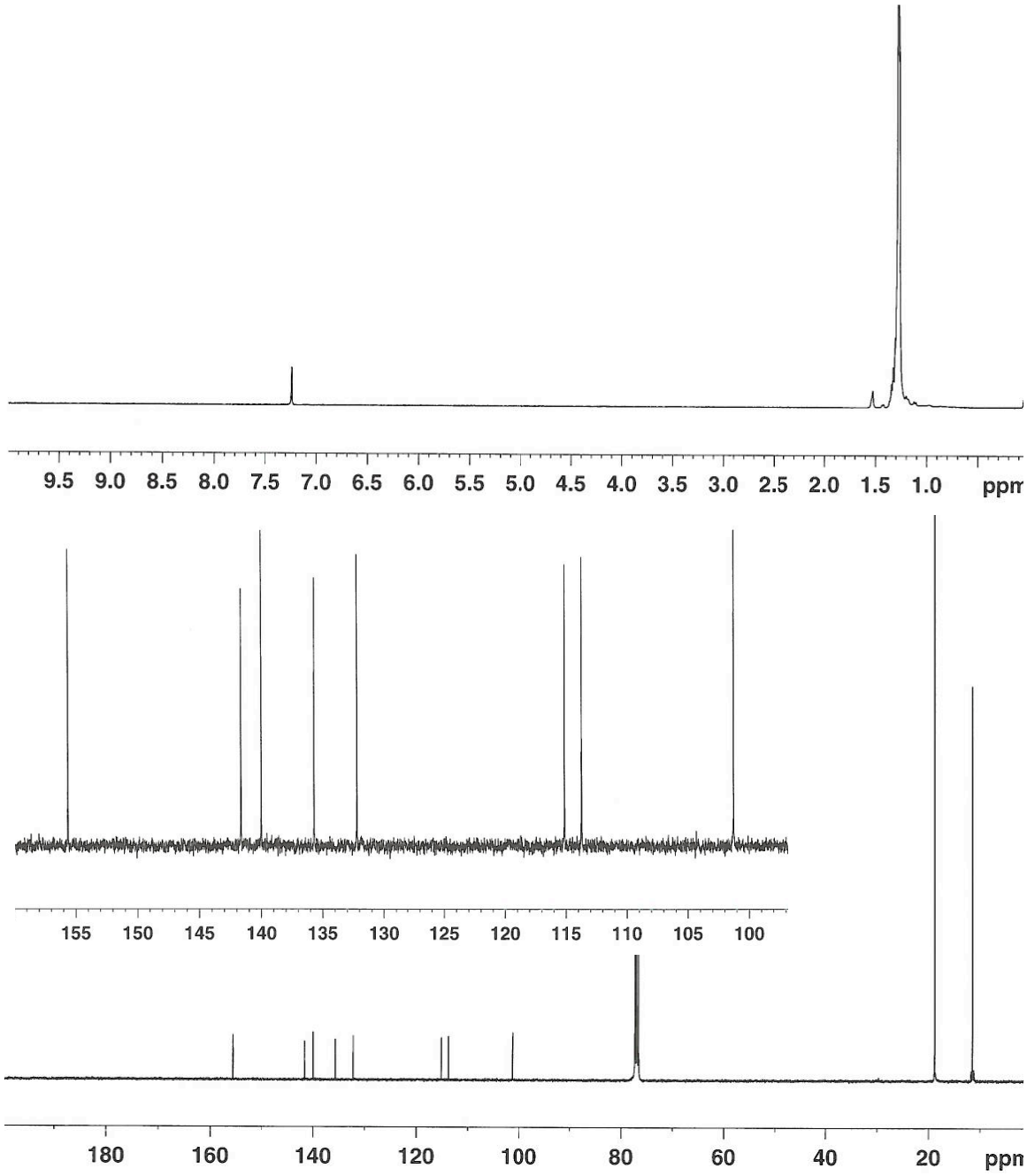

Figure 7.7. ^{1}H-NMR (top) and ^{13}C-NMR (bottom) of **7.2**.

7.4.5 UV-vis absorption and emission epctra of 7.1 and 7.2.

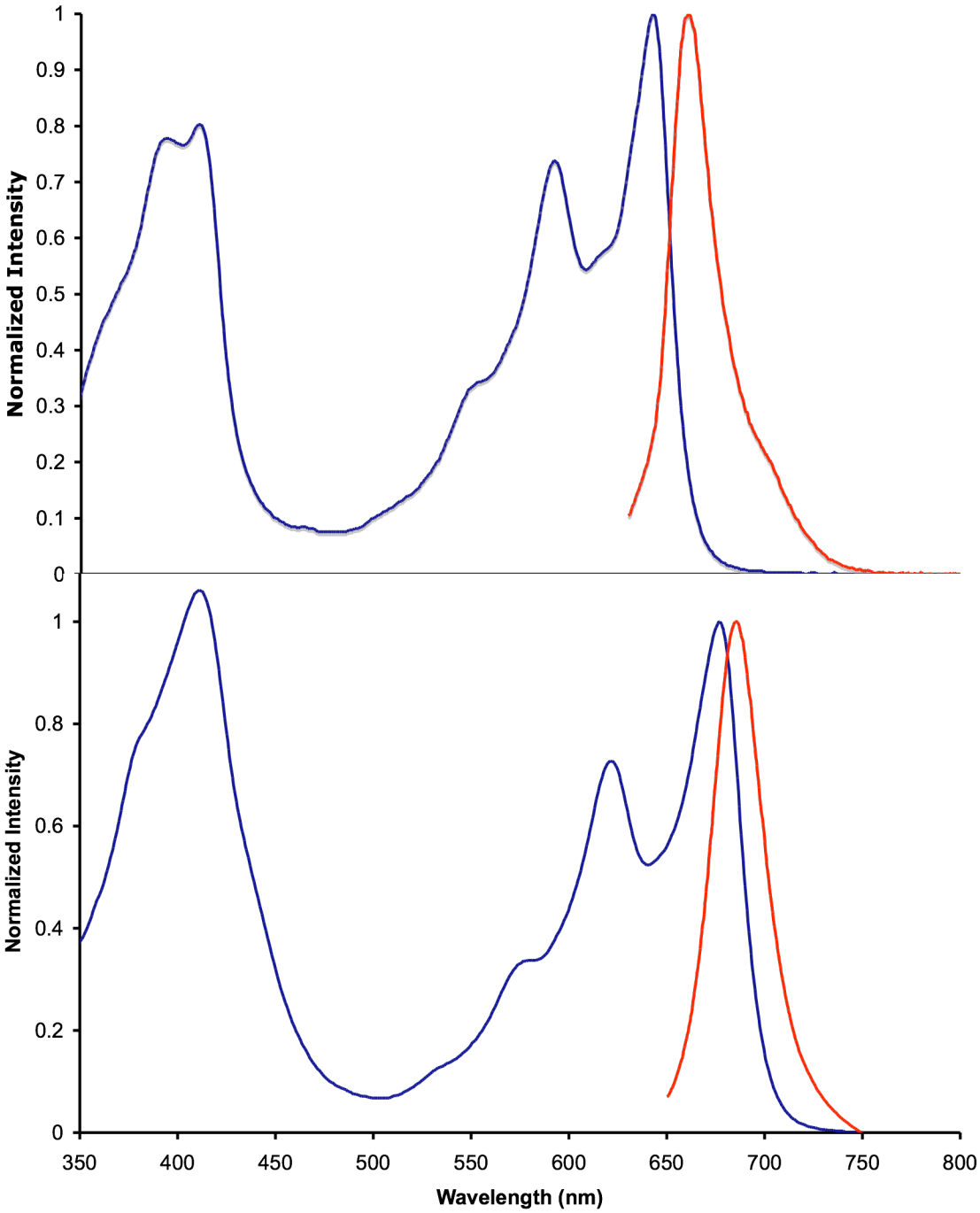

Figure 7.8. Normalized UV-vis absorption (blue) and emission (red) spectra of **7.1** (top) and **7.2** (bottom).

7.4.6 Single crystal X-ray structures of 7.1 and 7.2

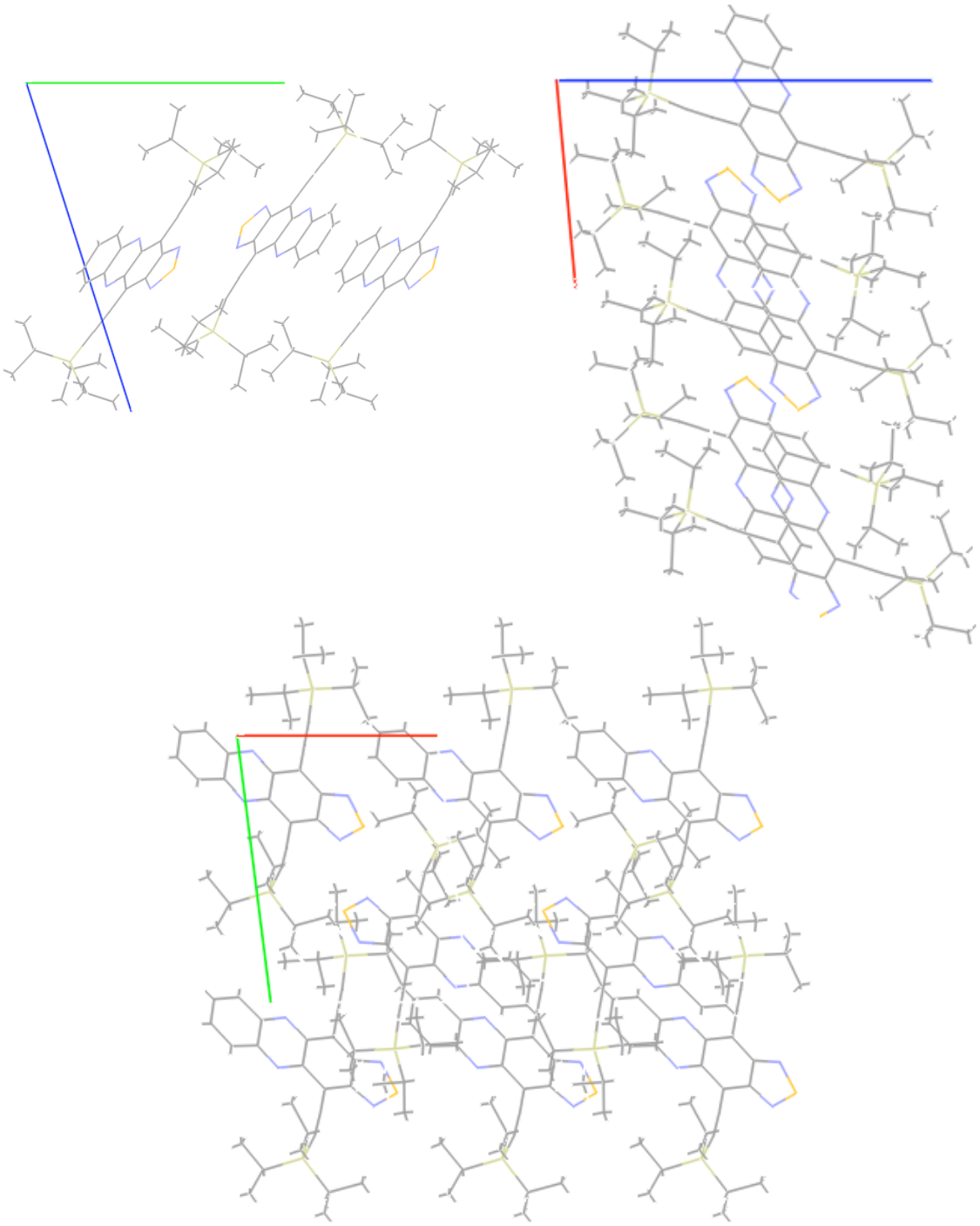

Figure 7.9. Single-crystal structure of **7.1**. Along the *a* axis (top left), *b* axis (top right) and *c* axis (bottom).

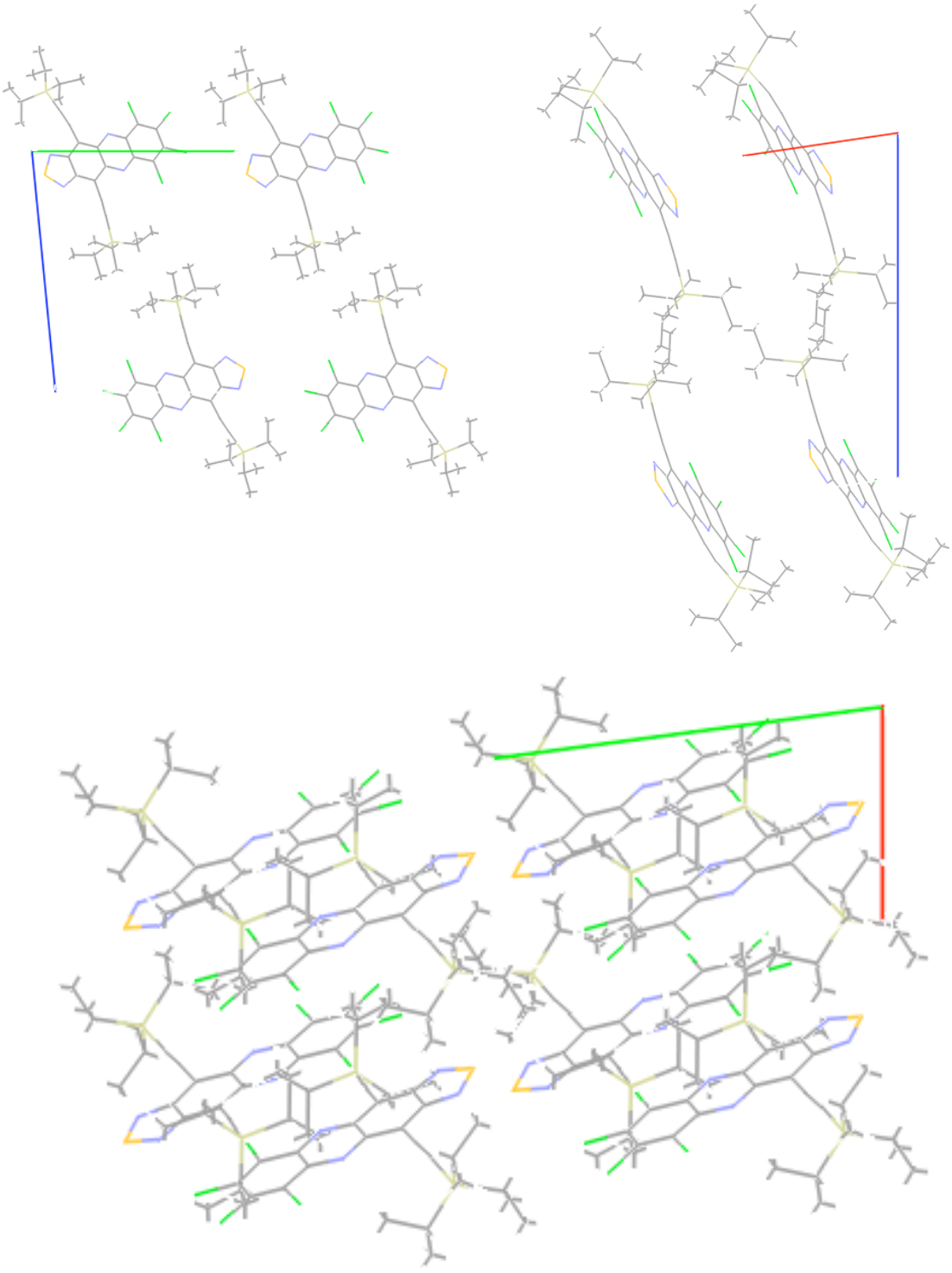

Figure 7.10. Single-crystal structure of **7.2**. Along the *a* axis (top left), *b* axis (top right), and *c* axis (bottom).

7.5 References

[1] R. Neidlein, T.V. Dao, A. Gieren, M. Kokkinidis, R. Wickens, H.P. Geserich, W. Ruppel. *Chem. Ber.* **1982**, *115*, 2898.

[2] [a] S. Miao, M.D. Smith, U.H.F. Bunz. *Org. Lett.* **2006**, *8*, 757. [b] S. Miao, P.v.R. Schleyer, J.I. Wu, K.I. Hardcastle, U.H.F. Bunz. *Org. Lett.* **2007**, *9*, 1073.

[3] A.L. Appleton, S. Miao, S.M. Brombosz, N.J. Berger, S. Barlow, S.R. Marder, K.I. Hardcastle, U.H.F. Bunz. *Org. Lett.* **2009**, *11*, 5222.

[4] S. Miao, A.L. Appleton, N.J. Berger, S. Barlow, S.R. Marder, K.I. Hardcastle, U.H.F. Bunz. *Chem. Eur. J.* **2009**, *15*, 4990.

[5] A.L. Appleton, S.M. Brombosz, S. Barlow, J.S. Sears, J-L. Brédas, S.R. Marder, U.H.F. Bunz. *Nature Comm*. **2010**, 1:90.

[6] M.L. Tang, A.D. Reichardt, P. Wei, Z. Bao. *J. Am. Chem. Soc.* **2009**, *131*, 5264.

[7] J.K. Politis, F.B. Somoza, J.W. Kampf, M.D. Curtis. *Chem. Mater.* **1999**, *11*, 2274.

[8] J.M. Thijssen. Computational Physics. 2nd Edition, 2007. Cambridge University Press.

CHAPTER 8

N,N-DIHYDROTETRAAZAHEPTACENE

8.1 Introduction

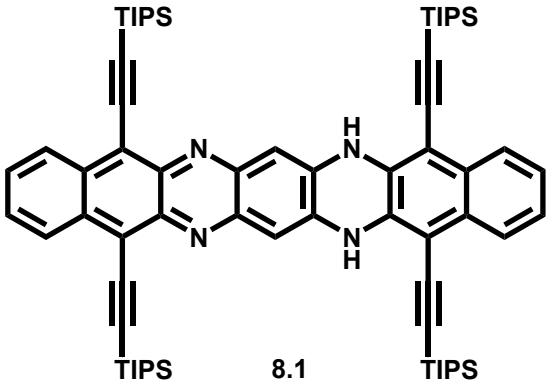

8.1

Scheme 8.1. Structure of compound **8.1**.

The search for synthetic routes toward higher order analogues of acenes (i.e. hexacene (**8.4**), heptacene (**8.5**), and nonacene (**8.6**)) has been a challenge (Scheme 8.2). In fact, compounds **8.4** and **8.5** can only be studied when embedded in a poly(methyl methacrylate) matrix so as to prevent thermal dimerization and oxidation.[1] Even in the matrix, compound **8.5** degraded within four hours. However, the achievement of Neckers et al. was critical, as the synthesis of heptacene had been disputed in the literature for almost 65 years, and the last reported synthesis of **8.5** had been in a Ph.D. dissertation, however the NMR spectra were indicative of dimerized products.[2] If **8.5** is prepared in solution, it is trapped by oxygen as a result of its extremely high reactivity as a Diels-Alder diene.[3,1a] As the parent compounds **8.4**-**8.6** are too reactive to fully characterize

and study under normal laboratory conditions, derivatives thereof needed to be synthesized.

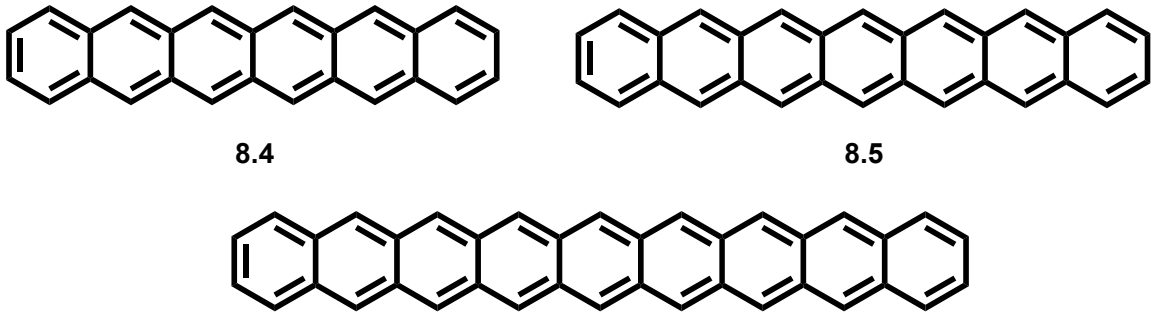

8.4 **8.5**

8.6

Scheme 8.2. Structures of the parent polyaromatic hydrocarbons hexacene (**8.4**), heptacene (**8.5**), and nonacene (**8.6**).

In 2005, the group of J.E. Anthony synthesized functionalized hexacene (**8.7**) and heptacene (**8.8**),[4] following their success with TIPS-pent (**8.9**) and the concomitant stability and solubility achieved with silylethynyl groups (Scheme 8.3).[5] Compounds **8.7** and **8.8** are stable when stored as crystals for several months and one week, respectively; but both decompose in solution within as little as one day.[4] Looking to impart even better stability to **8.5** for solution-based characterization experiments, Wudl et al[6] synthesized **8.10a,b** and **8.11**. Compound **8.10a** was insoluble even in aromatic solvents and **8.10b**, although more soluble, was still too reactive to obtain a clean ^{1}H NMR spectrum. Fortunately, compound **8.11** was stable enough to perform solution-based analysis so that this compound has been described by the authors as "The Most Stable and Fully Characterized Functional Heptacene," which was used as the title of the paper. Even though they noted that in the single-crystal structure determined by X-ray

diffraction crystallography (the crystal is stable for extended periods of time, so long as it is not exposed to oxygen) there were no direct π-π interactions of the acene backbones. They are still exploring the potential of this material in organic electronic device applications. After completing an extensive study of substituent effects and their impact on the stability of pentacene derivatives,[7] the group of G.P. Miller applied their knowledge of the stability imparted by *o*-alkyl substituted phenyl derivatives and thioaryl or thioalkyl substitution in order to design and synthesize **8.12**-**8.15**.[8] What they found was that these thio-based substituents were much better than silylethynyl groups at preventing photooxidative degradation of pentacene.[7] The authors expected **8.12** to rapidly degrade, which it did; unfortunately, so did derivatives **8.13**-**8.14** such that only UV-vis characterization could take place. On the other hand, the combined effects of the *o*-alkyl phenyl substitutents and the thioaryl substituents rendered **8.15** fully characterizable.

In order to achieve the next great breakthrough, Miller et al. applied their knowledge gained from **8.12**-**8.15** by applying the same principles to nonacene in order to generate the first "Persistent Nonacene Derivative" **8.16** and less persistent derivative **8.17** (Scheme 8.4).[9] Although this work is synthetically beautiful, their characterization of these compounds is certainly not conclusive. The UV-vis-NIR spectrum more closely resembles that of a degraded heptacene derivative because of the relative intensities of the 500 nm region versus the NIR region. Wudl previously showed that degradation of heptacene is concomitant with the growth of vibronic progression around 500 nm corresponding to a tetracene-like degradation product.[6] A look at the ^{1}H NMR spectrum of **8.16** in the aromatic region, of which the two singlets (~8.75 ppm) were assigned to

protons on the C5, 11, 16, 22, 7, 9, 18, and 20 positions, shows these are not clean singlets. There appears to be other peaks surrounding the singlets and the region between 6.6-7.5 ppm is not well resolved. Although **8.16** was labeled as a "persistent" derivative, it was stable for only 24 minutes,[10] whereas **8.17** was stable for only a few minutes. This may explain why the UV-vis and ^{1}H NMR spectra are not perfect, as these take time to collect their entire data sets. Thus, the search continues for ambient stablility of the larger acenes.

Herein, we hope to provide a new synthetic methodology towards the synthesis of persistent heptacene derivatives and higher order analogues by introducing nitrogen substitution within the core of the acene framework. Importantly, the ambient stability of these larger acenes may be improved, which may make it possible to exclude some of the bulky protecting substituents that potentially preclude their use in organic electronic devices due to a lack of π-π interactions of their core structures in the solid state, a necessary attribute for the mobility of holes and/or electrons.

The main issue at hand is the availability of starting materials and synthetic methodologies. Within our group, we have developed the acenothiadiazoles,[11] which can be reduced to their *o*-diamine forms,[12] a key building block of nitrogen-containing linearly and nonlinearly annelated ring structures. To date, we have been able to synthesize *N,N*-dihydrotetraazaheptacene derivative **8.1**; although, it certainly appears possible to make pentacene and nonacene derivatives in the same fashion. We have also previously published a tetraazapentacene derivative and its dihydro congener synthesized by a different methodology.[13]

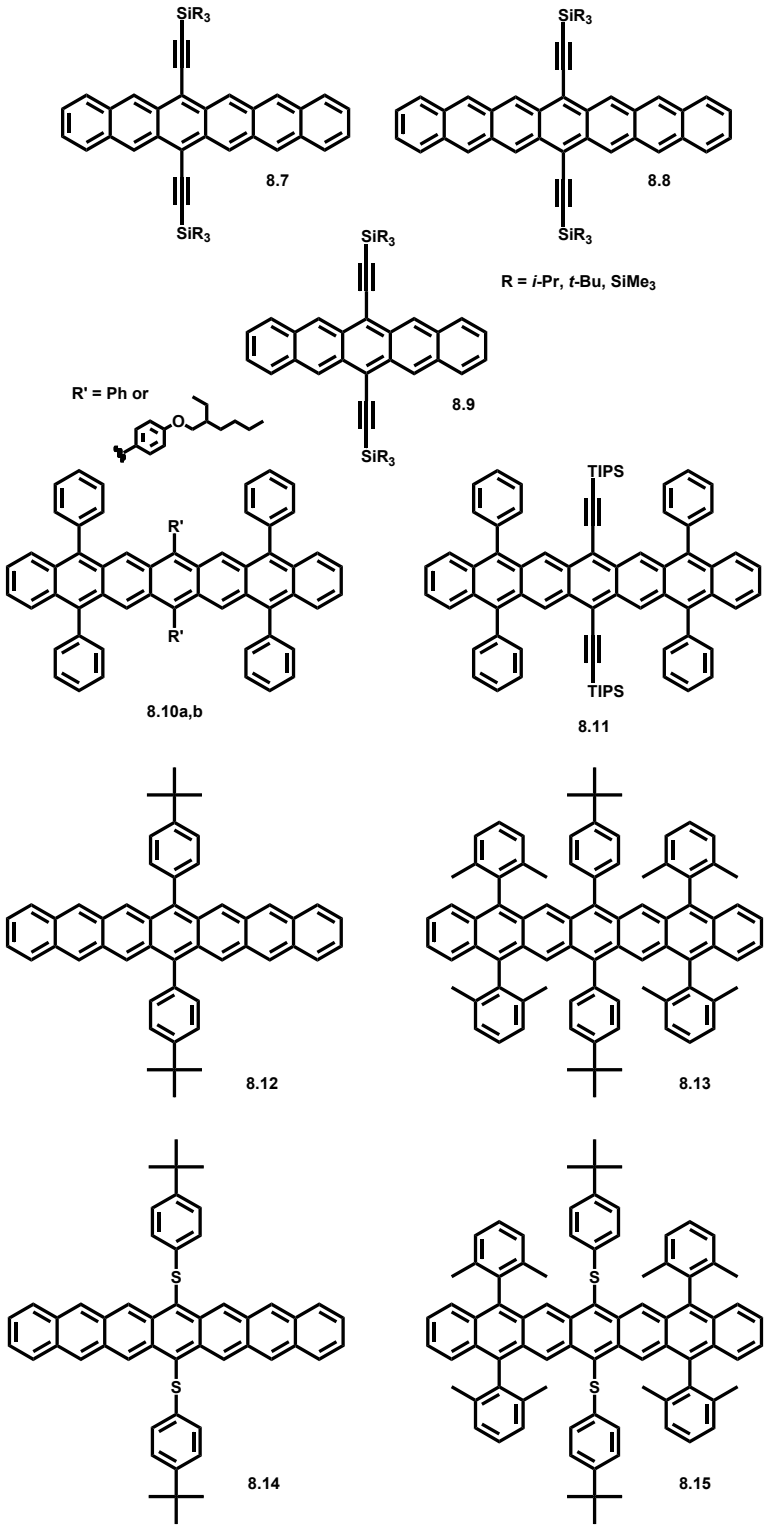

Scheme 8.3. Structures of hexacene and heptacene derivatives discussed within. The structure of TIPS-pent (**8.9**) is also shown.

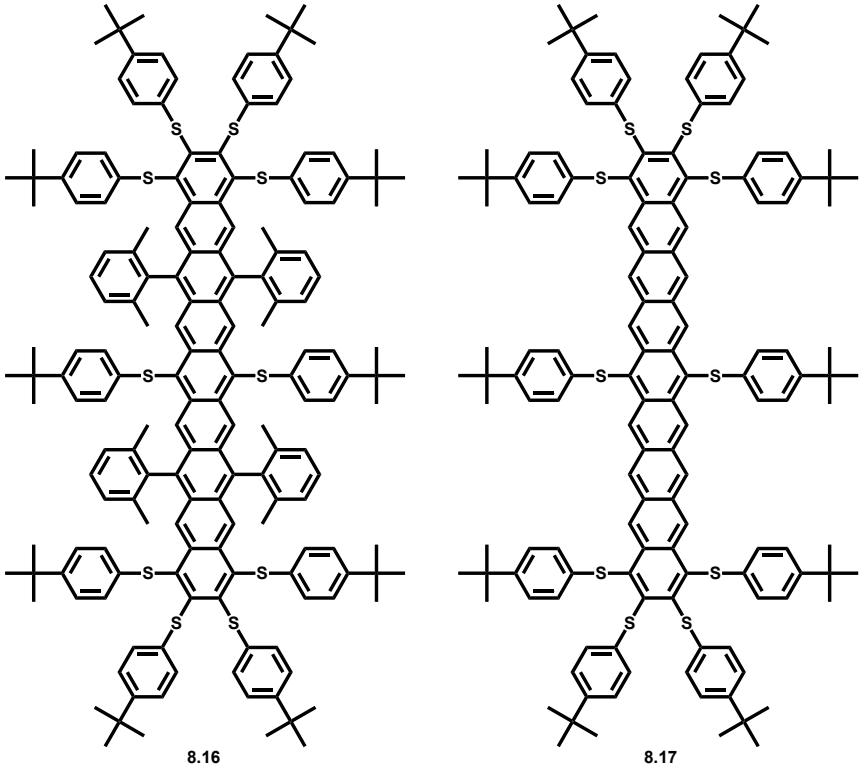

Scheme 8.4. The "persistent" nonacene derivative **8.16**, and its less substituted, less "persistent" congener **8.17**.

8.2 Results and Discussion

The synthesis (Scheme 8.5) of **8.1**[12a] takes place in a bomb tube with two equivalents of **8.2** and one equivalent of **8.3** dissolved in acetic acid and heated to its reflux temperature for multiple days resulting in 18.7% yield after purification of the crude reaction mixture. Compound **8.1** is a very dark purple/black solid that when dissolved in hexanes or dichloromethane produces a vibrantly purple solution displaying red fluorescence (Figure 8.1).

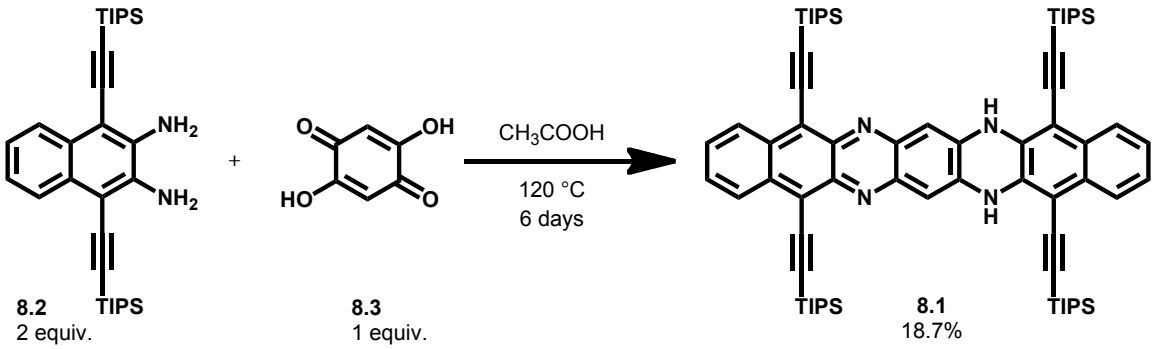

Scheme 8.5. Synthesis of **8.1**.

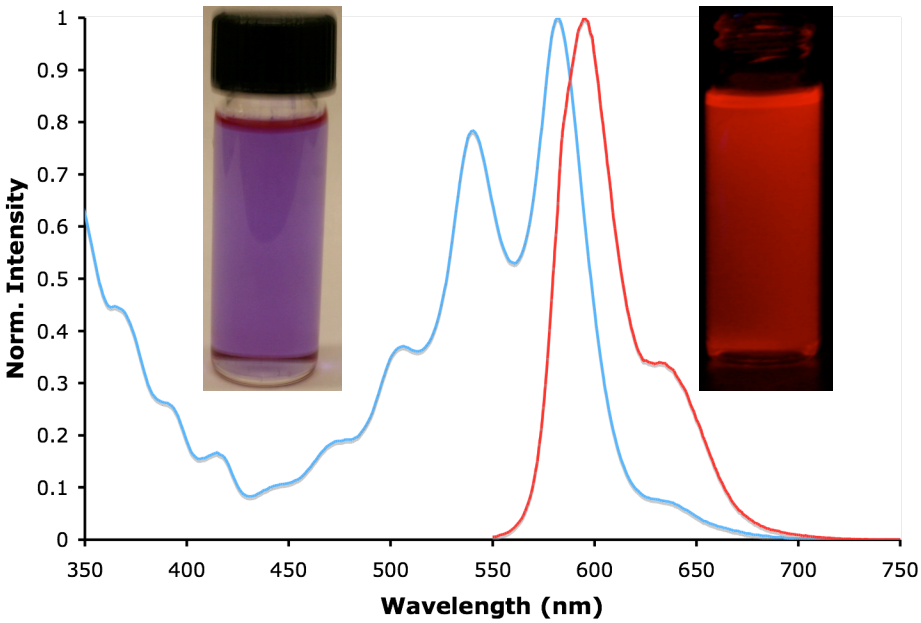

Figure 8.1. Normalized UV-vis absorption (blue) and emission (red) spectra of **8.1** in hexanes. Inset Right: Solution of **8.1** in dichloromethane under ambient lighting; Inset Left: Solution of **8.1** in dichloromethane under UV irradiation.

The vibronic fine structure in the absorption of **8.1** is a hallmark of the larger acenes[4,6] and heteroacenes.[11-13] The small Stokes shift of ~400 cm^{-1} is likely due to the rigidity of **8.1**, even though it contains two NH units within the linear array. The UV-vis spectrum of **8.1** appears closely related to our diazatetracene derivatives because the λ_{max}

of absorption is around 600 nm.[12a] This is likely a result of the NH units causing a disruption in the π-system across the entire core structure. The molar absorptivity of **8.1** was found to be ~30,000 $cm^{-1}M^{-1}$ at the λ_{max} of absorption, a new record for all of our *N*-heteroacene derivatives synthesized to date. The entire plot is shown in the Experimental section. The quantum yield of **8.1** in dichloromethane was determined to be 0.027 using 0.1 M quinine sulfate in sulfuric acid solution as a reference.

Single-crystals of **8.1** were grown from dichloromethane/hexanes solution (Figure 8.2). The molecules are planar in the solid-state and crystallographically disordered with respect to the nitrogens (50% occupancy by NH at each site due to symmetry). Unfortunately, however, it was clear that the use of four TIPS groups from the single-crystal X-ray structure obtained resulted in the heteroacene cores not having any direct overlap of their π faces. To make sure that this was the case in practice, a thin-film was drop-cast from dichloromethane and its UV-vis absorption spectrum is shown in Figure 8.3. Although there is a bathochromic shift in the long wavelength λ_{max} of 13 nm and tailing observed in the thin-film absorption profile, the overall solid state spectrum still retains its vibronic progression and spectral bandwidths thus indicating that there is no significant interaction of the π faces of adjacent molecules in drop-cast thin-films from dichloromethane solution onto quartz slides.

In order to determine whether or not **8.1** will undergo oxidation(s) and reduction(s), Dr. Steve Barlow performed cyclic voltammetry in deoxygenated THF or DCM using 0.1 M $^{n}Bu_4NPF_6$ and ferrocene was used as an internal reference. Compound

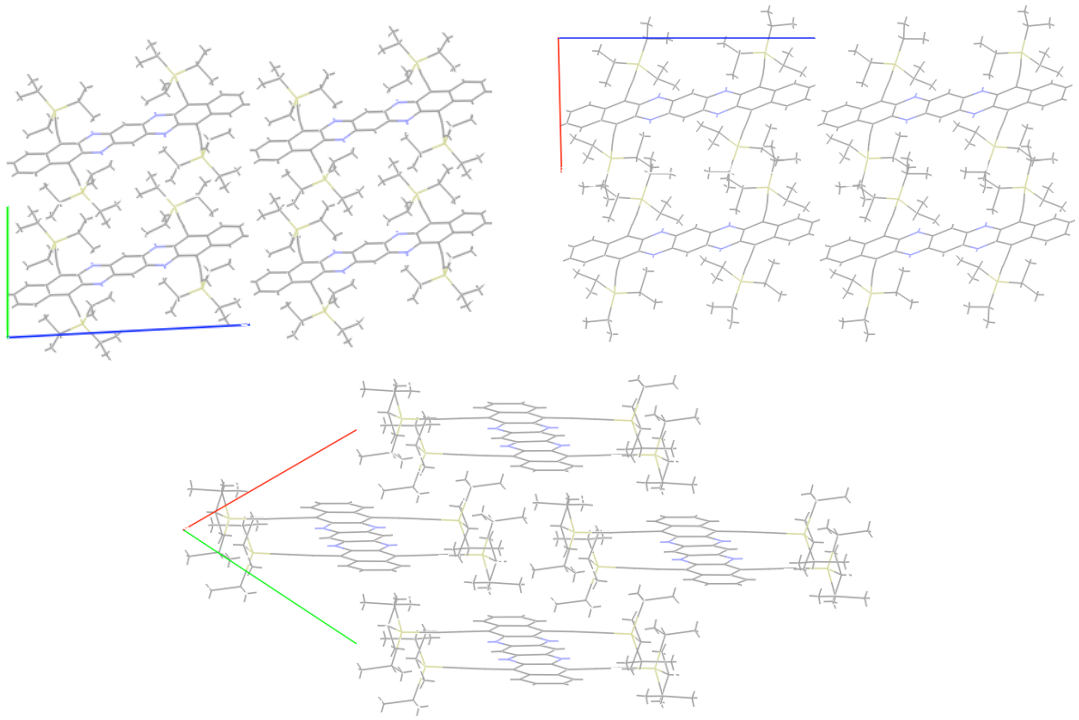

Figure 8.2. Single-crystal structure of **8.1**. Views: top left: along the *a* axis; top right: along the *b* axis; bottom: along the *c* axis.

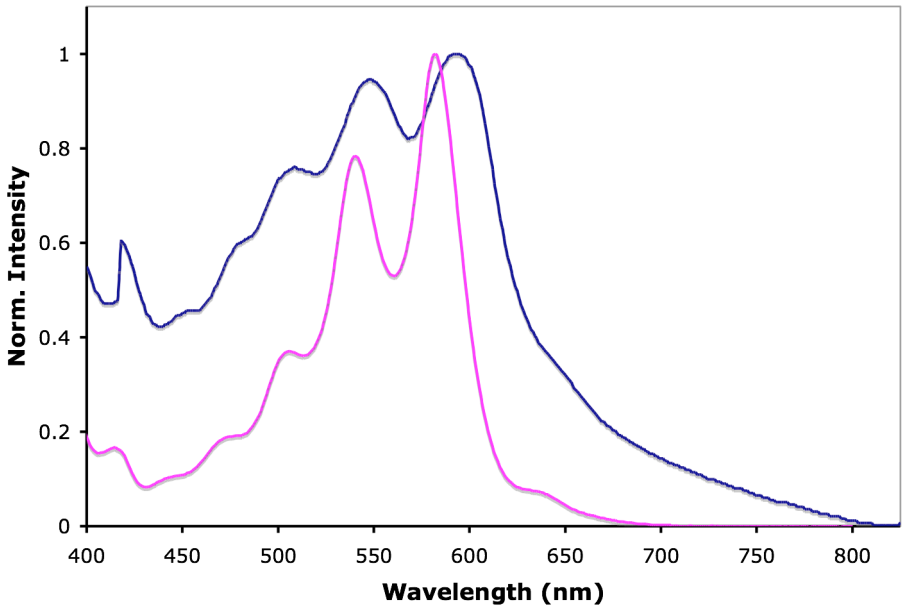

Figure 8.3. Normalized thin-film (blue) and hexane solution (pink) absorption spectra of **8.1**.

8.1 shows two successive, reversible reductions at -1.34 and -1.72 V with a third irreversible reduction at -2.19 V, all in THF. We were also able to observe an irreversible oxidation at +0.63 V in DCM.The electrochemical H-L gap of 1.97 V (difference between the first reduction and oxidation potentials) is in good agreement with our UV-vis absorption spectrum that shows a shoulder at 625 nm (1.98 eV). This is the first time that three successive reduction potentials have been observed in an acene or heteroacene small molecule. These redox potentials also show that **8.1** behaves similarly to our diazatetracene derivatives as the reduction potentials are nearly identical, however the oxidation potential occurs at 0.32 V less.[12a] Note: the working electrode was Pt and the potentiostat was a CH Instruments 620D.

Stability issues plague the larger acenes as described in the introduction. The longest-lived molecule is **8.7**,[4] a hexacene derivative, which will persist for several months in the solid state. Heptacene **8.8**[4] will only last one week in the solid state. All other molecules in the Introduction will rapidly degrade upon exposure to air and light. Drastically different is the stability of **8.1**, which will persist for more than one week in solution and three years (so far) in the solid state under ambient conditions![14] The ^{1}H NMR profiles of the original sample and the three-year old sample are shown in the Experimental section (Figure 8.4 and 8.6). There is no detectable degradation of the sample even after three years. It appears that core nitrogen substitution can stabilize the linearly annelated ring structure of the larger acenes, possibly allowing the use of fewer, less bulky substituents to prevent problems of degradation under ambient conditions and allow for communication between neighboring molecules through their π faces.

8.3 Conclusion

We have synthesized the first *N,N*-dihydrotetraazaheptacene derivative (**8.1**) and shown the stability of this compound to be significantly greater than any other acene derivative of analogous size reported to date. The synthetic methodology presented herein produces derivatives which have four TIPS groups. This number of TIPS groups (or other bulky appended substituents) has been shown to disrupt the π-π interactions in the solid-state,[6] as shown in Figure 8.2 and the solid-state absorption profile in Figure 8.3 of compound **8.1**. The larger *N*-heteroacenes (heptacene and higher order analogues) can be synthesized is shown to be possible and also that they are truly stable under ambient conditions. We are continuing to pursue *N,N*-dihydrotetraazanonacene, as well as synthetic methodologies that would allow for the utilization of only two TIPS groups on the central ring to improve the π-π interactions for application as the semi-conducting layer in an organic electronic device.

This manuscript has been submitted to the *Journal of the American Chemical Society*:

Anthony Lucas Appleton, Stephen Barlow, Seth R. Marder, Kenneth I. Hardcastle, Uwe H.F. Bunz. "*N,N*-Dihydrotetraazaheptacene: A Synthetic Strategy Towards Larger Acenes with Ambient Stability." **Submitted**.

8.4 Experimental Information

8.4.1 5,9,14,18-tetrakis((triisopropylsilyl)ethynyl)-6,17dihydro[b]benzo [6,7]quinoxalino [2,3-i]phenazine 8.1

In a 100 mL bomb tube was added **8.2** (0.400 g, 7.71 x 10^{-4} mol, 2 eq.) and **8.3** (0.054 g, 3.85 x 10^{-4}, 1 eq.), which were dissolved in acetic acid (30 mL). The reaction vessel was sealed and heated to 120 ºC for six days while stirring. The reaction was cooled to room temperature and extracted with DCM (50 mL), The organic layer was washed with H_2O (100 mL x 2), dried with sodium sulfate, and the solvent removed *in vacuo*. The crude mixture was purified by column chromatography on silica gel using hexanes/dichloromethane (3:1 *v/v*). Compound **8.1** was isolated as a dark purple solid (0.080 g, 18.7% yield). m.p. = stable up to 400 ºC; IR (KBr, cm^{-1}) 3375, 3055, 2958, 2931, 2719, 2434, 2360, 2133, 1739, 1720, 1596, 1569, 1488, 1461, 1377, 1261, 1226, 1153, 1107; ^{1}H NMR (400 MHz, δ in $CDCl_3$) 8.60 (AA' of AA'BB', 2H), 7.94 (AA" of AA"BB", 2H), 7.62 (s, 2H), 7.54 (BB' of AA'BB', 2H), 7.35 (BB" of AA"BB", 2H), 6.82 (s, 2H), 1.296-1.289 (m, broad, 42H), 1.255 (m, broad, 42H); ^{13}C NMR (100 MHz, $CDCl_3$) 145.70, 141.25, 135.77, 134.07, 130.90, 129.25, 127.31, 126.95, 125.96, 125.13, 119.07, 105.89, 105.70, 105.05, 103.40, 101.69, 99.49, 19.00, 18.92, 11.66, 11.36; accurate mass for $C_{70}H_{96}N_4Si_4$: *m/z* = 1104.6485 [M^+], calc. *m/z* = 1104.6712.

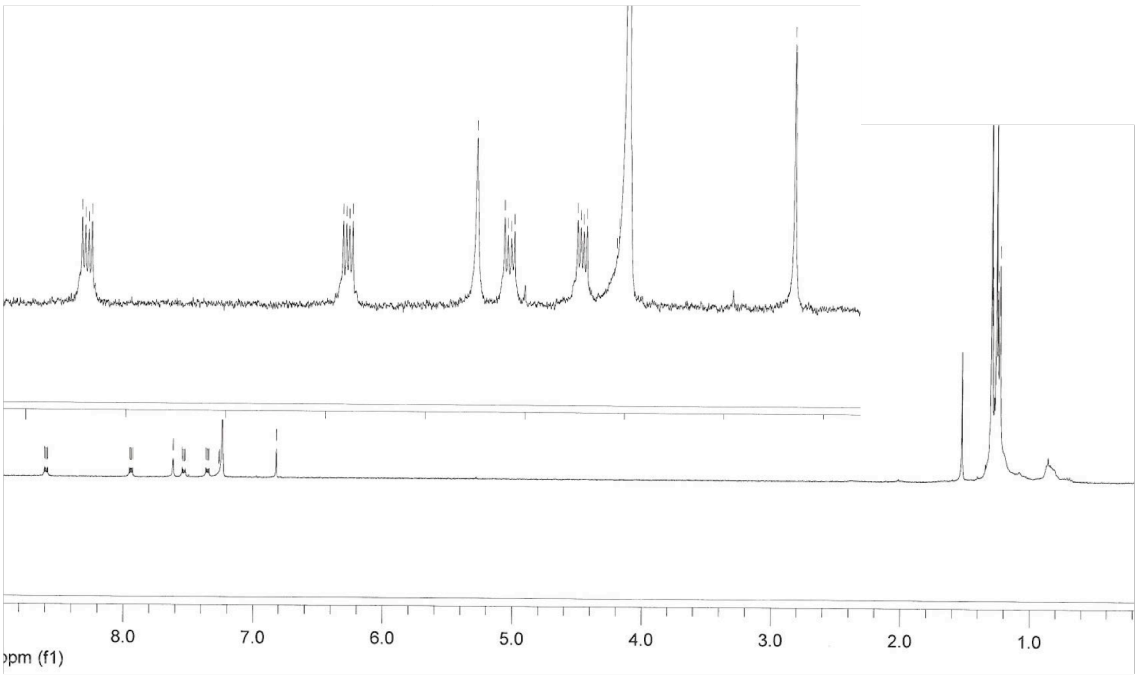

Figure 8.4. ^{1}H NMR of the compound **8.1** (October 2007).

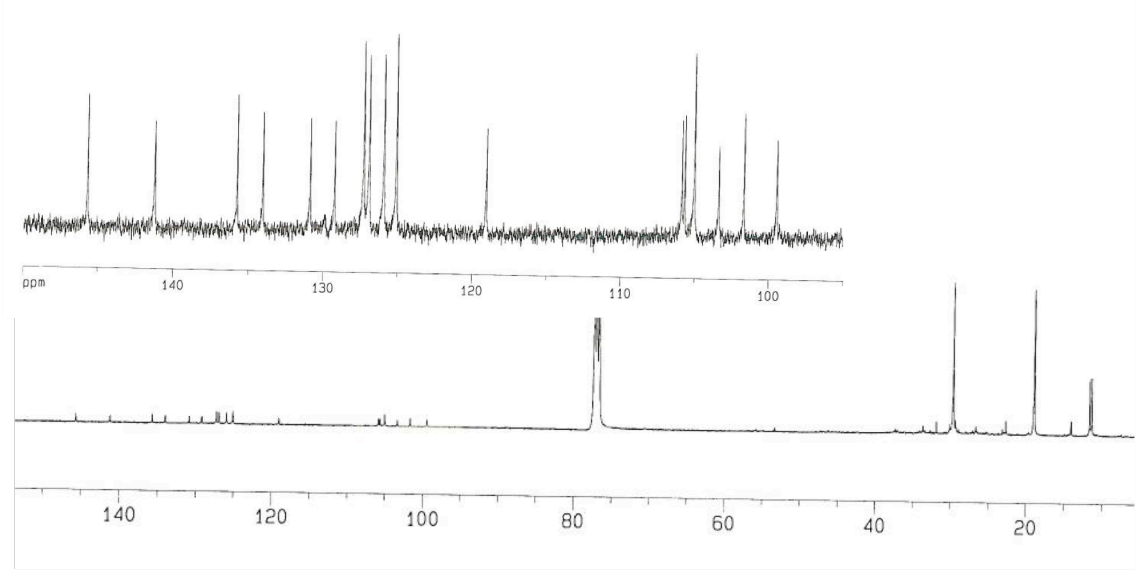

Figure 8.5. ^{13}C NMR of compound **8.1**, 10 mm NMR tube with ns = 40,000.

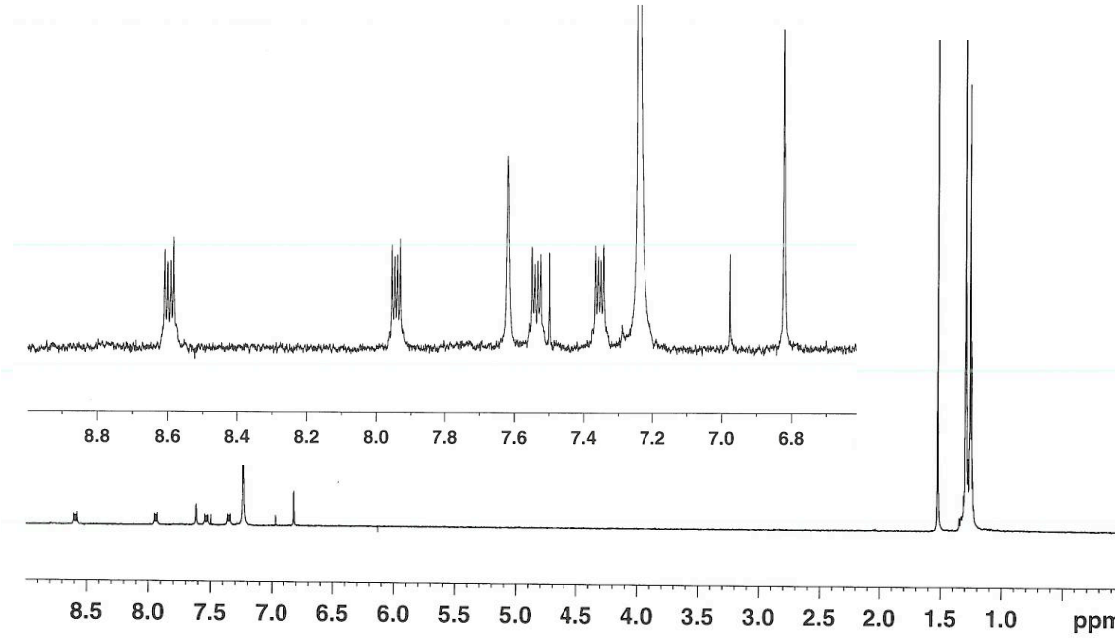

Figure 8.6. ^{1}H NMR of compound **8.1** (October 2010).

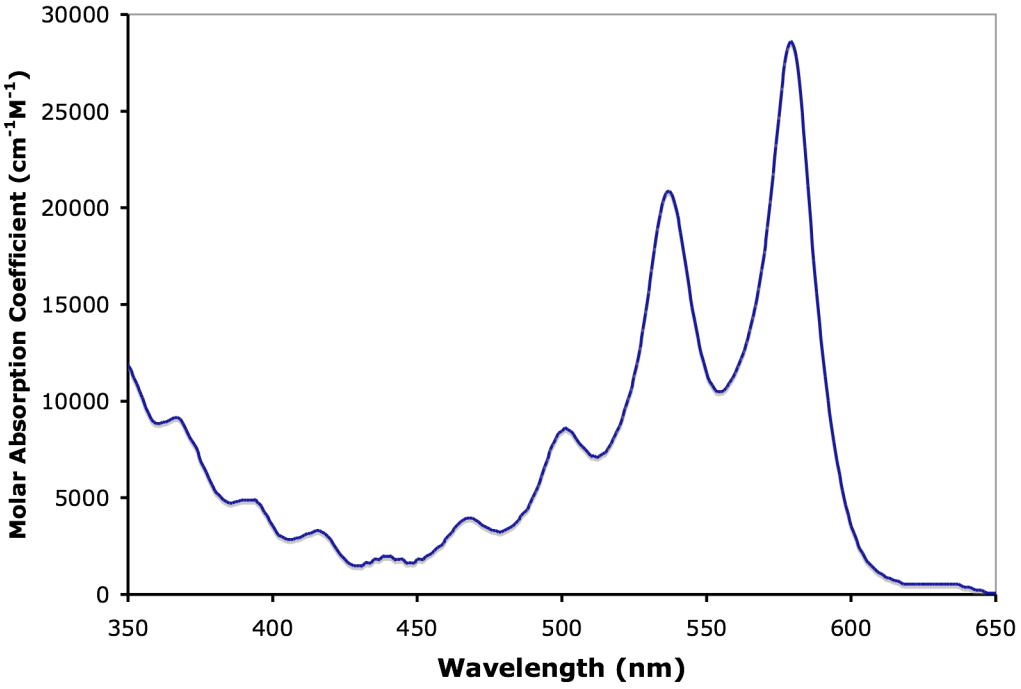

Figure 8.7. Molar absorptivity profile of compound **8.1** in hexanes.

8.5 References

[1] [a] R. Mondal, B.K. Shah, D.C. Neckers. *J. Am. Chem. Soc*. **2006**, *128*, 9612; [b] R. Mondal, C. Tonshoff, D. Khon, D.C. Neckers, H.F. Bettinger. *J. Am. Chem. Soc.* **2009**, *131*, 14281.

[2] [a] E. Clar. *Ber. Dtsch. Chem. Ges*. **1942**, *75B*, 1330; [b] B. Boggiano, E. Clar. *J. Chem. Soc.* **1957**, 2681; [c] C. Marschalk. *Bull. Soc. Chim*. **1943**, *10*, 511; [d] W.J. Bailey, C. Liao. *J. Am. Chem. Soc*. **1955**, *77*, 992; T. Fang. Heptacene, Octacene, Nonacene, Supracene and Related Polymers. Ph.D. Thesis, Univ. of California, Los Angeles, CA, 1986.

[3] P.v.R. Schleyer, M. Manoharan, H. Jiao, F. Stahl. *Org. Lett*. **2001**, *3*, 3643.

[4] M.M. Payne, S.R. Parkin, J.E. Anthony. *J. Am. Chem. Soc.* **2005**, *127*, 8028.

[5] [a] J.E. Anthony, D.L. Eaton, S.R. Parkin. *Org. Lett.* **2002**, *4*, 15; [b] A. Maliakal, K. Raghavachari, H. Katz, E. Chandross, T. Siegrist. *Chem. Mater.* **2004**, *16*, 4980.

[6] D. Chun, Y. Cheng, F. Wudl. *Angew. Chem. Int. Ed.* **2008**, *47*, 8380.

[7] I. Kaur, W. Jia, R. Kopreski, S. Selvarasah, M.R. Dokmeci, C. Pramanik, N.E. McGruer, G.P. Miller. *J. Am. Chem. Soc.* **2008**, *130*, 16274.

[8] I. Kaur, N.N. Stein, R.P. Kopreski, G.P. Miller. *J. Am. Chem. Soc*. **2009**, *131*, 3424.

[9] I. Kaur, M. Jazdzyk, N.N. Stein, P. Prusevich, G.P. Miller. *J. Am. Chem. Soc*. **2010**, *132*, 1261.

[10] Scott M. Brombosz personal communication with Polina Prusevich.

[11] A.L. Appleton, S. Miao, S.M. Brombosz, N.J. Berger, S. Barlow, S.R. Marder, K.I. Hardcastle, U.H.F. Bunz. *Org. Lett*. **2009**, *11*, 5222.

[12] [a] S. Miao, S.M. Brombosz, P.v.R. Schleyer, J.I. Wu, S. Barlow, S.R. Marder, K.I. Hardcastle, U.H.F. Bunz. *J. Am. Chem. Soc.* **2008**, *130*, 7339; [b] A.L. Appleton, S.M. Brombosz, S. Barlow, J.S. Sears, J-L. Brédas, S.R. Marder, U.H.F. Bunz. *Nature Comm*. **2010**, 1:90.

[13] S. Miao, A.L. Appleton, N.J. Berger, S. Barlow, S.R. Marder, K.I. Hardcastle, U.H.F. Bunz. *Chem. Eur. J.* **2009**, *15*, 4990.

[14] The original sample was prepared in October 2007 for single-crystal X-ray diffraction analysis. The same sample has been continuously exposed to atmospheric conditions; exposure to light has not been continuous, but the sample has been in contact with light for extended periods of time. The original ^{1}H NMR is shown in Figure 8.4 followed by a

^{1}H NMR taken of the same sample in October 2010 (Figure 8.6), without performing any purification.

CHAPTER 9

CONCLUSION

9.1 Introduction

The work presented herein has greatly expanded the materials available for applications in the area of organic electronics, as well as sensory materials in aqueous environments, and provided insight into the optoelectronic trends of differentlty substituted *N*-heteroacene derivatives. From a single set of three key starting materials, the acenothiadiazoles, we have been able to synthetically access many more derivatives that possess an array of properties and functionalities. This work has also influenced the synthesis of new derivatives by different means of synthetic methodologies in order to further advance available materials and understand their properties. Scheme 9.1 shows the structures of all materials discussed throughout this concluding chapter and Table 9.1 tabulates key results. First we will begin with a brief summary of each chapter, followed by a look at several promising properties of selected materials, then future synthetic endeavors, and finally concluding remarks.

9.2 Chapter Summaries

Chapter 2 serves as the foundation of this thesis, as the materials prepared acted as the starting materials for several chapters that followed and laid the groundwork for future projects. Compounds **2.1**-**2.3** gave us insight into several key properties for device application. The R-groups can be easily modified using different alkynyllithiums during

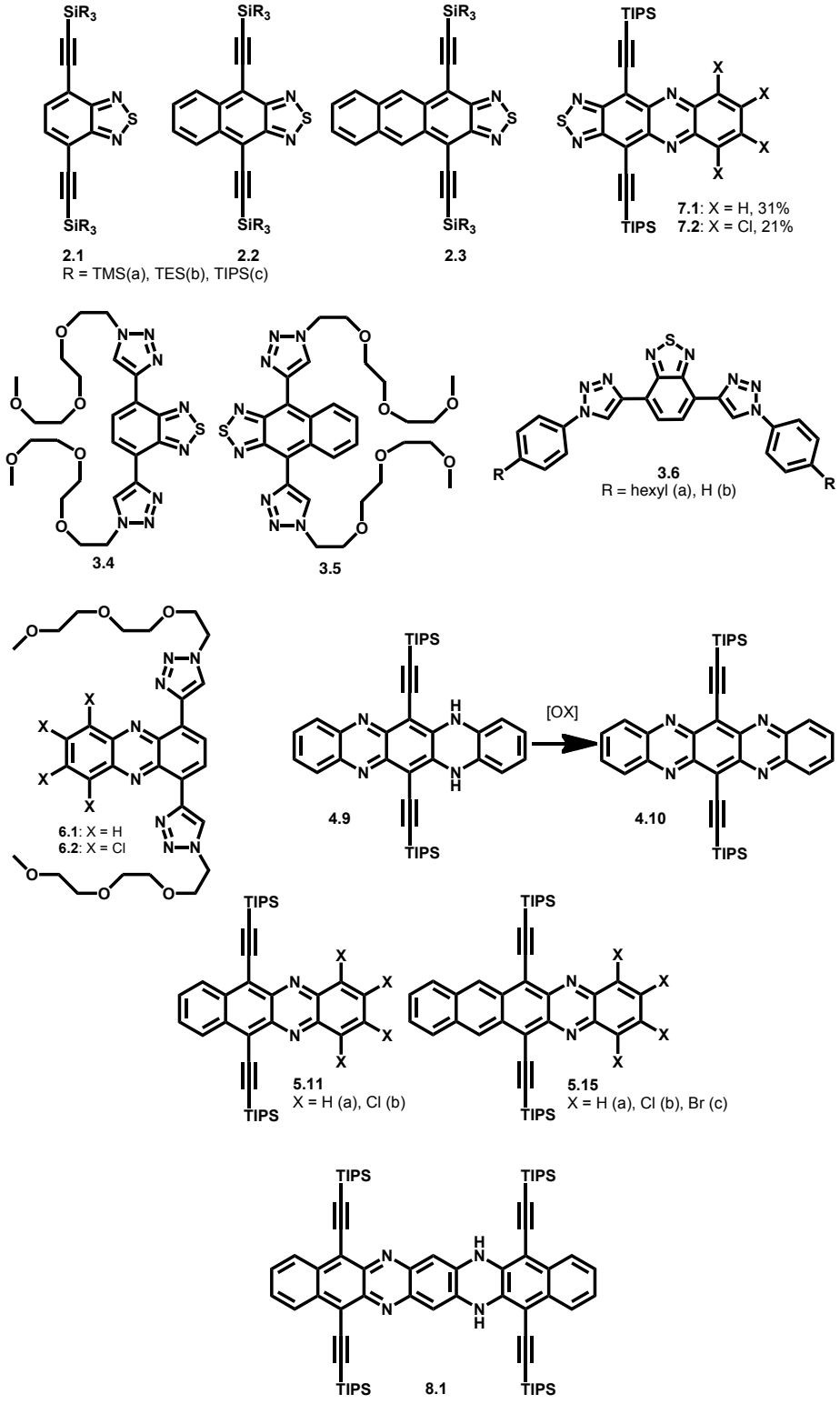

Scheme 9.1. Compounds discussed in Chapter 9.

Table 9.1. Compiled data.

Compound	**2.1c**	**2.2c**	**2.3c**	**4.9**	**4.10**	**TIPS-pent**[d]	**5.11a**	**5.11b**	**5.15a**	**5.15b**	**5.15c**	**7.1**	**7.2**	**8.1**
ABS Max (nm)	385	532	654	521	681	645	571	620	693	759	761	644	677	579
Molar Absorptivity ($cm^{-1}M^{-1}$)	12282	17600	19570	ND	ND	20000	22694	17227	19092	12863	10249	19278	15022	28594
EM Max (nm)	442	538	659	525	694	-	583	630	714	-	-	661	686	596
Quantum Yield[a]	0.94	0.28	0.01	ND	ND	-	0.09	0.02	<0.01	-	-	ND	ND	0.027
H-L (ABS) Gap (eV)	3.24	2.34	1.89	2.37	1.82	1.92	2.17	2.00	1.79	1.63	1.63	1.93	1.83	2.14
$1/t_0$ (s^{-1})	-	-	8.2×10^7	-	-	-	3.0×10^8	1.6×10^8	1.5×10^8	5.6×10^7	2.9×10^7	1.5×10^8	1.1×10^8	2.2×10^8
HOMO (eV)	-5.90[b]	-5.38[b]	-5.03[b]	-4.93[b]	-5.29[b]	-4.6	-5.72[g]	-6.03[g]	-5.37[g]	-5.66[g]	ND	-6.0[g]	-6.28[g]	ND
LUMO (eV)	-2.67[b]	-2.98[b]	-3.16[b]	-2.14[b]	-3.43[b]	-2.7	-3.35[g]	-3.78[g]	-3.50[g]	-3.89[g]	ND	-3.9[g]	-4.32[g]	ND
H-L (calc) Gap (eV)	3.23	2.40	1.87	2.79	1.86	1.9	2.37	2.25	1.87	1.77	ND	2.1	1.96	ND
E0/- (V)	ND	ND	-1.18[c]	-1.82[c]	-0.79[c]	-1.7	-1.19[f]	-0.92[f]	-1.05[f]	-0.79[f]	-0.79[f]	-0.84[h]	-0.57[c]	-1.34[c]
E-/2- (V)	ND	ND	-1.78[c]	-	-1.23[c]	-	-1.73[f]	-1.51[f]	-1.51[f]	-1.32[f]	-1.23[f]	-1.14[h]	-1.16[c]	-1.72[c]
E0/+ (V)	ND	ND	+0.74[c]	+0.32[c]	-	0.38	+0.99[f]	+1.11[f]	+0.68[f]	+0.83[f]	+0.80[f]	+1.17[h]	-	+0.63[h]
E+/2+ (V)	ND	ND	-	-	-	-	-	-	-	-	-	-	-	-
H-L (CV) Gap (V)	ND	ND	1.92	2.14	-	2.1	2.18	2.03	1.73	1.62	1.59	2.01	-	1.97

a: quinine sulfate in 0.1 M H_2SO_4 (aq) as reference; b: TMS derivatives were used, obtained by SPARTAN 08/Windows using the B3LYP method (continued) with the 6-31G**//6-31G** basis sets; c: 0.1 M $^nBuNPF_6$ THF solution, ferrocenium/ ferrocene as reference; d: J.E. Anthony et al. *J. Am. Chem. Soc.* **2001**, *123*, 9482, Swartz et al. *Org. Lett.* **2005**, *7*, 3163, Wurthner et al. *ChemPhysChem*. **2006**, *7*, 793, Griffith et al. *J. Phys. Chem. C*. **2008**, *112*, 20518; e: N. Nijegorodov et al. *Spectrochim Acta Part A*. **1997**, *53*, 1813; f: 0.1 M $^nBuNPF_6$ MeCN:toluene (1:1, *v/v*) solution, ferrocenium/ferrocene as reference; g: desilylated versions by DFT using the B3LYP/6-311+G* basis set; h: 0.1 M $^nBuNPF_6$ DCM colution, ferrocenium/ferrocene as reference.

synthesis. Different R-groups for **2.3** were shown to change the solid-state packing via single-crystal X-ray analysis and thin-film absorption spectra. The use of TIPS showed little change between solution and solid-state absorption spectra. However, the use of TES or TMS produced thin-film's with UV-vis absorption spectra that were indicative of π-π interactions due to spectral broadening and a decrease in the energy of the absorption onset. Size-dependent optical properties were observed across this series, with the largest member (**2.3**) having the lowest energy λ_{max} of absorption. Through computational studies, we found that this was due to a destabilizing effect on the HOMO and stabilizing effect on the LUMO as the core structure's size increased across the series.

Chapters 3 and 6 showed the utility of several derivatives via deprotection followed by the Click reaction to produce molecules that possessed a single binding pocket for certain metal cations. Compounds **3.4** and **3.5** become quenched upon the addition of Cu(II), as well as compound **6.1**. Compound **3.4** also showed binding towards Ni(II), while compound **6.1** showed binding towards Ag(I). The size of the acenothiadiazole core did not significantly effect the binding of metal cations (ie. **3.4** versus **3.5**), however halogenation of **6.1** (ie. **6.1** → **6.2**) nearly turns off the fluorescence response to metal cations. Fluorescent lifetimes for **3.4**, **3.5**, and **6.1** are at least 4 ns, thus indicating the potential to be used in complex biological matrices with time-gated detection. Interestingly, the bis(triazole) formation appears to confer two metal binding pockets, however after coordination to one site the other becomes too electron poor to effectively bind another metal cation. Finally, it was determined that the triazole unit is a poor electronic conduit as shown by the optoelectronic properties of derivative **3.6**.

Chapter 4 provided key insight and direction for later chapters. Compound **4.10** is obtained from its dihydro precursor (**4.9**) easily via manganese oxide oxidation. The TIPS substitution, analogous to TIPS-pent, conferred good solubility, stability, and promoted a brickwork style packing motif. The symmetrical diaza units around the central TIPS groups allowed facile reduction, but did not significantly alter the HOMO-LUMO gap when compared to TIPS-pent. This work fueled our pursuit of derivatives with facile reducibility (increased electron affinity), and intrigued us as to how, synthetically, lower energy electronic transitions could be achieved.

Chapter 5 was an exploration into the synthesis of soluble, asymmetrical diazatetracene and diazapentacene derivatives (**5.11a,b** and **5.15a-c**). The large bathochromic shifts upon halogenation of diazaacenes versus acenes was very interesting. Through computational studies, we found that diazaacenes possess a disjoint frontier molecular orbital structure for their HOMO, an effect not observed in the analogous acene series even if halogenated. Their LUMO (delocalized across the entire core) energies were more stabilized than their HOMO (disjoint structure) energies upon halogenation in the 1, 2, 3, 4 positions. This allowed for an absorption range of 571-761 nm to be "tuned in" and redox potentials that span 0.5 eV in their first reduction and first oxidation potentials among members of the same series. The absorption spectra of their thin-films were indicative of π-π interactions of the heteroacene cores, a promising result for device application. The optoelectronic tunability of these derivatives could prove beneficial in the future design of new materials for application in organic electronics.

Chapter 7 was an exploration into the limits of electron affinity and ionization potential of the large acenothiadiazole **2.3c**. Using pyrazine substitution at the 5 and 10

positions (**7.1**) and halogenation (**7.2**) of carbons 6-9 resulted in the lowest energy required for a first reduction potential thus far in our work, -0.57 V, for compound **7.2**. There was no significant change in the long wavelength λ_{max} for all three compounds, however halogenation resulted in a significant decrease in molar absorptivity as observed in chapter 5. We performed computational studies to better understand the optoelectronic properties observed for these thiadiazolophenazine derivatives as compared to **2.3c**. The reason for a significant decrease in the first reduction potential of **7.2** is due to the LUMO being stabilized by almost 0.75 eV relative to **2.3c**. The LUMO and HOMO are stabilized by almost the same amount, a very different result when compared to Chapter 5. The reason for this is that the HOMO undergoes less destabilizing effects upon pyrazine insertion and/or halogenation of the thiadiazole core (electron withdrawing moieties are now symmetrically substituted around the core structure, similarly **4.10**). Very interesting were the results of single-crystal analyses and thin-film absorption profiles. Although **7.1**, **7.2**, and **2.3c** possess nearly identical packing parameters, their thin-film absorption profiles could not be any different. In fact, these profiles more closely resemble **2.3a**, even though their R groups are drastically different, indicating π-π interactions of their cores when either drop-cast or spin-coated from solution. To date, **7.1** and **7.2** show the greatest potential of being able to be cast from solution in a device and act as an air-stable electron-transporting small molecule.

Chapter 8 was an attempt to push the limits of our synthetic methodologies in order to produce the first higher order core nitrogen-containing analogues of heptacene and nonacene. Unfortunately, *N,N*-dihydrotetraazanonacene was unable to be synthesized in a similar fashion as *N,N*-dihydrotetraazaheptacene (**8.1**). The instability of

the larger acenes (i.e. hexacene, heptacene, and nonacene) is such that they cannot be studied for any length of time outside of a matrix. Appending bulky substituents increased the longevity of these materials, but they are still too reactive under ambient conditions. Our derivative **8.1**, on the other hand, is significantly more stable such that it can remain for three years under ambient conditions in the solid state. Compound **8.1** undergoes three successive reductions, which is the first time we have observed three successive reduction potentials in any of our materials. Single-crystal X-ray analysis revealed that the use of four TIPS groups prevents π-π interactions in the solid-state, which was confirmed by comparison of its solution and solid-state UV-vis profiles. Although we have prepared the most stable heptacene derivative to date, its use as a hole- or electron-transporting molecule appears hindered by the numerous TIPS groups.

9.3 Promising Properties

Although we were unable to produce any meaningful results in terms of electron and/or hole mobility values by utilizing these materials as the semi-conducting layer in a TFT, we have still been able to expand the scope of materials and their properties (Table 9.1). We will now take a look at the potential of some of these materials if applied as the electron-transporting layer in an OPV with TIPS-pent as the hole-transporting layer. First, we will explore their UV-vis properties, followed by a comparison of their HOMO and LUMO levels, which are two key features in the design of an OPV. Lastly, we will explore the possibility of a bulk heterojunction device solution-cast from a single molecule.

Compared to TIPS-pent (λ_{max}, ε = 20,000),[13] the molar absorption coefficients of our materials are on the same order of magnitude. Within the acenothidiazoles, ε scales with increasing the size of the core; introduction of a pyrazine moiety (**2.3c → 7.1**) does not alter this value significantly, however halogenation (**7.1 → 7.2**) causes an almost 25% drop. This same drop is observed in all our nonhalogenated versus halogenated *N*-heteroacene derivatives. Interestingly, ε has an opposite trend for the diazaacene series compared to the acenothiadiazoles, as it drops from **5.11a** to **5.15a** by 15%. The largest ε value was obtained for **8.1**, which is also the largest member at seven linearly annelated rings.

Another way to compare the strength of X → X* is by calculating the oscillator strength for the first optoelectronic transition. Recall, that in Chapter 5 we were able to show that this transition is greater than 80% HOMO to LUMO in character for our diazatetracene and diazapentacene series. The oscillator strength ($1/\tau_0$, s^{-1}) is calculated by Equation 2, which has been adapted from reference:[1]

$$\frac{1}{\tau_0} = 8 \times 2303\pi c \overline{\nu_{ul}}^2 n^2 N^{-1} \int \varepsilon d\bar{\nu} \qquad (9.1)$$

where *c* is the speed of light in a vacuum, $\overline{\nu_{ul}}$ is the frequency of the transition in cm^{-1} at the λ_{max} of absorption, *n* is the refractive index of the medium, *N* is Avogadro's number, and ε is the molar absorptivity coefficient ($M^{-1}cm^{-1}$) at specified frequency $\bar{\nu}$ (cm^{-1}). The integration was taken from the minimum before the first electronic transition to the lower energy portion of the spectrum. This is simply another way of reporting the molar absorptivity profile of the entire first electronic transition. This may be a better way of evaluating the ability of the molecule to absorb light as it is not just the λ_{max}'s ε value, but

also takes into account the approximate area (integration) under the curve of the first electronic transition. From highest to lowest, the ranking is as follows: **5.11a**, **8.1**, **5.11b**, **5.15a**/**7.1**, **7.2**, **2.3c**, **5.15b**, and **5.15c** (Table 9.1). From these calculations, it is clear that bromination can severely impact the probability (the strength of the oscillation from the ground to first excited state) of this first electronic transistion by 81% (**5.15a** → **5.15c**) and chlorination causes a 27, 47, and 63% drop (**7.1** → **7.2**, **5.11a** → **5.11b**, and **5.15a** → **5.15b**), respectively. Also, the addition of one more annelated ring (**5.11a** → **5.15a**) results in a 50% decrease in the diazaacene series. Oddly enough, pyrazine moiety substitution and peripheral chlorination led to an overall increase (**2.3c** → **7.2**) within the thiadiazolophenazines. It appears that diazatetracene moieties (**5.11** and **8.1**) show the largest area under the curve for their first electronic transition, and that halogenation, in most cases, should be avoided when attempting to maximize the molar absorptivity of *N*-heteroacene materials.

For all compounds considered (Scheme 9.1, Table 9.1), our HOMO energies range from -4.93 to -6.28 eV, and our LUMO energies range from -2.14 to -4.32 eV. At the extremes are compounds **4.9** and **7.2** (as a note, these calculations have not been performed on **8.1** or derivatives thereof). Compound **4.9** is intrinsically electron rich as it is a diarylamine derivative, and **7.2** in intrinsically electron poor as is contains a thiadiazole unit and pyrazine moiety within the core and four chlorine atoms around the periphery. This is to be expected from first principles. Some trends are noteworthy. The addition of linearly annelated rings (**2.1c** → **2.2c** → **2.3c** and **5.11a** → **5.15a** and **5.11b** → **5.15b**) causes the HOMO to become more destabilized and the LUMO to become more stabilized across the series, leading to an overall decrease in the HOMO-LUMO

gap, an increase of the wavelength in the λ_{max} of absorption (decrease in energy), and a decrease in the first redox potentials. Chlorination (**5.11a → 5.11b**, **5.15a → 5.15b**, **7.1 → 7.2**) decreases the energies of both HOMO and LUMO, however the LUMO is stabilized to a greater extent than the HOMO, again leading to an increase in the λ_{max} of absorption, a decrease in the first reduction potential, but an increase in the first oxidation potential (we were unable to observe an oxidation potential for **7.2** under the conditions of our cyclic voltammetry experiments). These trends could be very useful as a way of designing the next generation of *N*-heteroacene derivatives depending on what properties are desirable for application in an organic electronic device.

According to the work of Bao et al[2] correlating HOMO/LUMO energy levels with carrier types, electron transport is observed when the LUMO is less than -3.15 eV and hole transport is not observed when the HOMO is below -5.6 eV on OTS treated surfaces with top contact gold electrodes. Accordingly, we could observe hole mobility values only for **2.1c**, **2.2c**, and **4.9**; ambipolar characteristics for **2.3c**, **4.10**, and **5.15a**; and electron mobility values only for **5.11a**, **5.11b**, **5.15b**, **7.1**, and **7.2**. This could mean that **2.3c**, **4.10**, **5.11a**, **5.11b**, **5.15a**, **5.15b**, **7.1**, and **7.2** could potentially be the electron-transporting layer in a heterojunction-based OPV.

An indirect comparison can be made to an OPV of reference based on pentacene and C60 which shows an efficiency of almost 2%.[3] The work of Kippelen et al and others have found that the upper-limit of the open circuit voltage (V_{OC}) depends largely on the relative energy levels of the donor and acceptor. More specifically, it correlates with the offset between the HOMO of the donor (D) and the LUMO of the acceptor (A). In the pentacene/C_{60} OPV, the offset of pentacene's HOMO and C_{60}'s LUMO is 0.8 eV,

Table 9.2. Tabulated theoretical V_{OC} values and the LUMO-LUMO offset of TIPS-pent and our compounds in the table based on a theoretical OPV.

Compound	**2.3c**	**4.10**	**5.11a**	**5.11b**	**5.15a**	**5.15b**	**7.1**	**7.2**
Est. V_{OC} (V)	1.44	1.17	1.25	0.82	1.1	0.71	0.7	0.28
L-L Offset (eV)	0.46	0.73	0.65	1.08	0.8	1.19	1.2	1.62

which produced experimental V_{OC} values on the order of 0.4 V even when other aspects of the device had been modified.[3] In our theoretical cases, we will use TIPS-pent as the hole-transporting layer and our molecules as the electron-transporting layer (Table 9.2). The largest estimated upper-limit V_{OC} was using **2.3c** as the electron-transporting layer, unfortunately this compound does show π-π interactions in the solid-state, but an easy modification of the R group to either TMS or TES could overcome this. However, **4.10**, **5.11a**, and **5.15a** all show estimated upper-limit V_{OC} values larger than 1.1 V, and all of these compounds show π-π interactions in the solid-state as well as packing parameters that are similar to the brickwork motif observed in TIPS-pent.[14] This is very promising indeed. Molecules **5.11b**, **5.15b**, and **7.1** all show estimated upper-limit V_{OC} values between 0.7-0.82 V, and molecule **7.2** showed a dismal estimated upper-limit V_{OC} of 0.28 V.

The efficiency of these devices also depends on the absorption of photons within the active layer, a process that C60 negligibly participates in past 450 nm as its molar absorptivity coefficients are less than 1000 and begin to completely die off past 650 nm.[4] Our molecules, on the other, absorb with similar efficiencies compared to TIPS-pent and have absorption windows that stretch out past 750 nm. In fact, molecule **5.15b** absorbs well past 760 nm in the solid-state and has an estimated V_{OC} with TIPS-pent of 0.71 V,

only 0.09 V less than the offset between C_{60}'s LUMO and pentacene's HOMO. The idea of avoiding lowering the H-L gap due to a decrease in V_{OC} is valid, but also lowering both HOMO and LUMO in an effort to achieve air-stable electron transport will also result in materials with small V_{OC} values in the theoretical example above. This may indicate that a new hole-transporting material may need to be developed in order to accommodate devices that could potentially operate in the presence of oxygen.

A factor that cannot be determined here that would greatly enhance (or perhaps destroy) this argument is the degree of wavefunction overlap that could be achieved between TIPS-pent and **5.15b**. However, the key overlap is between the LUMO of TIPS-pent and the LUMO of **5.15b**, as this represents a critical step in a functioning OPV: electron transfer from the LUMO of the donor to the LUMO of the acceptor (provided in this case the donor absorbs the photon). Also important is that this state (TIPS-pent (+) and **5.15b** (-)) be lower in energy than the bound electron-hole pair, such that the charges can be efficiently separated. In all cases (not just **5.15b**), the LUMO-LUMO offset between TIPS-pent and the electron-transporting molecule of interest is on the order of 0.5 eV and greater (pentacene and C60 have a LUMO-LUMO offset of 1.1 eV;[3] TIPS-pent and **5.15b** have a LUMO-LUMO offset of 1.2 eV). This energy difference should be able to overcome the exciton binding energy, which has been estimated at a few tenths (0.3-0.5) of an eV,[5] potentially resulting in efficient charge separation at the donor-acceptor interface. These results may appear promising, but do not mean anything until all resources of device fabrication have been exhausted or a functioning device is fabricated.

It certainly appears counter intuitive at first, but it may be possible to produce a heterojunction OPV fabricated by solution processing of only a single molecule! As the example, take compounds **4.9** and **4.10**. Compound **4.10** is produced by oxidation of compound **4.9**. This oxidation can be achieved quickly by use of manganese dioxide, or allowing **4.9** to be exposed to ambient conditions for a period of time. Their HOMO and LUMO levels appear promising for this application as discussed above: the LUMO-LUMO offset is 1.29 eV and the HOMO(D, **4.9**)-LUMO(A, **4.10**) offset is 1.5 eV (almost double that of pentacene/C_{60}). These materials should also pack quite similarly. The really interesting part is how to fabricate the device. After the synthesis of **4.9** (either working quickly during purification or doing so in an inert environment), it must be transferred into an oxygen-free glovebox where it can be dissolved in a solvent (i.e. chloroform), and then solution-processed onto an appropriate surface (i.e. ITO), and then have an appropriate counter electrode deposited on top or just probe the surface with a metal contact (i.e. aluminum). At first, there should be no photo current upon exposure to light (there is no heterojunction yet), however if we were to allow oxygen to bleed into the environment to varying levels and/or exposure times we could begin to oxidize **4.9** into **4.10** at varying rates. The really interesting part would be to observe the photocurrent over time as this oxidation takes place. This may not be the case, as oxygen may trap the electrons; thus, it may be best to remove the oxygen after a certain time if no photocurrent is observed and either vacuum seal the device or anneal the device followed by vacuum sealing in order to observe a photocurrent under illumination. This would be very exciting, as once the device has expired due to oxygen leakage, the material could be recycled by hydrogenation[6] if it could be recovered.

9.4 Future Synthetic Endeavors

We have been able to show that the condensation of an *o*-diamine with an *o*-dione is a reliable reaction. In fact, within our group we have explored the condensation of *o*-diones that would result in a nonlinearly annelated ring structures. We have found that these materials display properties for application as OLEDs due to their solid-state packing structure, which results in the ability of the materials to have solid-state fluorescence in colors across the spectrum. To date, we have not found a condensation reaction by this means that fails.

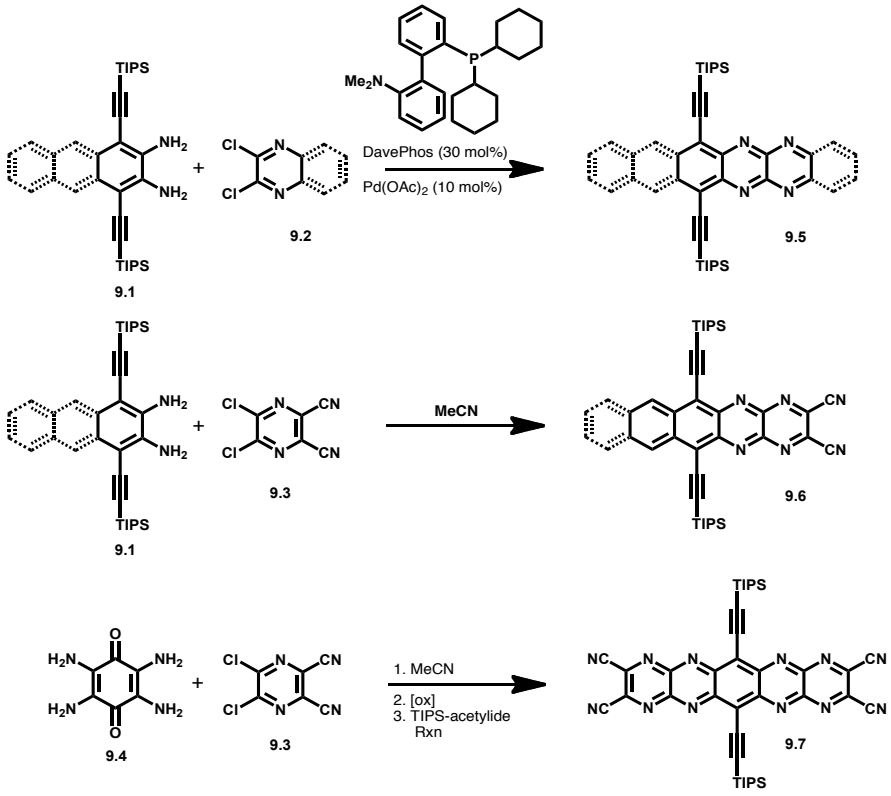

Scheme 9.2. Synthetic roadmap to future small molecules.

Other options to explore that could potentially result in materials for organic electronic applications would be the condensation of an *o*-halogen with our various *o*-diamines (Scheme 9.2). The first reaction[7] is that of 2,3-dichloropyrazine or 2,3-dichloroquinoxaline (**9.2**) with an *o*-diamine of choice (**9.1**). This would produce varying sized linearly annelated ring structures from three up to six rings. The dihydro derivatives may be produced first, which we should be able to oxidize into the fully aromatic form, similar to our tetraza- and diazapentacenes.[8] The second reaction[9] to be explored is the condensation of 2,3-dichloro-5,6-dicyanopyrazine (**9.3**) with an *o*-diamine of choice (**9.1** or **9.4**) to produce up to five linearly annelated ring structures. These products (**9.5**-**9.7**) could result in materials with extremely high electron affinities and ionization potentials (very low lying LUMO and HOMO levels), such that air-stable electron transport may be observed upon device fabrication. Their dihydro congeners may also show hole transport. These materials (**9.5** and **9.6**) could potentially absorb into the IR region of the solar spectrum due to a much more disjoint HOMO and stabilized LUMO than we have previously observed in our recent publication.[8b]

It is very interesting to see just how far compounds **9.5**-**9.7**'s HOMO and LUMO can be stabilized. Especially intriguing is compound **9.7**, which has a total of eight nitrogens within the pentacene unit itself. This number of aza nitrogens has been suggested by computational studies[10] to be required for electron transport, but synthetically was a challenging task as to how to incorporate so many nitrogens. Now, it appears, that this number of aza nitrogens can be synthetically achieved in a pentacene structure. Also, the use of the dicyano moiety of **9.3** should further improve facile electron injection by additionally stabilizing the LUMO. And because of the electron

deficient nature of this structure and its similarity to TIPS-pent, the solid-state packing could be extremely close (*d* spacing ≤ 3.3 Å).[8a] This could potentially help improve the transfer integral, representing wavefunction overlap, to better improve overall charge-carrier mobility.

Every material, up to this point, has been a small molecule. However, our recent work on metal sensor synthesis was able to show the ability to isolate stable, terminal alkynes.[11] These stable terminal alkynes could be a monomer for polymer synthesis to expand on the properties of poly(aryleneethynylene)s (PAEs) by Sonogashira coupling to a 1,4-diiodobenzene derivative.[12] Depending on the substitution of the diiodobenzene, different properties for different applications could be conferred. Very interesting would be a PAE displaying a robust quantum yield in the red part of the spectrum, a property potentially conferred by the use these stable terminal alkynes, which possess an already small H-L gap.

9.5 Concluding Remarks

This is a very exciting time for the organic electronic materials synthetic chemist. Our materials appear destine for many applications in synthesis and materials due to the ability to easily modify the core structure (optoelectronic properties), the R groups (solid-state packing/stability), and provide certain handles for postfunctionalization or incorporation into polymers. There is almost no limit for the driven synthetic chemist working with these materials.

9.6 References

[1] S.J. Strickler, R.A. Berg. *J. Chem. Phys*. **1962**, *37*, 814.

[2] M.L. Tang, A.D. Reichardt, P. Wei, Z. Bao. *J. Am. Chem. Soc.* **2009**, *131*, 5264.

[3] W.J. Potscavage, A. Sharma, B. Kippelen. *Accounts of Chem. Res*. **2009**, *42*, 1758. See also references 18-20 and 21-25 within.

[4] R.N. Thomas. *Analytica Chimica Acta*. **1994**, *289*, 57.

[5] B. Kippelen, J-L. Brédas. *Energy & Environmental Science*. **2009**, *2*, 251.

[6] S. Miao, S.M. Brombosz, P.v.R. Schleyer, J.I. Wu, S. Barlow, S.R. Marder, K.I. Hardcastle, U.H.F. Bunz. *J. Am. Chem. Soc.* **2008**, *130*, 7339.

[7] D.S. Surry, S.L. Buchwald. *Angew. Chem. Int. Ed*. **2008**, *47*, 6338.

[8] [a] S. Miao, A.L. Appleton, N.J. Berger, S. Barlow, S.R. Marder, K.I. Hardcastle, U.H.F. Bunz. *Chem. Eur. J.* **2009**, *15*, 4990; [b] A.L. Appleton, S.M. Brombosz, S. Barlow, J.S. Sears, J-L. Brédas, S.R. Marder, U.H.F. Bunz. *Nature Communications*. **2010**, 1:90.

[9] J. Nishida, Naraso, S. Murai, E. Fujiwara, H. Tada, M. Tomura, Y. Yamashita. *Org. Lett.* **2004**, *6*, 2007.

[10] M. Winkler, K.N. Houk. *J. Am. Chem. Soc.* **2007**, *129*, 1805.

[11] Y. Zhang, A.L. Appleton, S.M. Brombosz, A.J. Zappas, X. Qian, U.H.F. Bunz. "Amphiphilic phenazine and halogenated-phenazine bistriazoles and their metal-binding properties." *Chem. Comm.* **Submitted**.

[12] U.H.F. Bunz. *Macromol. Rapid Commun.* **2009**, *30*, 772.

[13] J.E. Anthony, J.S. Brooks, D.L. Eaton, S.R. Parkin. *J. Am. Chem. Soc.* **2001**, *123*, 9482.

[14] J.E. Anthony, D.L. Eaton, S.R. Parkin. *Org. Lett.* **2002**, *4*, 15.